Perylene Bisimide and Acene Derivatives as Organic Semiconductors in OTFTs

Dissertation zur Erlangung des
naturwissenschaftlichen Doktorgrades
der Julius-Maximilians-Universität Würzburg

vorgelegt von
Rüdiger Schmidt
aus Paderborn

Würzburg 2008

Eingereicht am 01.08.2008
bei der Fakultät für Chemie und Pharmazie

1. Gutachter: Prof. Dr. Frank Würthner
2. Gutachter:
der Dissertation

1. Prüfer: Prof. Dr. Frank Würthner
2. Prüfer:
3. Prüfer:
des Öffentlichen Promotionskolloquiums:

Tag des Öffentlichen Promotionskolloquiums:

Doktorurkunde ausgehändigt am:

für meine Eltern

Acknowledgement / Danksagung

Meinem Doktorvater, Herrn Prof. Dr. Frank Würthner danke ich für die Überlassung des sehr interessanten und vielseitigen Forschungsthemas, seine fundierte wissenschaftliche Betreuung, die zahlreichen Anregungen und die ausgezeichneten Arbeitsbedingungen in seinem Arbeitskreis. Auch die Möglichkeit im Rahmen einer Industriekooperation mit der BASF sehr eigenständig mit verschiedenen Forschungsgruppen kooperieren zu können, hat sehr zu dem erfolgreichen Abschluss meiner Arbeit beigetragen.

Bei Herrn Dr. Chantu Saha-Möller möchte ich mich für die große Geduld bei den Überarbeitungen der Publikationen und Teilen der vorliegenden Doktorarbeit bedanken.

Ein großer Dank gilt auch meinem Kooperationspartner in Stanford/USA. Die sehr erfolgreichen Transistor-Messungen von Herrn Dr. Joon Hak Oh, Herrn Dr. Mang Mang Ling und Frau Dr. Shuhong Liu in der Gruppe von Frau Prof. Dr. Zhenan Bao waren unverzichtbar für die Evaluierung meiner neuen Substanzen (Kapitel 5) im Rahmen der BASF-Kooperation.

Ein besonderer Dank geht an die BASF SE in Ludwigshafen, die Teile der vorliegenden Arbeit im Rahmen ihres Verbundprojektes „Organische Photovoltaik“ finanziert hat.

Herrn Dr. Martin Könemann, Herrn Dr. Rüdiger Sens, Herrn Dr. Felix Eickemeyer und Herrn Dr. Peter Erk möchte ich auch für die gute Zusammenarbeit bei Synthesen, Patenten und Publikationen im Rahmen der Kooperation herzlich danken.

Herrn Dr. Dirk Leusser und Herrn Prof. Dr. Dietmar Stalke sowie Herrn Dr. Fabian Seeler, Herrn Dr. Krystof Radacki und Herrn Prof. Dr. Holger Braunschweig danke ich für die Unterstützung bei den Röntgenstrukturanalysen.

Frau Dr. Ute Baumeister danke ich für die Möglichkeit der XRD-Messung des flüssigkristallinen Perylenbisimids

Herrn Joachim Bialas und Frau Manuela Deppisch danke ich für ihre ausgezeichnete Unterstützung und Kooperation im Labor und die Großsynthesen von „FSAB“ Produkten.

Bei Herrn Dr. Matthias Grüne und Frau Elfriede Ruckdeschel bedanke ich mich für die Aufnahme von ^{19}F- und Hochtemperatur ^{1}H-Spektren und bei Herrn Dr. Michael Büchner und Herrn Fritz Dadrich für die Anfertigung von Massenspektren.

Herrn Andre Klopf und Frau Katrin Lipsius danke ich für ihre zuverlässige und tatkräftige Unterstützung während ihrer Ausbildungszeit zum Chemielaboranten.

Mein Dank gilt weiterhin Frau Ana-Maria Krause für Durchführung und Beratung bei cyclovoltammetrischen Messungen, insbesondere bei den schwerlöslichen Perylenderivaten.

Ein großes Dankeschön geht an Frau Cornelia Röger für ihre tolle Kooperation, ausgezeichnetes Teamwork und Hilfsbereitschaft im Labor.

Auch bei Herrn Peter Osswald und Frau Stefanie Rehm möchte ich mich für die Hilfe und Diskussionsbereitschaft in all den Jahren bedanken.

Frau Christiana Toussaint danke ich für ihre Unterstützung bei allen organisatorischen Angelegenheiten.

Bei Herrn Brunner möchte ich mich für die kompetente Hilfe bei Computerfragen bedanke.

Allen früheren und aktuellen Mitarbeitern des Arbeitskreises danke ich für die schöne Zeit und viele lustige Abende im Labor und in der Stadt.

Meiner Familie und insbesondere meinen Eltern danke ich für die unschätzbare Unterstützung.

Allen meinen alten Freunden, Christian, Fabian, Kristina, Stefanie, Thomas, Conny, Valerie und Andreas danke ich für eine schöne Promotionszeit.

Marina danke ich für ihre Geduld, Hilfe und dass ich immer Rückhalt bei ihr gefunden habe.

List of Abbreviations

AFM	atomic force microscopy
APCI	atmospheric pressure chemical ionisation
CNC^+	(*N,N*-dimethylimidazolidino)-tetramethylguanidinium
CuPc	copper phthalocyanine
CV	cyclic voltammetry
DCM	dichloromethane
DSC	differential scanning calorimetry
DT-TTF	dithiophene-tetrathiafulvalene
EI	electron impact ionization
ESI	electrospray ionization
F_{16}-CuPc	hexadecafluoro copper phthalocyanine
Fc	ferrocene
Halex	halogen exchange reaction
HOMO	highest occupied molecular orbital
HR	high resolution
IPES	inverse photoemission spectroscopy
LC	liquid crystal/crystalline
LUMO	lowest unoccupied molecular orbital
MALDI	matrix-assisted laser desorption injection
NBA	naphthalene tetracarboxylic acid bisanhydride
NBI	naphthalene tetracarboxylic acid bisimide
NMP	*N*-methyl-2-pyrrolidone
NMR	nuclear magnetic resonance
OLED	organic light emitting diode
OFET	organic field effect transistor
OTFT	organic thin film transistor
OTS	octadecyltriethoxysilane
PBI	perylene tetracarboxylic acid bisimide
P3HT	poly-3-hexylthiophene
PR-TRMC	pulse-radiolysis time-resolved microwave conductivity
PTCBI	perylene tetracarboxylic acid bisbenzimidazole
RT	room temperature
SCLC	space-charge-limited current

TBAHFP	tetrabutylammonium hexafluorophosphate
THF	tetrahydrofurane
TMS	tetramethylsilane
TOF	time of flight
UPC	ultraviolet photoemission spectroscopy
UV	ultraviolet
Vis	visible

Table of Content

Chapter 1

Introduction and aim of thesis

Transistors are among the most important inventions of the 20th century and omnipresent in our everyday life. These electronic devices can be found in communication and automation technologies, and all kinds of computer systems. They are used for amplification or switching of electronic signals by allowing very large current flow, when only a small current or voltage is applied.

Despite extensive use of crystalline silicon and other inorganic materials for the fabrication of electronic devices, especially transistors, these rigid and expensive materials are not properly suited for several unique electronic applications. Organic semiconductors can close this gap, as they exhibit many desirable attributes. The potential flexibility of organic devices is a key factor for many future innovative products as foldable displays[1] or organic solar cells[2] (Figure 1).

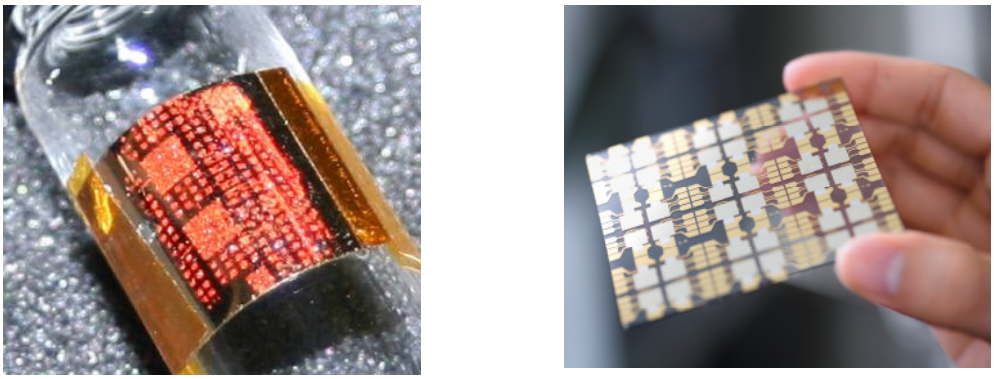

Figure 1. Flexible organic thin film transistors (OTFTs) (left) and organic solar cells (right), with permission from Prof. Z. Bao (http://www.news.com/i/ne/p/2006/bendy_210x186.jpg) and Dr. F. Eickemeyer (BASF SE).

Worth mentioning are also other devices,[3] e.g. disposable RFID (radio frequency identification) tags for replacing the bar codes on products in the supermarket,

display drivers, nonvolatile memories, and sensors. These components are based on organic thin film transistors (OTFTs) and they can be produced by vacuum deposition or spin-coating processes. The latter technique is only suitable for well-soluble organic compounds but enables printing and casting from solution to achieve low-cost and large area applications.[4] Furthermore, the physical, chemical, and electronic properties of organic compounds can be tuned quite easily over a wide range, which allows the design of perfectly aligned compounds with adjusted electronic levels for the active layer in OTFTs and related electronic and optoelectronic devices.[5]

Although organic semiconductors have attracted a lot of scientific attention during the last decade, many major challenges are still confronting the field of organic electronics. Solution-deposited semiconductors typically lack high performance in the thin layer and the devices of many organic n-type materials are not environmentally stable. Therefore, organic semiconductors with improved solubility and film-forming properties without concern for atmospheric exposition are in demand. Furthermore, the availability of stable high performance n- and p-type materials is essential for various applications such as diodes and complementary circuits.[6]

Concerning organic p-type semiconductors, unsubstituted acene derivatives, especially pentacene, have been intensively investigated in organic thin-film transistors (OTFT, Figure 2) with outstanding mobilities up to 3 cm^2/Vs,[7] even though the π–π interactions in the solid state are limited due to the well-known herringbone packing of the molecules. Single crystalline transistors showed even values up to 35 cm^2/Vs.[8]

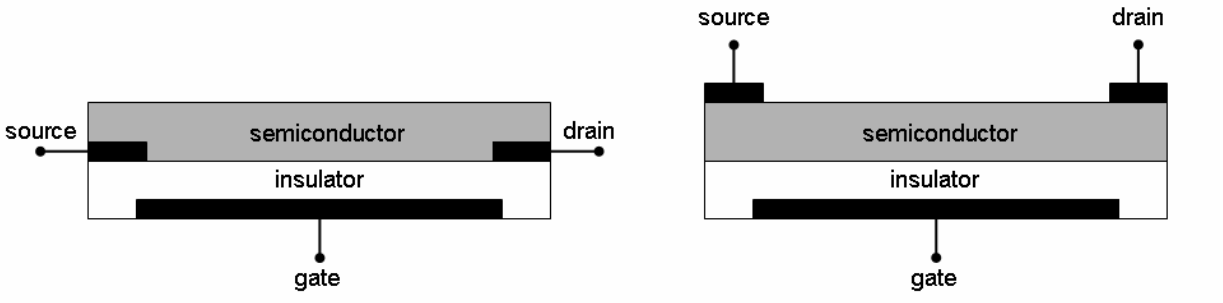

Figure 2. OTFT setup, bottom-contact (left), top-contact (right)

As many of such acene derivatives suffer from a very poor solubility, only processing by vacuum deposition can be applied. Therefore, highly soluble acene

derivatives with outstanding stability towards oxidation are required for large scale production of cheap electronic devices. In addition, the solid state packing can be modified to achieve parallel orientation of the dyes, which can lead to significantly higher charge carrier mobilities.[9] Thus, the development of new acene derivatives with above described properties was the aim of the first part of this thesis.

However, the performance of TFTs based on organic n-type semiconductors lags still behind that of p-type materials. Though many organic n-type semiconductors already revealed higher mobilities than amorphous silicon or other common p-type semiconductors, most electronic devices based on n-type organic materials are only stable under inert gas or vacuum. This makes a serious deployment of these compounds very difficult and new high performance air-stable compounds are in demand. Several rylene bisimide derivatives exhibit air-stable field effect mobilities,[10] especially, perylene tetracarboxylic acid bisimides (PBIs)[10b] are highly promising in this field of research. However, for the most literature known cases either quite low mobilities or other unexpected difficulties were reported and the attributes of PBIs for OTFTs still have to be improved. As perylene bisimide dyes can be modified in many different manners in bay and imide positions, the search for new PBI derivatives which exhibit high air-stable mobilities in OTFTs was the main goal of this thesis.

Chapter 2 gives an overview on the history, device principles and applications of organic semiconductors in thin film transistors. Furthermore, the performance of common organic p- and n-type semiconductors is illustrated and possibilities for potential improvements concerning stability and packing motives are discussed.

Chapter 3 presents the synthesis and characterization of highly soluble acene derivatives. The packing of the compounds in the solid state is elucidated and the charge carrier mobilities in OTFTs prepared by spin-coating techniques are investigated.

Chapter 4 focuses mainly on the synthesis of novel core-fluorinated perylene bisimide dyes. Different synthetic pathways are discussed and the solid state packing of a fluorinated perylene bisimide is presented exemplarily. In addition, the imide substituents are varied to obtain insoluble pigments, crystalline compounds as well as highly soluble liquid crystalline dyes.

Chapter 5 describes the synthesis of four different kinds of electron-deficient perylene bisimides that are suitable for applications as n-type semiconductors. The combination of electron-withdrawing groups in the imide positions with different

halogen substituents (fluorine to bromine) at the bay positions is presented. With X-ray diffraction analysis of several solvent-free single crystals, the influence of the arrangement in the solid state, especially the (non)planarity of the π–systems, on the performance in OTFTs prepared by vacuum deposition is discussed. The coherence of air-stability of the devices and the special packing of the molecules are explained on the basis of several examples.

Chapter 6 is the summary of this thesis in English and in **Chapter 7** a summary in German is given.

References and Notes

[1] For flexible displays, see: (a) S. R. Forrest, *Nature* **2004**, *428*, 911-918; (b) C. D. Sheraw, L. Zhou, J. R. Huang, D. J. Gundlach, T. N. Jackson, M. G. Kane, I. G. Hill, M. S. Hammond, J. Campi, B. K. Greening, J. Francl, J. West, *Appl. Phys. Lett.* **2002**, *80*, 1088-1090; (c) L. Zhou, A. Wanga, S.-C. Wu, J. Sun, S. Park, T. N. Jackson, *Appl. Phys. Lett.* **2006**, *88*, 083502.

[2] For organic solar cells, see: (a) L. Schmidt-Mende, A. Fechtenkötter, K. Müllen, E. Moons, R. H. Friend, J. D. MacKenzie, *Science* **2001**, *293*, 1119-1122; (b) P. Peumans, S. Uchida, S. R. Forrest, *Nature* **2003**, *425*, 158-162; (c) S. E. Shaheen, C. J. Brabec, N. S. Sariciftci, F. Padinger, T. Fromherz, J. C. Hummelen, *Appl. Phys. Lett.* **2001**, *78*, 841-843; (d) C. W. Tang, *Appl. Phys. Lett.* **1986**, *48*, 183-185.

[3] (a) D. J. Gundlach, *Nat. Mater.* **2007**, *6*, 173-174; (b) B. Yoo, T. O. Jung, D. Basu, A. Dodabalapur, B. A. Jones, A. Faccetti, M. R. Wasielewski, T. J. Marks, *Appl. Phys. Lett.* **2006**, *88*, 082104; (c) Y. Noguchi, T. Sekitani, T. Someya, *Appl. Phys. Lett.* **2006**, *89*, 253507; (d) Y. Watanabe, K. Kudo, *Appl. Phys. Lett.* **2005**, *87*, 223505; (e) R. C. G. Naber, B. de Boer, P. W. M. Blom, D. M. de Leeuw, *Appl. Phys. Lett.* **2005**, *87*, 203509; (f) R. C. G. Naber, B. de Boer, P. W. M. Blom, D. M. de Leeuw, *Appl. Phys. Lett.* **2005**, *87*, 203509; (g) H. Sirringhaus, N. Tessler, R. H. Friend, *Science* **1998**, *280*, 1741-1744.

[4] (a) H. Klauk, *Nat. Mater.* **2007**, *6*, 397-398; (b) K. J. Lee, M. J. Motala, M. A. Meitl, W. R. Childs, E. Menard, A. K. Shim, J. A. Rogers, R. G. Nuzzo, *Adv.*

Mater. **2005**, *17*, 2332-2336; (c) H. Sirringhaus, *Adv. Mater.* **2005**, *17*, 2411-2425; (d) M. M. Ling, Z. Bao, *Chem. Mater.* **2004**, *16*, 4824-4840.

[5] For representative reviews and highlights, see: (a) J. E. Anthony, *Angew. Chem.* **2008**, *120*, 460-492; *Angew. Chem. Int. Ed*. **2008**, *47*, 452-483; (b) A. Facchetti, *Mater. Today* **2007**, *10*, 28-37; (c) A. Dodabalapur, *Mater. Today* **2006**, *9*, 24-39; (d) F. Würthner, R. Schmidt, *ChemPhysChem* **2006**, *7*, 793-797; (e) J. E. Anthony, *Chem. Rev.* **2006**, *106*, 5028-5048; (f) A. Dodabalapur, *Nature* **2005**, *434*, 151-152; (g) C. R. Newman, C. D. Frisbie, D. A. da Silva Filho, J.-L. Brédas, P. C. Ewbank, K. R. Mann, *Chem. Mater.* **2004**, *16*, 4436-4451; (h) C. Reese, M. Roberts, M. Ling, Z. Bao, *Mat. Today* **2004**, *7*, 20-27; (i) T. W. Kelley, P. F. Baude, C. Gerlach, D. E. Ender, D. Muyres, M. A. Haase, D. E. Vogel, S. D. Theiss, *Chem. Mater.* **2004**, *16*, 4413-4422; (j) C. D. Dimitrakopoulos, P. R. L. Malenfant, *Adv. Mater.* **2002**, *14*, 99-117; (k) H. E. Katz, Z. Bao, S. L. Gilat, *Acc. Chem. Res.* **2001**, *34*, 359-369.

[6] For recent examples, see: (a) H. Klauk, U. Zschieschang, J. Pflaum, M. Halik, *Nature* **2007**, *445*, 745-748; (b) K. Hizu, T. Sekitani, T. Someya, J. Otsuki, *J. Appl. Phys. Lett.* **2007**, *90*, 093504; (c) A. Dodabalapur, *Mater. Today* **2006**, *9*, 24-39; (d) S. Nadkarni, B. Yoo, D. Basu, A. Dodabalapur, *Appl. Phys. Lett.* **2006**, *89*, 184105; (e) S. De Vusser, S. Steudel, K. Myny, J. Genoe, P. Heremans, *Appl. Phys. Lett.* **2006**, *88*, 162116.

[7] H. Klauk, M. Halik, U. Zschieschang, G. Schmid, W. Radlik, W. Weber, *J. Appl. Phys.* **2002**, *92*, 5259-5263.

[8] O. D. Jurchescu, J. Baas, T. T. M. Palstra, *Appl. Phys. Lett.* **2004**, *84*, 3061-3063.

[9] M. M. Payne, S. R. Parkin, J. E. Anthony, C. Kuo, T. N Jackson, *J. Am. Chem. Soc.* **2005**, *127*, 4986-4987.

[10] For air-stable rylene derivatives see: (a) B. A. Jones, A. Facchetti, T. J. Marks, M. R. Wasielewski, *Chem. Mater.* **2007**, *19*, 2703-2705; (b) A. J. Jones, M. J. Ahrens, M.-H. Yoon, A. Facchetti, T. J. Marks, M. R. Wasielewski, *Angew. Chem.* **2004**, *116*, 6523-6526; *Angew. Chem. Int. Ed.* **2004**, *43*, 6363-6366; (c)

H. E. Katz, A. J. Lovinger, J. Johnson, C. Kloc, T. Siegrist, W. Li, Y.-Y. Lin, A. Dodabalapur, *Nature* **2000**, *404*, 478-481, (d) H. E. Katz, J. Johnson, A. J. Lovinger, W. Li, *J. Am. Chem. Soc.* **2000**, *122*, 7787-7792.

Chapter 2

State of Knowledge

Abstract: This chapter gives an overview on the development, device principles, and applications of organic thin film transistors. Different methods for charge carrier mobility measurements are described and the most important n- and p-type organic semiconductors are illustrated by various examples. The special focus lies on perylene bisimide and acene derivatives, and their strengths and shortcomings in organic electronic devices are discussed.

2.1 History of Organic Field-Effect Transistors

Semiconductor microelectronics are omnipresent in everyday live of our advanced society, though the development of field-effect transistors (FETs) started only about 80 years ago. The principle of the first inorganic FET was patented by the German physicist *Lilienfeld* in 1926,[1] but he did not establish the operability of his devices. Thus, his invention was unnoticed by the industry and finally forgotten. About 20 years later the first working transistors were designed by *Bardeen*, *Brattain*, and *Shockley* at Bell Laboratories (USA) and in 1956 they were awarded with the Nobel price in physics for their pioneering research and discovery of the transistor effect. While these initial quite primitive transistors gradually replaced the formerly used vacuum tubes in many electronic applications, fifty more years of research were needed to develop the today's typical metal-oxide-semiconductor field-effect transistors (MOSFET) based on silicon.[2] These transistors are the most frequently built components by the mankind and millions of them found their way in processors of computers and other microelectronic devices.

The field-effect in transistor devices can also be used to determine the charge carrier mobility in solid materials. Such thin-film transistors (TFTs)[3] consist of deposited thin layers of metallic contacts and semiconducting and dielectric layers. This design principle turned out to be essential for large area applications where single crystalline silicon can not be applied any more. Nowadays hydrogenated amorphous silicon (α-Si:H) TFTs are indispensable for active-matrix liquid-crystal displays.

The structure of TFTs is also adequate for the application of low mobility compounds such as organic semiconductors, that were already described in the late 1940ies, but up to 1980ies only little research efforts were made in this area and few compounds (e.g. phthalocyanines) were investigated.[4] The invention of an organic heterojunction solar cell by *Tang* et al[5] and the development of thin film transistors with polymers[6] and small molecules[7] revived a broader scientific interest in undoped organic semiconductors. However, the performance of these first organic thin-film transistors (OTFTs) remained rather low, while the development of organic light emitting diodes (OLEDs) based on vacuum deposited films and polymers made much faster progress and led to already commercially available products as OLED displays.[8] Nevertheless, in recent years the performance of OTFTs improved drastically and, since the charge carrier mobilities outbalanced those of amorphous silicon,[9] industries have initialized research programs in this field. In the near future different products based on OFETs

(organic field effect transistor) such as radio-frequency identification (RFID) tags (for replacing the bar code),[10] other printable single use electronics,[11] chemical sensors,[10d,12] display drivers,[13] nonvolatile memories,[14] and flexible displays[10d,15] seem to be within reach.

2.2 Different Classes of Semiconductors

Semiconductors are divided into the intrinsic and the extrinsic classes.[16] An intrinsic semiconductor is an insulator at very low temperature, but the band gap is small enough that the conduction band can partly be populated at room temperature. E.g. undoped silicon belongs to this class (Figure 1).

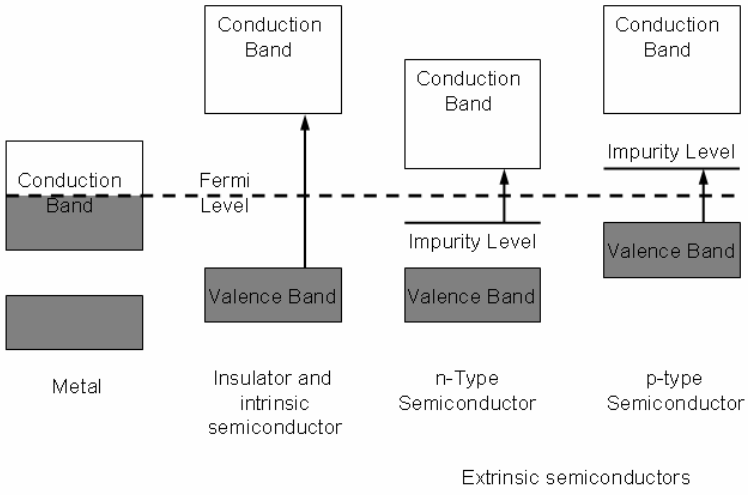

Figure 1. Energy diagrams of a metal, an insulator or intrinsic semiconductor and extrinsic semiconductors.[16]

Doping of intrinsic inorganic semiconductors induces localized energy levels close to the conduction (n-type) or valence (p-type) band edge (Figure 1, extrinsic semiconductors). By this technique the energy for the introduction of an electron or hole is tremendously lowered and the compound becomes more suitable for the common devices. But only few inorganic materials can be produced with sufficient purity, while most organic semiconductors are contaminated with relatively high amounts of both kinds (p- and n-type) of impurities. Due to these intrinsic impurities in organic semiconductors doping in the range of some ppm (parts per million) like silicon has no significant effect, whereas higher doping in the range of some percent will transfer the organic semiconductor into a conductor and make the compounds useless for electronic devices. Hence, organic semiconductors are more similar to insulators than in-

organic semiconductors and different models for the charge transport in the solid state were described in literature.[16,17]

2.3 Charge Carrier Transport in Organic Materials

The charge transport mechanism in molecular organic solids differs significantly from that of inorganic semiconductors as in organic materials normally ionic molecular states, i.e. radical cations and anions are involved.[18] In molecular solids electrons or holes have to move from one molecule to another and, compared to the single molecules in the gas phase, these ionic states are stabilized by polarization energies in the crystal. Due to these exciton binding energies the optical gap is significantly smaller than the single molecule gap to create an uncorrelated electron-hole pair (Figure 2, E_g and E_{opt}). Furthermore, the active layer in most OFETs is not single crystalline and the energy levels of valence and conduction bands of polycrystalline or amorphous layers are less discrete due to varying polarization energies of different molecular environments (Figure 3). The contribution of different defects or trapping states on the hopping transport was described by *Bässler* et al with a Gaussian distribution.[19] The spatial and energetic disorder in the semiconducting layer is proportional to the bandwidth of the Gaussian density of states.

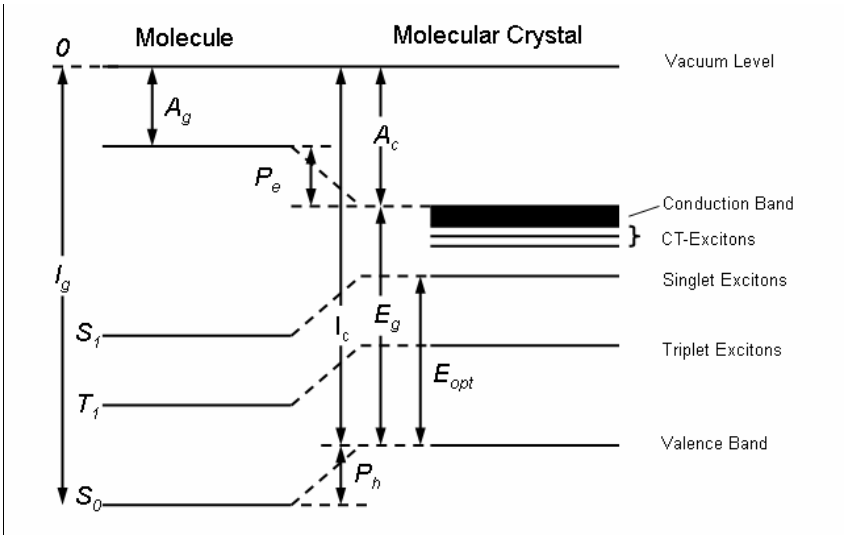

Figure 2. Energy levels of isolated molecule and molecular crystal. S_0, S_1, and T_1 = singlet and triplet states, I_g and A_g = ionization potential and electron affinity in gas phase, I_c and A_c = the respective quantities in crystal, P_e and P_h = polarization energies, E_g = single particle gap, E_{opt} = optical gap.[17a]

Otherwise the band transport model, as it can be used to describe carrier transport in silicon-based devices, can only be applied for highly ordered organic single crystals at low temperatures. Compared to inorganic materials the bandwidth of organic crystals

is still very small and the measured charge carrier mobilities range from 1 to ~35 cm^2/Vs which is comparable to the mobility in amorphous silicon.[20] For high purity crystals, different measurement techniques showed increasing mobilities with decreasing temperatures, suggesting band transport instead of hopping. This inverse temperature dependence of the charge carrier mobility μ can be expressed by equation 1.

$$\mu \propto T^{-n} \; with \quad n = 1...3 \tag{1}$$

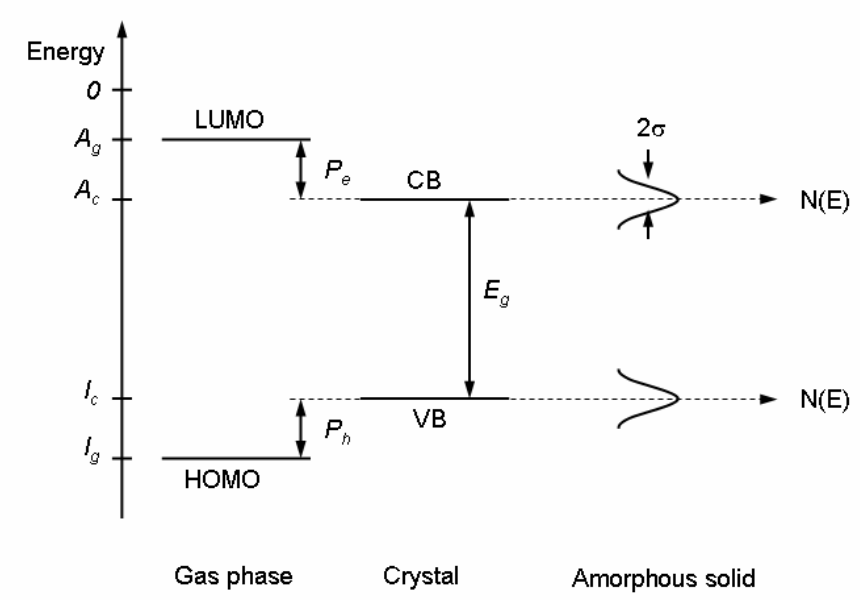

Figure 3. Energy levels of isolated molecule, molecular crystal, and amorphous solid. I_g and A_g = ionization potential and electron affinity in gas phase, I_c and A_c = the respective quantities in crystal, P_e and P_h = polarization energies, E_g = single particle gap.[17a]

In contrast to organic crystals, disordered organic materials do not form energy bands due to low molecular interactions between the molecules based on van der Waals forces. Some models have been developed to explain theoretically the temperature and electric-field dependency of charge carrier drift mobilities. The **Poole-Frenkel model** (equation 2) demonstrates empirically the temperature and electric-field dependencies of charge carrier mobilities.[18c,21] Many experimental results for organic disordered systems are in good accordance to this model.

$$\mu = \mu_0 \exp\left(\frac{E_0 - \beta_{PF}\sqrt{F}}{kT_{eff}}\right), T_{eff} = T^{-1} - T_0^{-1} \tag{2}$$

E_0 = activation energy in the absence of electric field, β_{PF} = the Poole-Frenkel coefficient, F = electric field, k = Boltzmann constant, T_0 = temperature at which the extrapolated data of Arrhenius plots for various electric fields intersect with one another, μ_0 = mobility at T_0.

According to the **small-polaron theory** the charge carrier hopping is supported by phonons.[18c,22] This means that charge carrier transport occurs by hopping of small polarons between localized states and the mobility of a small polaron in the limit of zero electric field can be calculated according to equation 3. The dependence of activation energy for charge transport in doped polymer systems on the spacing between the molecules has been explained with terms of this model.

$$\mu = (e\rho^2 / kT)P(\omega/2\pi)\exp\left[-\left(\frac{E_p}{2} - J\right)/kT\right] \quad (3)$$

μ = mobility, e = elementary charge, ω = phonon frequency, J = overlap integral, E_P = polaron binding energy, ρ = spacing between molecules, P = probability of a charge carrier hopping in the case of energy coincidence, adiabatic regime: P = 1, nonadiabatic regime: P < 1, k = Boltzmann´s constant, T = temperature.

The **disorder formalism** includes the energetic and positional disorder of the system.[18c,19,23] One assumes that the transport takes place by hopping through multiple localized states, which are influenced by the fluctuations of hopping site energy and intermolecular wave function overlap. The hopping site energy and intermolecular distance are in accordance with the Gaussian distributions. The mobility is given by the equation 4.

$$\mu = \mu_0 \exp\left[-\left(\frac{2\sigma}{3kT}\right)^2\right]\exp\left\{C\left[\left(\frac{\sigma}{kT}\right)^2 - \sum^2\right]\sqrt{F}\right\} \quad (4)$$

σ and Σ = parameters that characterize the energetic and position disorders, μ_0 = hypothetical mobility in the disorder-free system, F = electric field, C = empirical constant, k = Boltzmann´s constant, T = temperature.

Finally, the **multiple trapping and release model** assumes that highly concentrated localized levels act as traps for a defined delocalized band. By interacting with these levels the charge carriers are trapped and then released thermally. For the model some interactions are postulated. Carriers arriving at a defect are trapped with a very high probability near to 1 and the release of the carriers is thermally controlled. The drift mobility μ_D is related to the mobility μ_0 in the delocalized band by an expression of equation 5.[18b,24] This model is widely used to explain charge transport in amorphous silicon.

$$\mu_D = \mu_0 \alpha \exp\left(-\frac{E_t}{kT}\right) \quad (5)$$

μ_D = drift mobility, μ_0 = mobility in the delocalized band, α = ratio of the effective density of state at the delocalized band edge to the concentration of traps, E_t = distance between the trap level and delocalized band edge, , k = Boltzmann´s constant, T = temperature.

Besides charge carrier mobility, the charge carrier density is also of importance for the operation mode of the OTFT. The charge carrier density can be calculated with the equation 6. [17a]

$$n_i = N_0 \cdot \exp(-E_g / 2kT) \quad (6)$$

n_i = charge carrier density, E_g = energy gap, N_0 = effective density of states, k = Boltzmann´s constant.

With values of E_g = 2.5 eV and $N_0 = 10^{21}$ cm^{-3} for an exemplary organic semiconductor carrier densities of only n_i = 1 cm^{-3} can be found. Although the real density should be higher due to inevitable impurities, the corresponding value for silicon (E_g = 1.12 eV and $N_0 = 10^{19}$ cm^{-3}) is about $n_i = 10^{10}$ cm^{-3}. Therefore, it can be anticipated that particular impurities are responsible for charge carrier mobilities in organic materials, and it is always not for sure whether the obtained values are genuinely for the organic material or owing to some unintended dopants.

2.4 Architecture and Operation Mode of Thin-Film Transistors

The most OTFTs are built according to two different construction principles: the top-contact (TC) and the bottom-contact (BC) (Figure 4). Both structures have their pros and cons depending on the consistence of the active layer.[16]

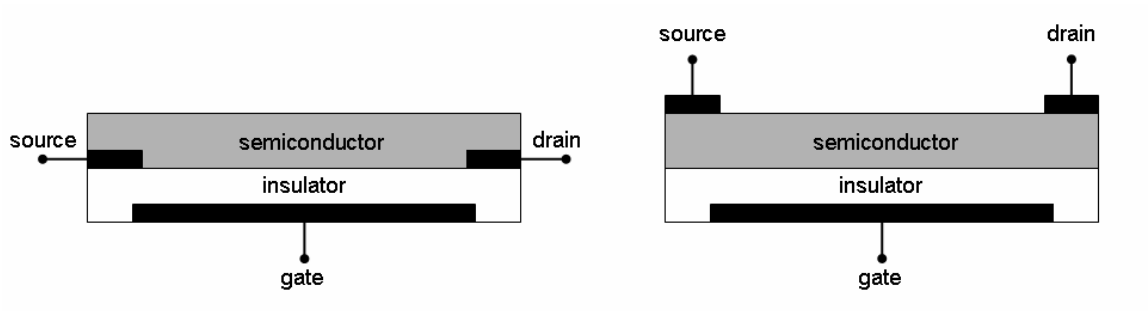

Figure 4. OTFT setup, bottom-contact (left), top-contact (right).

In general, TFTs are a combination of three electrodes, an insulator and a thin semiconducting layer. The source and drain electrodes are in direct contact with the semiconductor, while the gate electrode is insulated. In the case of bottom-contact device the organic thin layer is deposited onto the device in the last step, which allows microlithographic deposition of the source and drain electrodes before. This technique is not applicable to top-contact devices as the organic layers are quite fragile. That is why only deposition through shadow masks can be applied for top-contact devices

leading to an inferior resolution. The resistance between the contacts and semiconductor is normally lower for the top-contact device.

Furthermore, for each device the electrode material has to be adjusted to the applied organic semiconductor. Especially the Fermi level (or the work function) of the metal and the respective LUMO and HOMO levels of the compound have to be matched. The energy scheme in Figure 5 shows the respective positions of the energy levels of several known p- and n-type semiconductors and that of some common metals used as electrodes in TFTs. For example gold forms a good hole injection contact for copper phthalocyanine (CuPc) or pentacene, while electron injection is favored for perylene tetracarboxylic acid bisanhydride (PBA) or perfluorinated copper phthalocyanine (F_{16}-CuPc). For p-type semiconductors normally no negative charges can be injected into the far-off LUMO level (positive gate voltage), because the HOMO level is located much closer to the Fermi level of the metal of the electrodes. Generally, when the hole injection is more facile than the electron injection the organic semiconductor is called as p-type and vice versa as n-type.

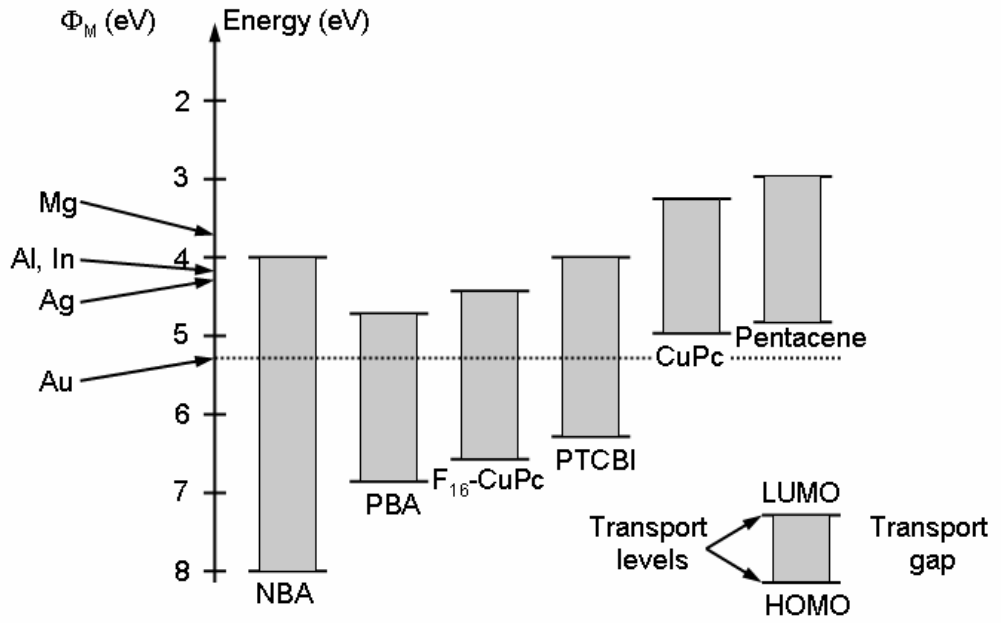

Figure 5. Comparison between the metal work functions (Φ_M) and the HOMO and LUMO positions, as determined by ultraviolet photoemission spectroscopy (UPS) and inverse photoemission spectroscopy (IPES) of various organic materials. The zero of the energy scale represents a common vacuum level. NBA = naphthalene tetracarboxylic acid bisanhydride; PBA = perylene tetracarboxylic acid bisanhydride; F_{16}-CuPc = hexadecafluoro copper phthalocyanine; PTCBI = perylene tetracarboxylic acid bisbenzimidazole; CuPc = copper phthalocyanine.[25]

The procedure for the thin film deposition is one of the most sensible production steps and has a strong impact on the performance of the device. The best method for small vaporable organic molecules is the deposition by **vacuum deposition tech-**

niques which is carried out by heating the material under reduced pressure (normally ultra high vacuum < 10^{-6} mbar).[18d] By this method the thickness and purity of the film can easily be controlled and the deposition rate and the substrate temperature can be adjusted as well. Since “chemically pure” organic semiconductors, synthesized and purified by normal chemical standards, contain substantial amounts of unknown impurities (in the range up to some percent) they have to be purified by zone vacuum sublimation, which can be performed several times in a row.

For compounds that decompose at higher temperatures the vacuum deposition technique is inappropriate. Therefore the deposition from solution by **spin-coating** is applied for polymers and thermally instable molecules. Spin-coating can also provide very homogeneous films, but the device performance is much lower due to little crystallinity of the active layer. Other developments are possible for liquid crystalline polymers, which self assemble after deposition in a highly ordered arrangement. Spin-coating techniques are generally praised as a very cheap way of device preparation which is essential for low cost electronics. However, during the last few years vacuum deposition methods have been steadily optimized and as a consequence the advances of solution processing are declining.

The **output and transfer characteristics** of an OTFT with a pentacene derivative[26] as active layer are depicted exemplarily in Figure 6. At lower drain voltage the current is proportional to gate and drain voltage following Ohm’s law (Figure 6, left). When finally the drain voltage approaches the gate voltage, the channel current becomes independent of the drain bias and the slope decelerates. This is called the saturated region (Figure 6, left, red area).

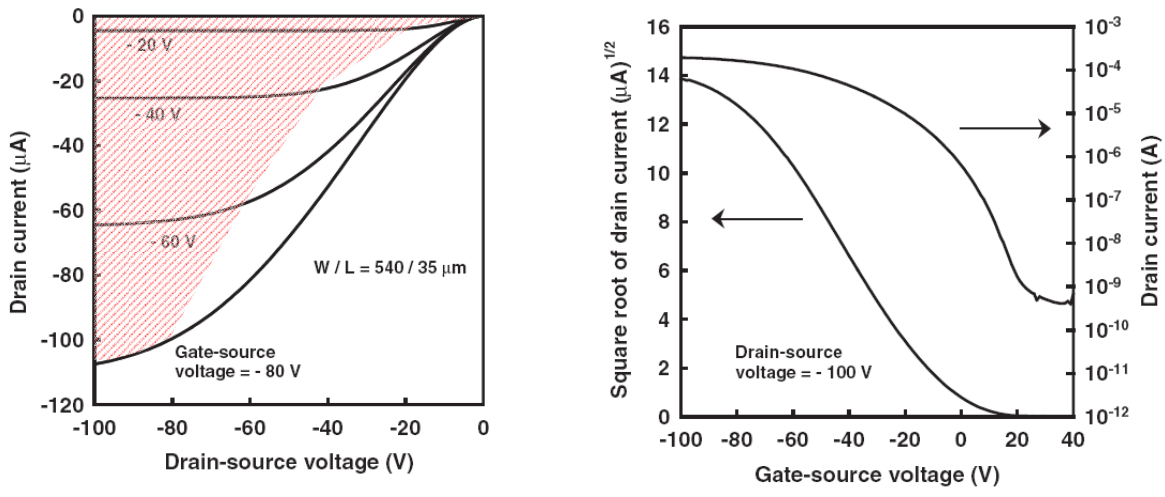

Figure 6. Output- (left) and transfer (right) characteristics for OTFT with a pentacene derivative, reproduced from ref [26] with permission from Wiley-VCH Verlag GmbH & Co. KGaA.

The current for the linear and saturated region is given by equations 7 and 8. Charge carrier mobility in the saturation regime can be obtained with equation 9.[18a] Another characteristic parameter is the threshold voltage, that is the gate voltage at which there are sufficient charge carriers in the active layer and the current starts to rise.

$$I_{dlin} = \frac{W}{L} C_i \mu (V_g - V_t) V_d \tag{7}$$

$$I_{dsat} = \frac{W}{2L} C_i \mu (V_g - V_t)^2 \tag{8}$$

$$\mu_{sat} = \frac{I_{dsat}}{(V_g - V_t)^2} \frac{2L}{WC_i} \tag{9}$$

W and L = channel width and length, respectively, C_i = insulator capacitance per unit area, V_g and V_d = gate and drain voltages, V_t = threshold voltage, $I_{dsat/lin}$ = current for linear/saturated region, μ_{sat} = mobility in saturated region.

In addition to the charge carrier mobility, the on/off ratio (equation 10) is another important TFT characteristic.[18d] It represents the ratio of the current when the device is switched off ($V_{SG} = 0$) and switched on ($V_{SG} \neq 0$) and is a very good indication for the purity of the organic semiconducting layer. When there are no impurities in the layer, charges can barely flow from source to drain electrode in the off state of the device leading to a high on/off ratio. Generally, the performance of a device can be read off from its transfer characteristics (Figure 6, right, I_{DS} vs V_{GS}), revealing an on/off ratio of about 10^6 and a mobility of 0.4 cm^2/Vs for this pentacene derivative (calculated with equations 9 and 10).

$$I_{on}/I_{off} = \mu C_i V_{SG} / 2\mu_r q N_A t \tag{10}$$

μ_r = charge carrier mobility, N_A = carrier concentration (off-state), t = semiconductor film thickness, q = electron charge, V_{SG} = current when device is switched off or on, C_i = insulator capacitance per unit area.

Next to the possibility of testing the organic semiconductor in TFTs, several other measurement setups have been established, the most known ones being the time of flight (TOF) and pulse-radiolysis time-resolved microwave conductivity (PR-TRMS). Furthermore mainly for pure organic single crystals the mobility can also be measured by the space-charge-limited current (SCLC) method.

For **TOF** measurements, an organic layer is embedded between two electrodes and irradiated by a laser pulse near to one of the electrodes.[18a] Depending on the polarity of the applied bias (and electric field) the photogenerated charges move across the

layer toward the other electrode where the time dependent current is recorded. For highly ordered crystalline materials nearly all charge carriers reach simultaneously the electrode, while in amorphous systems the signal is broadened. The mobility can then be calculated according to equation 11.

$$\mu = \frac{v}{F} = \frac{d}{Ft} = \frac{d^2}{Vt} \tag{11}$$

d = distance between the electrodes, F = electric field, t = averaged transient time, V = applied voltage.

PR-TRMC is better suited for the measurement of intrinsic mobilities and can even be used for bulk materials and single polymer chains in solution.[18a] The sample is excited by high energy electrons and some free charge carriers are created. With the reflected microwave power the change of the electrical conductivity $\Delta\sigma$ can be measured, which is dependent on the frequency and expressed by equation 12.[27] PR-TRMC values have to be considered as a possible maximum mobility value since the transport characteristics are assessed on a very small scale, e.g. even in the range of a single polymer chain. TOF values are normally smaller compared to the corresponding PR-TRMC values as for the former method the charge carriers have to cross the grain boundaries and interact with impurities.

$$\Delta\sigma = e\sum \mu N_{e-h} \tag{12}$$

$\Delta\sigma$ = change in electrical conductivity, $\Sigma\mu$ = sum of hole and electron mobilities, $N_{e\text{-}h}$ = density of generated electron-hole pairs, e = elementary charge.

Space-charge-limited current (SCLC) spectroscopy is a quite common method for the characterization of the electrical attributes of organic molecular crystals (Figure 7).[28]

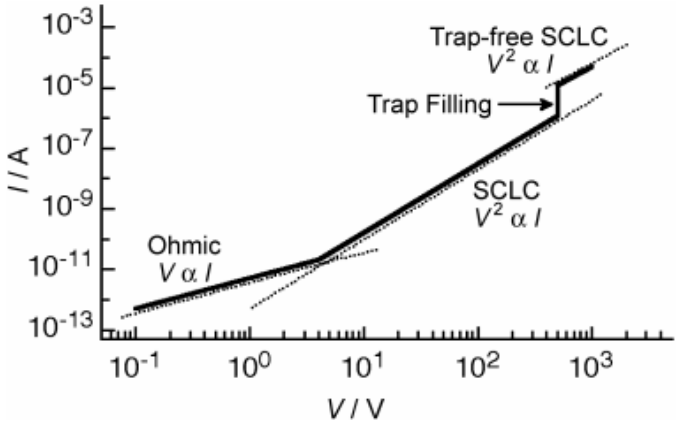

Figure 7. Current/voltage behavior of a crystalline sample reproduced from [28] with permission from Wiley-VCH Verlag GmbH & Co. KGaA.

In this setup an organic layer is sandwiched by two electrodes,[18a] and with the aquired current/voltage behavior at high electric fields (similar to TOF measurements) the mobility can be calculated. Figure 7 shows the crossover from the Ohmic regime to the space-charge-limited current at higher electric fields. In this region the current is proportional to the voltage squared ($V^2 \propto I$). When the electric field is further increased all traps are filled at once. Finally the trap-free SCLC region is reached, where the mobility can be determined most accurately. Even if the trap-free regime is not available by experiments, the lower limit for intrinsic mobilities can be obtained with the equation 13.

$$J_{TF} = \frac{9}{8}\varepsilon_0\varepsilon_r\mu\frac{V^2}{L^3} \tag{13}$$

J_{TF} = current density, V = applied bias voltage, ε_0 = permittivity of free space, ε_r = relative dielectric constant of medium, L = device thickness.

2.5 Influence of Molecular Packing on Charge Carrier Mobility

Besides the crystalline quality of the organic layer, the molecular order in the crystal itself is of significant importance for the charge carrier mobility.[29] Many unsubstituted organic molecules with conjugated π-systems (e.g. pentacene, rubrene, perylene, etc.) exhibit strong two-dimensional edge-to-face interactions leading to a “herringbone“ packing in the solid state. This packing supports two dimensional transport within the stacked layers, while the transport between the molecular layers is significantly lower. The anisotropy effect can easily be observed by charge carrier mobility measurements of single crystals in different directions, e.g. for pentacene single crystal values between 0.7 and 2.3 cm^2/Vs were found within the layers (measured from 0° to 360°)[30] and also rubrene showed significantly higher mobilities along the molecular π-stacking axis (Figure 8).[31] Although many organic molecules with “herringbone” structure exhibit very high charge carrier mobilities, this arrangement is *a priori* not perfect for the electronic properties of the material. Face-to-face interactions are predicted to cause stronger electronic coupling between the molecules.[32] Several research groups have made efforts to achieve this cofacial arrangement for pentacene[26] and tetrathiafulvalene (TTF)[33] derivatives and promising results were reported. Nevertheless, it has never been proved incontrovertible that cofacial arrangement is superior to “herringbone” order. One reason might be that nearly all cofacially ordered

molecules have a longitudinal or transverse shift along the stack due to the electrostatic repulsion, which reaches its maximum by a direct stacking of the π-systems. Such shifts have again a negative impact on the electronic intermolecular couplings leading to inferior charge carrier mobilities.

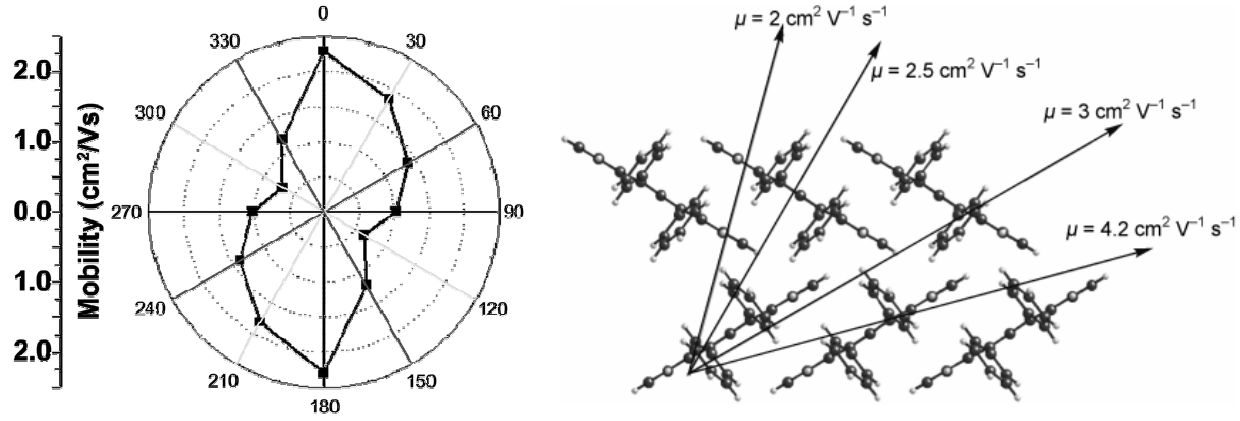

Figure 8. Polar plot illustrating the mobility anisotropy in a single-crystal pentacene FET (left) reproduced from ref [18a] with permission from the American Chemical Society, and mobility in a single crystal of rubrene as a function of source-drain electrode orientation (right) reproduced from ref [34] with permission from Wiley-VCH Verlag GmbH & Co. KGaA.

2.6 p-Type Organic Semiconductors

A selection of established organic p-type semiconductors is depicted in Figure 9. Pentacene (**1**), the famous member of the acene family, is maybe the most important organic p-type semiconductor material and already functions as a standard against which most new compounds are compared. Thin-film devices based on pentacene exhibit mobilities up to 3 cm^2/Vs,[35] while single crystal transistors reached mobilities up to 35 cm^2/Vs.[20a] The higher homologues of the acenes, e.g. hexacene are too susceptible to degradation (by oxygen and light), while the lower homologues (anthracene, tetracene) show lower mobilities compared to that of pentacene due to their less extended π-systems.

To overcome the disadvantages of the “herringbone” packing of pentacene (Figure 10), i.e. the oxygen and light sensitivity and the low solubility, functionalized acene derivatives (Figure 9, anthradithiophene **2**) have been developed. More detailed information about the performances and special abilities of acenes and their derivatives are given in Chapter 2.8.[34]

Rubrene (**3**) and diphenylanthracene (**4**) are structurally closely related to the unsubstituted acene derivatives. It is noteworthy that rubrene single crystal transistors

show very high mobilities up to 20 cm^2/Vs,[31] whereas no satisfactory results were reported for vacuum deposited thin-film devices, which might be attributed to inappropriate deposition mechanisms. Diphenylanthracene (**4**) single crystals exhibit hole carrier mobilities (3.7 cm^2/Vs) as well as electron carrier mobilities (13 cm^2/Vs) making this material a potential candidate for ambipolar applications.[36] Combination of the anthracene core with substituted thiophenes in compound **5** leads likewise to charge carrier mobilities in OTFTs of more than 0.5 cm^2/Vs.[37]

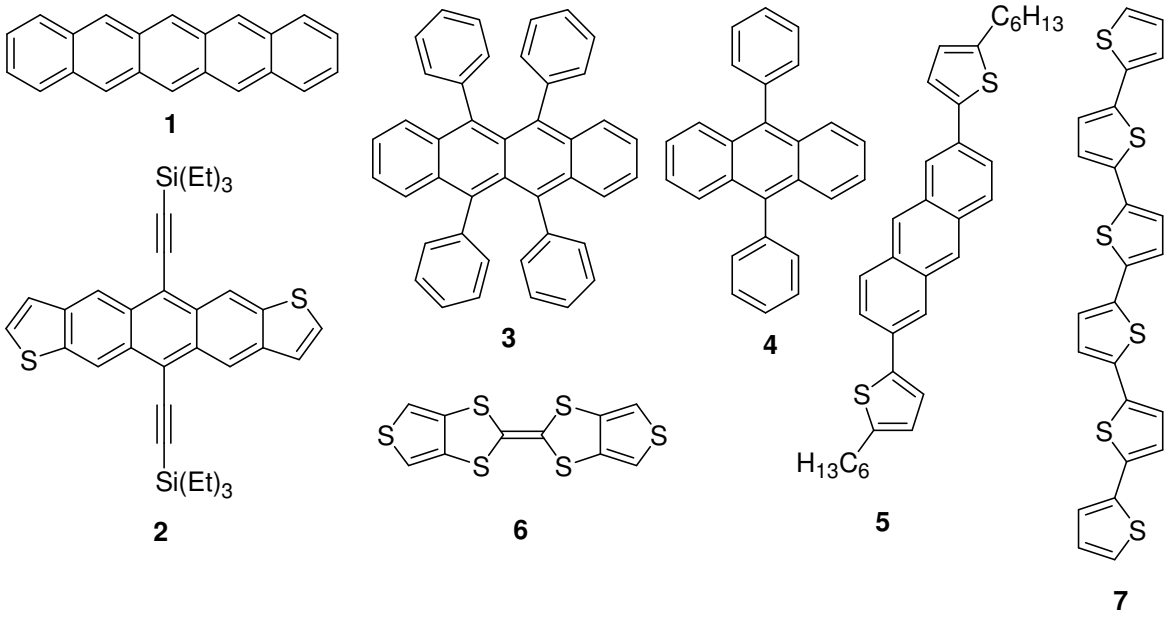

Figure 9. Chemical structures of a selection of (crystalline) organic p-type semiconductors.

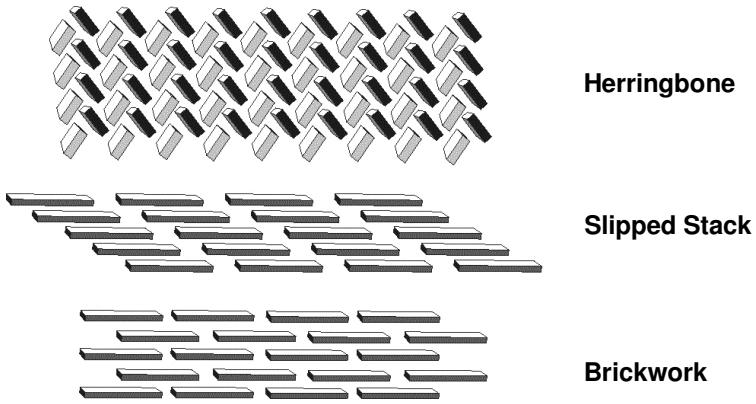

Figure 10. Packing motifs found for acene derivatives according to single X-ray analysis.

Tetrathiofulvalenes were mainly used as donors in highly conducting charge transfer salts. In recent years, the charge carrier mobilities of the pure compounds were investigated for the thin-film and single crystal transistors. For dithio-

phene-tetrathiafulvalene (DT-TTF, **6**) mobilities up to 1.4 cm^2/Vs were found for the single crystal device.[38]

(Oligo)thiophenes have attracted much scientific attention as they can be tuned over a wide range including highly crystalline derivatives and liquid crystalline polymers. Smaller molecules and oligomers, e.g. sexithiophene **7**,[39] have been investigated quite early in many applications but mobilities stayed rather low. Better results were obtained with regioregular *n*-hexyl substituted polymers (P3HT (**8**), Figure 11),[13a] reaching mobilities up to 0.1 cm^2/Vs. Recently, even higher values up to 0.7 cm^2/Vs have been reported for liquid crystalline thiophene polymers **9**.[40] The good performance of the polymers can be explained in terms of well-organized lamellae structure. Another advantage of thiophenes is that this class of compounds can easily be derivatized with electron-withdrawing groups like perfluorinated alkyl substituents, leading also to high performance n-type materials (**13** and **14**, see below 13).

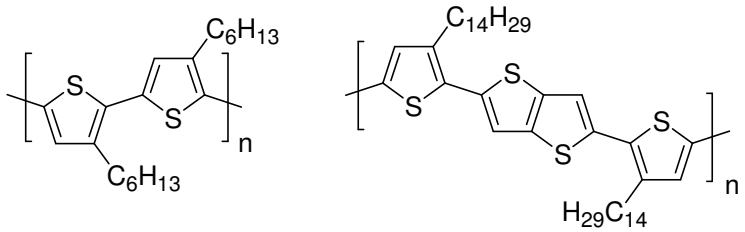

8 **9**

Figure 11. Chemical structures of high mobility p-type semiconducting polymers.

Besides polymers and crystalline materials, some liquid crystalline materials (hexabenzocoronene **10**, Figure 12)[41] showed high hole mobilities up to 0.5 cm^2/Vs in the liquid crystalline phase. Also triphenylene derivatives (e.g. **11**)[42] were intensively studied, but exhibited lower mobility due to their smaller and probably more mobile π–systems in the LC phase. In general such discotic liquid crystalline phases are achieved by surrounding discoid π–systems with long alkyl chains in the periphery. The self-assembly of these molecules in the liquid crystalline phases is advantageous, while the one-dimensional π-stacking in columns limits charge transport to only one dimension, which undermines the potential for applications without a precise alignment of the columns in the device. For other molecules with elongated shape, e.g. thiophene derivative **12**[43] two-dimensional smectic LC phases were found which, however, showed only minor mobilities (0.1 cm^2/Vs) due to the higher disorder in this phase.

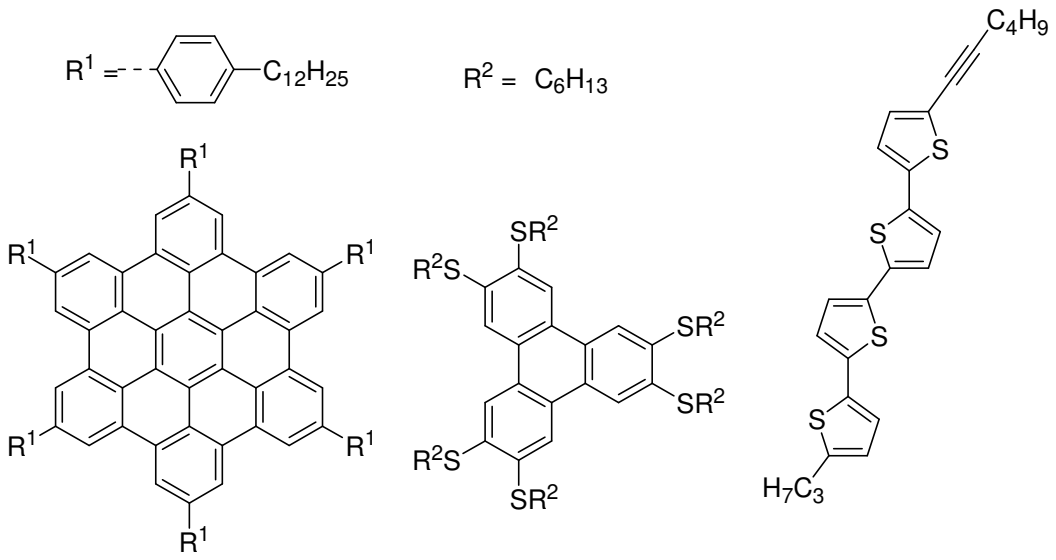

Figure 12. Chemical structures of liquid crystalline p-type semiconductors.

2.7 n-Type Organic Semiconductors

Until the end of the last century n-type organic semiconductors got less attention by the scientific community and the performance of their devices lagged behind the typical p-type materials. But within the last couple of years a larger number of organic n-type substances, whose electron charge carrier mobilities are already surpassing those of some common organic p-type or inorganic semiconductors like amorphous silicon, has been reported. These electron-poor semiconductors are obtained by the attachment of electron-withdrawing groups at formerly electron-rich aromatic π–cores. Typical withdrawing groups are carboxylic acids and imides, halogens, cyano substituents, or even perfluorinated alkyl and aryl substituents at the periphery of the molecule.

Very high electron mobilities were reported for different oligothiophenes **13**, **14** (0.50 and 0.60 cm^2/Vs, respectively)[44] and thiazoles **15**, **16** (1.83 and 0.30 cm^2/Vs, respectively)[45] with perfluorinated substituents (Figure 13). Obviously even the small trifluoromethyl substituent can be sufficient to achieve n-type semiconducting compounds. Interestingly, the core-fluorination of initially electron-rich copper phthalocyanine (**17**)[46] leads to n-type material displaying mobilities up to 0.03 cm^2/Vs, and the extensively studied p-type semiconductor pentacene shows electron mobilities up to 0.11 cm^2/Vs as a perfluorinated species **18**.[47] C_{60}-Fullerene (**19**) and its derivatives are among the few examples of n-type organic semiconductors without any elec-

tron-withdrawing groups and exhibit mobilities greater than 0.5 cm^2/Vs.[48] In special modified transistors values even up to 4.9 cm^2/Vs have been reported.[49] The charge carrier mobility of diindenoperylene (**20**) is not outstanding, but this compound possesses both n-type and p-type semiconductivity. Thus it is interesting for ambipolar applications.[50] Generally most of the devices based on above-mentioned compounds show good performances only under inert atmosphere or vacuum because oxygen and moisture can trap the electron charge carriers easily; therefore, their use in real applications is very limited. However, several rylene bisimides, e.g. derivatives **21** and **22**, are sufficiently air-stable making this class of organic semiconductors very promising for further investigation. These compounds will be discussed in detail in section 2.9 of this chapter.

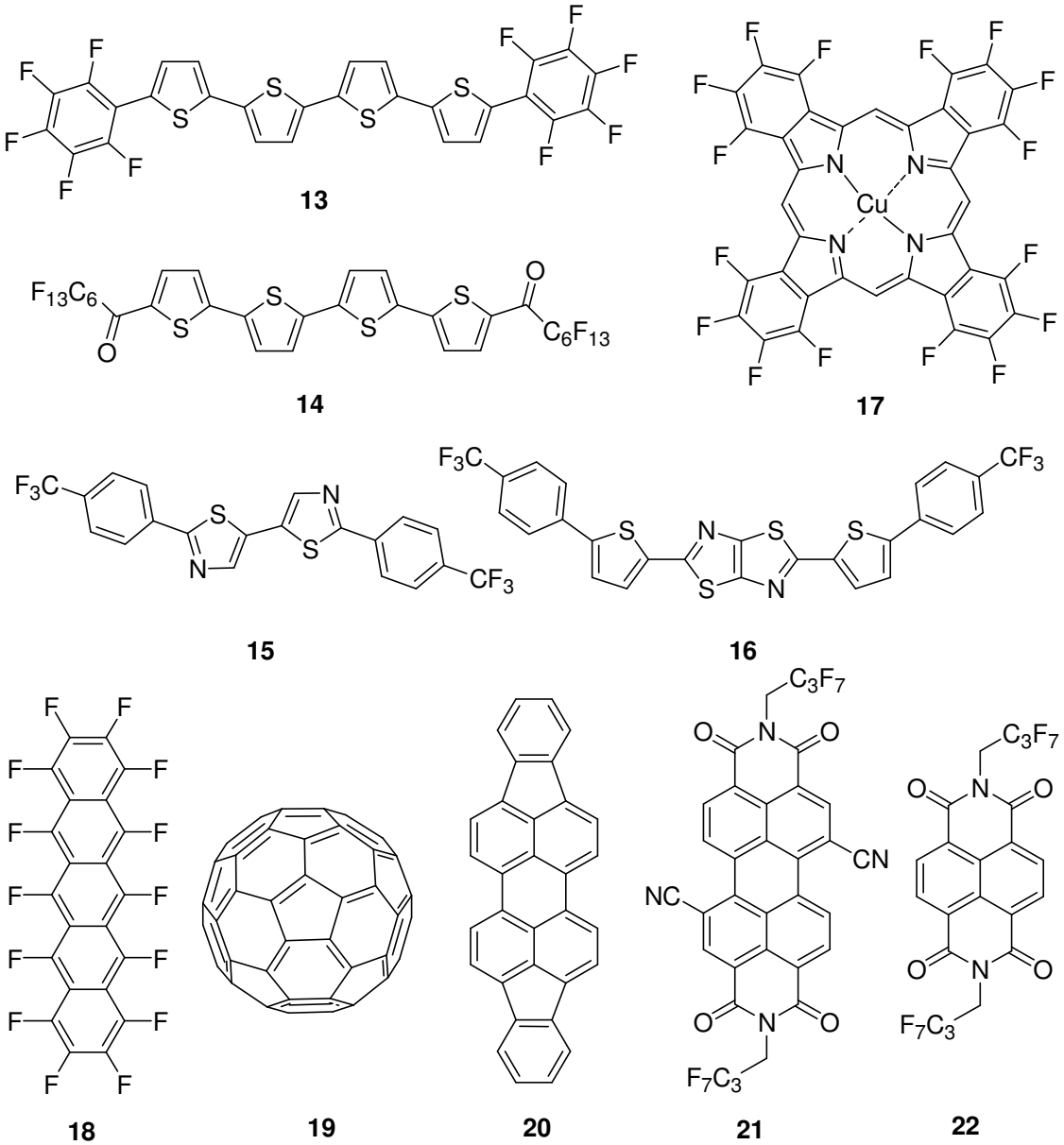

Figure 13. Chemical structures of different n-type organic semiconductors.

The chemical structures of the n-type semiconductors shown in Figure 13 reveal that fluorination is favorable for high performance organic n-type materials. The attachment of electron-withdrawing fluorine normally lowers the LUMO and the HOMO levels, facilitating the injection of electrons that converts originally p-type semiconductors such as oligothiophenes or even pentacene to n-type or ambipolar materials. The electronic attributes of molecules can be changed by the fluorine substituents. Thus, the unique properties of fluorinated hydrocarbons can be related to the special feature of this halogen atom, particularly, its electronegativity (Pauling scale EN = 4) that also leads to high polarization of the carbon-fluorine bond with strong bond energy (~450 kJ/mol).[51] This bond is 100 kJ/mol more stable than the carbon-chlorine bond and, therefore, can be seen as one of the reasons for the thermal and oxidative stability of fluorinated hydrocarbons. Some special properties of fluorinated organic compounds, in particular, the combined hydro- and lipophobicity are utilized for many industrial coatings.

The interactions between fluorine and hydrogen atoms of neighboring molecules are quite similar to conventional hydrogen bonding, but with lower energy. Fluorinated aromatic compounds have an inverted charge density distribution, which results in a positively charged center of fluorinated aromatic hydrocarbons in contrast to the corresponding halogen-free derivatives. This leads to strong interactions between fluorinated electron-poor aromatic rings and electron-rich non-fluorinated ones, e.g. benzene and hexafluorobenzene alone have a “herringbone” face-to-edge arrangement in the crystal (Figure 14, left), while a one to one mixture of them results in a face-to-face arranged complex (Figure 14, right) with a higher melting point.[52]

As molecules with larger partly fluorinated π-systems obey this rule as well highly ordered molecular stacking with efficient π-overlap may result in enhanced charge transport abilities for field effect transistor applications. This was already observed in the solid state of fluoroarene-thiophene oligomers.[44b]

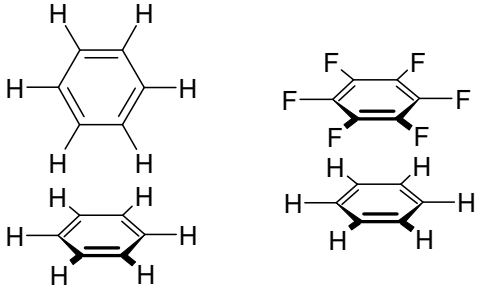

Figure 14. Single crystal arrangement of pure benzene and a 1/1 mixture with hexafluorobenzene.

2.8 Acenes and their derivatives in OTFTs

Although vacuum deposited thin films of pentacene show one of the highest p-type charge carrier mobilities, its physical and chemical attributes are not ideal for device fabrication. Its very pronounced insolubility makes the application of other deposition techniques nearly impossible and the “herringbone” packing in the solid state is not the best arrangement for charge transport. Since simple solution casting techniques are more attractive than vacuum deposition techniques for flexible electronic devices used in mass applications, in recent years efforts have been made to use soluble precursors **23**-**25** (Figure 15) of acenes in particular pentacene to facilitate solution deposition,[53] and indeed mobilities up to 0.89 cm^2/Vs were measured for such devices.[53b] However, the preparation of such soluble precursors is synthetic- cally challenging and a technically demanding annealing process is required to realize high-order thin films. Alternatively, semiconducting molecules may be structurally modified toward better solubility for spin-coating, to direct desirable supramolecular order in the solid state and to improve stability towards oxygen and light. Noteworthy that the attachment of bulky substituents at the central phenyl ring, the simplest variation for acenes, imparts many beneficial properties to acenes.

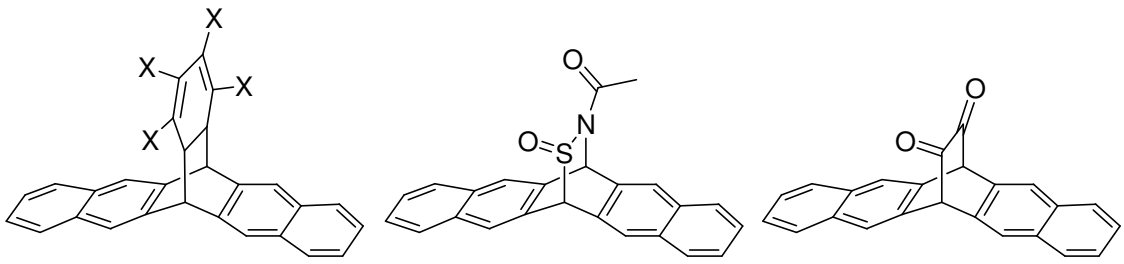

23 **24** **25**

Figure 15. Soluble precursors for the deposition of pentacene from solution.[53]

Based on this approach *Anthony* and co-workers developed some promising acene derivatives bearing two trialkylsilylethynyl groups at the central ring from anthracene **26** up to heptacene **30** (Figure 16).[26,54] Initially, they focused on the pentacene **28** and anthradithiophene **2** derivatives and later on the higher and lower homologues were synthesized for the evaluation of their electronic properties and complementing the ascending series.

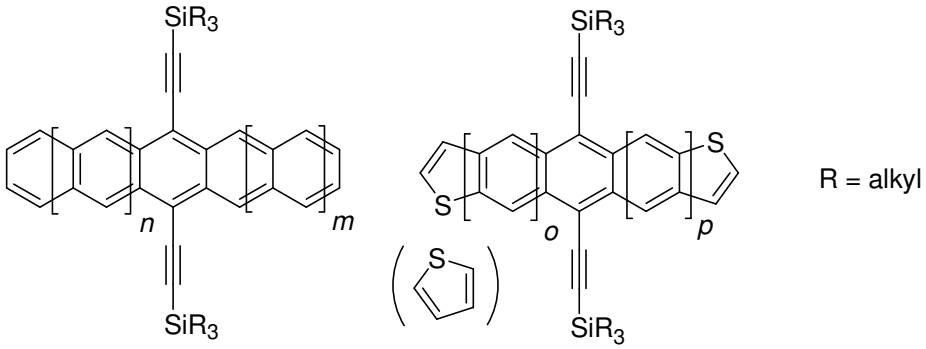

26: $n = 0$, $m = 0$
27: $n = 0$, $m = 1$
28: $n = 1$, $m = 1$
29: $n = 2$, $m = 1$
30: $n = 2$, $m = 2$

2: $o = 1$, $p = 1$
31: $o = 1$, $p = 2$
32: $o = 2$, $p = 2$

Figure 16. Series of acene derivatives synthesized by *Anthony* et al.[26,54]

These bis-silylethynylated acenes, especially the four- and five-ring derivatives **27**, **28**, and **2**, exhibit several remarkable features compared to the respective parent polycyclic aromatic hydrocarbons. Bis-silylethynylation of acenes lowers their propensity towards cycloaddition, increases the solubility, and affects the molecular packing in the solid state. Thus, the series of bis-triisopropylsilylethynylated acene derivatives allows to derive relationships between molecular properties like oxidation/reduction potential, chemical and photochemical stability, absorption wavelength (corresponding to band gap), and material properties like molecular arrangement in the solid state and charge carrier mobility in the OFETs. The performance of these derivatives did not outbalance vacuum deposited OFETs based on unsubstituted pentacene (0.40 cm^2/Vs for a vacuum deposited triisopropylsilyl substituted pentacene **27**),[54a] but the high solubility enabled the devices fabrication by spin-coating of **2** from solution to give transistors with mobilities up to 1.00 cm^2/Vs.[55] For OFETs prepared by spin-coating techniques, this value is surprisingly high as a well-ordered highly crystalline thin layer is difficult to obtain from solution.

The improved stability of the diisopropylsilyl pentacene is demonstrated by its 50-times slower degradation in air-saturated tetrahydrofuran solution compared to the unsubstituted compound.[56] In the dark, even oxygen saturated solutions did not lead to considerable decomposition after 24 hours. This is, indeed, a highly promising feature for solution processing of organic semiconductors by spin-coating techniques. The higher stability achieved by proper substitution is not limited to the pentacene derivative. For higher bis-silylethynylated homologues the synthesis and characterization became only possible due to this stabilizing effect of the substituents.

The electronic features of higher acenes and polyacenes have been the subject of many theoretical studies and controversial discussions.[57] Early computations at the B3LYP/6-31G* level indicated a triplet ground state for oligoacenes higher than hexacene.[57c] In a later reinvestigation it has been shown, however, that the singlet wave function constructed from restricted Kohn-Sham orbitals possesses a triplet instability, and should be discarded in favor of a UB3LYP description.[57b] At this level of theory, higher polyacenes have a finite HOMO-LUMO gap and a singlet ground state with significant multiconfigurational character. Although the functionalized heptacene derivatives do not match perfectly with the electronic structure of the parent unsubstituted acene, their synthesis allowed a detailed examination of related acene structure. Neither ^{1}H NMR nor EPR spectroscopy provided evidence for a triplet diradical ground state.[58] Furthermore, the correlation of the HOMO-LUMO energy gap (Figure 17, here approximated from the absorption maxima of the most bathochromic optical transition) versus the inverse number of annulated aromatic rings shows a perfectly linear behavior for the whole available series of bis-silylethynylated acenes and allows extrapolation to an energy gap for the infinite polyacene chain of 0.35 eV (corresponding to an absorption wavelength of 3500 nm), which substantiates the computationally predicted small, but existent nonzero band gap for polyacenes.[57c, 59]

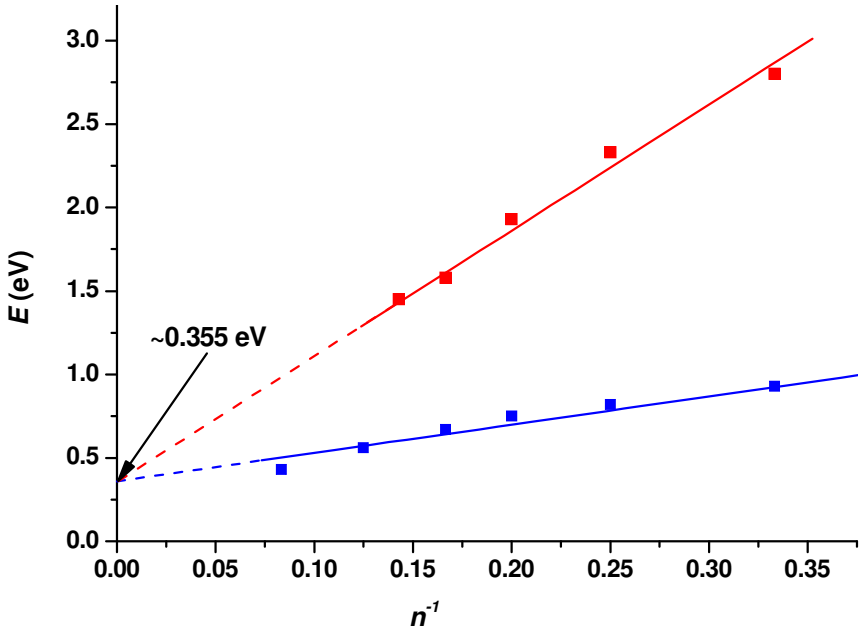

Figure 17. Correlation of electronic band gap versus the inverse number of annulated rings (n^{-1}) for *Anthony´s* series of bis-silylethynylated acenes (red) and for *Osuka´s* series of annulated porphyrins (blue).[59]

Whilst this value is still rather unreliable due to an extrapolation of about 1 eV from the last experimental value for the heptacene derivative, for annulated porphyrins *Osuka* and co-workers[60] have recently observed absorption maxima (about 2900 nm) that are close to the value predicted for the infinite polyacene chain of bis-silylethynylated acenes. In this case, the extrapolation of the HOMO-LUMO gap shows exactly the same energy gap (0.36 eV) for infinite annulated porphyrins (Figure 17).

Most interesting from the application point of view is the novel homologous series of bis-silylethynylated dithienoacenes (Figure 16). Advantages of these compounds are the extension of the conjugated system by two thiophene rings which leads to more stable radical cations and possible electronic coupling by sulfur-sulfur interactions in the solid state in addition to π-π overlap. Thus, dithienoanthracene **2** (Figure 16, R = ethyl) shows a significantly higher charge carrier mobility (1 cm^2/Vs) than the corresponding pentacene derivative **28** (Figure 16, R = ethyl), despite a higher ionization energy and a larger HOMO-LUMO gap.

Besides the above-mentioned interesting molecular properties of functionalized acenes in solution, even more fascinating attributes are found for the solid state materials. The first outstanding feature is given by the unique molecular arrangement in the solid state, the second by the high charge carrier mobilities in spin-coated OFETs, fabricated by Jackson's group.[26,54a,58]

According to *Desiraju* and *Gavezzotti* the packing of unsubstituted polycyclic aromatic hydrocarbons is governed by a delicate balance of π–π stacking and C–H–π interactions.[61] Based on a detailed analysis of 32 representative crystal structures all four classes of observed packing motifs could be related to the size, shape, and C/H ratio of the respective molecules. All parent acenes fall into the class of "herringbone" structures owing to the dominance of "glide"-promoting C-H-π contacts versus "stack"-promoting aromatic surface (Figure 10, top). Although high charge carrier mobilities are observed for such herringbone-packed pentacenes, chemical intuition would suggest better prospects for acenes with direct π–π overlap. Such arrangements are now indeed observed for many silylethynylated pentacenes and dithienoacenes that exhibit 1-D slipped-stack e.g. dithienoanthracene **2**, (Figure 16, R = isopropyl) or 2-D "brickwork" arrangement e.g. pentacene **28**, (Figure 16, R = isopropyl).[26,54,55,58] These arrangements assure a close distance of about 3.5 Å between the molecules with a high contact area between their π–faces (up to 7.7 $Å^2$ for "brickwork" ar-

rangement). However, only the 2-D brickwork packing provides charge carrier mobility in two different directions as demanded for successful implementation in devices without alignment layers.

Next to these *peri*-functionalized acene derivatives some other synthetical approaches have been undertaken. By inducing a dipole a brickstone like arrangement can also be observed in the solid state of **33** (Figure 18).[62] Although an "ideal" packing was observed, the charge carrier mobility was low (0.05 cm^2/Vs). But this can also be explained by the electron-withdrawing character of the quinone group leading to a less electron-rich molecule.

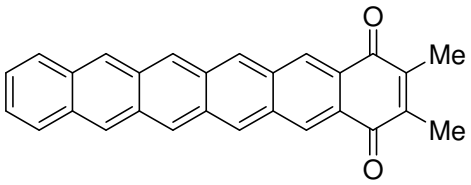

33

Figure 18. Hexacenequinone as an example for an acene-like derivative with a dipole.

(Hetero)acenes with alkyl chains at the periphery, e.g. **34** and **35**, were investigated since 1998 and showed mobilities up to 0.3 cm^2/Vs (Figure 19).[63] This molecular design indeed improved the solubility, but does not affect the sensibility toward oxygen in a positive way (e.g. preventing of cycloaddition by sterical demanding substituents etc.) Therefore this approach seems to be less attracitve compared to *peri*-substituted acenes.

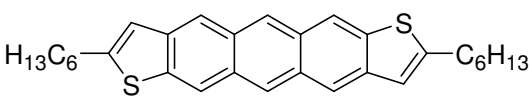

34

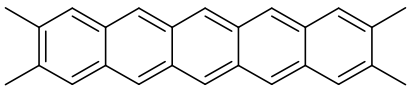

35

Figure 19. Alkyl-substituted acene derivatives.

2.9 Perylene and naphthalene bisimide derivatives in OTFTs

The industrial application of perylene tetracarboxylic acid bisimides (PBIs) started already in the 1950ies as pigment dyes in coatings due to their insolubility, excellent chemical stability, high extinction coefficients and other favorable properties. New fields of application were found during the last decades when many research groups started searching for novel potential n-type semiconductors and the first PBIs and

naphthalene tetracarboxylic acid bisimides (NBIs) were tested in OTFTs.[64] The initially quite low mobilities of the first devices, e.g. **40**, (Figure 20) was overcome by other PBI derivatives[65] and employing better preparation techniques. In 2006 one of the highest measured value was reported (**39**, 2.10 cm^2/Vs)[65g] for n-type semiconductors. The n-type semiconductivity and therewith the high electron affinity can be attributed to the strong electron-withdrawing imide groups in the molecular structure (Figure 21). Although an impressive number of PBIs with different imide and bay substituents has been reported,[66] examples for in TFTs successfully tested PBI derivatives are still quite limited.

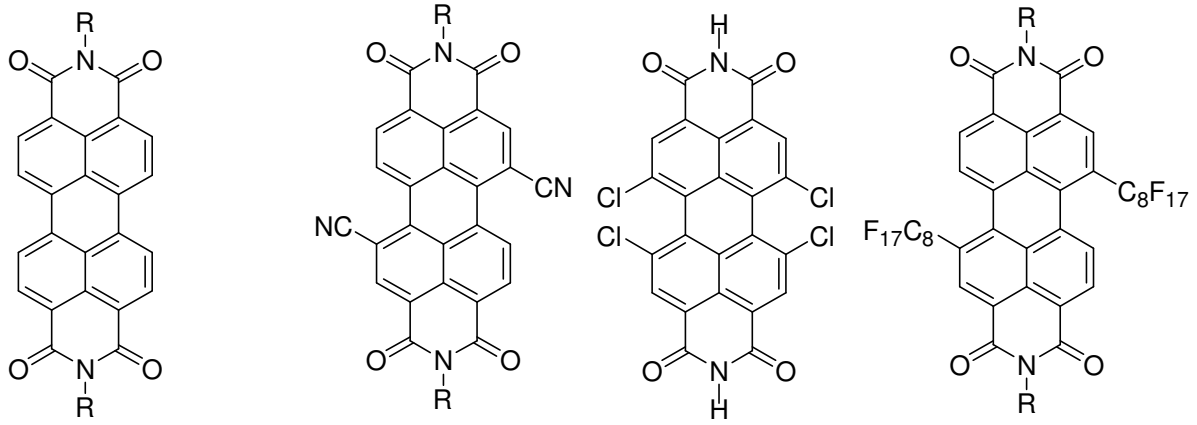

36: R = C_5H_{11}
37: R = C_8H_{17}
38: R = $C_{12}H_{25}$
39: R = $C_{13}H_{27}$
40: R = phenyl
41: R = perfluorophenyl
42: R = 2-phenylethyl

43: R = CH_2CF_3
44: R = $CH_2C_3F_7$
45: R = $CH_2C_7F_{15}$
46: R = C_8H_{17}
47: R = cyclohexyl
48: R = perfluorobenzyl
49: R = 4-trifluormethylphenyl

50

51: R = $CH_2C_3F_7$
52: R = C_4H_9

Figure 20. Structures of perylene bisimide dyes that were investigated as vacuum deposited n-type semiconductors in OTFTs.

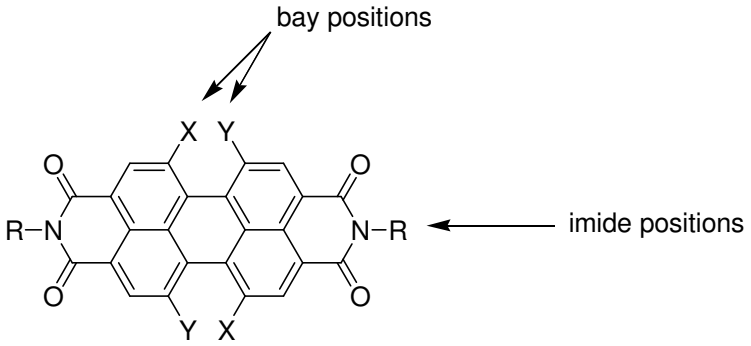

Figure 21. Synthetically easy available positions to “tune” the electronic properties of PBIs.

As revealed by theoretical calculations, the electronic properties of the imide substituents have very little effect on the absorption and emission properties of the PBIs

since LUMO and HOMO orbitals have a knot at the imide position (Figure 22, based on AM1 calculations).[67] This means that the relative position of the frontier orbitals (revealed by cyclic voltammetry), and not the band gap itself, are changed, making the color of the dyes independent of the potential electron-donating or -withdrawing abilities of the imide substituents. This attribute can be used for tuning the redox potentials of PBIs without influencing the optical properties by choosing the appropriate imide groups.

The first single crystal studies of in bay position unsubstituted PBIs were already published more than 25 years ago and it was found that the imide substituents have no influence on the structural parameters (bond lengths and angles) of the perylene core.[68] Moreover, the π-systems of the PBIs were, as expected, nearly perfectly planar and the two individual naphthalene subunits were found to be linked by $C(sp^2)$–$C(sp^2)$ single bonds with an average length of about 1.46 Å.

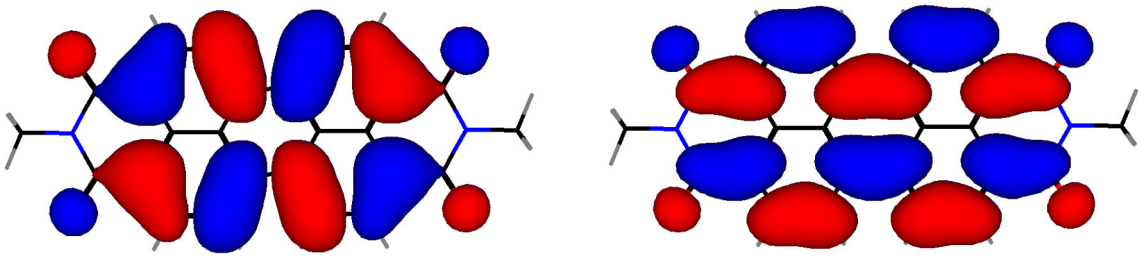

Figure 22. HOMO (left) and LUMO (right) of PBIs based on AM1 calculations.

By contrast, bay substituents have strong effects on the structural and (opto)electronical properties of PBIs. Depending on the size of the bay substituents (halogens, aryl(oxy), amines, etc.) the flat π-system is distorted and torsion angles up to 37° (for a tetrachlorinated PBI) have been found for several di- and tetrasubstituted PBIs.[69] This twist apparently hinders an adequate overlap between the aromatic systems of neighboring molecules and might be an explanation for the fact that nearly all so far reported crystalline PBI derivatives with a good performance in an OTFT possess a quite planar π–system (Figure 20, Table 1). Notably, also the dicyano PBIs **43**-**49** have a flat aromatic core. Electron-withdrawing bay substituents such as halogen or cyano seem to improve of n-type semiconducting abilities of dyes since these substituents increase the electron affinity.

Table 1: Charge carrier mobilities of crystalline PBIs measured in TFTs prepared by vacuum deposition, derivatives **43**, **48**, and **49** are not listed due to very low performance.[65j]

Year of publication	compound	Charge carrier mobility (cm^2/Vs)	
		glove box	air
2008[65j]	**45**	n.a.	0.05
2008[70]	**51**	n.a.	0.03
2008[70]	**52**	0.05	0.05
2007[65d]	**50**	0.18	0.04
2007[65d]	**42**	0.11	0.09
2007[65i]	**41**	0.06	0.04
2006[65g]	**39**	2.10	instable
2006[65f]	**46**	0.14	0.14
2005[65h]	**39**	0.60	instable
2004[65c]	**44**	0.64	0.64
2004[65e]	**38**	0.20	instable
2004[65c]	**47**	0.10	0.10
2004[65e]	**36**	0.10	instable
2002[65b,e]	**37**	0.60	instable
1996[64a]	**40**	2×10^{-5}	instable

A closer look at the already published PBI charge carrier mobilities (Table 1) reveals that since 2004 the main focus laid on the preparation of air stable devices, which are essential for potential everyday applications. Nevertheless, the obtained charge carrier mobilities of air-stable devices (**44**, 0.64 cm^2/Vs) stayed significantly below the highest values (**39**, 2.10 cm^2/Vs) achieved for sensitive building blocks. Since 2004 no real improvements for air-stable TFTs based on PBIs were reported. The latest synthetic approach led to PBIs with two perfluorinated alkyl chains in bay positions (**51** and **52**, Figure 20), showing air stable charge carrier transport. Due to the high twisting of the perylene core the packing was not very dense and the mobilities were rather low.[70]

In general, the comparison of the reported charge carrier mobilities under ambient conditions is difficult. Details about the exact experimental conditions are rarely given in literature, though the length of the exposition and the storage of the devices are very important for a serious scientific interpretation. Furthermore, controversial explanations are found for the air-stability of PBI derivatives. *Marks* and co-workers concluded, that either a sufficient high reduction potential (including an overpotential to the reaction of charge carriers and oxygen) or closed packed perfluorinated alkyl chains will lead to a stable performance of the device under exposure to air.[71] On the other hand, *Klauk* and coworkers tested different “air-stable” PBI derivatives over 500 days and

could not confirm these conclusions.[65j] An exponential decrease of the performance of the devices was observed, independent of the solid state arrangement of the dyes.

Besides the vaporable small PBI derivatives, charge carrier mobilities of crystalline[69a] and liquid crystalline[72] PBI dyes **53**-**60** have also been published (Figure 23, Table 2 and Table 3). Pulse-radiolysis time-resolved microwave conductivity (PR-TRMS) or time of flight (TOF) setups were used for the mobility measurement of these derivatives. As mentioned before, PR-TRMC values have to be considered as the possible maximum charge carrier mobilities, since only the transport in a very small domain of the active organic layer is tested. The obtained mobilities can therefore not be compared with the potential performance in a thin film transistor setup. Furthermore, even in the higher ordered crystalline phase the mobilities stayed beyond the best values achieved for PBIs in OTFTs.

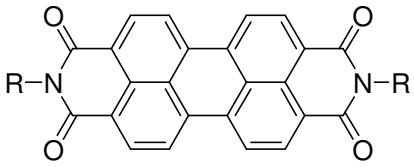

53: R = tridodecyloxyphenyl
54: R = tridodecylphenyl
55: R = $C_{12}H_{25}$
56: R = $C_{18}H_{37}$

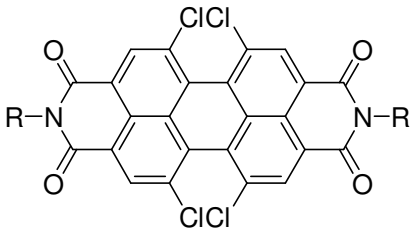

57: R = tridodecyloxyphenyl
58: R = 2-diisopropylphenyl
59: R = 4-dodecylphenyl
60: R = $C_{12}H_{25}$

Figure 23. Structures of selected (liquid) crystalline perylene bisimide dyes with charge carrier mobilities measured by PR-TRMC technique.

Table 2: Charge carrier mobilities of selected liquid crystalline PBIs obtained by PR-TRMC measurements.

Year of publication	compound	Charge carrier mobility (cm^2/Vs)	
		Crystalline phase	LC phase
2007[72b]	**54**	0.05	0.003
2005[72a]	**57**	0.08	0.02
2000[72a]	**53**	0.01	0.02
2000[65a]	**56**	0.21	0.11

Table 3: Charge carrier mobilities of selected crystalline PBIs obtained by PR-TRMC measurements.

Year of publication	compound	Charge carrier mobility (cm^2/Vs)
2004[69a]	**58**	0.01
2004[69a]	**60**	0.14
2004[69a]	**59**	0.05
2004[69a]	**55**	0.04

Independent on the (liquid) crystallinity of organic semiconductors, the packing of the π–systems has probably the largest impact on the performance of the device. Unfortunately, the solid state arrangement of PBIs tested in OTFTs has seldom been clarified (Figure 24, right).[65c] Even so, more than 20 structures[68,73] of unsubstituted PBIs were reported, allowing a closer look at their packing behavior in the crystal. The studies on the solid state packing of these quite insoluble pigments were originally made for the investigation of their crystallochromy. Though the absorption spectra of these similar PBI dyes in solution are identical, the colors of the crystals range from red to maroon to red-violet and even to black. *Graser* and *Hädicke* established empirically the relationship between overlap of the π-systems in the stacks (along with the transverse and longitudinal shifts) and color of the solid state. Only in a much defined area of shifts (see “black crystal“, Figure 24) the interactions of the π–systems in the crystals lead to a black color of the solid state absorption spectra.

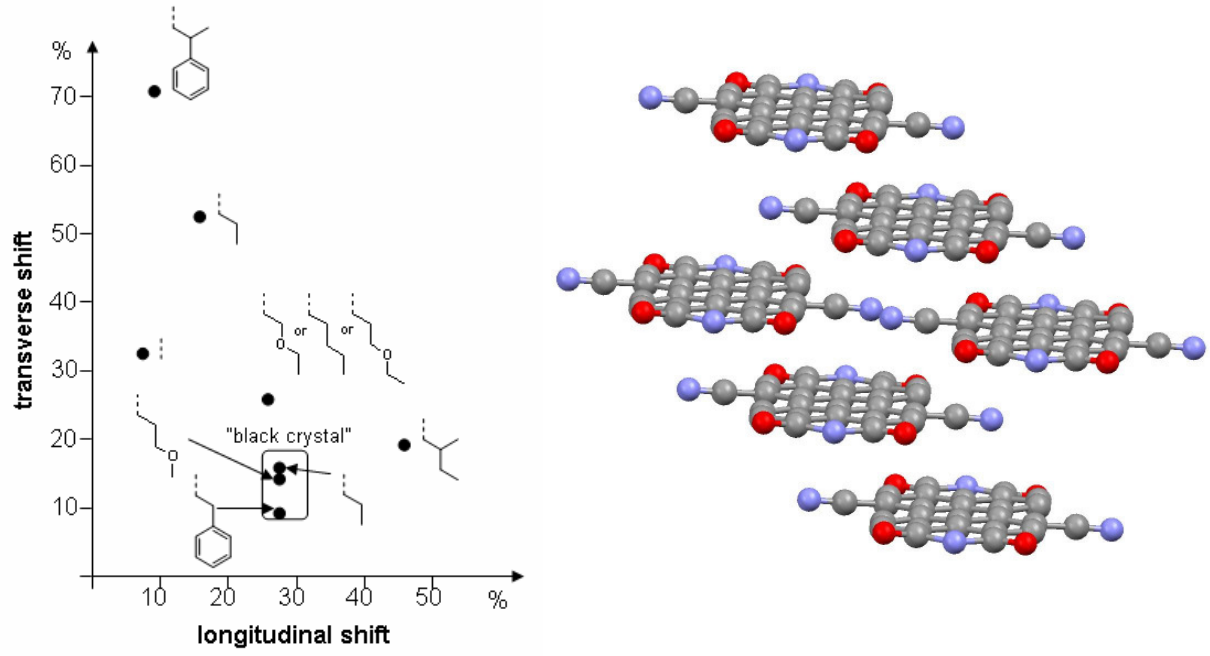

Figure 24. Transverse and longitudinal shifts of the π–sytems of PBIs in the crystal stacks with different substituents in the imide position (left);[68b] crystal structure (made of the corresponding cif file) of the dicyano PBI (right) with the highest mobility in air-stable OTFT (imide substituents omitted for clarity).[65c]

Even in some single crystals (e.g propyl substituent, Figure 24) of one compound, stacks with different overlap (27% and 53%) have been observed leading to a “mixture” of different colors. The color change to black is potentially important for application in organic solar cells, as the absorption of these dyes can be extended over the whole visible spectrum.[74] The ideal overlap of the π-systems for maximal charge carrier

mobility in OTFTs is actually not known, but the above-mentioned study on the impact of different imide substituents on the packing reveals that the prediction of packing properties is rather difficult. An intelligent “crystal engineering”, which would make many synthetical efforts redundant, seems to lie far ahead. Indeed *Graser* and *Hädicke* recapitulated at the end of their studies that a reliable prediction of crystal packing only by examining the structure of a single molecule is nearly impossible.

Besides PBIs, naphthalene biimides **61**-**65** (Figure 25, Table 4) were also tested for their charge carrier mobilities. Although their overall performance could not yet reach the mobilities of the best perylene derivatives, these compounds have some quite promising attributes as well. Due to their wider band gap (~3.0 eV) they do not have a significant visible absorption and are suitable for transparent organic optoelectronics.[75] Furthermore, NBIs with perfluorinated alkyl chains (**62** and **63**, Figure 25) were the first published air-stable rylene derivatives in OFETs.[76] However the perfluorinated octyl group resulted in a lowered mobility compared to that of the parent fluorine-free hydrocarbon (Table 4).

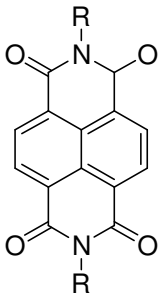

61: R = H
62: R = $CH_2C_3F_7$
63: R = $CH_2C_7F_{15}$
64: R = C_8H_{17}

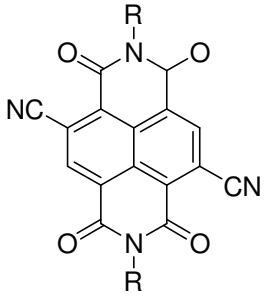

65: R = C_8H_{17}

Figure 25. Structures of the most important naphthalene bisimides dyes used as vacuum deposited n-type semiconductors in OTFTs.

Table 4: Charge carrier mobilities of some crystalline NBIs obtained from TFTs prepared by vacuum deposition.

Year of publication	compound	Charge carrier mobility	
		glove box	air
2007[75]	**65**	0.15 cm^2/Vs	0.11 cm^2/Vs
2000[76]	**64**	0.16 cm^2/Vs	instable
2000[76]	**63**	0.05 cm^2/Vs	0.05 cm^2/Vs
2000[76]	**62**	0.01 cm^2/Vs	0.01 cm^2/Vs
1996[64b]	**61**	10^{-4} cm^2/Vs	~10^{-6} cm^2/Vs

The recent outstanding synthetic achievement for NBIs was realized by the successful preparation of a cyanated derivative **65**.[75] However, the mobilities were quite similar to corresponding PBIs leading to an air-stable fluorine-free compound.

2.10 Concluding Remarks

In this chapter the current state of development for organic semiconductors, especially small molecules for vacuum deposition or spin-coating techniques has been presented. While high performance p-type semiconductors lack sufficient solubility, the operational performance and device stability of n-type systems lag behind their counterparts. The examples discussed here demonstrate the need of new organic semiconductors for practical applications without having the above-mentioned drawbacks.

2.11 References and Notes

[1] J. E. Lilienfeld, US Patent 1 745 175, **1930**.

[2] D. Kahng, US Patent 3 102 230, **1963**.

[3] P. K. Weimer, *Proc. IRE* **1962**, *50*, 1462-1469.

[4] (a) D. F. Barbe, C. R. Westgate, *J. Phys. Chem. Solids* **1970**, *31*, 2679-2687; (b) F. Ebisawa, T. Kurokawa, T. Ando, *J. Appl. Phys.* **1983**, *54*, 3255-3259.

[5] C. W. Tang, *Appl. Phys. Lett.* **1986**, *48*, 183-185.

[6] (a) A. Tsumura, K. Koezuka, T. Ando, *Appl. Phys. Lett.* **1986**, *49*, 1210-1212; (b) A. Tsumura, K. Koezuka, T. Ando, *Synth. Metals* **1988**, *25*, 11-23; (c) J. H. Burroughes, C. A. Jones, R. H. Friend, *Nature* **1988**, *335*, 137-141.

[7] (a) G. Horowitz, D. Fichou, X. Z. Peng, Z. G. Xu, F. Garnier, *Solid State Commun.* **1989**, *72*, 381-384; (b) G. Horowitz, X. Z. Peng, D. Fichou, F. Garnier, *J. Appl. Phys.* **1990**, *67*, 528-532.

[8] For a recent review on OLEDs, see: B. Geffroy, P. le Roy, C. Prat, *Polym. Int.* **2006**, *55*, 572-582.

[9] Y. Y. Lin, D. J. Gundlach, S. F. Nelson, T. N. Jackson, *IEEE Electron. Device Lett.* **1997**, *18*, 606-608.

[10] (a) P. F. Baude, D. A. Ender, M. A. Haase, T. W. Kelley, D. V. Muyres, S.D. Theiss, *Appl. Phys. Lett.* **2003**, *82*, 3964-3966; (b) D. J. Gundlach, *Nat. Mater.* **2007**, *6*, 173-174; (c) Y. Watanabe, K. Kudo, *Appl. Phys. Lett.* **2005**, *87*, 223505; (d) A. Dodabalapur, *Mater. Today* **2006**, *9*, 24-39.

[11] (a) M. M. Ling, Z. Bao, *Chem. Mater.* **2004**, *16*, 4824-4840; (b) H. Klauk, *Nat. Mater.* **2007**, *6*, 397-398.

[12] (a) Y. Noguchi, T. Sekitani, T. Someya, *Appl. Phys. Lett.* **2006**, *89*, 253507; (b) B. K. Crone, A. Dodabalapur, R. Sarpeshkar, A. Gelperin, H. E. Katz, Z. Bao, *J. Appl. Phys.* **2002**, *91*, 10140-10146.

[13] (a) H. Sirringhaus, N. Tessler, R. H. Friend, *Science* **1998**, *280*, 1741-1744; (b) C. D. Sheraw, L. Zhou, J. R. Huang, D. J. Gundlach, T. N. Jackson, M. G. Kane, I. G. Hill, M. S. Hammond, J. Campi, B. K. Greening, J. Francl, J. West, *Appl. Phys. Lett.* **2002**, *80*, 1088-1090.

[14] R. C. G. Naber, B. de Boer, P. W. M. Blom, D. M. de Leeuw, *Appl. Phys. Lett.* **2005**, *87*, 203509.

[15] (a) K. J. Lee, M. J. Motala, M. A. Meitl, W. R. Childs, E. Menard, A. K. Shim, J. A. Rogers, R. G. Nuzzo, *Adv. Mater.* **2005**, *17*, 2332-2336; (b) L. Zhou, A. Wanga, S.-C. Wu, J. Sun, S. Park, T. N. Jackson, *Appl. Phys. Lett.* **2006**, *88*, 083502; (c) D. Voss, *Nature* **2000**, *407*, 442-444; (d) F. Würthner, *Angew. Chem.* **2001**, *113*, 1069-1071; *Angew. Chem. Int. Ed.* **2001**, *40*, 1037-1039; (e) S. R. Forrest, *Nature* **2004**, *428*, 911-918.

[16] *Organic Electronics* (Ed. H. Klauk), Wiley-VCH, Weinheim, Germany, **2006**.

[17] For more details about organic electronics, see: (a) *Physics of Organic Semiconductors* (Ed. W. Brütting), Wiley-VCH, Weinheim, Germany, **2005**; (b) *Organic Molecular Solids* (Eds. M. Schwoerer, H. C. Wolf), Wiley-VCH, Weinheim, Germany, **2007**.

[18] For reviews on charge transport in organic semiconductors, see: (a) V. Coropceanu, J. Cornil, D. A. da Silva Filho, R. Silbey, J.-L. Brédas, *Chem. Rev.* **2007**, *107*, 926-952; (b) G. Horowitz, *Adv. Mater.* **1998**, *10*, 365-377; (c) Y. Shirota, H. Kageyama, *Chem. Rev.* **2007**, *107*, 953-1010; (d) A. R. Murphy, J. M. J. Fréchet, *Chem. Rev.* **2007**, *107*, 1066-1096; (e) J. Zaumseil, H. Sirringhaus, *Chem. Rev.* **2007**, *107*, 1296-1323; (f) A. Facchetti, *Mater. Today* **2007**, *10*, 28-37.

[19] H. Bässler, *Phys. Status Solidi B* **1993**, *175*, 15-56.

[20] (a) O. D. Jurchescu, J. Baas, T. T. M. Palstra, *Appl. Phys. Lett.* **2004**, *84*, 3061-3063; (b) N. Karl, J. Marktanner, *Mol. Cryst. Liq. Cryst.* **2001**, *355*, 149-173.

[21] (a) W. D. Gill, *J. Appl. Phys.* **1972**, *43*, 5033-5040; (b) J. Frenkel, *Phys. Rev.* **1938**, *54*, 647-648.

[22] L. B. Schein, J. X. Mack, *Chem. Phys. Lett.* **1988**, *149*, 109-112.

[23] H. Bässler, *Phys. Status Solidi B* **1988**, *107*, 9-54.

[24] P. G. Le Comber, W. E. Spear, *Phys. Rev. Lett.* **1970**, *25*, 509-511.

[25] A. Kahn, N. Koch, W. Gao, *J. Polym. Sci. B, Polym. Phys.* **2003**, *41*, 2529-2548.

[26] C. D. Sheraw, T. N. Jackson, D. L. Eaton, J. E. Anthony, *Adv. Mater.* **2003**, *15*, 2009-2011.

[27] (a) J. M. Warman, M. P. de Haas, G. Dicker, F. C. Grozema, J. Piris, M. G. Debije, *Chem. Mater.* **2004**, *16*, 4600-4609; (b) F. C. Grozema, L. D. A. Siebbeles, *Intern. Rev. Phys. Chem.* **2008**, *27*, 87-138.

[28] R. W. I. de Boer, M. E. Gershenson, A. F. Morpurgo, V. Podzorov, *Phys. Status Solidi A* **2004**, *201*, 1302-1331.

[29] For a recent review on organic single-crystal FETs, see: C. Reese, Z. Bao, *Mater. Today* **2007**, *10*, 20-27.

[30] J. Y. Lee, S. Roth, Y. W. Park, *Appl. Phys. Lett.* **2006**, *88*, 252106.

[31] V. C. Sundar, J. Zaumseil, V. Podzorov, E. Menard, R. L. Willet, T. Someya, M. E. Gershenson, J. A. Rogers, *Science* **2004**, *303*, 1644-1646.

[32] (a) D. E. Janzen, M. W. Burand, P. C. Ewbank, T. M. Pappenfus, H. Higuchi, D. A. Da Silva Filho, V. G. Young, J. L. Brédas, K. R. Mann, *J. Am. Chem. Soc.* **2004**, *126*, 15295-15308; (b) J. Cornil, J.-L. Brédas, J. Zaumseil, H. Sirringhaus, *Adv. Mater.* **2007**, *19*, 1791-1799.

[33] M. Mas-Torrent, P. Hadley, S. T. Bromley, X. Ribas, J. Tarres, M. Mas, E. Molins, J. Veciana, C. Rovira, *J. Am. Chem. Soc.* **2004,** *126*, 8546-8553.

[34] For a current review on organic p-type semiconductors see: J. E. Anthony, *Angew. Chem.* **2008**, *120*, 460-492; *Angew. Chem. Int. Ed*. **2008**, *47*, 452-483.

[35] H. Klauk, M. Halik, U. Zschieschang, G. Schmid, W. Radlik, W. Weber, *J. Appl. Phys.* **2002**, *92*, 5259-5263.

[36] S. K. Tripathi, M. Heinrich, T. Siegrist, J. Pflaum, *Adv. Mater.* **2007**, *19*, 2097-2101.

[37] H. Meng, F. Sun, M. B. Goldfinger, G. D. Jaycox, Z. Li, W. J. Marshall, G. S. Blackman, *J. Am. Chem. Soc.* **2005**, *127*, 2406-2407.

[38] M. Mas-Torrent, M. Durkut, P. Hadley, X. Ribas, C. Rovira, *J. Am. Chem. Soc.* **2004**, *126*, 984-985.

[39] F. Garnier, R. Hjlaoui, A. Yassar, P. Srivastava, *Science* **1994**, *265*, 1684-1686.

[40] I. McCulloch, M. Heeney, C. Bailey, K. Genevicius, I. MacDonald, M. Shkunov, D. Sparrowe, S. Tierney, R. Wagner, W. Zhang, M. L. Chabinyc, R. J. Kline, M. D. McGehee, M. F. Toney, *Nat. Mater.* **2006**, *5*, 328-333.

[41] A. M. van de Craats, J. M. Warman, A. Fechtenkötter, J. D. Brand, M. A. Harbison, K. Müllen, *Adv. Mater.* **1999**, *11*, 1469-1472.

[42] (a) D. Adam, P. Schuhmacher, J. Simmerer, L. Häussling, K. Siemensmeyer, K. H. Etzbachi, H. Ringsdorf, D. Haarer, *Nature*, **2004**, *371*, 141-143; (b) A. M. van de Craats, J. M. Warman, *Synth. Metals* **2001**, *121*, 1287-1288; (c) I. Parschiv, M. Giesbers, B. van Lagen, F. C. Grozema, R. D. Abellon, L. D. A. Siebbeles, A. T. M. Marcelis, H. Zuilhof, E. J. R. Sudhölter, *Chem. Mater.* **2006**, *18*, 968-974.

[43] M. Funahashi, J. Hanna, *Adv. Mater.* **2005**, *17*, 594-598.

[44] (a) M. Yoon, S. A. DiBenedetto, A. Facchetti, T. J. Marks, *J. Am. Chem. Soc.* **2005**, *127*, 1348-1349; (b) M. Yoon, A. Facchetti, C. E. Stern, T. J. Marks, *J. Am. Chem. Soc.* **2006**, *128*, 5792-5801.

[45] (a) S. Ando, R. Muratami, J. Nishida, H. Tada, Y. Inoue, S. Tokito, Y. Yamashita, *J. Am. Chem. Soc.* **2005**, *127*, 14996-14997; (b) S. Ando, J. Nishida, H. Tada, Y. Inoue, Y. Yamashita, *J. Am. Chem. Soc.* **2005**, *127*, 5336-5337.

[46] (a) Z. Bao, A. Lovinger, J. Brown, *J. Am. Chem. Soc.* **1998**, *120*, 207-208; (b) D. G. de Oteyza, E. Barrena, J. O. Osso, H. Dosch, S. Meyer, J. Pflaum, *Appl. Phys. Lett.* **2005**, *87*, 183504; (c) R. Ye, M. Baba, Y. Oishi, K. Mori, K. Suzuki, *Appl. Phys. Lett.* **2005**, *86*, 253505; (d) M.-H. Yoon, C. Kom. A. Facchetti, T. J. Marks, *J. Am. Chem. Soc.* **2006**, *128*, 12851-12869.

[47] Y. Sakamoto, T. Suzuki, M. Kobayashi, Y. Gao, Y. Fukai, Y. Inoue, F. Sato, S. Tokito, *J. Am. Chem. Soc.* **2004**, *126*, 8138-8140.

[48] (a) T. W. Lee, Y. Byun, B. W. Koo, I. N. Kang, Y. Y. Lyu, C. H. Lee, S. Y. Lee, *Adv. Mater.* **2005**, *17*, 2180-2184; (b) S. Kobayashi, T. Nishikawa, T. Takenobu, S. Mori, T. Shimoda, T. Mitani, H. Shimotani, N. Yoshimoto, S. Ogawa, Y. Iwasa, *Nat. Mater.* **2004**, *3*, 317-322; (c) E. J. Meijer, D. M. de Leeuw, S. Setayesh, E. Veenendaal, B. H. Huisman, P. W. M. Blom, J. C. Hummelen, U. Scherf, T. M. Klapwijk, *Nat. Mater.* **2003**, *2*, 678-682; (d) S. Kobayashi, T. Takenobu, S. Mori, A. Fujiwara, Y. Iwasa, *Appl. Phys. Lett.* **2003**, *82*, 4581-4583; (d) R. C. Haddon, A. S. Perel, R. C. Morris, T. T. M. Palstra, A. F. Hebard, R. M. Fleming, *Appl. Phys. Lett.* **1995**, *67*, 121-123.

[49] K. Itaka, M. Yamashiro, J. Yamaguchi, M. Haemore, S. Yaginuma, Y. Matsumoto, M. Kondo, H. Koinuma, *Adv. Mater.* **2006**, *18*, 1713-1716.

[50] A. K. Tripathi, J. Pflaum, *Appl. Phys. Lett.* **2006**, *89*, 082103.

[51] For a review on the role of fluorine for electronic applications, see: F. Babudri, G. M. Farinola, F. Naso, R. Ragni, *Chem. Commun.* **2007**, 1003-1022.

[52] G. W. Coates, A. R. Dunn, L. M. Henling, J. W. Ziller, E. B. Lobkovsky, R. H. Grubbs, *J. Am. Chem. Soc.* **1998**, *120*, 3641-3649.

[53] (a) P. T. Herwig, K. Müllen, *Adv. Mater.* **1999**, *11*, 480-483; (b) A. Afzali, C. D. Dimitrakopoulos, T. L. Breen, *J. Am. Chem. Soc.* **2002**, *124*, 8812-8813; (c) H. Yamada, Y. Yamashita, M. Kikuchi, H. Watanabe, T. Okujima, H. Uno, T. Ogawa, K. Ohara, N. Ono, *Chem. Eur. J.* **2005**, *11*, 6212-6220.

[54] (a) S. A. Odem, S. R. Parkin, J. E. Anthony, *Org. Lett.* **2003**, *5*, 4245-4248; (b) M. M. Payne, S. R. Parkin, J. E. Anthony, C. Kuo, T. N. Jackson, *J. Am. Chem. Soc.* **2005**, *127*, 8028-8029.

[55] M. M. Payne, S. A. Odom, S. R. Parkin, J. E. Anthony, *Org. Lett.* **2004**, *6*, 3325-3328.

[56] (a) A. Maliakal, K. Raghavachari, H. Katz, E. Chandross, T. Siegrist, *Chem. Mater.* **2004**, *16*, 4980-4986; (b) P. Coppo, S. G. Yeates, *Adv. Mater.* **2005**, *17*, 3001-3005.

[57] (a) M. Bendikov, F. Wudl, D. F. Perepichka, *Chem. Rev.* **2004**, *104*, 4891-4945; (b) M. Bendikov, H. M. Duong, K. Starkey, K. N. Houk, E. A. Carter, F. Wudl, *J. Am. Chem. Soc.* **2004**, *126*, 7416-7417; (c) K. N. Houk, P. S. Lee, M. Nendel, *J. Org. Chem.* **2001**, *66*, 5517-5521.

[58] M. M. Payne, S. R. Parkin, J. E. Anthony, C. Kuo, T. N Jackson, *J. Am. Chem. Soc.* **2005**, *127*, 4986-4987.

[59] F. Würthner, R. Schmidt, *ChemPhysChem.* **2006**, *7*, 793–797.

[60] A. Tsuda, A. Osuka, *Science* **2001**, *293*, 79-82.

[61] G. R. Desiraju, A. Gavezzotti, *Acta Cryst.* **1989**, *B45*, 473-482.

[62] Q. Miao, M. Lefenfeld, T.-Q. Nguyen, T. Siegrist, C. Kloc, C. Nuckolls, *Adv. Mater.* **2005**, *17*, 407-412.

[63] (a) J. G. Laquindanum, H. E. Katz, A. J. Lovinger, *J. Am. Chem. Soc.* **1998**, *120*, 664-672; (b) H. Meng, M. Bendikov, G. Mitchell, R. Helgeson, F. Wudl, Z. Bao, T. Siegrist, C. Kloc, C.-H. Chen, *Adv. Mater.* **2003**, *15*, 1090-1093.

[64] (a) G. Horowitz, F. Kouki, P. Spearman, D. Fichou, C. Nogues, X. Pan, F. Garnier, *Adv. Mater.* **1996**, *8*, 242-245; (b) J. G. Laquindanum, H. E. Karz, A. Dodabalapur, A. J. Lovinger, *J. Am. Chem. Soc.* **1996**, *118*, 11331-11332.

[65] (a) C. W. Strujik, A. B. Sieval, J. E. J. Dakhorst, M. Van Dijk, P. Kimkes, R. B. M. Kohorst, H. Donker, T. J. Schaafsma, S. J. Picken, A. M. van de Craats, J. M. Warman, H. Zuilhof, E. J. R. Sudhölter, *J. Am. Chem. Soc.* **2000**, *122*, 11057-11066; (b) P. R. L. Malenfant, C. D. Dimitrakopoulos, J. D. Gelorme, L. L. Kosbar, T. O. Graham, *Appl. Phys. Lett.* **2002**, *80*, 2517-2519; (c) A. J. Jones, M. J. Ahrens, M.-H. Yoon, A. Facchetti, T. J. Marks, M. R. Wasielewski, *Angew. Chem.* **2004**, *116*, 6523-6526; *Angew. Chem. Int. Ed.* **2004**, *43*, 6363-6366; (d) M.-M. Ling, P. Erk, M. Gomez, M. Könemann, J. Locklin, Z. Bao, *Adv. Mater.* **2007**, *19*, 1123-1127; (e) R. J. Chesterfield, J. C. McKeen, C. R. Newman, P. C. Ewbank, D. A. da Silva Filho, J.-L. Brédas, L. L. Miller, K. R. Mann, C. D. Frisbie, *J. Phys. Chem. B* **2004**, *108*, 19281-19292; (f) B. Yoo, T. Jung, D. Basu, A. Dodabalapur, B. A. Jones, A. Facchetti, M. R. Wasielewski, T. J. Marks, *Appl. Phys. Lett.* **2006**, *88*, 082104; (g) S. Tatemichi, M. Ichikawa, T. Koyama, Y. Taniguchi, *Appl. Phys. Lett.* **2006**, *89*, 112108; (h) D. J. Gundlach, K. P. Pernstich, G. Wilckens, M. Grüter, S. Haas, B. Batlogg, *J. Appl. Phys.* **2005**, *98*, 064502; (i) H. Z. Chen, M. M. Ling, X. Mo, M. M. Shi, M. Wang, Z. Bao, *Chem. Mater.* **2007**, *19*, 816-824; (j) R. T. Weitz, K. Amsharov, U. Zschieschang, E. B. Villas, D. K. Goswami, M. Burghard, H. Dosch, M. Jansen, K. Kern, H. Klauk, *J. Am. Chem. Soc.* **2008**, 10.1021/ja074675e.

[66] (a) F. Würthner, *Chem. Commun.* **2004**, 1564-1579; (b) A. C. Grimsdale, K. M. Müllen, *Angew. Chem.* **2005**, *117*, 5732-5772; *Angew. Chem. Int. Ed.* **2005**, *44*, 5592-5629; (c) F. Würthner, *Pure Appl. Chem.* **2006**, *78*, 2341-2350.

[67] F. Pichierri, *J. Mol. Struct. (Theochem)* **2004**, *686*, 57-63.

[68] (a) F. Graser, E. Hädicke, *Liebigs Ann. Chem.* **1980**, 1994-2011; (b) F. Graser, E. Hädicke, *Liebigs Ann. Chem.* **1984**, 483-494; (c) E. Hädicke, F. Graser, *Acta Crystallogr., Sect. C* **1986**, *42*, 189-195; (d) E. Hädicke, F. Graser, *Acta Crystallogr., Sect. C* **1986**, *42*, 195-198; (e) G. Klebe, F. Graser, E. Hädicke, J. Berndt, *Acta Crystallogr., Sect. B* **1989**, *45*, 69-77.

[69] (a) Z. Chen, M. G. Debije, T. Debaerdemaeker, P. Osswald, F. Würthner, *ChemPhysChem* **2004**, *5*, 137-140; (b) F. Würthner, V. Stepanenko, Z. Chen, C. R. Saha-Möller, N. Kocher, D. Stalke, *J. Org. Chem.* **2004**, *69*, 7933-7939; (c) S. Leroy-Lhez, J. Baffreau, L. Perrin, E. Levillain, P. Hudhomme, *J. Org. Chem.* **2005**, *70*, 6313-6320; (d) P. Osswald, D. Leusser, D. Stalke, F. Würthner, *Angew. Chem.* **2005**, *117,* 254–257; *Angew. Chem. Int. Ed.* **2005**, *44*, 250-253; (e) P. Osswald, F. Würthner, *J. Am. Chem. Soc.* **2007**, *129*, 14319–14326.

[70] Y. Li, L. Tan, Z. Wang, H. Qian, Y. Shi, W. Hu, *Org. Lett.* **2008**, *10*, 529-532.

[71] B. A. Jones, A. Facchetti, M. R. Wasielewski, T. J. Marks, *J. Am. Chem. Soc.* **2007**, *129*, 15259-15278.

[72] (a) M. G. Debije, Z. Chen, J. Piris, R. B. Neder, M. M. Watson, K. Müllen, F. Würthner, *J. Mater. Chem.* **2005**, *15*, 1270-1276; (b) Z. Chen, V. Stepanenko, V. Dehm, P. Prins, L. D. A. Siebbeles, J. Seibt, P. Marquetand, V. Engel, F. Würthner, *Chem. Eur. J.* **2007**, *13*, 436-449.

[73] P. Zugenmaier, J. Duff, T. L. Bluhm, *Cryst. Res. Technol.* **2000**, *35*, 1095-1115.

[74] (a) J. Mizuguchi, *J. Appl. Phys.* **1998**, *84*, 4479-4486; (b) B. A. Gregg, *J. Phys. Chem.* **1996**, *100*, 852-859.

[75] B. A. Jones, A. Facchetti, T. J. Marks, M. R. Wasielewski, *Chem. Mater.* **2007**, *19*, 2703-2705.

[76] (a) H. E. Katz, A. J. Lovinger, J. Johnson, C. Kloc, T. Siegrist, W. Li, Y.-Y. Lin, A. Dodabalapur, *Nature* **2000**, *404*, 478-481; (b) H. E. Katz, J. Johnson, A. J. Lovinger, W. Li, *J. Am. Chem. Soc.* **2000**, *122*, 7787-7792.

Chapter 3

Highly soluble acene derivatives for organic thin film transistors

Abstract: Four solution-processible trimethoxyphenylethynyl-substituted acene derivatives bearing substituents in the central ring of parent acenes have been synthesized. The bulky substituents were taken to achieve high solubility in different organic solvents and to change the solid state packing from “herringbone” to a more favored 2D brickstone arrangement. Therefore the solid state packing of two derivatives was examined by X-ray analysis. The disubstituted acene derivatives show high atmospheric stability both in solid state and in solution. These favourable properties facilitated the fabrication of thin film transistors with the given disubstituted acenes by the convenient solution processing, spin-coating technique. Field effect mobilities up to 1.9×10^{-5}cm^2/Vs and on/off ratios up to 10^3 were observed for these devices which show only minor decrease upon exposure to air.[a]

[a] Charge carrier mobilities were measured at the University of Stuttgart by. S. Göttling in the group of Prof.Dr. N. Frühauf (Institut für Systemtheorie und Bildschirmtechnik). This chapter has been published: R. Schmidt, S. Göttling, D. Leusser, D. Stalke, A.-M. Krause, F. Würthner *J. Mater. Chem.* **2006**, *16*, 3708–3714.

3.1 Introduction

During the last decade, organic thin film transistors (OTFTs) have become increasingly more attractive for various electronic applications as more convenient processes for their fabrication have become accessible compared to amorphous silicon based technologies.[1] Notably, devices based on organic semiconductors have some advantages due to their high flexibility, low weight and different ways of easy processability. On the other hand, OTFTs cannot achieve the high switching frequency of single crystalline silicon because of an inherently lower mobility and structural disorder of organic compounds in their solid state. But the values of the switching frequencies of organic electronic materials have already approached the speed of conventional amorphous inorganic devices. Thus, organic semiconductors are promising for flexible, inexpensive and large area applications that do not demand high switching frequency, e.g. electronic papers and displays,[2] sensors[3] and disposable microelectronics[4] (barcodes, smart cards, RFID tags, memory devices, etc.).

In the recent years, unsubstituted acenes have been intensively investigated as organic semiconductors with the result that OTFTs based on parent pentacene have exhibited so far the best performance with field effect mobilities up to 3 cm^2/Vs for vacuum deposited and 35 cm^2/Vs for single crystal devices, respectively,[5] despite the lack of π–π interactions in the solid state due to the well-known herringbone packing of acene molecules.[6] As parent pentacene suffers from a very deficient solubility, it can, therefore, be processed either by vacuum deposition or in form of soluble precursors.[7] While vacuum deposition techniques are needed for high performance OTFTs,[8] deposition from solution will facilitate the large scale production of electronic devices for disposable applications. Therefore, highly soluble acene derivatives are indeed in demand.[9]

Anthony and coworkers have shown that the solubility problem of acenes, in particular pentacene, may be encountered by introducing properly chosen substituents in their central positions.[10] For the design of soluble acenes the following aspects are of importance: Recent studies have demonstrated that the charge carrier mobility in organic semiconductors is dependend on the interaction between the π–systems.[11] Therefore, a small distance between the π–surfaces of molecules[9] and well-ordered parallel-orientated stacks can be very beneficial toward high charge carrier mobilities.[10a] Accordingly, the electronic abilities of

devices can be improved by circumventing the edge-to-face arrangement in solid state.[10b] Bulky substituents are helpful to force the molecules to form a 2-D brickstone network in crystals with strong π–π overlap that can facililtate higher mobility in p- and n-type semiconducting organic layers.[8c,10c,d] Moreover, it has been shown that some substituents can provoke a higher stability of acene derivatives against oxidative and other decomposition processes.[12]

Bearing in mind the above-mentioned aspects the disubstituted acene derivatives **3**, **5**, **7** and **9** (Scheme 1) were designed with the aim to achieve high solubility that enables processing of acenes by convenient spin-coating, instead of high temperature vacuum deposition techniques. The sterically demanding phenylethynyl substituents are chosen to prevent herringbone packing and, on the other hand, to promote π–π overlap for higher electronic transport properties. Furthermore, it is expected that in these extended chromophoric systems charge carrier mobility may not be limited to the acene core, but also expands to the π–system of the substituents owing to the high planarity of the whole molecule. OTFTs of the newly synthesized disubstituted acene derivatives were fabricated by spin-coating from solution and they exhibit appreciable field effect mobility.

3.2 Synthesis

The disubstituted acene derivatives **3**, **5**, **7** and **9** were prepared by nucleophilic reaction of lithiated 5-ethynyl-1,2,3-trimethoxybenzene **1** with the respective quinone, followed by *in situ* reduction of the resultant diol by tin(II)-chloride and diluted hydrochloric acid (Scheme 1). The quinones **4**, **6** and **8** were synthesized by aldol condensation of the corresponding dialdehyde and ketone by literature methods.[10c,d,13] Starting material **1** was prepared from trimethoxybenzaldehyde, which was converted to the corresponding dibromoalkene by Corey-Fuchs reaction and subsequently treated with *n*-butyllithium to afford the ethynyl compound **1**.[14]

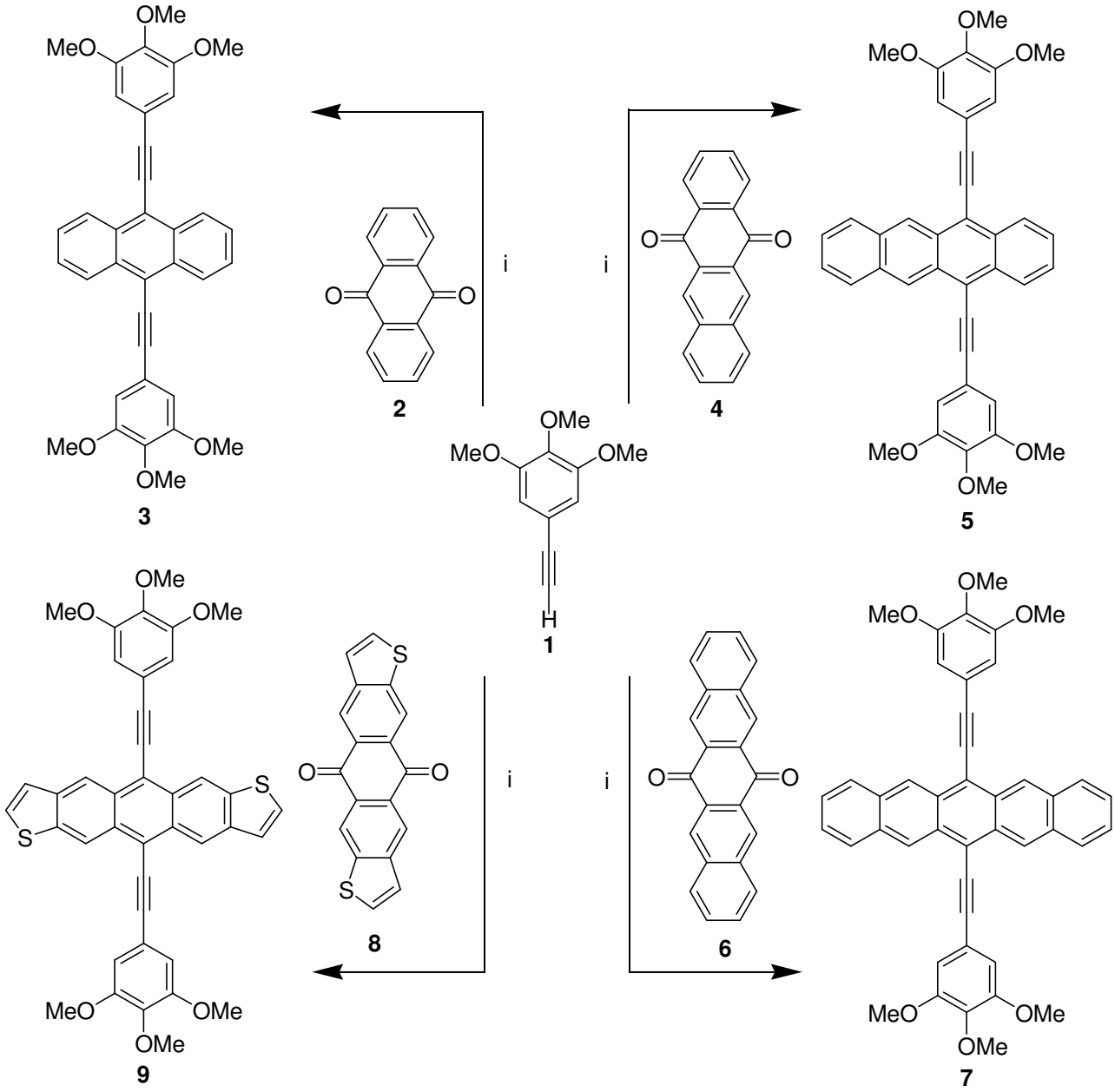

Scheme 1. Synthesis of acenes **3**, **5**, **7** and **9**. Reagents and conditions: i) *n*- BuLi, -78 °C, 30 min; addition of the respective quinone, RT, 60 min; $SnCl_2$, HCl, RT. Yields: 91% **3**, 45% **5**, 21% **7** and 45% **9**. Note that quinone **8** and the corresponding dithienoanthracene **9** are isomere mixtures.

3.3 Optical and Electrochemical Properties

The optical properties of the highly soluble disubstituted acenes were investigated by UV/Vis absorption and fluorescence spectroscopy in dichloromethane. The strongest absorption bands of these compounds appear at 280 to 330 nm. In the visible region, the acenes **3**, **5** and **7** exhibit significant absorption bands at 475 nm, 560 nm and 667 nm, respectively (Figure 1, left). The dithienoanthracene derivative **9** shows a similar spectrum as tetracene **5**, but with a batochromically shifted

absorption maximum at 572 nm (Figure 1, right). It is interesting to note that the absorption bands of the disubstituted acenes are significantly red shifted compared to those of the respective unsubstituted compounds. This bathochromic shift can be attributed to the extension of the chromophoric system by phenylethynyl groups.

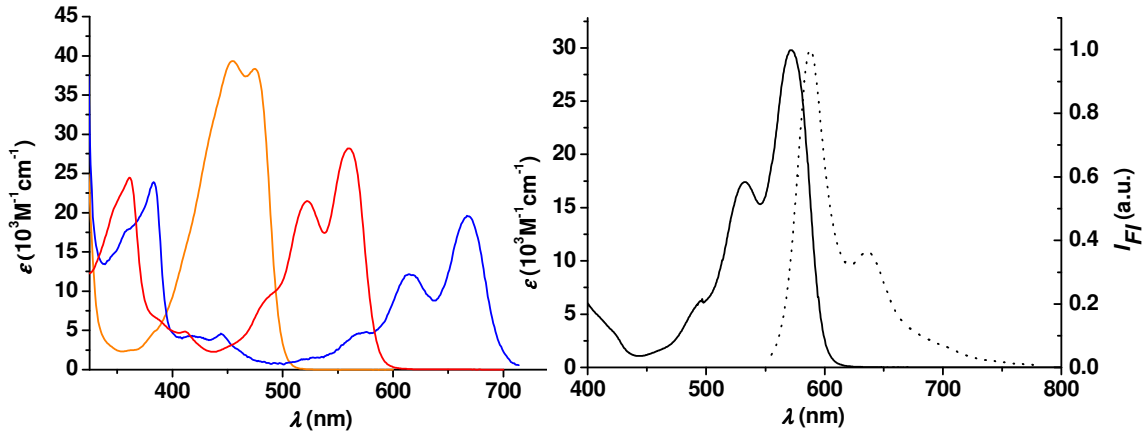

Figure 1. UV/Vis absorpiton spectra of acene derivatives **3**, **5** and **7** in dichloromethane (left) and UV/Vis absorption (solid line) and fluorescence (dashed line, λ_{ex} = 450 nm) spectra of **9** in dichloromethane (left).

The acene derivatives **3**, **5**, **7** and **9** are moderate to highly fluorescent in dichloromethane and chloroform solutions and their quantum yields (in dichloromethane) range from 19% to 86% (Table 1). Noteworthy, the disubstituted tetracene **5** possesses a higher fluorescence quantum yield (86%) than that of similar phenylethynyltetracene derivatives,[15] which contain alkyl (81%), or no substituents (66%) at the phenyl rings. This reveals that the electron-rich methoxy groups in the periphery of the present acene derivatives do not have any detrimental effect on the fluorescence of the chromophoric system.

Table 1: Absorption and fluorescence maxima ($\lambda_{abs/em}$) and fluorescence quantum yields (ϕ_{fl}) of acene derivatives in dichloromethane.

Acene	λ_{abs} (nm)	ε (M^{-1} cm^{-1})	λ_{em} (nm)	ϕ_{fl}[a]
3	455	39300	457	0.58
5	560	28200	571	0.86
7	667	19600	681	0.19
9	572	29800	588	0.82

[a] ϕ_{fl} ± 0.03; determined with fluorescein (0.1 M, NaOH) served as reference for **3**, *N,N'*-di(2,6-diisopropylphenyl)-1,6,7,12-tetraphenoxyperylene-3,4:9,10-tetracarboxylic acid bisimide in $CHCl_3$ as reference for **5** and **9** and Nile Blue in ethanol as reference for **7**.

The fact that all thin films in our electronic devices were amorphous, UV/Vis spectra of these films (Figure 2) can provide further information on the electronic

coupling between the π–systems in the solid state. For anthracene **3** we observe a very slight shift of about 5 nm of the absorption maximum, followed by tetracene **5** and dithienoanthracene **9** with 18 and 19 nm, respectively. The strongest batochromic shift is exhibited by the pentacene **7** thin film with 34 nm, which can be taken as an indication for a stronger electronic coupling between neighboring chromophores in the solid state compared to the smaller homologues.

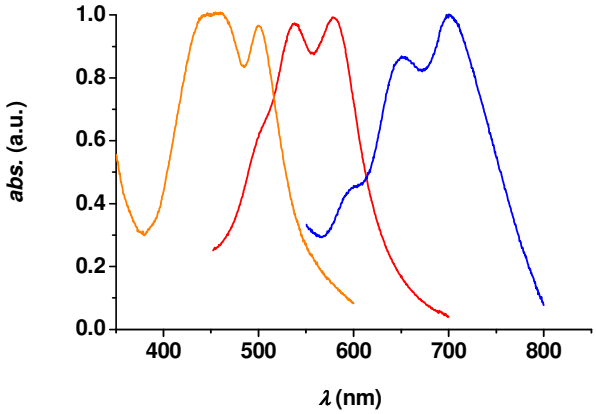

Figure 2. Thin film UV/Vis absorption spectra of acene derivatives **3** (orange), **5** (red) and **7** (green) prepared by dropcasting.

The redox behaviour of the disubstituted acene derivatives **3**, **5**, **7** and **9** were investigated by cyclic voltammetry (CV) employing ferrocene as internal standard for the calibration of potential. In Table 1 the redox potentials of these acene derivatives and, for comparison, their parent compounds are given. While the oxidation process of **3**, **5** and **7** is irreversible, dithienoanthracene **9** exhibits two reversible oxidation (at 355 and 736 mV) and one reversible reduction (at -1645 mV) waves (Figure 3). It is remarkable that the first oxidation potentials of disubstituted anthracene **3** and tetracene **5** derivatives are significantly lower than those of their parent compounds, while the oxidation potential of the disubstituted pentacene **7** is slightly higher compared with that of its parent hydrocarbon. These data might indicate that the disubstituted anthracene and tetracene derivatives are oxidatively less stable than the respective unsubstituted compounds, while the pentacene derivative **7** is somewhat more resistant than its parent compound. Nevertheless, the solutions of **5**, **7** and **9** did not show any sign of decomposition under ambient laboratory conditions after several hours. All compounds can be stored for months under argon atmosphere without any degradation. Anthracene derivative **3** is stable even under exposition of light and air.

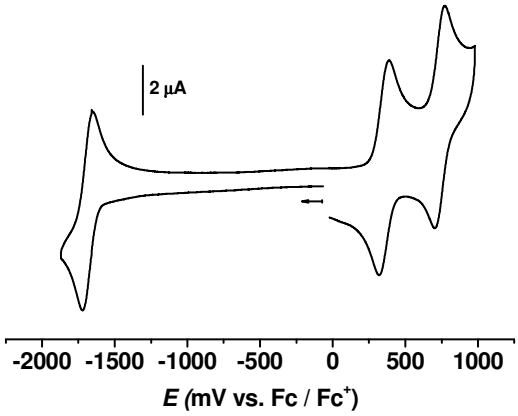

Figure 3. Cyclic votammogram of **9** in DCM using ferrocene as internal standard.

Table 2: First oxidation potentials (in V vs Fc/Fc^+) of **3**, **5**, **7** and **9** and their parent hydrocarbons.

comp.	disubstituted[a]	unsubstituted[a]
3	0.60	0.95
5	0.45	0.52
7	0.29	0.28
9	0.36	n.a.

[a] performed in 0.1 M solution of the supporting electrolyte Bu_4NPF_6 in dichloromethane, Pt electrode, scan rate of 150 mV/s for **3**, **5** and **7** and 250 mV/s for **9**, ferrocene served as internal standard.

3.4 X-ray analysis

As the structural features of organic materials in solid state are of particular importance for their semiconducting properties, e.g. charge carrier mobilities, acene derivatives **3** and **5** were analyzed by single crystal X-ray diffraction. For this purpose, anthracene **3** was recrystallized from dichlormethane and methanol to afford cubic orange crystals. X-ray characterization of **3** revealed a 1-D side-shifted stack in solid state (Figure 4). The overlap of the π–systems with face-to-face interactions is about 50% with a distance of 3.39 Å. Except for two methoxy substituents, the whole molecule displays a nearly flat symmetric molecular geometry, which enables a close molecular packing without inclusion of any solvent molecules. Furthermore, the molecule lies about an inversion centre.

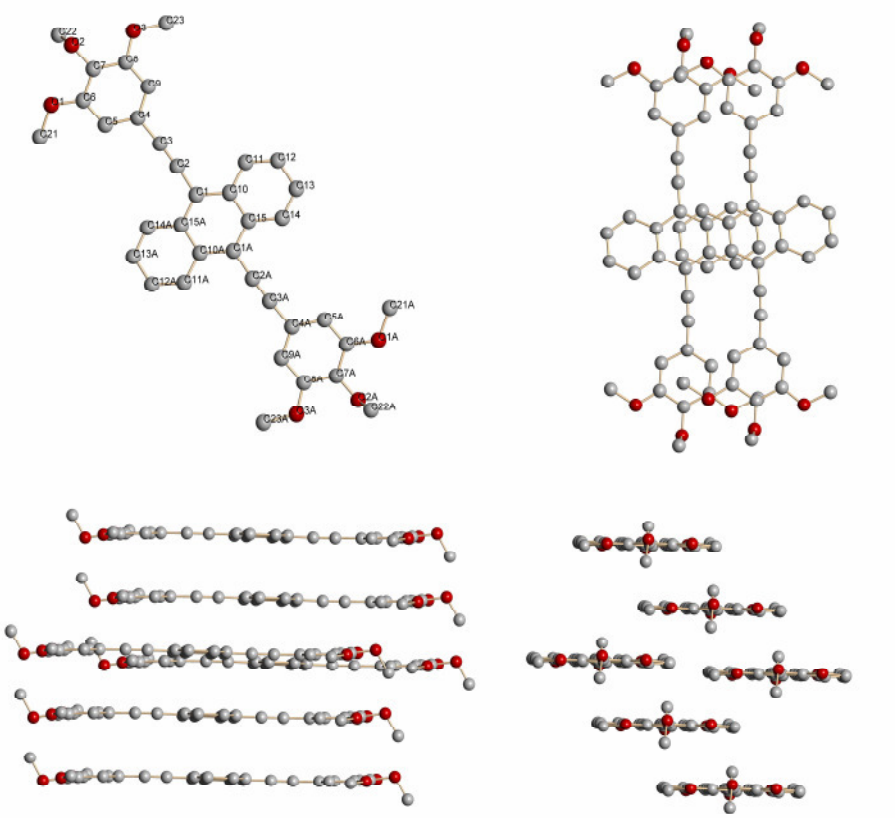

Figure 4. Crystal structure of **3**: molecular structure (top left), view on stacked p-system (top right), view along the short molecule axis (bottom left), view along the long axis (bottom right). The plane in front is darker for better visualization. The additional "A" letters in the labels indicate that these atoms are at equivalent positions, created by symmetry operation (2-x, 2-y, 1-z).

Crystals of tetracene **5** (dark red needles) were grown from chloroform and degassed methanol under argon atmosphere. As in the case of **3**, solid state structure of **5** exhibits 1-D stacks, but those are organized in a side-shifted face-to-edge arrangement (Figure 5, bottom), similar to the herringbone structure of parent pentacene. However, the surfaces of the π–systems are not exactly perpendicular to each other, as it is generally the case for herringbone structures. This can be attributed to the steric demand of the substituents in these molecules. Furthermore, chloroform molecules were enclosed in the lattice structure with a 2:1 ratio of $CHCl_3$/**5**. No 2-D brickstone arrangement was observed as seen for related compounds of *Anthony* and coworkers[10] and the spatial cavity between the 1-D stacks was filled with solvent molecules. Nevertheless, as the phenyl substituentes, which are face-to-edge (approx. 85°) arranged (Figure 5, bottom left) to the next tetracene core, are part of the whole π-system of the molecule, electronic interactions between the stacks might be possible in two different dimensions.

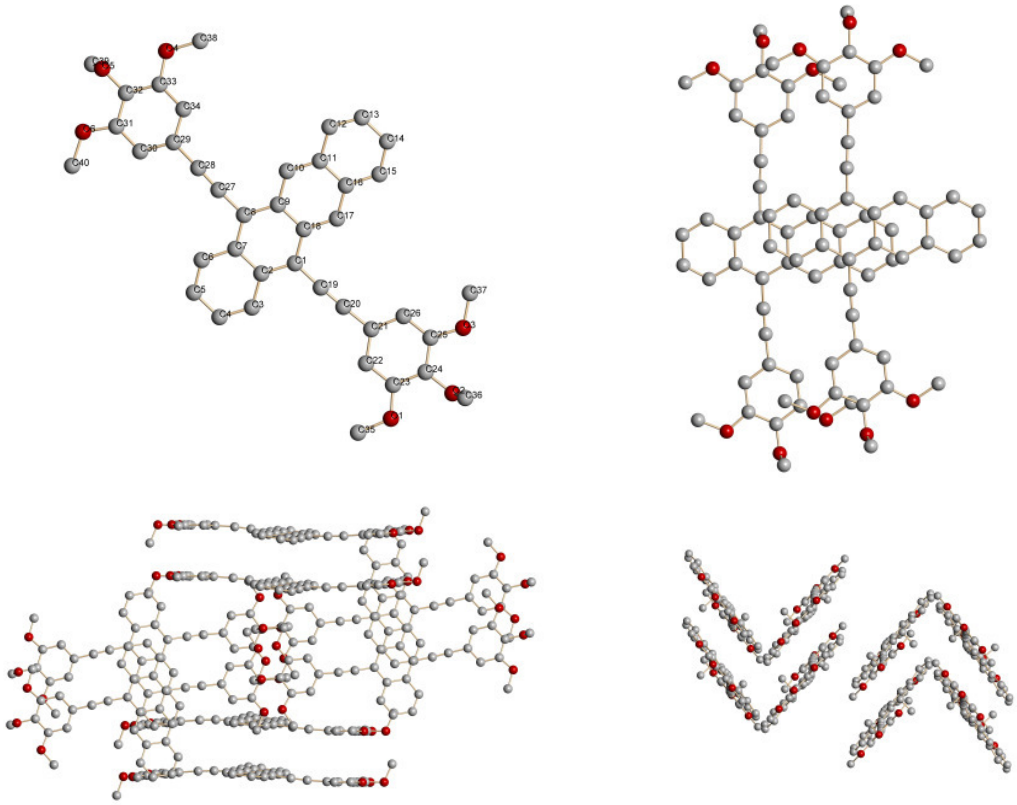

Figure 5. Crystal structure of **5**: molecular structure (top left), view on stacked π-system (top right), view along the long molecule axis (bottom left), view along the short axis (bottom right). Chloroform molecules are omitted for clarity. The plane in front is more dark for better visualization.

3.5 Thin Film Transistors

The OTFTs of acene derivatives **3**, **5**, **7** and **9** were prepared by spin-coating of their solution on surfaces. The devices were prepared and measured by S. Göttling in the group of Prof. Dr. N. Frühauf. Dichloromethane was used as solvent for **3**, **5** and **7**, while ethyl acetate was applied for compound **9**. A silicon dioxide (SiO_2) wafer was used as substrate. The dielectric was grown by anodic oxidation on sputtered aluminia with a thickness of 60 nm. The gate electrode was made from aluminium, while the source and drain electrodes were constructed from sputtered gold. A saturated solution of the present acenes was coated across the surface of the devices and the solvent was evaporated in a stream of nitrogen gas. All acene derivatives formed uniform, but amorphous thin films from solutions. The thickness of the active layers of devices was measured with a surface profiler and ranged from 35 (**7**) and 40 (**5**) up to 65 nm (**9**). The OTFT spin-coated with anthracene derivative **3** did not show any field effect controlled conductivity. The tetracene compound **5** exhibited a small hole mobility of roughly 10^{-6} cm^2/Vs. The on/off ratio could not be determined exactly due to the increase of the current for positive voltage. The

dithienoanthracene derivative **9** showed a field effect mobility of 8×10^{-6} cm^2/Vs with an on/off ratio of 6×10^2. After four days exposition to air under clean room conditions, the on/off ratio decreased to 1.4×10^2 due to the higher off-conductivity, apparently caused by oxidation processes. The best performance was observed for the device with pentacene derivative **7**. Figures 6 show the input and output characteristics of the OTFT of **7** with a field effect mobility of 1.9×10^{-5} cm^2/Vs and an on/off ratio of 10^3. A highly favourable feature, in regard to potential applications, of this device is its atmospheric stability; thus, only minor decrease in OTFT characteristics of **7** could be observed after exposure to ambient air and light over 3 days (Figure 6, left).

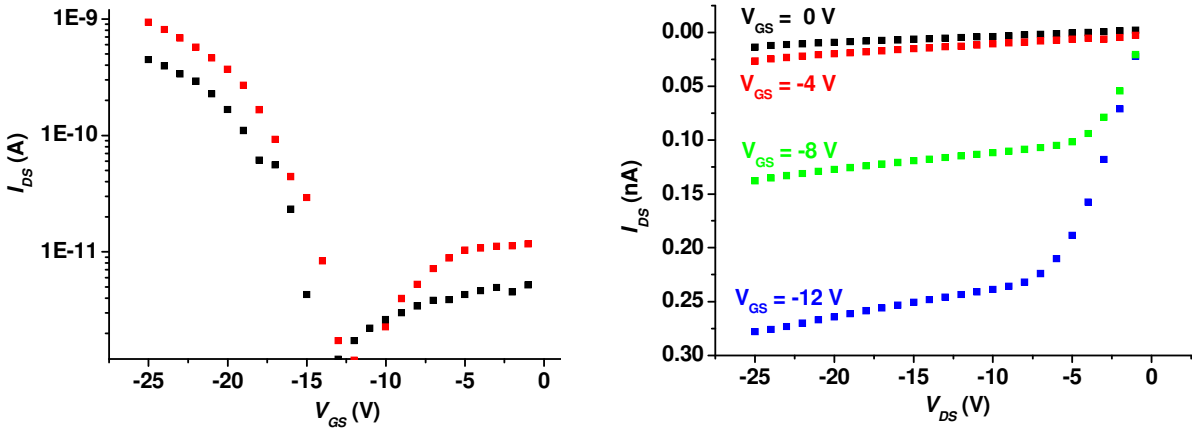

Figure 6. Input characteristics (drain current versus gate voltage) of pentacene derivative **7**, (red = measured directly after coating, black = measured after 3 days) (left); Output characteristics (drain current versus drain voltage) of **7** (right); OTFT with a channel width of 100 µm and a channel length of 10 µm on aluminum oxide dielectric of 60 nm.

The AFM image of the thin layer of pentacene **7** shows a channel width of 100 µm with a length of 10 µm on an aluminum oxide dielectric. The height of the semiconducting layer was about 35 nm. The image shows a highly amorphous structure perforated with holes formed on evaporation of the solvent. The off-characteristics of the OTFT with **7** are similar to those of the devices with vacuum deposited unsubstituted pentacene. However, the on-currents are about three orders of magnitude smaller, which is presumably caused by the disordered amorphous structure of **7** on thin films.

Due to the very low vapour pressure and poor thermal stability of higher acene derivatives **5**, **7** and **9**, their vacuum deposition was not possible at higher temperatures. Only the anthracene derivative **3** could be vacuum deposited and its charge carrier mobility was determined as 0.033 cm^2/Vs.

3.6 Conclusions

We have presented here promising solution-processible amorphous acene-based organic semiconductors bearing substituents in the central ring of parent acenes. Thus, a homologue series of trimethoxyphenylethynyl-substituted acene derivatives were synthesized that are highly soluble in different organic solvents, e.g. dichloromethane, chloroform and ethyl acetate. The present disubstituted acene derivatives show high atmospheric stability both in solid state and in solution. These favorable properties facilitated the fabrication of thin film transistors with the given disubstituted acenes by the convenient solution processing, spin-coating technique. Field effect mobilities up to 1.9×10^{-5} cm^2/Vs and on/off ratios up to 10^3 were observed for these devices which show only minor decrease upon exposure to air.

3.7 Experimental Section

Materials and Methods. 3-thiophenecarboxaldehyde, 1,4-dihydroxy-naphthalene, 1,4-cyclohexanedione, phthaldialdehyde, 3,4,5-trimethoxybenzaldehyde, carbontetrabromide and *n*-BuLi (2.5 M) in hexane were purchased from commercial sources, i.e. Merck, Fluka, Aldrich, or Fluka. All chemicals were used without further purification; solvents were purified and dried according to literature procedures:[16] tetrahydrofurane (THF) from Na/benzophenone and dichloromethane from CaH_2.

Thin layer chromatography. Thin layer chromatography was performed on aluminium foils which were coated with silica gel 60 F_{254} and a concentration zone, purchased from Merck KGaA (Hohenbrunn, Germany).

Column chromatography. Flash and normal pressure column chromatography were done using silica gel Si60 (mesh size 0.032-0.063 mm) from Merck KGaA (Hohenbrunn, Germany) as stationary phase.

Mass Spectrometry (MS). MALDI-TOF mass spectrometry was performed on a Bruker Autoflex II spectrometer (Bruker Daltronics GmbH, Bremen, Germany). EI and FAB mass spectrometry was performed on a Finnigan MAT 90 spectrometer using

3-nitrobenzylalcohol as a matrix for sample preparation.

Melting points. Melting points were determined using a Olympus Bx41 polarization microscope (Olympus GmbH, Hamburg, Germany) equipped with a heating table (THMS 600, Linkam, Great Britain) and are uncorrected.

NMR spectroscopy. ^{1}H NMR spectra (400 MHz) were recorded on Bruker Advance 400 spectrometer; chemical shifts in $CDCl_3$ are given relative to $CHCl_3$ (δ = 7.26 ppm). ^{13}C NMR spectra (101 MHz) were recorded on Bruker Avance 400 spectrometer.

Spectroscopy. Absorption spectra were recorded on a Perkin Elmer Lambda 40 spectrophotometer. Fluorescence emission and excitation spectra were recorded on a PTI QM4-2003 fluorescence spectrometer and corrected against photomultiplier and lamp intensity. A long wavelength range emission corrected photomultiplier R928 was used. Fluorescence quantum yields were determined in CH_2Cl_2 vs *N,N'*-di(2,6-diisopropylphenyl)-1,6,7,12-tetraphenoxy-perylene-3,4,9,10-tetracarboxylic acid bisimide (ϕ_{fl} = 0.96 in $CHCl_3$) for **5** and **9**, in CH_2Cl_2 vs fluorescein (0.1 M, NaOH) for **3** and Nile Blue in ethanol as reference for **7**.[17] The given quantum yields are averaged from values measured at three different excitation wavelengths with (A < 0.05) in the absorption maximum (standard deviation < 3% of the given values). For these measurements spectroscopic grade (Uvasol) dichloromethane and chloroform were used without further purification.

Electrochemical Analysis. Cyclic voltammetry (CV) was performed with a standard commercial electrochemical analysor in a three electrode single-component cell under argon. Dichloromethane (HPLC grade) was used as solvent that was dried over calciumhydride and degassed prior to measurement. The supporting electrolyte tetrabutylammonium-hexafluorophosphate was recrystallized from ethanol/water and dried in high vacuum. The measurements were carried out at a concentration of 10^{-4} M with ferrocene as internal standard for the calibration of potential. Working electrode: Pt disc; reference electrode: Ag/AgCl; auxiliary electrode: Pt wire.

X-ray analysis. The data of the single crystal structures of **3** and **5** were collected from shock-cooled crystals on a BRUKER SMART-APEX diffractometer with D8 goniometer (graphite-monochromated Mo-Kα radiation, λ = 0.71073 Å) equipped with a low temperature device at 100(2) K.[18] An empirical absorption correction was employed using SADABS 2.05.[19] The structures were solved by direct methods (SHELXS-97)[20] and refined by full-matrix least squares methods against F^2 (SHELXL-97).[21]

R values: $R1 = \Sigma||F_o|-|F_c||/\Sigma|F_o|$, $wR2 = [\Sigma w(F_o^2-F_c^2)^2/\Sigma w(F_o^2)^2]^{0.5}$, $w = [\sigma^2(F_o^2)+(g_1P)^2+g_2P]^{-1}$, $P = 1/3[\max(F_o^2,0)+2F_c^2]$. All non-hydrogen atoms were refined with anisotropic displacement parameters. All hydrogen atoms of the molecules were assigned ideal positions and refined isotropically using a riding model with U_{iso} constrained to 1.2 or 1.5 times the U_{eq} of the parent atom. Crystallographic data (excluding structure factors) for the structures reported in this paper have been deposited with the Cambridge Crystallographic Data Centre as supplementary publication no. CCDC-294143 (**3**) and CCDC-294144 (**5**).

Preparation of the dielectric. The substrate with a structured metal layer of aluminum is used as the anode and a metal plate as the cathode in an electrolyte bath. The electrolyte must be electrically conductive and for the aluminum layer the pH-value must be between 6 and 8 otherwise the aluminum layer is dissolved. During anodisation the current density is kept constant, while the voltage increases linearly with the oxide thickness. Metal ions migrate onto the surface of the metal and react with OH^- anions of the electrolyte. One part of the oxide grows into the metal and the other grows on the metal surface. The voltage defines the thickness of the oxide.

Preparation of the OTFTs. Al_2O_3 is used as the dielectric layer in organic thin film transistors (OTFT). OTFT structures are fabricated on glass substrates. Bottom gate, bottom contact OTFTs are processed using aluminum as gate metallization. The surface of the structured aluminum is anodized forming the oxide layer. As drain and source contact material gold is sputtered and patterned. Finally, the acene derivatives were spin-coated as semiconducting layer. The layer was dried under stream of nitrogen gas.

For the OTFTs a channel length l = 10 µm is chosen and the channel width is w = 100 µm. The mobility µ and the threshold voltage V_{th} are extracted from saturation

region of the transfer characteristic. The on/off ratio is based on the maximum and the minimum value of I_{DS}.

Synthesis of acene derivatives 3, 5, 7 and 9

5-ethynyl-1,2,3-trimethoxybenzene[14] and the corresponding quinones (tetracene-5,12-dione, pentacene-6,13-dione and anthradithiophenequinone)[10c,d,13] were synthesized according to literature.

General procedure for the synthesis of acene derivatives

To a solution of 5-ethynyl-1,2,3-trimethoxybenzene (**1**) in dry THF, *n*-butyllithium (2.5 M) in hexane was added by a syringe with stirring under argon atmosphere at -78 °C. The reaction mixture was gradually warmed to room temperature, subsequently the appropriate quinone was added and the solution was stirred for additional 1 h at RT. Afterwards, dilute HCl (10%) saturated with Sn(II)-chloride was added and the mixture was then extracted (3 x 20 ml) with CH_2Cl_2. The combined organic phases were dried with Na_2SO_4 and the solvent was removed *in vacuo*.

9,10-Bis-(3,4,5-trimethoxyphenylethynyl)-anthracene (3)

Anthracene derivative **3** was prepared according to the general procedure using 1.50 g (7.80 mmol) 5-ethynyl-1,2,3-trimethoxybenzene (**1**), 20 ml THF, 4.9 ml (7.84 mmol) *n*-butyllithium-hexane (1.6 M solution), 447 mg (2.15 mmol) anthraquinone **2** and 10 ml of HCl (10%) saturated with Sn(II)-chloride. The orange, highly fluorescent crude product was purified by flash chromatography (100% $CHCl_3$, R_f = 0.31) to obtain **3** as an orange solid (1.09 g, 91%).

Mp: 235 °C; ^{1}H NMR ($CDCl_3$): δ 8.67 (m, 4H), 7.66 (m, 4H), 7.00 (s, 4H), 3.98 (s, 12H), 3.93 (s, 6H); ^{13}C NMR ($CDCl_3$): δ = 153.7, 139.8, 132.5, 127.6, 127.2, 118.4, 117.8, 109.4, 102.9, 85.8, 61.4, 56.7; MS (Maldi (pos.-mode, chloroform)): 558.8 (M^+), calculated 558.2 ($C_{36}H_{30}O_6$); Anal. calcd. for $C_{36}H_{30}O_6$: C, 77.40; H, 5.41; found: C, 77.03; H, 5.46%; UV/Vis (CH_2Cl_2): λ_{max}/nm (ε_{max} /$M^{-1}cm^{-1}$) = 455 (39300), 475 (38300); fluorescence (CH_2Cl_2): λ_{max} = 457 nm, fluorescence quantum yield ϕ_{fl} = 0.58; electrochemistry (CH_2Cl_2, 0.1M TBAHFP, vs. ferrocene): E^{ox} (Acene/Acene$^+$) = 0.60 V.

Single crystals of **3** were obtained by recrystallization from dichloromethane and methanol.

Crystal data of compound 3. $C_{36}H_{30}O_6$, orange cubes, triclinic, a = 5.0294(11), b = 7.47771(17), c = 19.701(4) Å, α = 97.683(4)°, β = 92.558(4)°, γ = 109.440(4)°, V = 689.2 Å^3, T = 100 K, space group P-1, Z = 1, μ(Mo-Kα) = 0.091 mm^{-1}, 11591 reflections measured, 2729 unique (R_{int} = 0.0356), $R1[I>2\sigma(I)]$ = 0.0516, $wR2$ = 0.1326 (all data), g_1 = 0.0714, g_2 = 0.2452 for 235 parameters.

5,12-Bis-(3,4,5-trimethoxyphenylethynyl)-tetracene (5)

Tetracene derivative **5** was prepared according to general procedure using 894 mg (4.67 mmol) 5-ethynyl-1,2,3-trimethoxybenzene (**1**), 20 ml THF, 1.65 ml (4.65 mmol) *n*-butyllithium-hexane (2.5 M solution), 400 mg (1.55 mmol) tetracene-5,12-dione **4** and 10 ml of HCl (10%) saturated with Sn(II)-chloride. The purple, highly fluorescent crude product was purified by flash chromatography (100% $CHCl_3$) to obtain **5** as a dark red solid (377 mg, 45%).

Mp: 222 °C; ^{1}H NMR ($CDCl_3$): δ 8.66 (m, 2H), 8.11 (m, 2H). 7.59 (m, 2H), 7.49 (m, 2H), 7.06 (s, 4H), 4.00 (s, 12H), 3.95 (s, 6H); MS (FAB, 3-nitrobenzylalcohol): 608.4 (M^+), calculated 608.2 ($C_{40}H_{32}O_6$); Anal. calcd. for $C_{40}H_{32}O_6$: C, 78.93; H, 5.30; found: C, 78.85; H, 5.54%; UV/Vis (CH_2Cl_2): λ_{max}/nm (ε_{max} /M^{-1}cm^{-1}) = 560 (28200), 523 (21500); fluorescence (CH_2Cl_2): λ_{max} = 571 nm, fluorescence quantum yield ϕ_{fl} = 0.86; electrochemistry (CH_2Cl_2, 0.1M TBAHFP, vs. ferrocene): E^{ox} (Acene/Acene$^+$) = 0.45 V.

Recrystallization from chloroform and methanol afforded single crystals of **5**.

Crystal data of compound 5. $C_{42}H_{34}O_6$, violet needles, monoclinic, a = 35.241(3), b = 5.6021(5), c = 20.1942(18) Å, β = 90.868(2)°, V = 3986.4 Å^3, T = 100 K, space group $P2_1/c$, Z = 4, μ(Mo-Kα) = 0.478 mm^{-1}, 46446 reflections measured, 7040 unique (R_{int} = 0.0370), $R1[I>2\sigma(I)]$ = 0.0544, $wR2$ = 0.1138 (all data), g_1 = 0.0281, g_2 = 8.0463 for 493 parameters.

6,13-Bis-(3,4,5-trimethoxyphenylethynyl)-pentacene (7)

Pentacene derivative **7** was prepared according to general procedure using 400 mg (2.08 mmol) 5-ethynyl-1,2,3-trimethoxybenzene (**1**), 15 ml THF, 1.4 ml (2.24 mmol) *n*-butyllithium-hexane (1.6 M solution), 125 mg (0.41 mmol) pentacene-6,13-dione (**6**) and 6 ml of HCl (10%) saturated with Sn(II)-chloride. The crude product was purified by flash chromatography (100% $CHCl_3$), followed by a precipitation from saturated dichloromethane solution with methanol, to obtain **7** as a blue solid (55 mg, 21%).

Mp:198 °C; ^{1}H NMR ($CDCl_3$): δ9.20 (m, 4H), 8.01 (s, 4H), 7.42 (m, 4H), 7.11 (s, 4H), 4.03 (s, 12H), 3.98 (s, 6H); MS (Maldi (pos.-mode, chloroform)): 658.3 (M^+), 658.2 calculated ($C_{44}H_{34}O_6$); Anal. calcd. for $C_{44}H_{34}O_6$: C, 80.22; H, 5.20; found: C, 79.35; H, 5.52%; UV/Vis (CH_2Cl_2): λ_{max}/nm (ε_{max} /$M^{-1}cm^{-1}$) = 667 (19600), 614 (12100); fluorescence (CH_2Cl_2): λ_{max} = 681 nm, fluorescence quantum yield ϕ_{fl} = 0.19; electrochemistry (CH_2Cl_2, 0.1M TBAHFP, vs. ferrocene): E^{ox} (Acene/Acene$^+$) = 0.29 V.

5,11-Bis-(3,4,5-trimethoxyphenylethynyl)-dithienoanthracene (9)

Dithienoanthracene derivative **9** was prepared according to general procedure using 155 mg (81 mmol) 5-ethynyl-1,2,3-trimethoxybenzene (**1**), 20 ml THF, 0.32 ml (0.80 mmol) *n*-butyllithium-hexane (2.5 M solution), 60.0 mg (0.19 mmol) anthradithiophenequinone (**8**) and 10 ml of HCl (10%) saturated with Sn(II)-chloride. The purple, highly fluorescent crude product was purified by flash chromatography (100% $CHCl_3$, R_f = 0.31), followed by precipitation from a saturated dichloromethane solution with methanol, to obtain **9** as a violet solid (30.0 mg, 35%).

Mp: 250 °C; ^{1}H NMR ($CDCl_3$): δ9.13-9.21 (m, 4H), 7.48-7.58 (m 4H), 7.08 (m, 4H), 4.01 (m, 12H), 3.96 (s, 6H); MS (FAB, pos.-mode): 670.5 (M^+), calculated 670.1 ($C_{40}H_{30}O_6S_2$); UV/Vis (CH_2Cl_2): λ_{max}/nm (ε_{max} /$M^{-1}cm^{-1}$) = 572 (29800), 533 (17499); fluorescence (CH_2Cl_2): λ_{max} = 588 nm, fluorescence quantum yield ϕ_{fl} = 0.82; electrochemistry (CH_2Cl_2, 0.1M TBAHFP, vs. ferrocene): E^{ox} (Acene/Acene$^+$) = 0.36 V.

3.9. References and Notes

[1] (a) T. W. Kelley, P. F. Baude, C. Gerlach, D. E. Ender, D. Muyres, M. A. Haase, D. E. Vogel, S. D. Theiss, *Chem. Mater.* **2004**, *16*, 4413-4422; (b) C. Reese, M. Roberts, M. Ling, Z. Bao, *Mat. Today* **2004**, *7*, 20-27; (c) M. Bendikov, F. Wudl, D. F. Perepichka, *Chem. Rev.* **2004**, *104*, 4891-4946 ; (d) C. D. Dimitrakopoulos, P. R. L. Malenfant, *Adv. Mater.* **2002**, *14*, 99-117; (e) F. Würthner, *Angew. Chem.* **2001**, *113*, 1069-1071; *Angew. Chem. Int. Ed.* **2001**, *40*, 1037-1039; (f) H. Klauk, *Nat. Mater.* **2007**, *6*, 397-398; (g) A. Dodabalapur, *Mater. Today* **2006**, *9*, 24-39; (h) A. Facchetti, *Mater. Today* **2007**, *10*, 28-37.

[2] (a) C. D. Sheraw, L. Zhou, J. R. Huang, D. J. Gundlach, T. N. Jackson, M. G. Kane, I. G. Hill, M. S. Hammond, J. Campi, B. K. Greening, J. Francl, J. West, *Appl. Phys. Lett*. **2002**, *80*, 1088-1090; (b) H. E. A. Huitema, G. H. Gelinck, J. B. P. H. van der Putten, K. E. Kuijk, C. M. Hart, E. Cantatore, P. T. Herwig, A. J. J. M. van Breemen, D. M. de Leeuw, *Nature* **2001**, *414*, 599; (c) L. Zhou, A. Wanga, S.-C. Wu, J. Sun, S. Park, T. N. Jackson, *Appl. Phys. Lett.* **2006**, *88*, 083502.

[3] (a) Z. Zhu, J. T. Mason, R. Dieckmann, G. G. Malliaras, *Appl. Phys. Lett*. **2002**, *81*, 4643-4645; (b) C. Bartic, A. Campitelli, S. Borghs, *Appl. Phys. Lett.* **2003**, *82*, 475-477; (c) B. K. Crone, A. Dodabalapur, R. Sarpeshkar, A. Gelperin, H. E. Katz, Z. Bao, *J. Appl. Phys.* **2002**, *91*, 10140-10146; (d) Y. Noguchi, T. Sekitani, T. Someya, *Appl. Phys. Lett.* **2006**, *89*, 253507.

[4] (a) D. Voss, *Nature* **2000**, *407*, 442-444; (b) B. Crone, A. Dodabalapur, Y.-Y. Lin, R. W. Filas, Z. Bao, A. LaDuca, R. Sarpeshkar, H. E. Katz, W. Li, *Nature* **2000**, *403*, 521-523; (c) B. Yoo, T. O. Jung, D. Basu, A. Dodabalapur, B. A. Jones, A. Faccetti, M. R. Wasielewski, T. J. Marks, *Appl. Phys. Lett.* **2006**, *88*, 082104; (d) R. C. G. Naber, B. de Boer, P. W. M. Blom, D. M. de Leeuw, *Appl. Phys. Lett.* **2005**, *87*, 203509; (e) H. Klauk, *Nat. Mater.* **2007**, *6*, 397-398.

[5] (a) H. Klauk, M. Halik, U. Zschieschang, G. Schmidt, W. Radlik, W. Weber, *J. Appl. Phys.* **2002**, *92*, 5259-5263; (b) O. D. Jurchescu, J. Baas, T. T. M. Palstra, *Appl. Phys. Lett*. **2004**, *84*, 3061-3063; (c) T. W. Kelley, D. V. Muyres, P. F. Baude, T. P. Smith, T. D. Jones, *Mat. Res. Soc. Symp. Proc.* **2003**, Vol 771.

[6] For a recent review on acenes, see: J. E. Anthony, *Angew. Chem.* **2008**, *120*, 460-492; *Angew. Chem. Int. Ed*. **2008**, *47*, 452-483.

[7] (a) P. T. Herwig, K. Müllen, *Adv. Mater.* **1999**, *11*, 480-483; (b) A. Afzali, C. D. Dimitrakopoulos, T. L. Breen, *J. Am. Chem. Soc.* **2002**, *124*, 8812-8813; (c) H. Yamada, Y. Yamashita, M. Kikuchi, H. Watanabe, T. Okujima, H. Uno, T. Ogawa, K. Ohara, N. Ono, *Chem. Eur. J.* **2005**, *11*, 6212-6220.

[8] (a) J. A. Merlo, C. R. Newman, C. P. Gerlach, T. W. Kelly, D. V. Muyres, S. E. Fritz, M. F. Toney, C. D. Frisbie, *J. Am. Chem. Soc.* **2005**, *127*, 3997-4009; (b) H. Meng, F. Sun, M. B. Goldfinger, G. D. Jaycox, Z. Li, W. J. Marshall, G. S. Blackman, *J. Am. Chem. Soc.* **2005**, *127*, 2406-2407; (c) S. Ando, R. Muratami, J. Nishida, H. Tada, Y. Inoue, S. Tokito, Y. Yamashita, *J. Am. Chem. Soc.* **2005**, *127*, 14996-14997.

[9] (a) F. Würthner, R. Schmidt, *ChemPhysChem* **2006**, *7*, 793-797; (b) R. D. McCullough, *Adv. Mater.* **1998**, *10*, 93-116.

[10] (a) M. M. Payne, S. R. Parkin, J. E. Anthony, C. Kuo, T. N Jackson, *J. Am. Chem. Soc.* **2005**, *127*, 4986-4987; (b) C. D. Sheraw, T. N. Jackson, D. L. Eaton, J. E. Anthony, *Adv. Mater.* **2003**, *15*, 2009-2011; (c) C. R. Swartz, S. R. Parkin, J. E. Bullock, J. E. Anthony, A. C. Mayer, G. G. Malliaras, *Org. Lett.* **2005**, *7*, 3163-3166; (d) M. M. Payne, S. A. Odom, S. R. Parkin, J. E. Anthony, *Org. Lett.* **2004**, *6*, 3325-3328.

[11] J. Cornil, D. Beljonne, J.-P. Calbert, J-L. Brédas, *Adv. Mater.* **2001**, *13*, 1053-1067.

[12] (a) A. Maliakal, K. Raghavachari, H. Katz, E. Chandross, T. Siegrist, *Chem. Mater.* **2004**, *16*, 4980-4986; (b) P. Coppo, S. G. Yeates, *Adv. Mater.* **2005**, *17*, 3001-3005.

[13] B. Serpaud, Y. Lepage, *Bull. Chem. Soc. Fr.* **1977**, 539-542.

[14] N. J. Lawrence, F. A. Ghani, L. A. Hepworth, J. A. Hadfield, A. T. McGown, R. G. Pritchard, *Synthesis* **1999**, *9*, 1656-1660.

[15] (a) S. A. Odom, S. R. Parkin, J. E. Anthony, *Org. Lett.* **2003**, *5*, 4245-4248; (b) D. R. Maulding, B. C. Roberts *J. Org. Chem*. **1968**, *34*, 1734-1736.

[16] *Purification of Laboratory Chemicals* (Eds. D. D. Perrin, W. L. Amarego, D. R. Perrin), Pergamon Press Ltd., Oxford, **1980**.

[17] R. Gvishi, R. Reisfeld, Z. Burshtein, *Chem. Phys. Lett.* **1993**, *213*, 338-334.

[18] (a) T. Kottke, D. Stalke, *J. Appl. Crystallogr.* **1993***, 26,* 615-619; (b) T. Kottke, R. J. Lagow, D. Stalke*, J. Appl. Crystallogr*. **1996**, *29*, 465-468; (c) D. Stalke, *Chem. Soc. Rev*. **1998**, *3*, 117-178.

[19] G. M. Sheldrick, *SADABS 2.05: Program for Area Detector Absorption Correction*, University of Göttingen, **2002**.

[20] G. M. Sheldrick, *Acta Crystallogr. Sect. A,* **1990**, *46*, 467-473.

[21] G. M. Sheldrick, *SHELXL-97 – Program for Structure Refinement*, University of Göttingen, **1997**.

Chapter 4

Synthetic Routes to Core-fluorinated Perylene Bisimide Dyes and their Properties

Abstract: A broad spectrum of core-fluorinated perylene bisimide dyes with varied substituents at imide positions have been synthesized by imidization of the difluoro-substituted perylene bisanhydride with the respective amines or by nucleophilic halogen exchange reaction (Halex process) of the corresponding dibromo- and tetrachloro-substituted perylene bisimides with potassium fluoride. More interestingly, core-fluorinated perylene bisimide pigments containing no imide groups could be obtained for the first time by deprotection of methylbenzyl substituents at imide N atoms. The solubility of the synthesized derivatives ranges from insoluble pigments to highly soluble liquid crystalline compounds. Compared with the parent unsubstituted perylene bisimides, these fluorinated dyes display hypsochromically shifted absorption and fluorescence spectra with fluorescence quantum yields up to unity enabling bright yellow emission. The electrochemical properties of these electron-poor perylene bisimides and the packing properties of a tetra-fluorinated derivative in solid state have been presented.[a]

[a] A part of this chapter was published: F. Würthner, P. Osswald, R. Schmidt. T. E. Kaiser, H. Masikkamäki, M. Könemann, *Org. Lett*. 2006, *8,* 3765-3768.

4.1 Introduction

Organic semiconductors have gained great attention due to their promising applications in organic field effect transistors (OFETs),[1] light emitting diodes (OLEDs),[2] and solar cells.[3] Whilst several classes of organic materials with high p-type charge carrier mobility had been known for long time, their n-type counterparts have become available only recently. One general approach toward n-type semiconducting materials is the attachment of perfluorinated substituents at electron poor π–conjugated cores, e.g., naphthalene bisimides[4] and thiazols,[5] or even at originally electron rich π–conjugated systems, e.g., oligothiophenes,[6] acenes,[7] and phthalo- cyanines.[8] Among organic n-type semiconductors, perylene bisimide dyes (PBIs) are very auspicious candidates as in bay area (1,6,7,12-position) unsubstituted perylene bisanhydrides and PBIs are considered to be the archetype n-type semiconducting materials. Their applications in solar cell devices and OFETs have been demonstrated.[9] Recently, high charge carrier mobilities up to 2.1 cm^2/Vs were determined for vapor-deposited films.[9c] PBIs bearing four chlorine atoms in the bay positions have also been investigated for applications in thin film transistors, and charge carrier mobilities up to 0.18 cm^2/Vs were determined for vapor-deposited films.[10] Furthermore, the introduction of two strongly electron-withdrawing cyano groups in the bay area has significantly improved the applicability of PBI dyes with air-stable charge carrier mobilities up to 0.64 cm^2/Vs.[11a] Surprisingly, no core-fluorinated PBIs are known in literature, which might be explained by the more challenging synthetic accessibility compared to the chlorinated or brominated PBIs.

Nevertheless, the introduction of electron-withdrawing and, in particular, fluorine groups afforded significant improvements of the n-type semiconducting properties for several classes of organic semiconductors.[11] Thus, in this work perylene bisimide dyes bearing two or four fluorine atoms at the bay position were synthesized for the first time. Nucleophilic displacement of bromine or chlorine by fluoride ions appeared to be a promising strategy for the synthesis of core-fluorinated perylene bisimides.[12] Indeed, fluorine atoms could be introduced into the bay position of perylene bisimides by nucleophilic substitution of brominated or chlorinated PBIs with potassium fluoride in tetrahydrothiophene-1,1-dioxide (sulfolane) as solvent in the presence of (*N,N*-dimethylimidazol-idino)-tetramethylguanidinium chloride (CNC^+, Scheme 1). The latter was recently used as an efficient catalyst for such Halex reactions.[13] Alternatively, the common transfer catalyst 18-crown-6 can be used for this purpose.

Core-fluorinated perylene bisimides without imide substituents are also of interest as the corresponding parent compound itself is a n-type semiconductor, and incorporation of fluorine atoms into the bay are will enhance its electron-accepting properties. However, such core-fluorinated PBIs are so far not known. Here we report that di- and tetrafluorianted PBIs with N-H imide functionality are accessible by a novel deprotection procedure developed in our group.[14]

4.2 Synthesis

The core-fluorinated perylene bisimides **4** and **5** were synthesized either by imidization or halogen exchance reaction as outlined in Scheme 1. The starting material perylene bisanhydride **1**[15] was obtained from the BASF SE, while the precursor PBIs **2** and **3** were synthesized according to literature methods.[16]

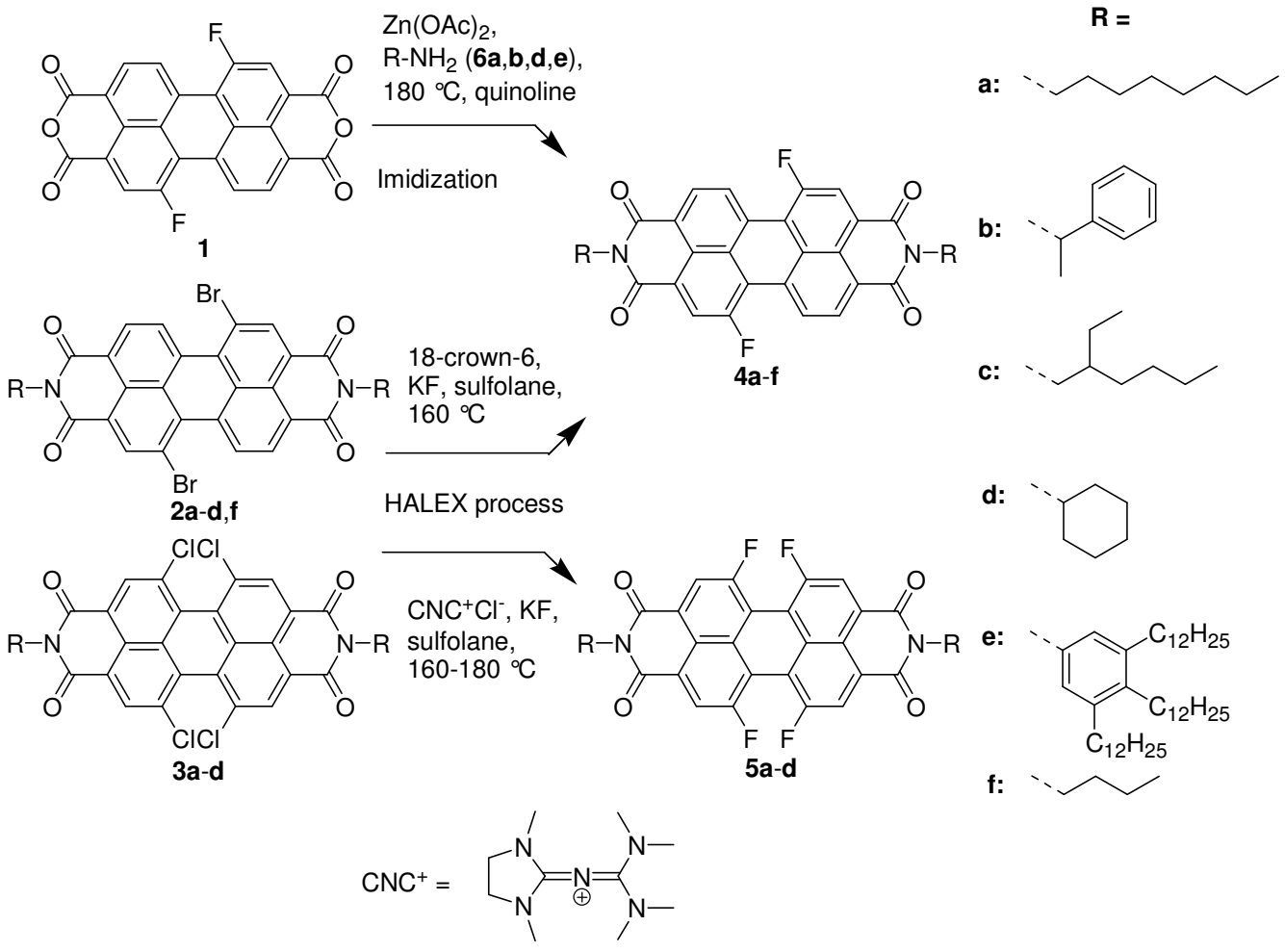

Scheme 1. Synthesis of PBIs **4** and **5**.

Imidization of difluorinated perylene bisanhydride **1** with amines **6a**,**b**,**d** or **e** afforded the corresponding difluorinated perylene bisimides **4a**,**b**,**d** and **e** in relatively lower yields (<27%, see Table 1). The reasons for these unsatisfactory yields might be, on the one hand, the insufficient purity of the starting material **1**[15] and on the other hand, facile nucleophilic exchange of fluorine atoms by aliphatic amines. Indeed, the reaction of perylene bisanhydride **1** with an excess of octylamine afforded high amounts of a green byproduct with a NH-octyl substituents in bay position. Thus, the Halex process of the dibrominated perylene bisimides **2a**-**d** and **f** was chosen to obtain the difluorinated products **4a**-**d** and **f** in better yields. This reaction was carried out in sulfolane with potassium fluoride and catalytic amounts of 18-crown-6 and, indeed, significantly higher yields (between 25 and 60%, Table 1) were achieved. Notably, the use of CNC^+ catalyst for this reaction was less successful.[17]

Table 1: Yields (%) of difluorinated PBIs **4a-f** by imidization of PBA **1** or Halex reaction of PBIs **2a**-**d**, **f** .

	yield (%)	
PBI	Imidization	Halex reaction[a]
4a	13	59[17]
4b	27	60
4c	[b]	46
4d	10	46[17]
4e	12	[b]
4f	[b]	25

[a] catalyst: 18-crown-6; [b] Not performed.

The Halex reaction of tetrachlorinated perylene bisimides **3a**-**e** afforded the corresponding tetrafluorinated PBIs **4a**-**c** in lower yields (Table 2), while for PBI **3d** no conversion was observed. The deficient yields can be explained by the sterical congestion imparted by four halogen atoms and the required four step reaction sequence for halogen exchange. For this Halex reaction, the CNC^+ catalyst was used, as this catalyst was developed particularly for the chloride-fluoride exchange,[13] while 18-crown-6 is a quite general phase transfer catalyst. The solubility of PBIs in sulfolane has a strong influence on the yield as for the insoluble PBI **3d**[17] no conversion could be observed and the yield (3%) of less soluble dye **5a** was significantly lower than those for the better soluble compounds **5b** and **c** (20 and 18%). Replacement of the CNC^+ with the 18-crown-6 catalyst led to even lower yields or decomposition, respectively.

Table 2: Yields of tetrafluorinated PBIs **5a**-**d** by Halex process of chlorinated PBIs **3a**-**c**.

PBI	**5a**	**5b**	**5c**
yield (%)	3	20[a]	18[a]

[a] These yields are based on the conversion of the PBIs **3b** and **3c**, respectively, as about 50% of the starting materials was recouverd (see Experimental section).

More interstingly, the core-fluorinated PBIs with NH imide groups **4h** and **5h** could be synthesized for the first time by cleavage of the α-methyl-benzyl imide substituents of **4b** and **5b**, respectively, with boron tribromide in dichloromethane in nearly quantitative yields (Scheme 2). These fluorinated PBIs are insoluble pigments that could be characterized only by mass spectrometry. Noteworthy, that the above-mentioned deprotection method is applicable not only to PBI derivatives bearing electron-withdrawing bay substituents, but also to those containing electron-donating core substituents such as amines[14a] and aryloxy groups.[18] Thus, boron tribromide mediated deprotection of α-methyl-benzyl imide substituents is a general method with broad scope for the synthesis of core-substituted perylene bisimides with NH imide functionalities.

By saponification of **5c** the tetrafluorinated perylene bisanhydride **7** could be obtained in a yield of 94%. Mass spectrometry revealed an impurity of a trifluoro-hydroxy substituted perylene that obviously originated from nucleophilic substitution of one fluorine by potassium hydroxide. The saponification of **4c** led also to an insoluble compound, but the desired product could neither be isolated nor identified.

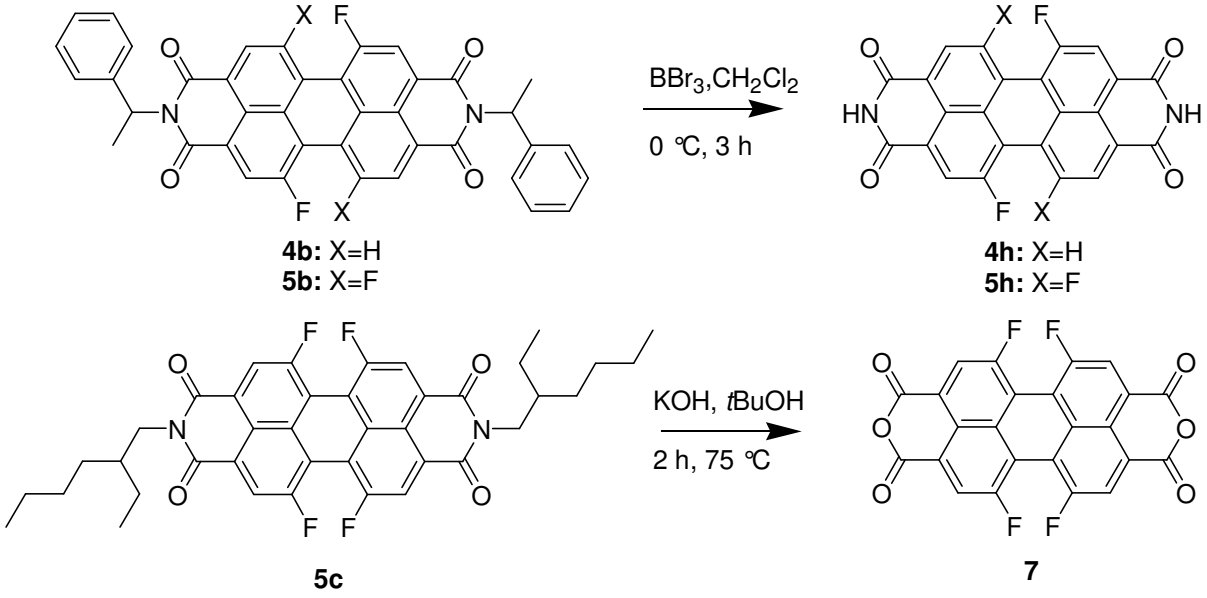

Scheme 2. Synthesis of PBIs **4h**, **5h** and bisanhydride **7**.

4.3 Optical Properties

The optical properties of the perylene bisimide dyes **4** and **5** were investigated by UV/Vis and fluorescence spectroscopy. Absorption and fluorescence spectra of difluorinated PBI **4f** and tetrafluorinated derivative **5b** are shown as representative examples in Figure 1 and the optical data for all compounds are collected in Table 3. The absorption spectra of difluorinated compounds **4a**-**f** show a well-defined vibronic fine structure of the S_0-S_1 transition with maxima between 508 and 511 nm, depending on the imide substituent. The absorption and emission maxima of difluorinated derivatives are hypsochromically shifted by 16 and 17 nm, respectively, in comparison with those of the related unsubstituted PBI derivatives. Such hypsochromic shifts are unprecedented for PBI dyes and enable for the first time bright yellow fluorescence colors for this class of fluorophores. The similar absorption coefficients and vibronic progressions in the spectra of difluorinated and unsubstituted perylene bisimides are in agreement with a flat, rather than a twisted, perylene core as demonstrated for single crystal X-ray analysis of a difluorinated PBI derivatve.[17]

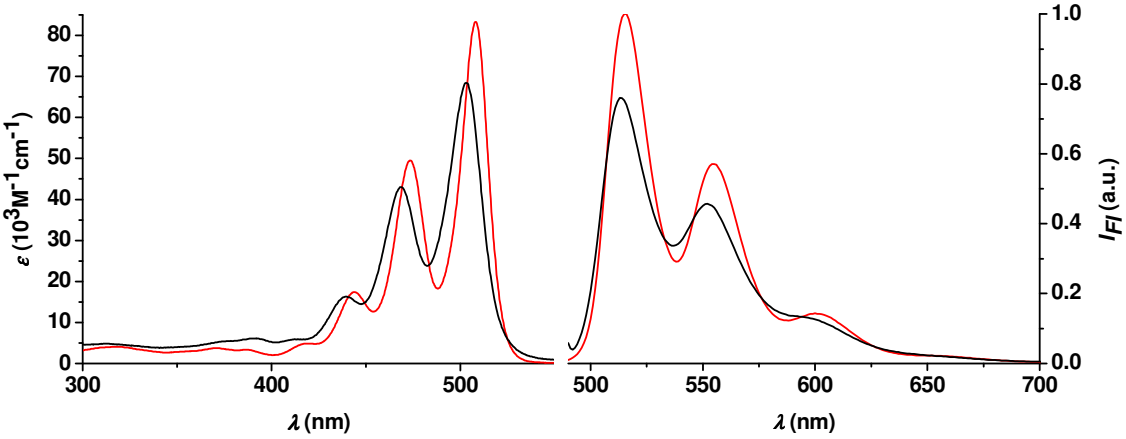

Figure 1. UV/Vis absorption spectra (left) and fluorescence emission (right) spectra of **4f** (red) and **5b** (black) in dichloromethane.

The absorption maxima for tetrafluorinated PBIs **5a**-**c** are even further shifted to shorter wavelength (503 to 500 nm). Their extinction coefficients are considerably decreased at an average of 19% compared to those of difluorinated derivatives **4a**-**f** which can be attributed to the twist of the perylene core in former compounds as demonstrated for **5a** by X-ray analysis (see below). The fluorescence spectra of all core-fluorinated PBIs fulfill the mirror image condition as exemplified for compounds **4f** and **5b** in Figure 1. The core-fluorinated PBIs presented here possess rather small Stokes shifts (5-12 nm) indicating the quite rigid structure of the molecules. Nearly all

of the dyes exhibit very high fluorescence quantum yields (85-100 %) which corresponds very well with the values reported for unsubstituted PBI derivatives. The only exception is liquid crystalline dye **4e**, which has lower fluorescence quantum yield of 35%. This value is in good accordance with the low quantum yields of dyes with identical imide substituents,[19] where the fluorescence quenching can be explained by photo-induced electron transfer process to the electron rich imide substituents.

Table 3: UV/Vis absorption and fluorescence emission properties of core fluorinated perylene bisimide dyes **4** and **5** in DCM.

PBI	λ_{abs} [nm]	ε [M^{-1} cm^{-1}]	λ_{em} [nm]	ϕ_{fl}[a]
4a[17]	508	81300	514	1.00
4b	510	80900	518	0.98
4c	508	76600	516	1.00
4d[17]	508	89000	513	0.98
4e	511	96900	518	0.35
4f	508	83300	515	1.00
5a[17]	500	66000	509	0.88
5b	503	68400	514	0.85
5c	501	71900	513	1.00

[a] ϕ_{fl} ± 0.03 (average deviction); the quantum yields were determined at three different wavelenghts with *N,N´*-di(2,6-diisopropyl-phenyl)-perylene-3,4:9,10-tetracarboxylic acid bisimide (ϕ_{fl} = 1.00 in chloroform) as reference (for details see Experimental part).

4.4 Electrochemical Properties

The electrochemical properties of core-fluorinated PBIs **4** and **5** were investigated by cyclic voltammetry and their reduction potentials are given in Table 4. Exemplified cyclic voltammograms for **4b** and **5c** are shown in Figure 2. The fluorinated PBIs exhibit two reversible reduction waves, whereas within the accessible scanning range in dichloromethane no oxidation waves could be detected. The first reduction waves for **4a**-**f** were observed at -1.02 V to -1.08 V vs. Fc/Fc^+, while the second reduction waves appeared at -1.26 V to -1.29 V. Both first and second reduction waves of tetrafluorinated PBIs **5a**-**c** were observed at slightly higher potentials (-0.98 and -1.21 V vs. Fc/Fc^+), indicating that the tetrafluorinated perylene bisimides are easier to reduce than the corresponding difluorinated derivatives, as expected. In regard to imide substituents on redox properties, aromatic substituents (e.g. **4e**) lead to a decrease of the reduction potential by 20-50 mV compared to primary aliphatic

substituents. This increase or decrease can be explained by the moderate electron withdrawing effect of the aromatic.

Interestingly, the influence of the fluorine core-substituents is very small as the core-unsubstitued reference compound *N,N´*-di(cyclohexyl)-perylene-3,4:9,10-tetracarboxylic acid bisimide shows under identical conditions a first reduction potential of about -1.10 V which is only 20 mV lower than the potential of the difluorinated compound **4d**, but still significantly lower (>200 mV)[20] than those for core-chlorinated or brominated PBIs.

Table 4: First and second half-wave reduction potentials (in V vs Fc/Fc^+) of core-fluorinated perylene bisimides **4** and **5**

PBI	E (PBI/PBI^-)[V][a]	E (PBI^-/PBI^{2-})[V][a]	ε LUMO [eV][b]
4a	-1.04	-1.26	-3.76
4b	-1.04	-1.25	-3.76
4c	-1.07	-1.28	-3.73
4d	-1.08	-1.29	-3.72
4e	-1.02	-1.26	-3.78
4f	-1.04	-1.25	-3.76
5a	-0.98	-1.22	-3.82
5b	-0.98	-1.21	-3.82
5c	-0.98	-1.21	-3.82

[a] Measured in 0.1 M solution of Bu_4NPF_6 in dichloromethane with a scan rate of 100 mV/s; ferrocene served as internal standard; [b] calculated according to literature methods using the equation: ε LUMO = -4.8eV–(E(PBI/PBI^-).[21]

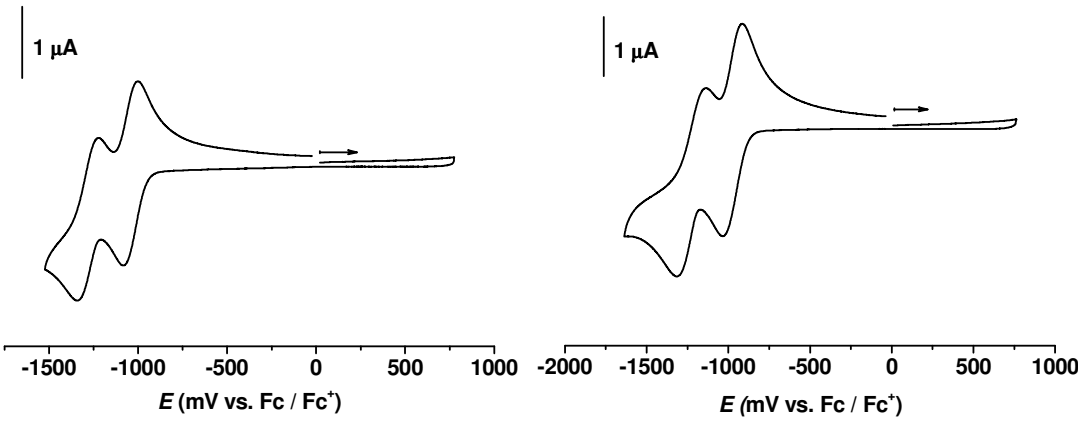

Figure 2. Cyclic voltammograms of **4b** (left) and **5c** (right).

4.5 Properties in the Solid State

A solvent free single crystal of **5a** suitable for X-ray analysis could be obtained by slow evaporation of a dichloromethane solution. The molecular structure **5a** is depicted

in Figure 3. For derivative **5a**, bearing four fluorines at the bay position, the twisting of the perylene core was surprisingly unsymmetrical, but, as expected, significantly larger than for difluorinated perylene bisimide dyes.[17] Thus, the dihedral angle on the one bay area is ~17° (carbon atoms C16-C4-C3-C22), the other being ~28° (carbon atoms C24-C5-C7-C15). The extended twist angle for **5a** can mainly be attributed to the repulsive interactions of the strongly electronegative fluorine atoms at the bay area.

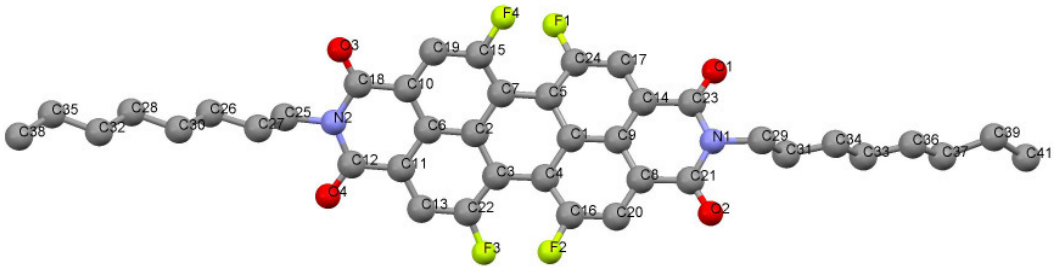

Figure 3. Ball and stick representation of the molecular structure of PBI **5a** in the crystal.

The unsymmetrical distortion is most probably induced by packing effects and intermolecular interactions in the crystal lattice, allowing a denser arrangement in the solid state. The fluorine atoms possess a van-der-Waals radius of 135 pm, which is in between that of oxygen (140 pm) and hydrogen (120 pm). Due to this small size of the fluorine atom, the difluorinated PBI exhibits a nearly planar perylene core quite similar to the unsubstituted PBIs,[22] while e.g. tetraphenoxy-substituted PBIs possess a torsion angle of 25-30° in the solid state.[23] The crystal packing of **5a** is shown in Figure 4. The dyes are arranged in stacks along the a axis of the unit cell, but the stacked molecule share less than 50% of their perylene core surface. Two molecules of **5a** with opposite chirality are found in one unit cell (blue = *P*-enantiomer, red = *M*-enantiomer). Furthermore, no solvent molecules are embedded in the crystal lattice, which is quite unusual for a perylene molecule of this size and only the outer areas of the octyl substituents were partly disordered. The chirality induced by the twist of the bay area can be observed also in crystal structures of other tetrasubstituted perylene bisimide dyes,[23b] and only very recently the enantiomers of a tetrabromo-substituted PBI were found to be conformationally stable at room temperature.[24]

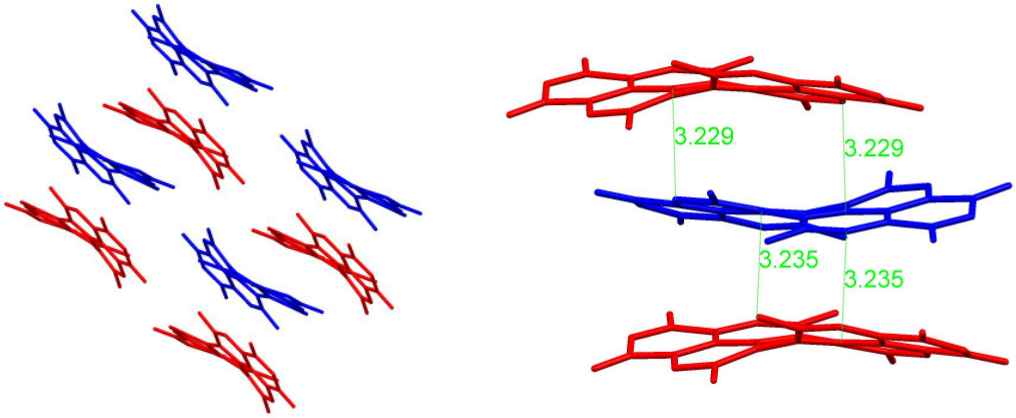

Figure 4. Crystal packing of **5a**, the *P*-enantiomers are blue, the *M*-enantiomers red colored (left). Distances between naphthalene subunits of the two neighbouring molecules are given in Å (right).

The closest intermolecular contacts of about 2.4 Å, which can be assigned to CH···O contacts, are found between the hydrogens of a perylene core and the oxygens of an imide group. The clostest π–π interactions are given between neighboring molecules of opposite chirality in one stack and range between 3.2-3.3 Å, which is smaller than the interplane spacing of graphite.[25] The intermolecular distances between the π–surfaces of naphthalene units in a stack are quite similar, thus no preferential dimer formation is given. Furthermore, as shown in Figure 5, the lipophilic aliphatic octyl chains and the aromatic perylene cores are well separated in the crystal. This packing should enable at least a two dimensional charge carrier transport along the PBI stacks, hence this PBI is potentially interesting for an application as active layer in OTFTs.

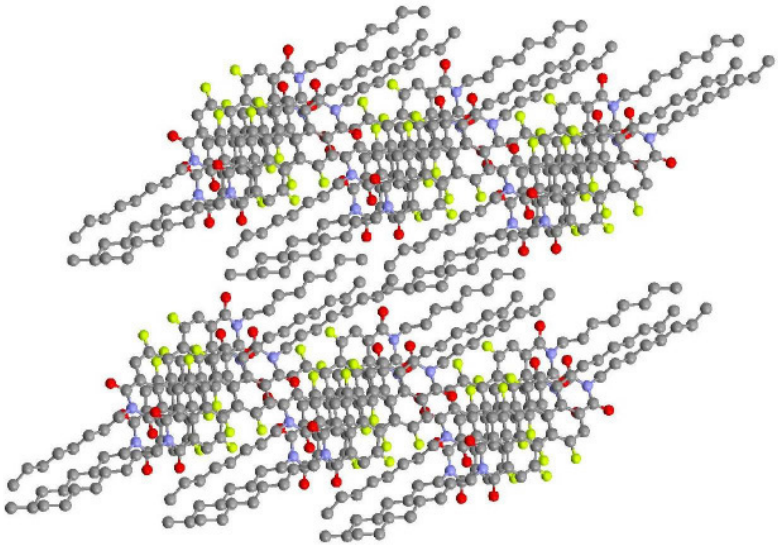

Figure 5. Separation of aliphatic imide substituents and aromatic cores for PBI **5** in the crystal.

4.6 Examination of the Mesophase Properties of 4e

Several tridodecylphenyl substituted perylene bisimide derivatives are known in literature[19] and they exhibit liquid crystalline mesophases. Therefore the liquid crystalline properties of PBI **4e** were examined by DSC and polarization microscope studies. As the single crystal X-ray analysis of a difluorinated PBI derivative revealed a nearly planar π–system with a very low torsion angle of about 3°,[17] the potential π–π interactions of this compound in condensed state should be more similar to the core-unsubstituted PBI **8** than to that of the highly twisted dibrom- **9** or tetrachlorinated compounds **10** (Figure 6). The DSC thermogram of PBI **4e** (Figure 7) shows a LC to isotropic phase transition with an endothermic peak at 321 °C with ΔH of 19.7 kJ/mol (12.4 J/g) which is very similar to that of the core-unsubstituted reference compound **8** (Table 5).

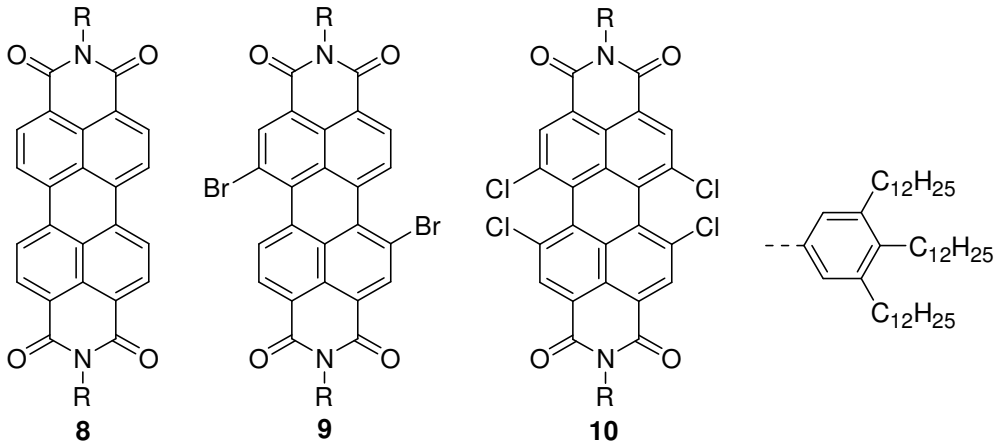

Figure 6. Literature known liquid crystalline PBI derivatives **8**, **9**, and **10**.

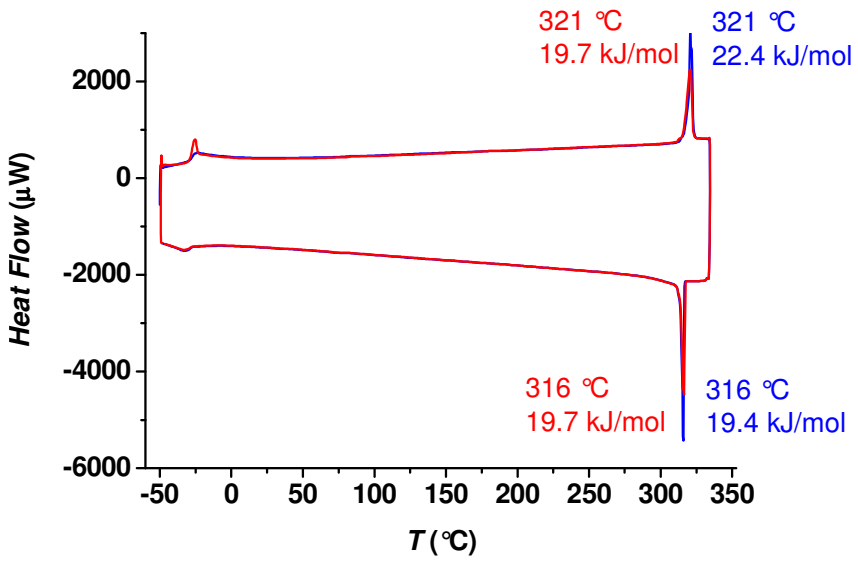

Figure 7. Differential scanning calorimetry profile of PBI **4e**: First heating and first cooling (blue line) and second heating (red line), heating rate 10 K/min.

Table 5: Clearing temperature *T*, transition enthalpies ΔH, and entropies ΔS for the LC to isotropic transitions of PBI **4e** and reference compounds.[19]

PBI	*T* [°C]	ΔH [kJmol^{-1}]	ΔS [Jmol^{-1}K^{-1}]
4e	321	19.7	33.2
8[19]	300	18.6	32.5
9[19]	160	2.7	6.2
10[19]	110	8.4	21.9

Under the polarizing optical microscope (Figure 8, left) a growing dendritic texture was observed for the LC phase, revealing a liquid crystalline columnar phase similar to **8**. Although the compound has still a quite high viscosity, shearing of **4e** at 200 °C was possible (Figure 8, right). These observations reveal that two fluorine atoms in bay position have only small impact on the optical, redox, and packing properties of perylene bisimide dyes compared to the core-unsubstituted derivatives.

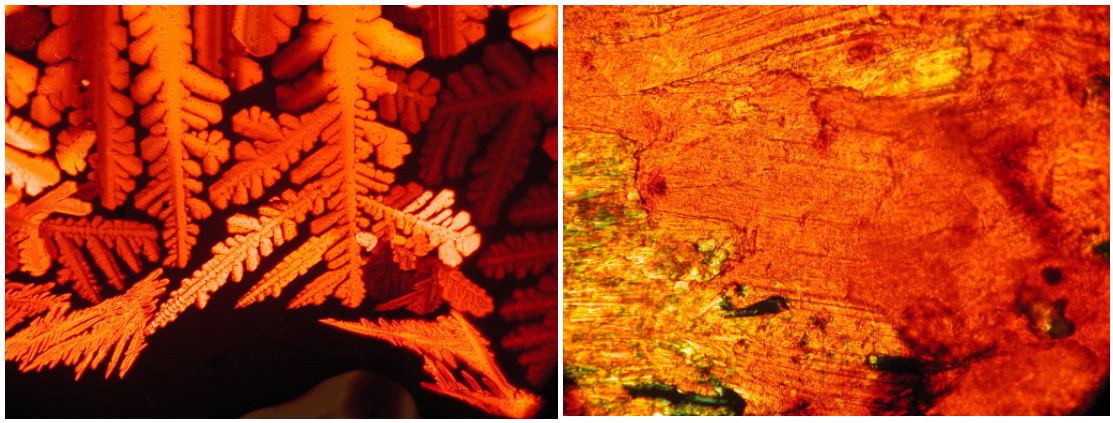

Figure 8. Growing optical texture of perylene bisimide **4e** at 285 °C, cooling rate 2K/min (left) and shearing of the sample at 200 °C (right).

The order of the LC phase was further determined by XRD-measurements done by Dr. Ute Baumeister at the University of Halle. On the wide angle X-ray scan several reflexes indicate a liquid crystalline and columnar mesophase. The longitudinal axes of the columns are oriented in favor parallel to the longitudinal axis of the sample. Sharp and intensely reflexes in the small angle region of the meridian fit to this hexagonal phase with a lattice parameter ***a*** = 28.8 Å. The stack distance within the columns can be determined from the intensive and quite sharp reflex at the outside of the equator of the recording (h = 3.35 Å). Calculation of the molecule volume in a crystal phase gives by using the increment method of Immirzi and Perini[26] a value of 2,480.8 Å^3. The volume of a column disc can be calculated to $\boldsymbol{a}^2 \times \sin(120°) \times h$ = 2,398.0 Å^3. According to these two values the number of molecules in the cross section of one such column is exactly one.

4.7 Conclusion

Two series of hitherto unknown di- and tetrafluorinated perylene bisimide dyes were synthesized and characterized. The direct imidization of the difluorinated perylene bisanhydride led to significant lower yields than the Halex conversion of the dibrominated perylene bisimides. The lower yields can be explained by the impure starting material and the tendency of these more sensible materials to undergo side reactions with highly nucleophilic amines. In case of the Halex reaction of tetrachlorinated perylene bisimides, decomposition of the desired product could not be circumvented. Therefore, the reaction had to be terminated after partial conversion of the starting material to avoid extended product decomposition. Nevertheless, the intermediate products and unreacted starting material could be isolated and re-used, leading to overall yields of about 20%.

The physical attributes of the disubstituted derivatives are, apart from the hypsochromic shift of the optical absorption and emission, quite similar to the corresponding unsubstituted dyes. The PBIs can also build up strong π–π interactions in the solid and liquid crystalline state due to their negligible torsion angle in the bay area. Nevertheless, the quadrupole moment of the dyes is changed by the two bay-substituents, which makes a modified packing of the dyes in the solid state quite probable. The structural attributes of tetrafluorinated derivatives are more similar to other tetrasubstituted dyes (e.g., tetrachloro). For one example the packing in solid state reveals close π–π distances between the naphthalene units of the twisted chromophores.

Since good π–π interactions are inevitable for high charge carrier mobilities, particularly the difluorinated chromophores represent a promising class of n-type semiconductors for organic electronic applications.

4.8 Experimental Section

Materials and methods. Dibrominated PBIs **2a,c,d,f** and tetrachlorinated PBIs **3a,c,d** were synthesized according to literature.[16] For the former compounds isomeric mixtures of the 1,7 and 1,6 isomers in a ratio of about 9:1 were used. The difluorinated perylene bisanhydride starting material was obtained from BASF SE. Potassium fluoride, zinc acetate, propionic acid, cyclohexylamine, 1-*n*-octylamine, ethylhexylamine, 1-*n*-butylamine, 1-phenylethylamine, sulfolane, 18-crown-6 and silica

gel (Si 60, 40-63 µm) were purchased from commercial source, i.e. Merck, Fluka, Aldrich, or Fluka, while tridodecylaniline was synthesized according to literature.[27] Potassium fluoride was dried in vacuum (60 °C/10^{-3} mbar), sulfolane was fractionally destilled under vacuum prior to use. All other chemicals and solvents were used as received. The catalyst (*N,N´*-dimethylimidazolidino)-tetramethylguanidinium chloride (CNC^+) was synthesized according to literature procedures.[28]

Thin layer chromatography. Thin layer chromatography was performed on aluminium foils which were coated with silica gel 60 F_{254} and a concentration zone, perchased from Merck KGaA (Hohenbrunn, Germany).

Column chromatography. Flash and normal pressure column chromatography were done using silica gel Si60 (mesh size 0.032-0.063 mm) from Merck KGaA (Hohenbrunn, Germany) as stationary phase.

Melting points. Melting points were determined using a Olympus Bx41 polarization microscope (Olympus GmbH, Hamburg, Germany) equipped with a heating table (THMS 600, Linkam, Great Britain) and are uncorrected.

NMR spectroscopy. ^{1}H NMR spectra (400 MHz) were recorded on Bruker Advance 400 spectrometer; chemical shifts in $CDCl_3$ are given relative to $CHCl_3$ (δ = 7.26 ppm). ^{19}F NMR spectra (376.5 MHz) were recorded on Bruker Avance 400 spectrometer , chemical shifts in $CDCl_3$ are given relative to $CCIF_3$ (δ = 0.0 ppm)

Absorption and fluorescence spectroscopy. For all measurements, spectroscopic grade solvents (Uvasol®) from Merck were used. UV/Vis spectra were measured in quartz glass cuvettes under ambient conditions unless otherwise stated. The measurements were performed with a PE 950 spectrometer (Perkin Elmer GmbH, Rodgau, Germany). Fluorescence emission and excitation spectra were recorded on a PTI QM4-2003 fluorescence spectrometer and corrected against photomultiplier and lamp intensity. The fluorescence quantum yields were determined by the optical dilute method[29] (A < 0.05) using *N,N´*-di(2,6-diiso- propylphenyl)-perylene-3,4:9,10-tetracarboxylic acid bisimide (ϕ_{fl} = 1.00 in chloroform)[12b] as reference.

X-ray analysis. The X-ray diffraction data for **5a** were collected on a Bruker X8 APEX diffractometer with a CCD area detector, using graphite-monochromated MoKα radiation. The structure was solved by employing direct methods, and refined and expanded by means of Fourier techniques with the SHELX software package (G. M. Sheldrick, SHELX-97, Universität Göttingen, 1997).[30] All non-hydrogen atoms were refined anisotropically. Hydrogen atoms were placed in idealized positions and included in structure factor calculations.

Single crystals of **5a** were obtained by recrystallization from dichloromethane and methanol.

Crystal data of compound 5a. $C_{40}H_{38}F_4N_2O_4$, orange needles, triclinic, space group P-1, a = 7.8097(4), b = 12.1717(7), c = 18.2517(11) Å, α = 75.605(1)°, β = 80.791(1)°, γ = 80.2050(1)°, V = 1643.3(2) Å^3, Z =2, ρ_{calc} = 1.388 g/cm^3, μ = 0.105 mm^{-1}, F-(000) = 720, T = 193(2) K, R_1 = 0.1024, wR_2 = 0.1829, 5792 independent reflections [$2\theta \leq 50.0°$] and 467 parameters.

Electrochemical analysis. Cyclic voltammetry (CV) was performed with a standard commercial electrochemical analyzer in a three electrode single-component cell under argon atmosphere. Dichloromethane (HPLC grade) was used as solvent and was dried over calciumhydride and degassed prior to measurement. The supporting electrolyte tetrabutylammonium-hexafluorophosphate was recrystallized from ethanol/water and dried in high vacuum. The measurements were carried out at a concentration of 10^{-4} M with ferrocene as internal standard for the calibration of potential. Working electrode: Pt disc; reference electrode: Ag/AgCl; auxiliary electrode: Pt wire.

General procedure A (imidization).

A mixture of difluorinated perylene bisanhydride **1**,[15] the respective amine and zinc acetate in quinoline was stirred at 180 °C under argon for 2 h. After cooling to room temperature, the reaction mixture was poured into 2N HCl and extracted with CH_2Cl_2. The organic layer was washed with 2N HCl and the solvent was under in vacuum. The crude product was first purified by silica gel column chromatography and subsequently precipitated from CH_2Cl_2/methanol to give red-orange solids.

General procedure B (Halex process).

A mixture of dibrominated perylene bisimide **2** or tetrachlorinated perylene bisimide **3**, KF and 18-crown-6 (for **2**) or (*N,N´*-dimethylimidazolidino)-tetramethylguanidinium chloride (CNC^+) (for **3**) in sulfolane was stirred at 160-180 °C for 6.5-27 h under argon. The reaction was quenched by addition of 10 mL water and the precipitate was separated by filtration, washed several times with water, and dissolved in CH_2Cl_2, dried over $MgSO_4$ and purified by silica gel column chromatography. After removing the solvent under reduced pressure, the obtained solid material was re-dissolved in dichloromethane and precipitated by addition of methanol and dried in vacuum (60 °C, 10^{-3} mbar, 1 day).

***N,N´*-Di(*n*-octyl)-1,7-difluoroperylene-3,4:9,10-tetracarboxylic acid bisimide (4a).**

a) According to general procedure **A**, the reaction of 44.0 mg (103 µmol) 1,7-difluoroperylene-3,4:9,10-tetracarboxylic acid bisanhydride **1**, 78.1 mg (604 µmol) 1-*n*-octylamine, 20.0 mg $Zn(OAc)_2$ in 5 mL quinoline afforded after column chromatography ($CHCl_3$:*n*-hexane = 4:1, and 7:3) 9 mg (14 µmol, 13%) of **2a** as an orange solid.

b) For details according to general procedure **B** see literature.[17]

Mp. 335-338 °C; ^{1}H NMR (400 MHz, $CDCl_3$): δ 9.13 (m, 2H), 8.74 (m, 2H), 8.51 (m, 2H), 4.21 (m, 4H), 1.77 (m, 4H), 1.49-1.21 (m, 20H), 0.88 (t, 6H, ^3J(H,H) = 6.8 Hz); ^{19}F NMR (376.5 MHz, $CDCl_3$): δ -102.99 (m); HR-MS (apci (pos.-mode, chloroform): 650.2947 (M^-), calculated 650.2962 ($C_{40}H_{40}F_2N_2O_4$); UV/Vis (CH_2Cl_2): λ_{max}/nm (ε_{max} /$M^{-1}cm^{-1}$) = 508 (81300), 474 (48400), 444 (17300); fluorescence (CH_2Cl_2): λ_{max} = 514 nm, fluorescence quantum yield ϕ_{fl} = 1.00; CV (CH_2Cl_2, 0.1 M TBAHFP, vs. Fc/Fc^+): $E_{1/2}$ (PBI/PBI^-) = -1.04 V, $E_{1/2}$ (PBI^-/PBI^{2-}) = -1.26 V.

***N,N´*-Bis(α-methylbenzyl)-1,7-difluoro-3,4:9,10-tetracarboxylic acid bisimide (*rac.*) (4b).**

a) According to general procedure **A**, the reaction of 100 mg (0.233 mmol) 1,7-difluoroperylene-3,4:9,10-tetracarboxylic acid bisanhydride **1**, 200 mg (1.65 mmol) 1-phenylethylamin, 50.0 mg $Zn(OAc)_2$ in 12 mL quinoline afforded after column chromatography (CH_2Cl_2:pentane = 4:1) 40.0 mg (63.0 µmol, 27%) of **4b** as an orange

solid.

b) According to general procedure **B**, the reaction of 651 mg (1.36 mmol) *N,N´*-di(1-phenylethyl)-1,7-dibromo-3,4:9,10-tetracarboxylic acid bisimide (**2b**), 650 mg KF and 200 mg 18-crown-6 in 13 mL sulfolane afforded after column chromatography (CH_2Cl_2) 330 mg (0.52 mmol, 60%) of a red solid.

Melting range: 311-322 °C; ^{1}H NMR (400 MHz, $CDCl_3$): δ 9.04 (m, 2H), 8.63 (d, 2H, ^3J(H,H) = 7.8 Hz), 8.46 (d, 2H, ^3J(H,H) = 13.7 Hz), 7.51 (m, 4H), 7.34 (m, 4H), 7.2-7.3 (m, 2H), 6.54 (q, 2H, ^3J(H,H) = 7.2 Hz), 2.04 (d, 6H, ^3J(H,H) = 7.2 Hz); ^{19}F NMR (376.5 MHz, $CDCl_3$): δ -103.07; HR-MS (apci (pos.-mode, chloroform)): 635.1776 ($M+H^+$), calculated 635.1777 ($C_{40}H_{25}F_2N_2O_4$); UV/Vis (CH_2Cl_2): λ_{max}/nm (ε_{max} /$M^{-1}cm^{-1}$) = 510 (80900), 475 (47400), 445 (16600); fluorescence (CH_2Cl_2): λ_{max} = 518 nm, fluorescence quantum yield ϕ_{fl} = 0.98; CV (CH_2Cl_2, 0.1 M TBAHFP, vs. Fc/ Fc^+): $E_{1/2}$ (PBI/PBI^-) = -1.04 V, $E_{1/2}$ (PBI^-/PBI^{2-}) = -1.25 V.

***N,N´*-Di(2-ethylhexyl)-1,7-difluoro-3,4:9,10-tetracarboxylic acid bisimide (*rac.*) (4c).**

a) Reaction according to general procedure **A** has not been carried out.

b) According to general procedure **B**, the reaction of 590 mg (1.36 mmol) *N,N´*-Di(ethylhexyl)-1,7-dibromo-3,4:9,10-tetracarboxylic acid bisimide (**2c**), 590 mg KF and 295 mg 18-crown-6 in 20 mL sulfolane afforded after column chromatography (CH_2Cl_2) 270 mg (0.43 mmol, 46 %) of **4c** as a red solid.

Mp. 311-315 °C; ^{1}H NMR (400 MHz, $CDCl_3$): δ 9.12 (m, 2H), 8.68 (d, 2H, ^3J(H,H) = 8.0 Hz), 8.49 (d, 2H, ^3J(H,H) = 13.6 Hz), 4.15 (m, 4H), 1.97 (m, 2H), 1.2-1.5 (m, 16H), 0.96 (m, 6H), 0.90 (m, 6H); ^{19}F NMR (376.5 MHz, $CDCl_3$): δ -102.90; HR-MS (apci (pos.-mode, chloroform)): 650.2945 (M^-), calculated 650.2951 ($C_{40}H_{40}F_2N_2O_4$); UV/Vis (CH_2Cl_2): λ_{max}/nm (ε_{max} /$M^{-1}cm^{-1}$) = 508 (76600), 474 (45200), 444 (16000); fluorescence (CH_2Cl_2): λ_{max} = 516 nm, fluorescence quantum yield ϕ_{fl} = 1.00; CV (CH_2Cl_2, 0.1 M TBAHFP, vs. Fc/ Fc^+): $E_{1/2}$ (PBI/PBI^-) = -1.07 V, $E_{1/2}$ (PBI^-/PBI^{2-}) = -1.28 V.

***N,N´*-Di(cyclohexyl)-1,7-difluoroperylene-3,4:9,10-tetracarboxylic acid bisimide (4d).**

a) According to general procedure **A**, the reaction of 40.0 mg (93.4 µmol) of 1,7-difluoroperylene-3,4:9,10-tetracarboxylic acid bisanhydride (**1**), 86.7 mg (874 µmol) cyclohexylamine, 20.0 mg $Zn(OAc)_2$ in 5 mL quinoline yielded after column chromatography (CH_2Cl_2:*n*-pentane = 4:1 and 3:2) 5.0 mg (8.47 µmol, 10%) of **4d** as an orange solid.

b) For details according to general procedure **B** see literature.[17]

Mp. > 440 °C (decomposition); ^{1}H NMR (400 MHz, $CDCl_3$): δ 9.14 (dd, 2H, ^3J(H,H) = 8.4 Hz, ^3J(H,H) = 5.2 Hz), 8.69 (d, 2H, ^3J(H,H) = 7.7 Hz), 8.50 (d, 2H, ^3J(H,F) = 13.8 Hz), 5.04 (m, 2H), 2.56 (m, 4H), 1.20-2.00 (m, 16H); ^{19}F NMR (376.5 MHz, $CDCl_3$): δ -103.22 (m); HR-MS (ESI, CH_2Cl_2, acetonitrile 1:1): 590.2015 (M^-), calculated 590.2023 ($C_{36}H_{28}N_2O_4F_2$); UV/Vis (CH_2Cl_2): λ_{max}/nm (ε_{max} /$M^{-1}cm^{-1}$) = 508 (88000), 473 (52100), 444 (18300); fluorescence (CH_2Cl_2): λ_{max} = 513 nm, fluorescence quantum yield ϕ_{fl} = 0.98; CV (CH_2Cl_2, 0.1 M TBAHFP, vs. Fc/Fc^+): $E_{1/2}$ (PBI/PBI^-) = -1.08 V, $E_{1/2}$ (PBI^-/PBI^{2-}) = -1.29 V.

***N,N´*-Di(tridodecylphenyl)-1,7-difluoroperylene-3,4:9,10-tetracarboxylic acid bisimide (4e).**

a) According to general procedure **A**, the reaction of 100 mg (233 µmol) 1,7-difluoroperylene-3,4:9,10-tetracarboxylic acid bisanhydride (**1**), 550 mg (920 µmol) tridodecylaniline, 51.0 mg $Zn(OAc)_2$ in 13 mL quinoline yielded after column chromatography (CH_2Cl_2:*n*-pentane = 1:1, 1:3 and 2:3) 45.0 mg (28.0 µmol, 12%) of **4e** as an orange sticky solid.

b) Reaction according to general procedure **B** has not been carried out.

Mp. 321 °C; ^{1}H NMR (400 MHz, $CDCl_3$): δ 9.22 (m, 2H), 8.78 (d, 2H, ^3J(H,H) = 7.8 Hz), 8.58 (d, 2H, ^3J(H,F) = 13.5 Hz), 6.97 (s, 4H), 2.66 (t, 12H), 1.19-1.64 (m, 120H), 0.88 (m, 18H); ^{19}F NMR (376.5 MHz, $CDCl_3$): δ -102.83 (m); HR-MS (neg.-mode, apci, chloroform): 1587.2344 (M^-), calculated 1587.2352 ($C_{108}H_{160}F_2N_2O_4$); UV/Vis (CH_2Cl_2): λ_{max}/nm (ε_{max} /$M^{-1}cm^{-1}$) = 511 (96900), 476 (57300), 446 (20500); fluorescence (CH_2Cl_2): λ_{max} = 518 nm, fluorescence quantum yield ϕ_{fl} = 0.35; CV (CH_2Cl_2, 0.1 M TBAHFP, vs. Fc/Fc^+): $E_{1/2}$ (PBI/PBI^-) = -1.02 V, $E_{1/2}$ (PBI^-/PBI^{2-}) = -1.26 V.

***N,N´*-Di(*n*-butyl)-1,7-difluoroperylene-3,4:9,10-tetracarboxylic acid bisimide (4f).**

a) According to general procedure **A**, the reaction of 100 mg (151 µmol) *N,N´*-di(*n*-butyl)-1,7-dibromo-3,4:9,10-tetracarboxylic acid bisimide (**2f**), 100 mg KF and 35 mg 18-crown-6 in 5 mL sulfolane afforded after column chromatography (CH_2Cl_2) 20 mg (37.2 µmol, 25 %) of **4f** as a red solid.

b) Reaction according to general procedure **B** has not been carried out.

Mp. 375-377 °C; ^{1}H NMR (400 MHz, $CDCl_3$): δ 9.19 (m, 2H), 8.73 (d, 2H, ^3J(H,H) = 7.8 Hz), 8.54 (d, 2H, ^3J(H,F) = 13.5 Hz), 4.22 (m, 4H), 1.70-1.80 (m, 4H), 1.4-1.6 (m, 4H), 0.90-1.20 (t, 6H); ^{19}F NMR (376.5 MHz, $CDCl_3$): δ -103.12 (m); HR-MS (apci (pos-mode, acetonitrile, chloroform)): 538.1709 ($M+H^+$), calculated 538.1710 ($C_{32}H_{24}F_2N_2O_4$); UV/Vis (CH_2Cl_2): λ_{max}/nm (ε_{max} /$M^{-1}cm^{-1}$) = 508 (83300), 473 (49500), 444 (17400); fluorescence (CH_2Cl_2): λ_{max} = 515 nm, fluorescence quantum yield ϕ_{fl} = 1.00; CV (CH_2Cl_2, 0.1 M TBAHFP, vs. Fc/Fc^+): $E_{1/2}$ (PBI/PBI^-) = -1.04 V, $E_{1/2}$ (PBI^-/PBI^{2-}) = -1.25 V.

1,7-Difluoro-3,4:9,10-tetracarboxylic acid bisimide (4h)

A portion of 612 mg (0.96 mmol) *N,N´*-di(1-phenylethyl)-1,7-difluoro-3,4:9,10-tetracarboxylic acid bisimide (**4b**) were dissolved in 450 ml dry CH_2Cl_2 and cooled to 0 °C. Then 2.5 mL borontribromide were added and the solution was stirred for 3 h at RT. Afterwards the CH_2Cl_2 was removed in vacuum and the residue was poured into in a mixture of water and methanol. After treatment in an ultrasonic bath for 30 min the precipitate was filtered off and washed with water and CH_2Cl_2 to afford 390 mg (0.92 mmol, 96%) of a dark powder were obtained.

Mp. >450 °C (subl.); ^{1}H NMR (400 MHz, $CDCl_3$): insoluble compound; MS (EI (pos.-mode)): 426.0445(M^+), calculated 426.0447 ($C_{24}H_6F_4N_2O_4$).

***N,N´*-Di(*n*-octyl)-1,6,7,12-tetrafluoroperylene-3,4:9,10-tetracarboxylic acid bisimide (5a).**

According to general procedure **B** the reaction of 200 mg (270 µmol) *N,N´*-di(*n*-octyl)-1,6,7,12-tetrachloroperylene-3,4:9,10-tetracarboxylic acid bisimide (**3a**), 154 mg KF and 17 mg CNC^+ in 6.5 mL sulfolane at 170 °C for 28 h afforded after column chromatography (CH_2Cl_2:pentane = 3:2 and chloroform:pentane = 7:3) 5.2 mg

(8.00 µmol, 3%) of **5a** as an orange solid.

Mp. 237-242 °C; ^{1}H NMR (400 MHz, $CDCl_3$): δ8.49 (t, 4H, ^{3}J(H,F) = 5.2 Hz), 4.21 (t, 4H, ^{3}J(H,H) = 7.2 Hz), 1.76 (m, 4H), 1.47-1.24 (m, 20H), 0.88 (t, 6H, ^{3}J(H,H) = 6.9 Hz); ^{19}F NMR (376.5 MHz, $CDCl_3$): δ -94.27 (t, ^{3}J = 5.31 Hz); HR-MS (ESI (neg-mode, CH_2Cl_2, acetonitrile): 686.2762 (M^-), calculated 686.2768 ($C_{40}H_{38}F_4N_2O_4$); UV/Vis (CH_2Cl_2): λ_{max}/nm (ε_{max} /$M^{-1}cm^{-1}$) = 500 (66000), 466 (41300), 438 (15000); fluorescence (CH_2Cl_2): λ_{max} = 509 nm, fluorescence quantum yield ϕ_{fl} = 0.88; CV (CH_2Cl_2, 0.1 M TBAHFP, vs. Fc/Fc^+): $E_{1/2}$ (PBI/PBI^-) = -0.98 V, $E_{1/2}$ (PBI^-/PBI^{2-}) = -1.22 V.

***N,N´*-Bis(α-methylbenzyl)-1,6,7,12-tetrafluoroperylene-3,4:9,10-tetracarboxylic acid bisimide (5b).**

According to general procedure **A** the reaction of 1.00 g (1.36 mmol) *N,N´*-bis(α-methylbenzyl)-1,6,7,12-tetrachloroperylene-3,4:9,10-tetracarboxylic acid bisimide (**3b**), 1.25 g KF and 100 mg CNC^+ in 8 mL sulfolane at 160 °C for 5 h afforded after column chromatography (CH_2Cl_2:*n*-pentane = 2:1) 80.0 mg (43.0 µmol, 9%) of **5b** as an orange solid. Since 550 mg of starting material were re-isolated, the yield referring to the converted amounts of starting material **3b** is about 20 %.

Mp. 275-279 °C; ^{1}H NMR (400 MHz, $CDCl_3$): δ8.44 (t, 4H, ^{3}J(H,F) = 5.3 Hz), 7.34 (m, 4H), 7.51 (m, 4H), 7.26 (m, 2H), 6.54 (q, 2H, ^{3}J(H,H) = 7.3 Hz), 2.01 (d, 6H, ^{3}J(H,H) = 7.0 Hz); ^{19}F NMR (376.5 MHz, $CDCl_3$): δ -94.29 (t, ^{3}J(H,F) = 5.3 Hz); HR-MS (apci (neg.-mode, chloroform)): 670.1532 (M^-), calculated 670.1521 ($C_{40}H_{22}F_4N_2O_4$); UV/Vis (CH_2Cl_2): λ_{max}/nm (ε_{max} /$M^{-1}cm^{-1}$) = = 503 (68400), 468 (43000), 440 (16300); fluorescence (CH_2Cl_2): λ_{max} = 514 nm, fluorescence quantum yield ϕ_{fl} = 0.85; CV (CH_2Cl_2, 0.1 M TBAHFP, vs. Fc/Fc^+): $E_{1/2}$ (PBI/PBI^-) = -0.98 V, $E_{1/2}$ (PBI^-/PBI^{2-}) = -1.21 V.

***N,N´*-Di(2-ethylhexyl)-1,6,7,12-tetrafluoroperylene-3,4:9,10-tetracarboxylic acid bisimide (5c).**

According to general procedure **B** the reaction of 300 mg (400 µmol) *N,N´*-di(2-ethylhexyl)-1,6,7,12-tetrachloroperylene-3,4:9,10-tetracarboxylic acid bisimide (**3c**), 250 mg KF and 100 mg CNC^+ in 2.4 mL sulfolane at 160 °C for 2 h afforded after column chromatography (CH_2Cl_2 and CH_2Cl_2:*n*-hexane = 7:3) 30.0 mg

(43.0 µmol, 9%) of **5c** as an orange solid. Since 150 mg of starting material **3c** were re-isolated, the yield referring to the converted amounts of starting material **3c** is about 18 %.

Mp. 222 °C; ^{1}H NMR (400 MHz, $CDCl_3$): δ8.49 (t, 4H, ^{3}J(H,F) = 5.2), 4.16 (m, 4H), 1.95 (m, 2H), 1.43-1.25 (m, 16H), 0.97-0.88 (m, 12H); ^{19}F NMR (376.5 MHz, $CDCl_3$): δ -94.27 (t, ^{3}J(H,F) = 5.3 Hz); HR-MS ((apci (neg.-mode, chloroform)): 686.2783 (M^-), calculated 686.2773 ($C_{40}H_{38}F_4N_2O_4$); UV/Vis (CH_2Cl_2): λ_{max}/nm (ε_{max} /$M^{-1}cm^{-1}$) = 501 (71900), 466 (44900), 437 (16400); fluorescence (CH_2Cl_2): λ_{max} = 513 nm, fluorescence quantum yield ϕ_{fl} = 1.00, CV (CH_2Cl_2, 0.1 M TBAHFP, vs. Fc/Fc^+): $E_{1/2}$ (PBI/PBI^-) = -0.98 V, $E_{1/2}$ (PBI^-/PBI^{2-}) = -1.21 V.

1,6,7,12-Tetrafluoro-3,4:9,10-tetracarboxylic acid bisimide (5h).

A portion of 70.0 mg (104 µmol) of *N,N´*-di(1-phenylethyl)-1,6,7,12-tetrafluoro-3,4:9,10-tetra-carboxylic acid bisimide (**5b**) was dissolved in 15 mL dry CH_2Cl_2 under argon and cooled to 0 °C. Then 200 µL borontribromide were added and the solution is stirred for 3 h at RT. Afterwards the CH_2Cl_2 was removed in vacuum and the residue was poured into in a mixture of water and methanol. After treatment in an ultrasonic bath for 30 min the precipitate was filtered off and washed with water and CH_2Cl_2 to obtain 45.0 mg (97.0 µmol, 93%) of a red powder.

Mp. > 495 °C (decomp.); This compound is not soluble in common solvents, thus no ^{1}H NMR spectrum could be measured; HR-MS (EI (pos.-mode, chloroform)): 462.0255 (M^+), calculated 462.0260 ($C_{24}H_6F_4N_2O_4$)

1,6,7,12-Tetrafluoro-3,4:9,10 tetracarboxylic acid bisanhydride (7).

A mixture of 55.0 mg (80.0 µmol) *N,N´*-di(2-ethylhexyl)-1,6,7,12-tetrafluoro-3,4:9,10-tetracarboxylic acid bisimide (**5c**), 300 mg KOH, 200 µL water and 10 mL butanol was stirred at 75 °C for 2 h. Then the mixture was poured into 200 mL acetic acid and stirred for 5 h at 100 °C. The acetic acid was diluted with water and the product precipitated over night. The precipitate was filtered off and dried in vacuum to obtain 34.0 mg (75.0 µmol, 94%) of a dark powder were obtained.

Mp. > 450 °C (decomp.); MS (EI (pos.-mode)): 464.1 (M^+), calculated 464.0 ($C_{24}H_4F_4O_6$)

***N,N´*-Bis(α-methylbenzyl)-1,7-dibromo-3,4:9,10-tetracarboxylic acid bisimide (2b) (rac.).**

A mixture of 2.00 g (3.63 mmol) 1,7-dibromo-3,4:9,10-tetracarboxylic acid bisanhydride, 0.5 mL α-methylbenzylamine (*rac.*) and 10 mg $Zn(OAc)_2$ was stirred in 12 mL quinoline for 3 h at 130 °C. After cooling to RT the mixture was poured into 200 mL 2N HCl and the precipitate was filtered off and dried in vacuum. After column chromatography (CH_2Cl_2) 1.31 g (1.74 mmol, 48%) of a dark red solid were obtained.
^{1}H NMR (400 MHz, $CDCl_3$): δ9.46 (d, 2H, ^3J(H,H) = 8.2 Hz), 8.90 (s, 2H), 8.67 (d, 2H, ^3J(H,H) = 8.1 Hz), 7.51 (m, 4H), 7.34 (m, 4H), 7.2-7.3 (m, 2H), 6.54 (q, 2H, ^3J(H,H) = 7.2 Hz), 2.02 (d, 6H, ^3J(H,H) = 7.2 Hz); HR-MS (apci (pos.-mode, chloroform)): 755.0178 ($M+H^+$), calculated 755.0176 ($C_{40}H_{24}Br_2N_2O_4$).

***N,N´*-Bis(α-methylbenzyl)-1,6,7,12-tetrachloro-3,4:9,10-tetracarboxylic acid bisimide (3b) (rac.).**

A mixture of 3.00 g (5.66 mmol) 1,6,7,12-tetrachloro-3,4:9,10-tetracarboxylic acid bisanhydride, 7.5 mL (65.2 mmol) α-methylbenzylamine (*rac.*) and 1.00 g $Zn(OAc)_2$ were stirred in 65 mL quinoline at 180 °C for 4 h. After cooling to RT the mixture was poured into 300 mL 2N HCl and the precipitate was filtered off and dried in vacuum. After column chromatography (CH_2Cl_2) 3.70 g (5.03 mmol, 88%) of a dark red solid were obtained.
^{1}H NMR (400 MHz, $CDCl_3$): δ8.64 (s, 4H), 7.51 (m, 4H), 7.34 (m, 4H), 7.2-7.3 (m, 2H), 6.54 (q, 2H, ^3J(H,H) = 7.2 Hz), 2.01 (d, 6H, ^3J(H,H) = 7.2 Hz); HR-MS (apci (pos.-mode, chloroform)): 735.0414 (M^-), calculated 735.0406 ($C_{40}H_{23}Cl_4N_2O_4$).

4.9 References and Notes

[1] For representative reviews on OTFTs, see: (a) J. E. Anthony, *Angew. Chem.* **2008**, *120*, 460-492; *Angew. Chem. Int. Ed.* **2008**, *47*, 452-483; (b) A. Facchetti, *Mater. Today* **2007**, *10*, 28-37; (c) A. Dodabalapur, *Mater. Today* **2006**, *9*, 24-39; (d) C. R. Newman, C. D. Frisbie, D. A. da Silva Filho, J.-L. Brédas, P. C. Ewbank, K. R. Mann, *Chem. Mater.* **2004**, *16*, 4436-4451; (e) *Physics of Organic Semiconductors* (Ed. W. Brütting), Wiley-VCH, Weinheim, Germany, **2005**; (f) *Organic Molecular Solids* (Eds. M. Schwoerer, H. C. Wolf), Wiley-VCH,

Weinheim, Germany, **2007**; (g) M. M. Ling, Z. Bao, *Chem. Mater.* **2004**, *16*, 4824-4840.

[2] For a recent review on OLEDs, see: B. Geffroy, P. le Roy, C. Prat, *Polym. Int.* **2006**, *55*, 572-582.

[3] (a) C. W. Tang, *Appl. Phys. Lett.* **1986**, *48*, 183-185; (b) L. Schmidt-Mende, A. Fechtenkötter, K. Müllen, E. Moons, R. H. Friend, J. D. MacKenzie, *Science* **2001**, *293*, 1119-1122; (c) P. Peumans, S. Uchida, S. R. Forrest, *Nature* **2003**, *425*, 158-162; (d) S. E. Shaheen, C. J. Brabec, N. S. Sariciftci, F. Padinger, T. Fromherz, J. C. Hummelen, *Appl. Phys. Lett.* **2001**, *78*, 841-843.

[4] (a) H. E. Katz, A. J. Lovinger, J. Johnson, C. Kloc, T. Siegrist, W. Li, Y.-Y. Lin, A. Dodabalapur, *Nature* **2000**, *404*, 478-481; (b) H. E. Katz, J. Johnson, A. J. Lovinger, W. Li, *J. Am. Chem. Soc.* **2000**, *122*, 7787-7792.

[5] S. Ando, R. Muratami, J. Nishida, H. Tada, Y. Inoue, S. Tokito, Y. Yamashita, *J. Am. Chem. Soc.* **2005**, *127*, 14996-14997.

[6] (a) A. Facchetti, M.-H. Yoon, C. L. Stern, G. R. Hutchinson, M. A. Ratner, T. J. Marks, *J. Am. Chem. Soc.* **2004**, *126*, 13480-13501. (b) M.-H. Yoon, A. Facchetti, C. L. Stern, T. J. Marks, *J. Am. Chem. Soc.* **2006**, *128*, 5792-5801.

[7] (a) M. Sun, *Chem. Phys.* **2006**, *320*, 155-163; (b) Y. Sakamoto, T. Suzuki, M. Kobayashi, Y. Gao, Y. Fukai, Y. Inoue, F. Sato, S. Tokito, *J. Am. Chem. Soc.* **2004**, *126*, 8138-8140.

[8] (a) Z. Bao, A. J. Lovinger, J. Brown, *J. Am. Chem. Soc.* **1998**, *120*, 207-208; (b) D. G. de Oteyza, E. Barrena, J. O. Osso, H. Dosch, S. Meyer, J. Pflaum, *Appl. Phys. Lett.* **2005**, *87*, 183504; (c) R. Ye, M. Baba, Y. Oishi, K. Mori, K. Suzuki, *Appl. Phys. Lett.* **2005**, *86*, 253505; (d) M.-H. Yoon, C. Kom. A. Facchetti, T. J. Marks, *J. Am. Chem. Soc.* **2006**, *128*, 12851-12869.

[9] (a) C. W. Tang, *Appl. Phys. Lett.* **1986**, *48*, 183-185; (b) P. Peumans, A. Yakimov, S. R. Forrest, *J. Appl. Phys.* **2003**, *93*, 3693-3723; (c) S. Tatemichi, M. Ichikawa, T. Koyama, Y. Taniguchi, *Appl. Phys. Lett.* **2006**, *89*, 112108.

[10] M. M. Ling, P. Erk, M. Gomez, M. Könemann, J. Locklin, Z. Bao, *Adv. Mater.* **2007**, *19*, 1123-1127.

[11] (a) B. A. Jones, M. J. Ahrens, M.-H. Yoon, A. Facchetti, T. J. Marks, M. R. Wasielewski, *Angew. Chem.* **2004**, *116*, 6523-6526; *Angew. Chem. Int. Ed.* **2004**, *43*, 6363-6366; (b) Z. Bao, A. Lovinger, J. Brown, *J. Am. Chem. Soc.* **1998**, *120*, 207-208.

[12] (a) R. Iden, G. Seybold, (BASF AG) *Ger. Pat. Appl.*, DE 3434059 A1, **1985**; *Chem. Abstr.* **1985**, *103*, 38696q; (b) G.; Seybold, G. Wagenblast, *Dyes Pigm.* **1989**, *11*, 303-317; (c) Y. Zhao, M. R. Wasielewski, *Tetrahedron Lett.* **1999**, *40*, 7047-7050.

[13] A. Pleschke, A. Marhold, M. Schneider, A. Kolomeitsev, G.-V. Röschenthaler, *J. Fluorine Chem.* **2004**, *125*, 1031-1038.

[14] (a) H. Wang, T. E. Kaiser, S. Uemura, F. Würthner, *Chem.Commun.* **2008**, 181-1183; (b) PhD Thesis P. Osswald.

[15] The difluoroperylene bisanhydride was synthesized by conversion of the dibromo derivative in sulfolane and potassiumfluoride with 18-crown-6 as a catalyst by Dr. M. Könemann. The insoluble product had a high amount of different impurities and was used without further purification.

[16] For the synthesis of **2a**,**c**,**d**,**f**, see: (a) U. Rohr, C. Kohl, K. Müllen, A. van de Craats, J. Warman, *J. Mater. Chem.* **2001**, *11*, 1789-1799; b) A. Böhm, H. Arms, G. Henning, P. Blaschka, (BASF AG) German Pat. DE 19547209 A1, **1997**; *Chem. Abst.* **1997**, *127*, 96569g. For the synthesis of **3a**,**c**,**d** see: (c) D. Dotcheva, M. Klapper, K. Müllen, *Macromol. Chem.* **1994**, *195*, 1905-1911.

[17] F. Würthner, P. Osswald, R. Schmidt. T. E. Kaiser, H. Masikkamäki, M. Könemann, *Org. Lett.* **2006**, *8,* 3765-3768.

[18] T. Kaiser, H. Wang, V. Stepanenko, F. Würthner, *Angew. Chem.* **2007**, *119*, 5637–5640; *Angew. Chem. Int. Ed.* **2007**, *46*, 5541–5544

[19] Z . Chen, U. Baumeister, C. Tschierske, F. Würthner, *Chem. Eur. J.* **2007**, *13*, 450-465.

[20] F. Würthner, *Chem. Comm.* **2004**, 1564–1579.

[21] I. Seguy, P. Jolinat, P. Destrule, R. Mamy, H. Allouchi, C. Couseille, M. Cotrait, H. Bock, *ChemPhysChem* **2001**, *2*, 448-452.

[22] F. Graser, E. Hädicke, *Liebigs Ann. Chem.* **1980**, *12*, 1994-2011.

[23] (a) F. Würthner, A. Sautter, J. Schilling, *J. Org. Chem.* **2002**, *67*, 3037-3044; (b) P. Osswald, D. Leuser, D. Stalke, F. Würthner, *Angew. Chem.* **2005**, *117,* 254-257; *Angew. Chem. Int. Ed.* **2005**, *44*, 250-253.

[24] P. Osswald, F. Würthner, *J. Am. Chem. Soc.* **2007**, *129*, 14319–14326

[25] S. R. Forrest, M. L. Kaplan, P. H. Schmidt, *J. Appl. Phys.* **1984**, *55*, 1492-1507.

[26] A. Immirzi, B. Perini, *Acta Cryst. Sect. A* **1977**, *33*, 216-218.

[27] F. Würthner, Z. Chen, V. Dehm, V. Stepanenko, *Chem. Commun.* **2006**, 1188-1190.

[28] A. Pleschke, A. Marhold, M. Schneider, A. Kolomeitsev, G.-V. Röschenthaler, *J. Fluorine Chem.* **2004**, *125*, 1031-1038.

[29] *Principles of Fluorescence Spectroscopy* (Ed. J. R. Lakowicz), 2nd ed., Kluwer Academic/Plenum, New York, **1999**.

[30] (a) G. M. Sheldrick, *SADABS 2.05: Program for Area Detector Absorption Correction*, University of Göttingen, **2002**; (b) G. M. Sheldrick, *SHELXL-97 – Program for Structure Refinement*, Universität Göttingen, **1997**.

Chapter 5

Perfluorinated Perylene Bisimides as Air-Stable High Performance n-Type Organic Semiconductors

Abstract: The design of air-stable organic n-type semiconductors with outstanding charge carrier mobilities is an attractive research field since such materials may find many applications in organic thin film transistors (OTFTs) and related electronic and (opto)electronic devices. Four series of electron-deficient perylene bisimide (PBI) dyes were synthesized and characterized by MS, ^{1}H and ^{19}F NMR, UV/Vis and fluorescence spectroscopy in solution and solid state, and cyclic voltammetry. The charge carrier mobilities of all compounds were measured in thin film transistors prepared by vacuum deposition techniques and the best air-stable derivatives showed mobilities up to 1.44 cm^2/Vs and on/off ratios up to 10^9.[a] For the most promising candidates the packing in the solid state was investigated by X-ray analysis of the single crystals. The series of PBIs with ascending halogen atoms (fluorine to bromine) in bay position showed increasing torsion angles with saturation effect at the end. Further, sterically demanding imide substituents led to torsion of the imide groups hindering "convenient" π–π stacking of the dyes in solid state. From the correlation of charge carrier mobility and solid state packing it is concluded that high performance OTFTs are obtained from those derivatives that show close π–π contacts between the chromophores in the solid state.

[a] The charge carrier mobilities were measured at Stanford University by Dr. J. H. Oh, Dr. M. M. Ling, and S. Liu in the working group of Prof. Dr. Z. Bao.

5.1 Introduction

Organic semiconductors are the key component for many electronic and optoelectronic devices. Their possible applications range from organic photovoltaic cells[1] and light-emitting diodes (OLEDs)[2] to unconventional electronics, where traditional inorganic semiconductors cannot be employed. For the latter devices,[3] which include disposable low-cost microelectronics, radio-frequency identification (RFID) tags, sensors, electronic papers, and flexible displays, organic thin-film transistors (OTFTs) are most promising. Historically, the performance of n-type organic semiconductors has always been outmatched by the more intensively investigated p-type materials. Nevertheless, both kinds of high performance organic semiconductors are required for the fabrication of complementary integrated circuits, bipolar transistors, or organic p/n junctions[4] and easy access to these materials is desirable. Within the last couple of years a larger number of organic n-type substances, whose electron charge carrier mobilities are already surpassing those of some common organic p-type or inorganic semiconductors such as amorphous silicon, has been reported. Apart from high electron mobilities, practically useful n-type semiconductors should possess a sufficiently high electron affinity to allow for efficient electron injection from common metal electrodes into these materials.[5] Nearly all organic n-type semiconductors are conceptualized by attachment of strongly electron-withdrawing substituents such as imides, halogens, cyano or perfluorinated alkyl and phenyl groups on the formerly electron-rich aromatic systems. A plethora of synthetic research efforts was published recently and very high mobilities (> 2 cm^2/Vs) were reported for OTFTs of various different classes of electron poor aromatic derivatives.[6] However, a major drawback of many compounds described in the literature is the poor stability of devices operated under ambient conditions. Accordingly research on the development of new air-stable organic n-type semiconductors was amplified during the recent years.

Among the investigated organic n-type semiconductors, perylene bisimides are very promising candidates, even though the most outstanding mobility values (up to 2.10 cm^2/Vs)[6i,j] of the devices broke down under ambient conditions. *Wasielewksi*, *Marks* and coworkers demonstrated that thermodynamic stability of the generated charge carriers is hardly accessible by shifting the HOMO and LUMO, as a reduction potential greater than +0.57 V (vs SCE) is needed to avoid oxidation of the negative charges by oxygen.[7] So far no single PBI with such high reduction potential has been

reported, but an overpotential, already postulated by *deLeeuw* et al for doped polymers,[8] seems to hinder the oxidation of the charge carriers of the dye with E^{red} > -0.1V (vs SCE) as well. This concept was proved by the air-stability of several fluorine-free rylene bisimide derivatives (0.15 cm^2/Vs)[3d, 9] with strong electron-withdrawing cyano groups in bay positions (Figure 1, R = alkyl), exhibiting a reduction potential between the two above mentioned critical values.

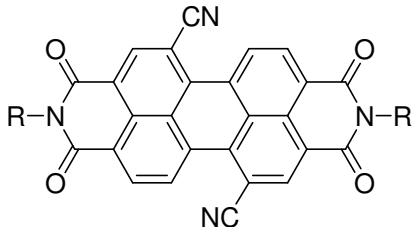

R = alkyl or perfluoroalkyl

Figure 1. Core-cyanated PBIs with different (perfluoro)alkyl imide substituents.

Another possible synthetic approach is the development of compounds which form a closely packed solid state that inhibits the intrusion of oxygen and moisture into the active π–stack layer. This concept was also intensively studied for the class of rylene bisimide dyes. Apart from one PBI (0.11 cm^2/Vs)[10] these compound have invariable perfluorinated substituents in their imide positions (Figure 2).[10,11,12,13] Exposure to humidity and oxygen could not decrease the performance of these field effect transistors significantly. The air-stability of these compounds was mainly explained with the special attributes of the substituents, which form a closer oxygen resistant packing in the solid state compared to derivatives with halogen-free imide substituents, since the LUMO of the most materials with fluorinated alkyl or phenyl groups (Figure 2) is still too high (E^{red} < -0.1V (vs SCE)) and the charge carriers can still be trapped under ambient conditions.

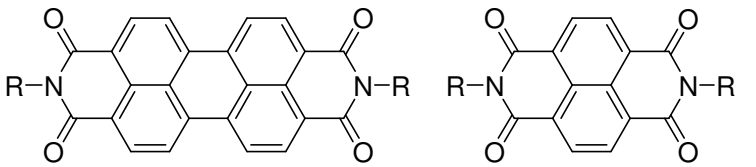

R = fluorinated alkyl
or phenyl substituents

Figure 2. Rylene bisimide dyes with perfluorinated imide substituents.

Up to now the best mobility was reported for a PBI derivative combining both concepts. A cyanated perylene dye (Figure 1, R = perflurobutyl) showed air-stable values of about 0.64 cm^2/Vs.[13] Unfortunately, the very low reduction potential allows already the existence of radical anions in the thin layer without any voltage at the gate

electrode, leading to “always on” transistors. Furthermore, the above mentioned reasons for the air-stability of the devices were already controversially debated in literature, since not all studies on PBIs could confirm the coherence of air-stability and densely packed perfluorinated alkyl chains.[14] Up to now no scientific explanation for the air-stability of organic n-type semiconductors is certainly evidenced and more investigations have to be undertaken.

Perylene bisimide dyes are very auspicious candidates for such studies and for electronic applications as well. The solid state packing and concomitant properties of PBIs can be tailored by introduction of appropriate substituents either in the imide position or by core substitution in the bay region and only a small part of promising PBIs has yet been investigated for employment in electronic applications. Substitution in the 1,6,7, and 12 position of the PBI backbones enforces a considerable twisting of the perylene skeleton out of planarity and the effect of this structural modification on the electrical and charge transport properties of these semiconductors is not yet well understood, though. Whereas intermolecular coupling might be reduced in core-twisted PBIs due to steric constraints, a slipped arrangement of these dyes might, on the other hand, help to prevent the formation of dimeric pairs that have been envisaged as potential electron traps. To elucidate the effect of successive bay substitution and to get a better understanding of the connection between solid state packing, OTFT performance, and ambient stability of the devices, a large library of differently halogenated perylene bisimide derivatives (Chart 1) has been synthesized in this work. The halogens are strongly electron-withdrawing groups and change significantly the redox potentials (and the LUMO) of these dyes, which might improve the charge carrier injection and the air stability of the devices. For the imide positions five different perfluorinated substituents were chosen for this work. They do not only influence the stability of the OTFTs towards oxygen but also change the arrangement of the dyes in the crystal.

Compounds **1a**-**e** and **2a**-**e** bear perfluorinated butyl or phenyl groups in the imide positions. The bay positions of series **1** and **2** were functionalized by fluorine, chlorine, and bromine substituents, respectively (Chart 1). The unsubstituted dyes were chosen as reference models and PBI derivative **2a** is a literature known air-stable semiconductor with a mobility of 0.06 cm^2/Vs.[12] Additionally, series **3** was investigated, since these compounds are a modification of a BASF “black pigment” dye which also proved to be an air-stable high performance n-type semiconductor[10] and is

avery promising candidate for applications in organic solar cells due to its strong absorbance over the whole visible range.[15]

Finally, a series of PBIs bearing perfluorinated alkyl amines of different length, namely **4a**, **1a**, and **4b**, were chosen to elucidate the influence of the chain length on packing and device performance.

Chart 1. Chemical structures of synthesized and investigated fluorinated PBI derivatives.

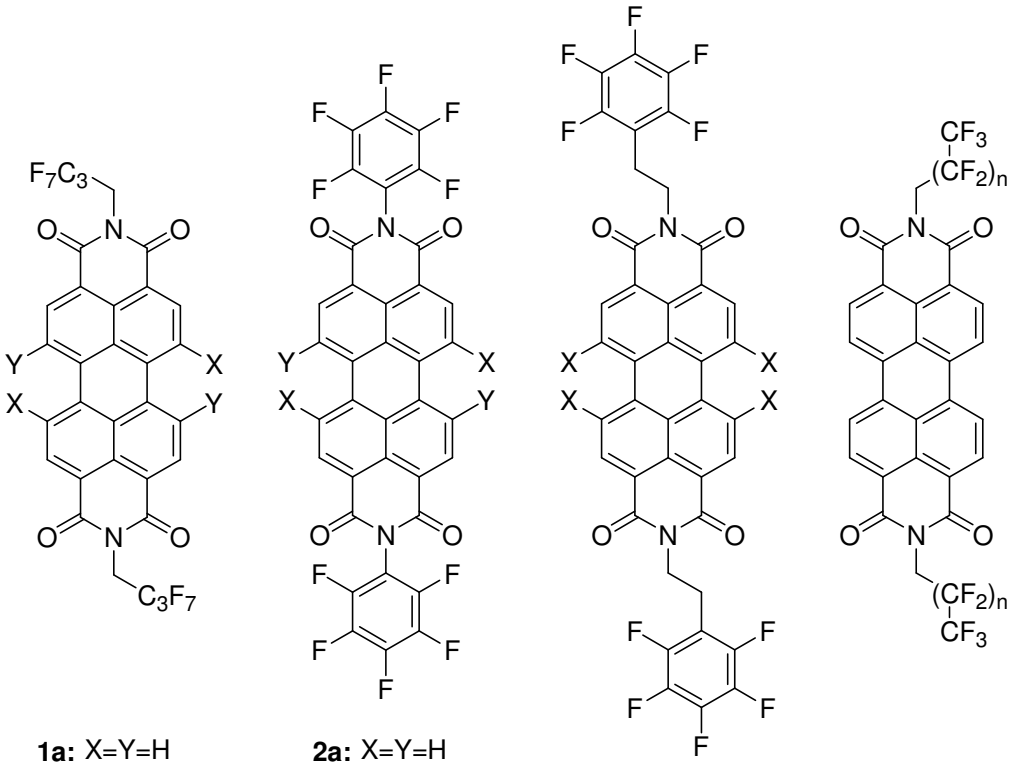

1a: X=Y=H
1b: X=H, Y=F
1c: X=Y=F
1d: X=Y=Cl
1e: X=Y=Br

2a: X=Y=H
2b: X=H, Y=F
2c: X=Y=F
2d: X=Y=Cl
2e: X=Y=Br

3a: X=H
3b: X=Cl

4a: n=0
1a: n=2
4b: n=3

5.2 Synthesis

The synthesis of all perylene bisimide derivatives **1**-**4** is depicted in Scheme 1, the reagents and conditions are given in Table 1 and 2. Starting materials **5a** and **5b** were donated by the BASF AG, anhydrides **5c**[16] and **5d** (isomeric pure and isomeric mixture)[17] were synthesized according to literature.

To receive PBIs **1a**,**d**-**f**, **3b**, **4a**, and **4b** a literature-known imidization procedure was chosen, taking NMP with catalytic amounts of acetic acid as a solvent.[13] Due to the very low nucleophilicity of the pentafluoroaniline high excess of the amine with catalytic

amounts of acetic acid in NMP had to be taken for the synthesis of **2d**-**f**. The introduction of fluorine in bay-position (products **1b**,**c** and **2b**) was achieved by the so-called Halex reaction.[18] The bromine (**1f** and **2f**) or chlorine (**1d**) atoms of the starting materials underwent nucleophilic substitution with potassium fluoride in sulfolane as solvent in the presence of 18-crown-6 or the CNC^+-catalyst, depicted in Scheme 1. PBIs **2a** and **3a** were synthesized in quinoline with zinc acetate.

Scheme 1. Synthesis of PBIs **1-4**.

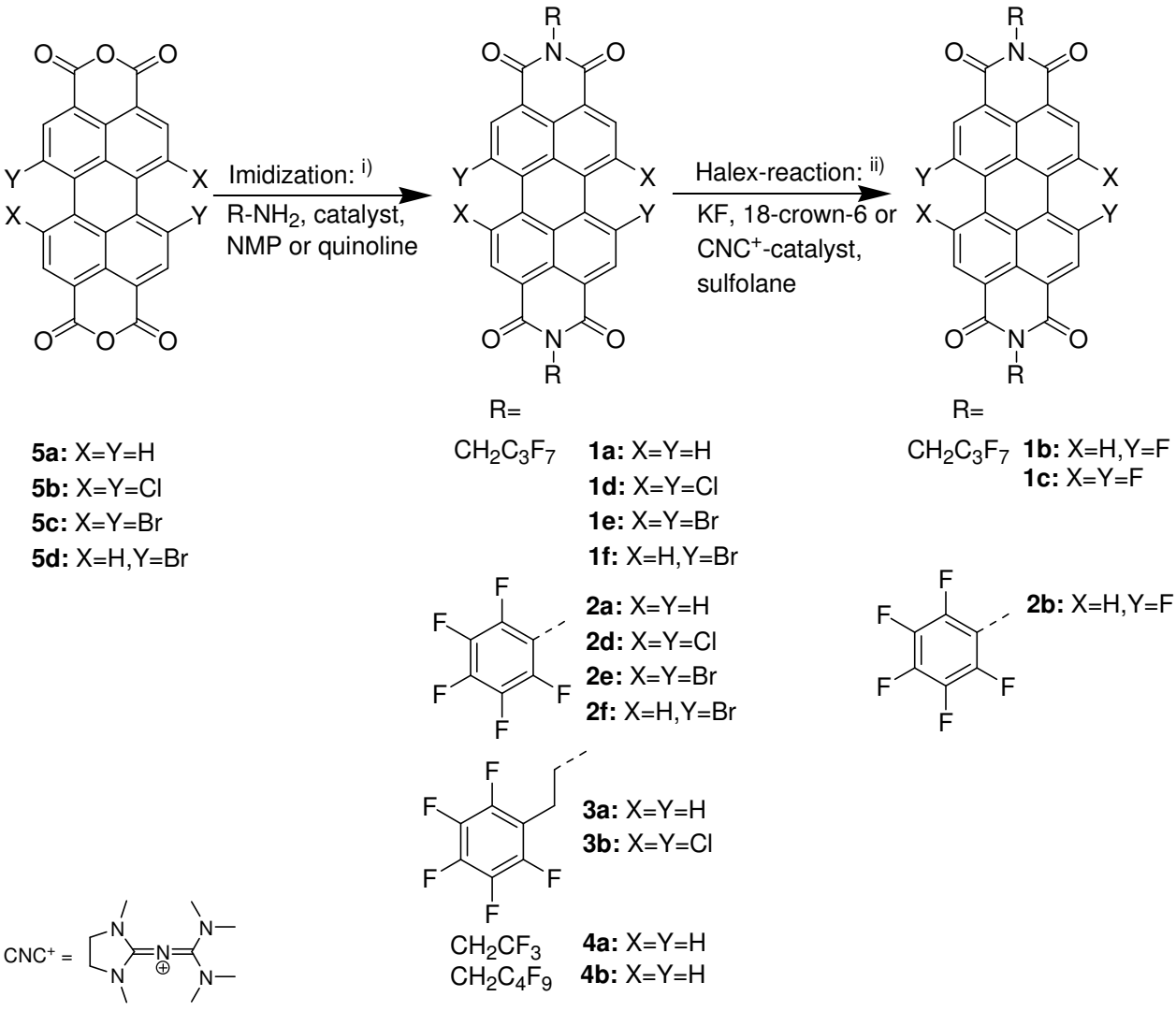

i) Imidization of the anhydrides **5a**-**d** with the corresponding amines to obtain PBIs **1a**,**d**-**f**, **2a**,**d**-**f**, **3a**,**b** and **4a**,**b**; for detailed conditions see Table 1.
ii) Halex reaction of PBIs **1d**,**f** and **2d**,**f** to obtain fluorinated PBIs **1b**,**c** and **2b**; for detailed conditions see Table 2.

Next to the low nucleophilicity of the amines, the solubility of the anhydride had also a large impact on the yields. The unsubstituted starting material **5a** reacted even under harsh conditions very slowly and the yields stayed mainly below 25%, even though

several optimizations were tried. Only imidization with the highly reactive trifluoroethylamine led to excellent yields of 88%.

Table 1: Reaction conditions, reagents and yields for the synthesis of **1a**,**d**-**f**, **2d**-**f**, **3b**, and **4a**,**b** by imidization of the corresponding anhydride in NMP, for **2a** and **3a** quinoline was taken as solvent.

comp.	yield (%)	anhydride	amine	catalyst	temp. (°C)	time (h)
1a	25	**5a**	$H_2NCH_2C_3F_7$	HOAc	200	48
1d	77	**5b**	$H_2NCH_2C_3F_7$	HOAc	90	5
1e	66	**5c**	$H_2NCH_2C_3F_7$	HOAc	90	5
1f	94	**5d**	$H_2NCH_2C_3F_7$	HOAc	90	5
2a	19	**5a**	$H_2NC_6F_5$	$Zn(OAc)_2$	200	7
2d	59	**5b**	$H_2NC_6F_5$	HOAc	160	28
2e	41	**5c**	$H_2NC_6F_5$	HOAc	160	28
2f	26	**5d**	$H_2NC_6F_5$	HOAc	160	28
3a	15	**5a**	$H_2N(CH_2)_2C_6F_5$	$Zn(OAc)_2$	180	12
3b	78	**5b**	$H_2N(CH_2)_2C_6F_5$	HOAc	90	2
4a	88	**5a**	$H_2NCH_2CF_3$	HOAc	200	48
4b	13	**5a**	$H_2NCH_2C_4F_9$	HOAc	200	48

Table 2: Reaction conditions, reagents and yields for the synthesis of **1b**,**c** and **2b**,**c** by Halex reaction with 18-crown-6 or CNC^+ as catalysts in sulfolane.

comp.	yield (%)	starting material	catalyst	temp. (°C)	time (h)
1b	32	**1f**	18-crown-6	160	0.75
1c	8	**1d**	CNC^+	160	2-3
2b	45	**2f**	18-crown-6	160	0.75

5.3 Examination of the optical attributes in solution and solid state.

The absorption and emission spectra of the five derivatives of series **1** in dichloromethane are depicted in Figures 3 and 4, respectively.

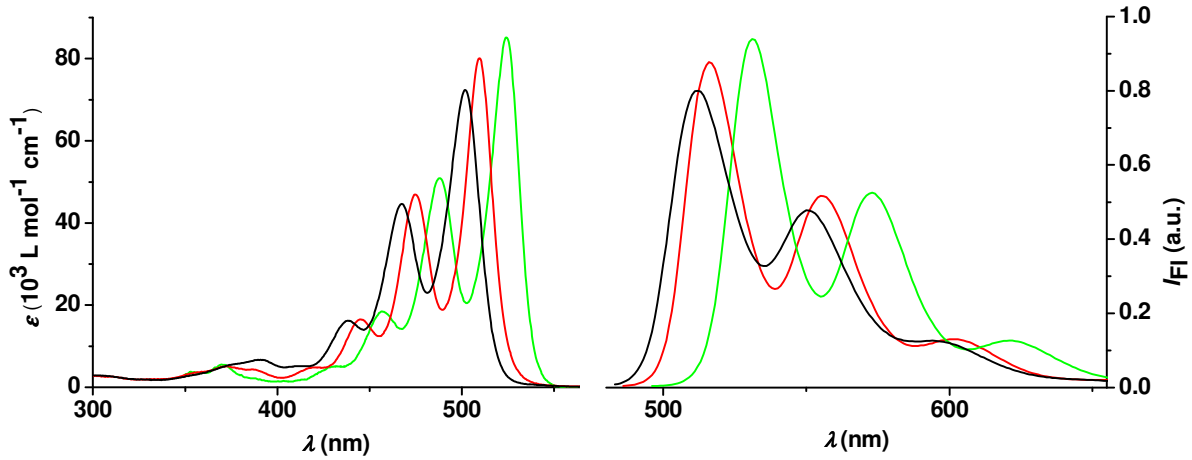

Figure 3. UV/Vis absorption (left) and fluorescence (right) of **1a** (green), **1b** (red) and **1c** (black) in dichloromethane.

The absorption spectra of **1a**-**c** reveal the typical optical characteristics of PBIs showing well defined vibronic fine structures (0-0, 0-1, 0-2 and 0-3 transitions) of the S_0-S_1 band with a maximum at 524 (**1a**), 509 (**1b**) and 502 nm (**1c**), respectively. The absorption coefficients are between 72 000 and 85 000 $M^{-1}cm^{-1}$, their decrease goes along with an increasing torsion angle of the perylene core.[19] The maxima of the fluorinated PBIs **1b** and **1c** are hypsochromically shifted by 15 (**1b**) or 22 (**1c**) nm compared to the unsubstituted perylene **1a**.

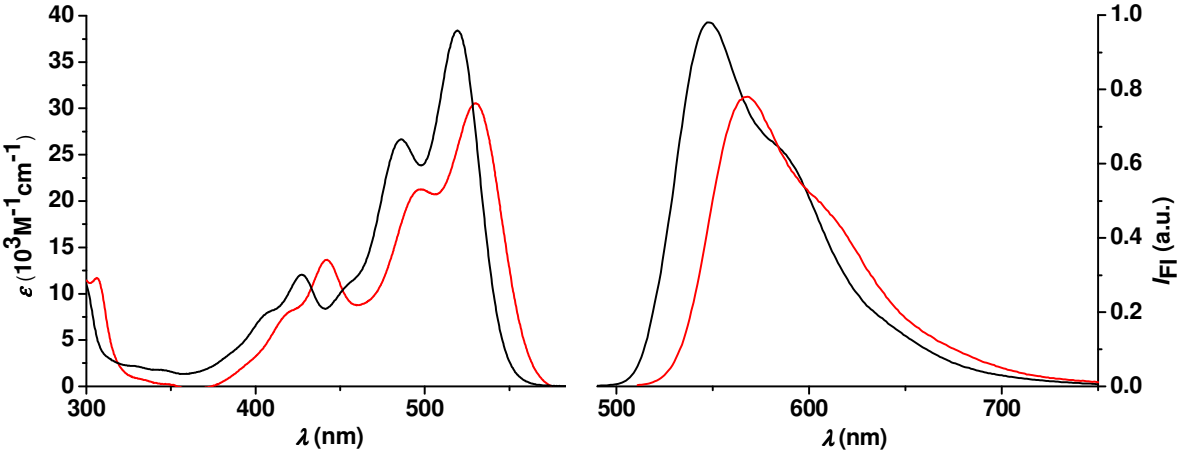

Figure 4. UV/Vis absorption (left) and fluorescence (right) of **1d** (black) and **1e** (red) in dichloromethane.

The maxima of the S_0-S_1 transition of **1d** and **1e** are located at 520 and 530 nm, respectively (Figure 4). Due to the loss of planarity of the aromatic core, the spectra exhibit less pronounced vibronic fine structures. Compared to the spectrum of **1a** the maximum of **1d** is shifted slightly hypsochromically by 4 nm, while the maximum of **1e** is shifted oppositely by 6 nm. The lower absorption coefficients of compounds **1d** and **1e** are in accordance with already published spectra of other tetrachlorinated[20] and tetrabrominated[21] PBIs. Moreover the decrease of the absorption coefficient of **1d** and **1e** (Table 3) can be attributed to the increasing twist of the aromatic core.

The fluorescence properties of series **1** are given in Table 3 and the normalized fluorescence spectra are shown in Figure 3 and 4. The emission spectra (Figure 3, right) of **1a**, **1b** and **1c** are in mirror image relative to the absorption spectra. The relative small Stokes shift of only 7-10 nm indicates a quite rigid structure of the molecules with little bond length alteration upon optical axcitation. All three derivatives exhibit very high fluorescence quantum yields between 90 and 100%. On the other hand, the Stokes shift of **1d** and **1e** is much larger (27 and 38 nm, respectively), implying a more pronounced change of the geometry between the ground and the excited states. Furthermore, the mirror image conditions are not perfectly

accomplished and derivative **1e** has the smallest quantum yield of only 54%. Nevertheless this is still a quite high value for a dye with four heavy atom substituents as well as a strongly twisted π–core.

The absorption and emission attributes of series **2** in DCM are very similar to **1**, except slightly bathochromically shifted maxima (about 3 nm) and higher extinction coefficients. The optical characteristics of **3b** and **4b** in solution are identical to the corresponding dyes **1d** and **1a**, respectively.

Table 3: Optical absorption and emission wavelengths, quantum yields in solution and solid state of series **1**, **2**, **3**, and **4** in DCM.

comp.	λ_{abs} (nm)	λ_{em} (nm)	ϕ_{fl} (solution)[a]	ϕ_{fl} (s.)[b]	ε($M^{-1}cm^{-1}$)	λ_{abs} (nm)(s.)[b,c]
1a	524	531	1.00	0.05	85200	489
1b	509	516	1.00	0.08	80100	504
1c	502	512	0.90	0.14	72400	505
1d	520	547	0.89	0.04	38400	521
1e	530	568	0.54	0.01	30500	533
2a	527	534	1.00	0.00	90200	500
2b	512	518	0.96	0.10	92600	482
2d	522	549	0.97	0.10	43100	530
2e	533	569	0.64	0.02	35100	540
3a	n.a.[d]	n.a.	n.a.	n.a.	n.a.	501
3b	520	546	0.93	0.04	40300	526
4a	n.a.[d]	n.a.	n.a.	0.01	n.a.	502
4b	524	530	1.00	0.01	78600	499

[a] ϕ_{fl} ± 0.03; [b] measured in solid state; [c] the absorption maxima in solid state were measured with a $BaSO_4$ trituration; [d] insoluble dye.

The solid state absorption spectra were measured with a 10^{-4} M $BaSO_4$ trituration of the dyes. For series **1** strongly altered absorption bands are observed only for **1a** and **1b**, indicating strong electronic interactions between the closely packed chromophores in the pulverized crystals (Figure 5, left). Though the absorption maximum of **1a** is hypsochromically shifted by 25 nm compared to the unsubstituted dye **1a**, two new shoulders appear at about 550 and 570 nm. The new broad absorption bands are responsible for the darker red color of the crystals of **1a**. These optical solid state properties are typical for unsubstituted perylene bisimide dyes with similar packing in the crystal (see below). Thus, perylene bisimide dyes with pentyl- or ethoxyethyl substituents in the imide positions exhibit similar longitudinal and transversal shifts for

the π–stacks in the crystal and also show bathochromically shifted absorption bands at 570 and 564 nm respectively.[22]

For **1b** these effects are less pronounced. The absorption maximum is marginally hypsochromically shifted by 5 nm and there is only one new small broadening at about 545 nm. This can be explained by the potentially smaller longitudinal or larger transverse shift of the molecules in the solid state (see section 5) leading to a much smaller overlap of the aromatic systems of the chromophores.

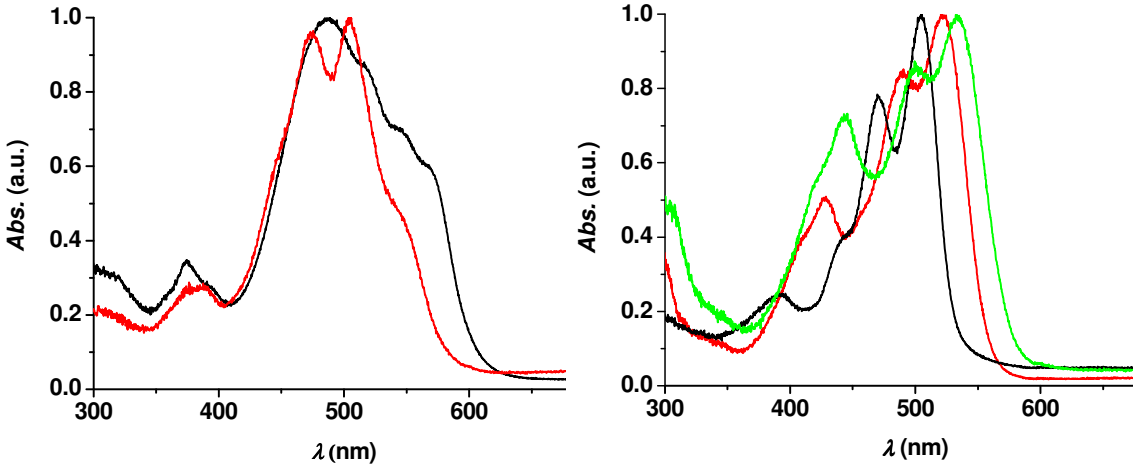

Figure 5. Solid state UV/Vis absorption spectra of the $BaSO_4$ trituration of **1a** (black) and **1b** (red) (left); and **1c** (black), **1d** (red), and **1e** (green) (right).

The spectra of the other dyes **1c**-**e** (Figure 5, right) showed only minor changes compared to the measurements of the monomers in solution (Figure 3 and 4). Thus, the absorption maxima and the fine structure in solid state and solution are corresponding to each other. This can be explained by the limited π–π interactions in the solid state, especially for **1d** and **1e**. Due to the strongly twisted aromatic core no close contacts between the aromatic units are possible and the colors of the crystals are consequently similar to those of the monomer solutions.

For compounds **2a** and **2b** with relatively planar aromatic systems again enhanced intermolecular π–π interactions are evident (Figure 6, left). Similar to solid state spectra of **1a** and **1b**, the maxima are shifted hypsochromically by 27 and 30 nm with respect to the monomer solutions in DCM, but second absorption bands appear at about 521 and 538 nm. This quite sterically demanding aromatic imide substituents do not hinder closed π–π–contacts in solid state, while slightly larger substituents in literature (e.g. 2,6-dimethylphenyl) exhibit marginal aromatic contacts but extremely expanded stacks (π–π distance = 6.65 Å) or large transverse shifts in the crystal structure.[22]

The solid state spectra of the tetrachlorinated and -brominated derivatives **2d** and **2e** (Figure 6, right) with highly twisted π–systems are very similar to the respective monomer spectra in solution, indicating that in this case the rather bulky bay substituents diminish significantly the potential interactions between the chromophores.

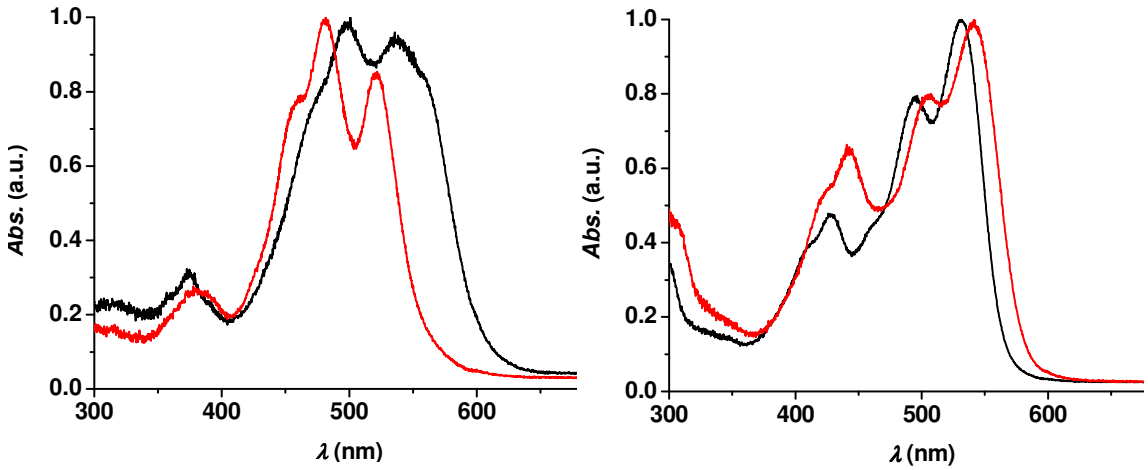

Figure 6. Solid state UV/Vis absorption spectra of the $BaSO_4$ trituration of **2a** (black) and **2b** (red) (left), and **2d** (red), and **2e** (black) (right).

Due to insolubility the absorption spectrum of dye **3a** was recorded only in solid state. Compared to the corresponding fluorine-free PBI, which is a industrial "black pigment",[23] the $BaSO_4$ trituration of **3a** (Figure 7) showed a significantly smaller bathochromic shift, rather resembling the solid state spectra of **1a** or **1b**.

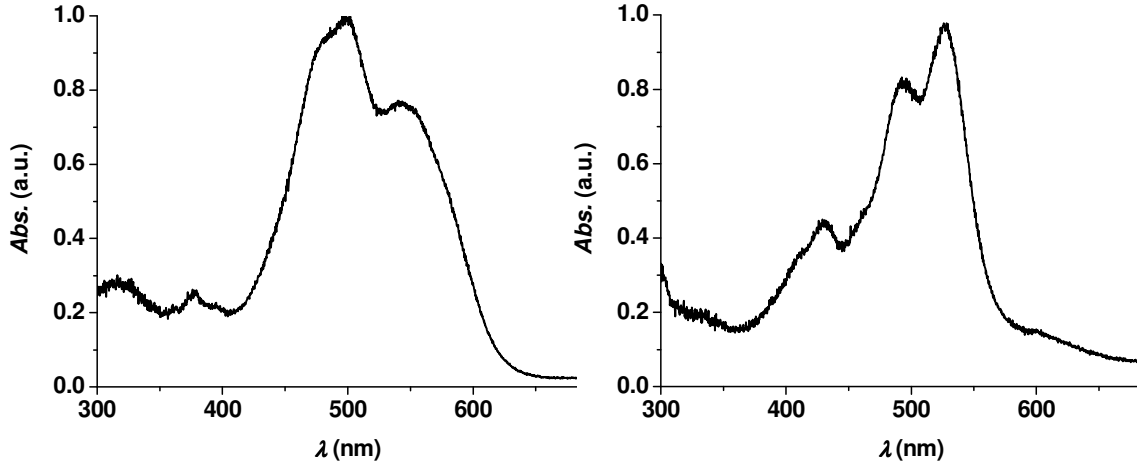

Figure 7. Solid state UV/Vis absorption spectra of the $BaSO_4$ trituration of **3a** (left) and **3b** (right).

The absorption maximum of **3a** was slightly hypsochromically shifted to 501 nm, but a new strong band at 543 nm is also observable. This band leads to the dark red color of the solid of **3a**. Though no single crystal could be obtained, the color differences of

the monomeric dye and the trituration are clear evidence for a significant change in solid state packing. By contrast, the solid state spectrum of the core-chlorinated derivative **3b** (Figure 7, Table 3) is again very similar to the other tetrachlorinated derivatives **1d** and **2d** with little π–π interactions between the chromophores.

The solid state spectra of **4a** and **4b** are very similar to those of **1a**. Compared to the monomer solution of **1a** the maxima are hypsochromically shifted to 502 and 499 nm respectively, while two additional bands appear at about 555 nm (Figure 8).

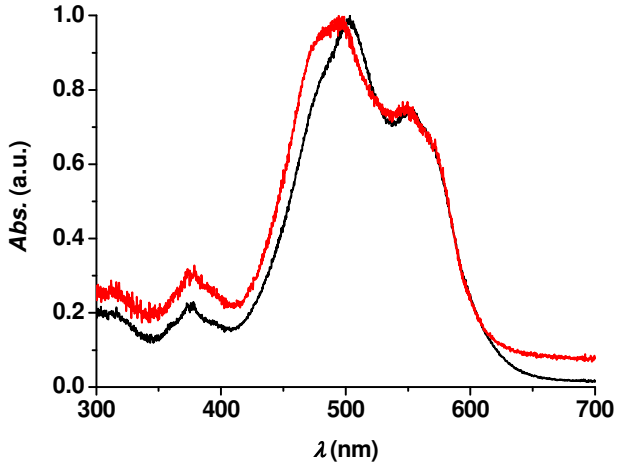

Figure 8. Solid state UV/Vis absorption spectra of the $BaSO_4$ trituration of **4a** (black) and **4b** (red).

5.4 Electrochemical Properties

The electrochemical properties of the soluble PBI derivatives were investigated by cyclic voltammetry and are summarized in Table 4. All dyes exhibit two reversible reduction waves, while no oxidation wave could be observed due to the limited scanning range in the given solvent. The increase of first and second reduction potentials for series **1** and **2** are depicted in Figure 9, while exemplary cyclic voltammograms of the unsubstituted PBI **1a** and the electron-poorest PBI **2e** are shown in Figure 10. The first reduction potentials of series **1** range from -0.95 eV (**1a**) to -0.70 eV (**1e**) (Table 4). Compared to other halogen-free alkyl substituted PBIs without core substituents (Figure 11), dye **1a** can be reduced more easily by about ~150 mV due to the electron-withdrawing effect of the perfluorinated butyl substituent. By bromination of the core (**1e**) the reduction potential is even elevated up to 400 mV in comparison to similar halogen-free hydrocarbons.

Table 4: Half-wave reduction potentials (in eV versus Fc/Fc^+) in dichloromethane and calculated LUMO energies of all soluble derivatives of series **1**, **2**, **3**, and **4**.

comp.	E (PBI/PBI^-)[eV][a]	E (PBI^-/PBI^{2-})[eV][a]	ε LUMO [eV][b]
1a	-0.95	-1.15	-3.85
1b	-0.92	-1.14	-3.88
1c	-0.87	-1.12	-3.93
1d	-0.74	-0.95	-4.06
1e	-0.70	-0.91	-4.10
2a	-0.88	-1.08	-3.96
2b	-0.86	-1.08	-3.94
2d	-0.69	-0.89	-4.11
2e	-0.64	-0.84	-4.16
3a	-1.01	-1.21	-3.79
3b	-0.81	-1.02	-3.99
4b	-0.96	-1.15	-3.84

[a] Measured in 0.1 M solution of Bu_4NPF_6 in dichloromethane with a scan rate of 100 mV/s, ferrocene served as internal standard; [b] determined according to literature methods (εLUMO = -4.8eV–(E(PBI/PBI^-)).[24]

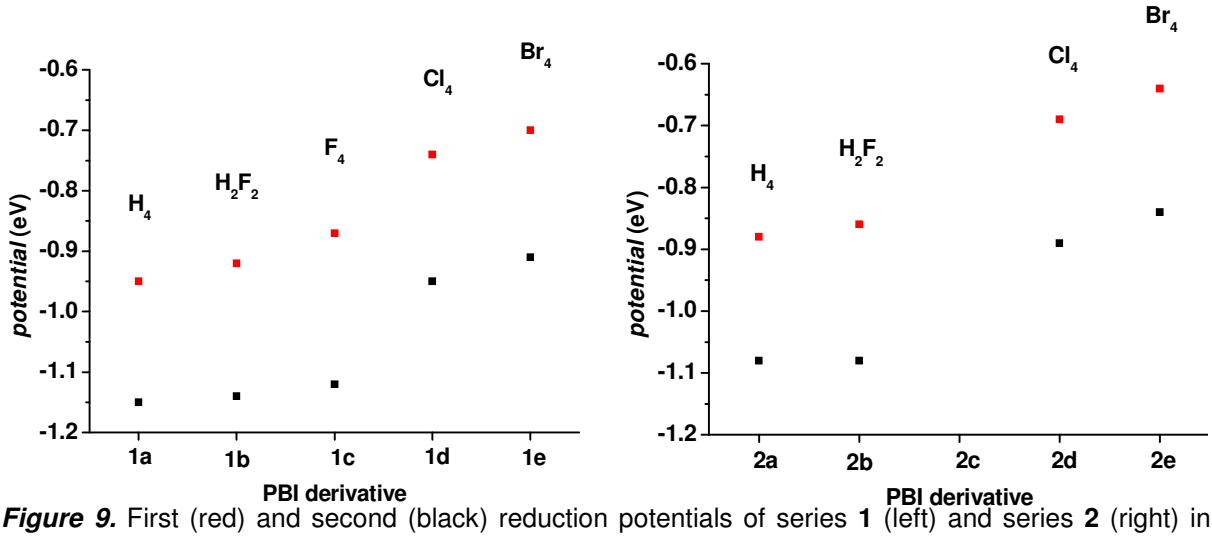

Figure 9. First (red) and second (black) reduction potentials of series **1** (left) and series **2** (right) in dependence of bay substituents in DCM using ferrocene as internal standard.

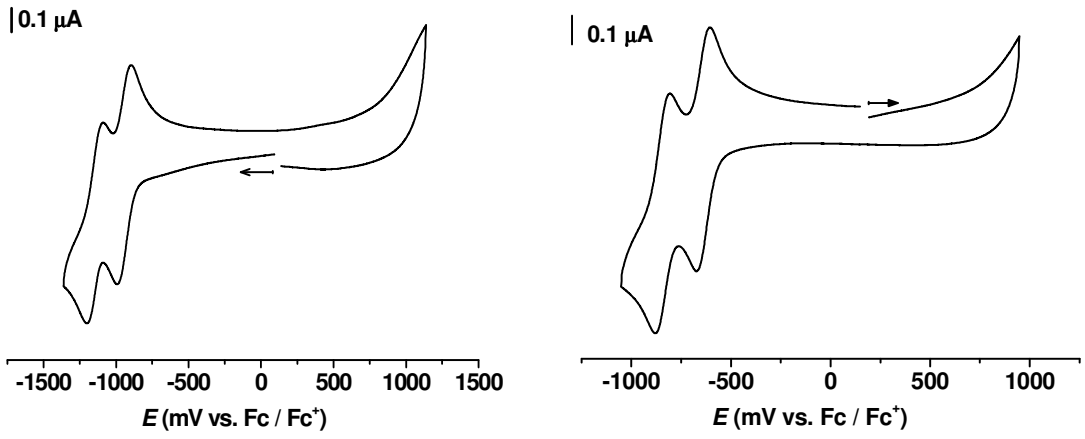

Figure 10. Cyclovoltamogramm of **1a** (left) and **2e** (right) in DCM using ferrocene as internal standard.

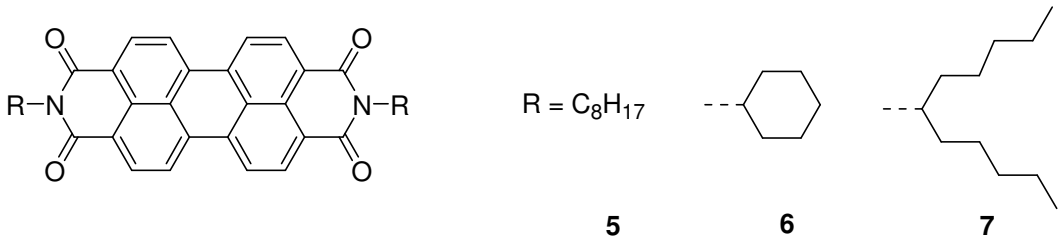

Figure 11. Halogen-free alkyl substituted PBIs.

Table 5: Half-wave reduction potentials (in eV versus Fc/Fc^+) in dichloromethane and calculated LUMO energies of all soluble derivatives of series **1**, **2**, **3**, and **4**.

comp.	E (PBI/PBI^-)[eV][a]	E (PBI^-/PBI^{2-})[eV][a]	ε LUMO [eV][b]
5	-1.13[c]	-1.32	-3.67
6	-1.10	-1.29	-3.70
7	-1.12	-1.37	-3.68

[a] Measured in 0.1 M solution of Bu_4NPF_6 in dichloromethane with a scan rate of 100 mV/s, ferrocene served as internal standard; [b] determined according to literature methods (εLUMO = -4.8eV–(E(PBI/PBI^-));[25] [c] due to low solubility concentration of the dye < 0.1M ("trace crossing effect").

Noteworthy is the quite small effect of the fluorine substitution of **1b** and **1c** (30 and 80 mV, respectively) compared with dye **1a** and the much larger increase (210 mV) by substitution with four chlorine atoms (**1d**). Dye **1e** with the tetrabrominated perylene core has the highest reduction potential in this series, although bromine possesses the smallest electronegativity in this row of halogens.

The dyes of series **2** bearing pentafluorophenyl substituents in the imide position can be reduced more easily than PBIs **1** as indicated by their first reduction potentials ranging from -0.88 eV (**2a**) to -0.64 eV (**2e**). The perfluorinated phenyl substituents can obviously withdraw electron density from the perylene core more easily. This effect has also been noted previously for fluorine-free aromatic and aliphatic imide substituents in literature.[26] The tendency in the row is equal to series **1** and the tetrabrominated compound **1e** is the electron-poorest dye of all derivatives studied in this work. The reduction potentials of PBIs **3a** and **3b** (Table 4) are in between those values of alkyl and perfluoro-alkyl substituted PBIs, which is not surprising as an additional CH_2 group is between the imide nitrogen and the electron withdrawing perfluoro-phenyl group. The redox properties of **4b** are as expected equal to **1a**.

5.5 Examination of the packing in the solid state.

For unambiguous assignment of the arrangement of the molecules in the solid state, crystallization experiments of all derivatives were carried out and five single crystals of

series **1** (**a**-**e**) and two single crystals of series **2** (**b**,**d**) suitable for X-ray diffraction could be obtained after several crystallization attempts. Solvent-free single crystals of compounds **1a**-**c**, **2b**, and **2d** were obtained by recrystallization from benzene (or toluene) or slow diffusion of methanol into chloroform, respectively. Single crystals of perylene bisimide dyes **1d** and **1e** of sufficient quality were very difficult to obtain, probably due to the pronounced twisting of the aromatic systems and the concomitant inclusion of solvent molecules. Hence no solvent-free crystals were obtained and benzene was embedded in both structures. The detailed crystallographic data are given in the experimental section.

Perylene bisimide **1a** crystallizes in the triclinic space group P-1 and the unsubstituted molecule shows a nearly planar π–system with a torsion angle of only 1.5° in bay position (C11-C9-C3-C5). The smallest C-C bond (1.38 Å) can be found in the perylene core between the C6 and C12. The longest bond length is, as expected, between the two naphthalene units (C3-C9, Figure 12) and corresponds with 1.47 Å to a $C(sp^2)$-$C(sp^2)$-single bond. The existence of these two individual naphthalene subunits in the perylene core was already revealed by *Graser* and *Hädicke* with the first X-ray single crystal analysis of different perylene bisimide dyes.[27]

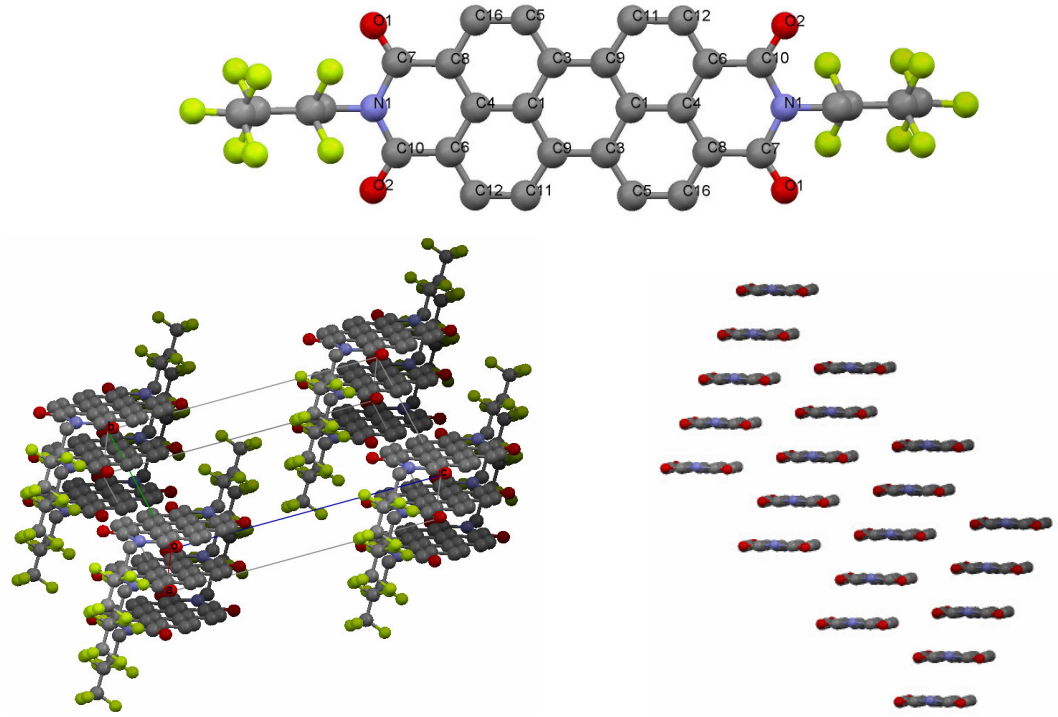

Figure 12. Single crystal structure with atom labels (top), packing with unit cell (left) and side view on the stacks (right, for clarity only the perylene part is shown) of **1a**.

In the crystal of **1a** the molecules are arranged in a slipped-stack face to face arrangement with a narrow π–π stacking of 3.31 to 3.35 Å (Figure 13), which is quite

similar to the interplane spacing of graphite.[28] The longitudinal (along the N-N axis, N-N distance ≈ 11.4 Å) displacement of the molecules is large (3.58 Å), but with a transverse displacement of only 1.21 Å the intermolecular π–π overlap is still over 50% (Figure 13, right). The closest distances (2.46 Å) between different perylene stacks can be found among the aromatic hydrogen atoms and the oxygens of the imide groups, which results in a very dense packing of the stacks

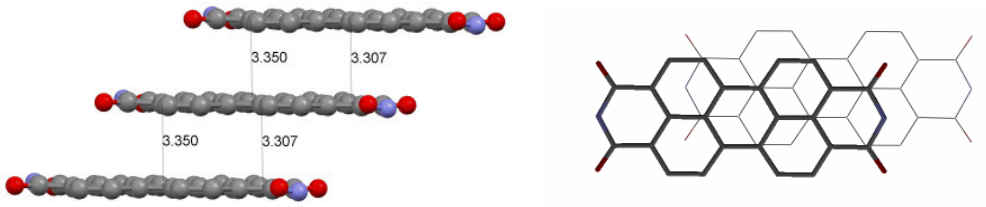

Figure 13. π–π-distances within the stack (left) and top view on the overlap of two neighboring molecules (right) of **1a**.

The difluorinated PBI derivative **1b** crystallizes in the monoclinic space group P2(1)/c. Since two fluorine atoms are small in size, the planarity of the molecules is not changed and the torsion angle in the bay area (C4-C3-C2-C1) is only slightly increased to 3.0° (Figure 14). Nevertheless, the solid state packing has changed from a slipped-stack to a typical “herringbone” arrangement with a close distance of 3.33 to 3.38 Å between the π–planes within a stack (Figure 15, left).

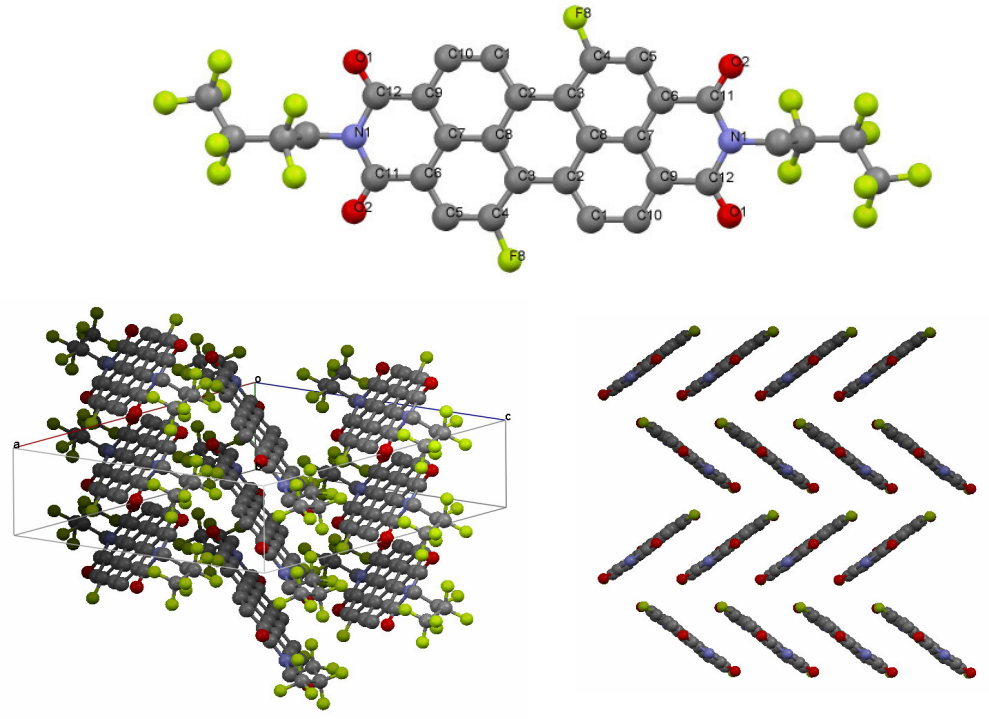

Figure 14. Single crystal structure with labels (top), packing with unit cell (left) and side view on the stacks (right, for clarity only the perylene part is shown) of **1b**.

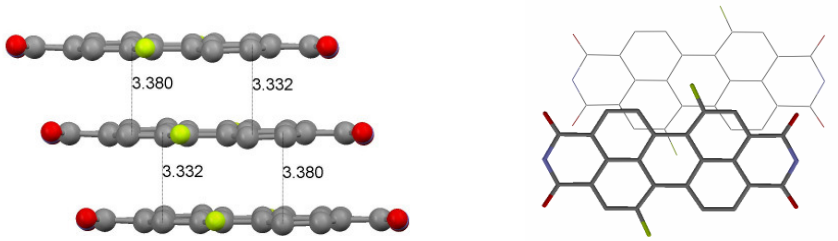

Figure 15. π–π distances within the stack (left) and top view on the overlap of two neighboring molecules (right) of **1b**.

This different arrangement might arise by the changed quadrupole of the dye due to the attachment of two fluorines in bay-position. Notably, the longitudinal shift (1.43 Å) of the molecules is significantly smaller than for **1a**, but the large transverse shift of 3.63 Å reduces the direct π–π overlap to less than ~5% (Figure 15, right). The closest distance between the stacks (2.49 Å) is now among a hydrogen atom in bay position of the perylene core and a fluorine atom of the alkyl chain. Next to the changed quadrupole another possible explanation for the different packing (compared to **1a**) could be the well known repulsion between electron-rich elements like oxygen and fluorine. For **1b** a similar arrangement is not possible, as in case of **1a** the terminal parts of the perfluorinated alkyl chains are in close distance to the hydrogens in bay position. Dye **1b** has two fluorines in bay position which would lead to a large repulsion between the fluorine atoms. Though this “herringbone” arrangement might not be perfect for an ideal charge carrier transport, the calculated density of this crystal structure is the highest (1.995 g/cm^3) in series **1** and **2**.

The tetrafluorinated perylene bisimide derivative **1c** crystallizes in the triclinic space group P-1. In this case another parameter, i.e. core-twisting, shows its influence on the packing, which provokes a much more complex arrangement (Figure 16). The repulsive interactions between the four strongly electronegative fluorine atoms in bay position distort the planar π–system which results in a twisting of the two naphthalene subunits. Due to packing effects and molecular interactions in the crystal lattice each molecule has two different dihedral angles in the bay area, 19.8° (C19-C20-C8-C7) and 25.1° (C23-C22-C10-C11), respectively (Figure 16, top). Also two different distances (1.46 and 1.47 Å) between carbon atoms (C10-C22, C8-C20, Figure 16, top) of the naphthalene subunits can be found, which is caused by the broken symmetry. Moreover, two molecules with opposite handedness are observed in the crystal structure in a ratio of 1/1. These atropisomers (*M*- and *P*-enantiomers) are only stable in the solid state due to low barrier of rotation in solution.[19] Though the naphthalene subunits of neighboring molecules are still parallel orientated to each other, two

different distances (3.18 and 3.28 Å, respectively) can be found along a stack (Figure 17, left).

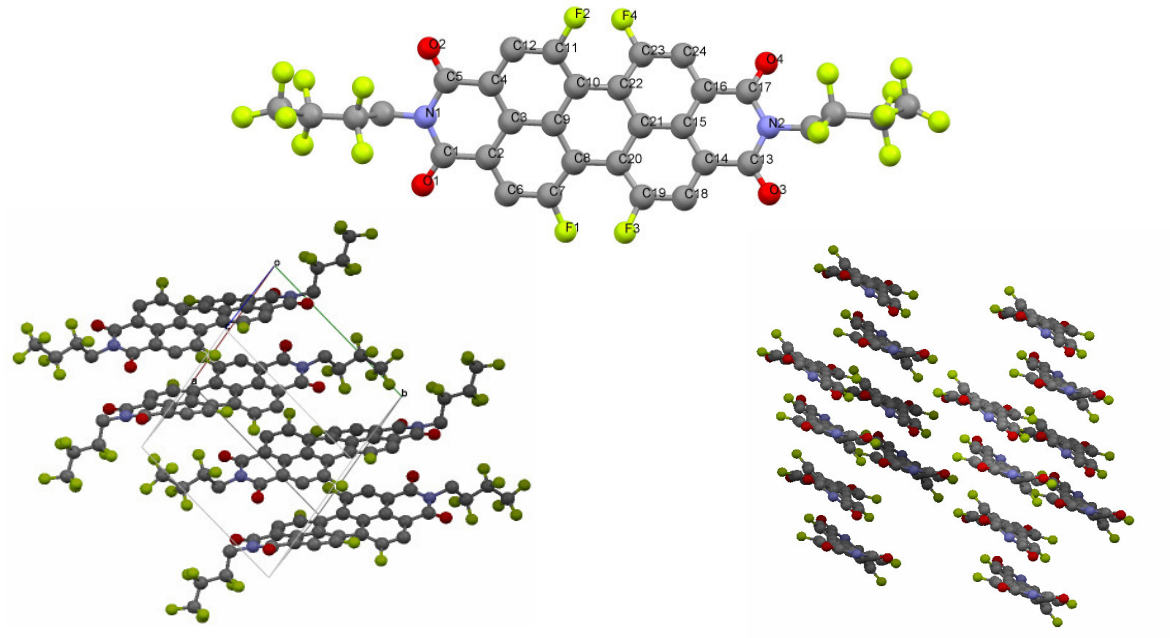

Figure 16. Single crystal structure with labels (top), packing with unit cell (left) and side view on the stacks (right, for clarity only the perylene part is shown) of **1c**.

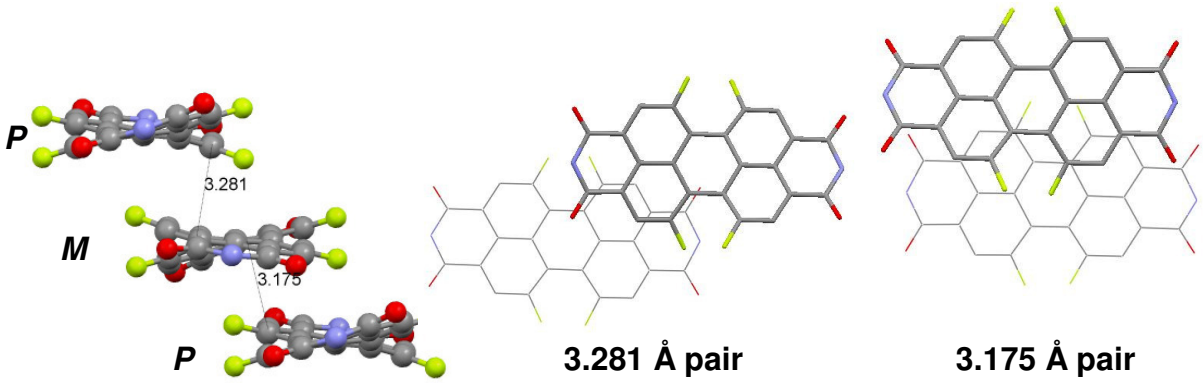

Figure 17. Minimal π–π-distances between the *M*- and *P*-enantiomers (left) and top view on the overlap of two closest neighbor molecules (middle, right) of **1c**.

These alternate arrangements of *M*- and *P*-enantiomers are quite common for solvent free crystals of tetrasubstituted perylene bisimide dyes and several examples are reported in the literature.[18,29] The closest intermolecular distance can be found, as in case **1a**, between an oxygen atom of an imide group and an aromatic hydrogen atom of a vicinal perylene. Because the twisting of the perylene core hinders a direct stacking the transverse shift of adjacent molecules is even higher (3.97 Å) than for **1b**, resulting in a negligible π–π overlap (Figure 17, right). Nevertheless the naphthalene subunits of vicinal perylene bisimides are oriented parallel to each other and these

arrangements led to an order of *M*- and *P*-layers (Figure 16). A shifted columnar stacking is less observable than in the other cases (**1a**,**b**).

As already mentioned, single crystals of **1d** with a sufficient quality for single crystal X-ray analysis could only be grown in aromatic solvents like benzene. This PBI crystallizes in the monoclinic space group C2. The four bulky chlorine atoms in bay position lead to high torsion angles of 34.8° (C19-C15-C22-C30) and 36.4°(C28-C9-C12-C8) (Figure 18, top).

Surprisingly the carbon-carbon bond length connecting the naphthalene subunits is quite small (1.43 and 1.44 Å) for this compound, even shorter than for the unsubstituted dye **1a**. In addition the crystal structure contains benzene molecules stack embedded in an alternating fashion along the b axis (Figure 19). With each naphthalene subunits one benzene molecule is associated with distances from 3.29 to 3.46 Å with a high overlap of the aromatic systems. This leads to “isomeric pure” crystals with only *M*-enantiomers in the whole single crystal. Furthermore, perpendicular layers of benzene molecules are embedded in these mixed stacks, separating them from each other in one direction (Figure 18, left).

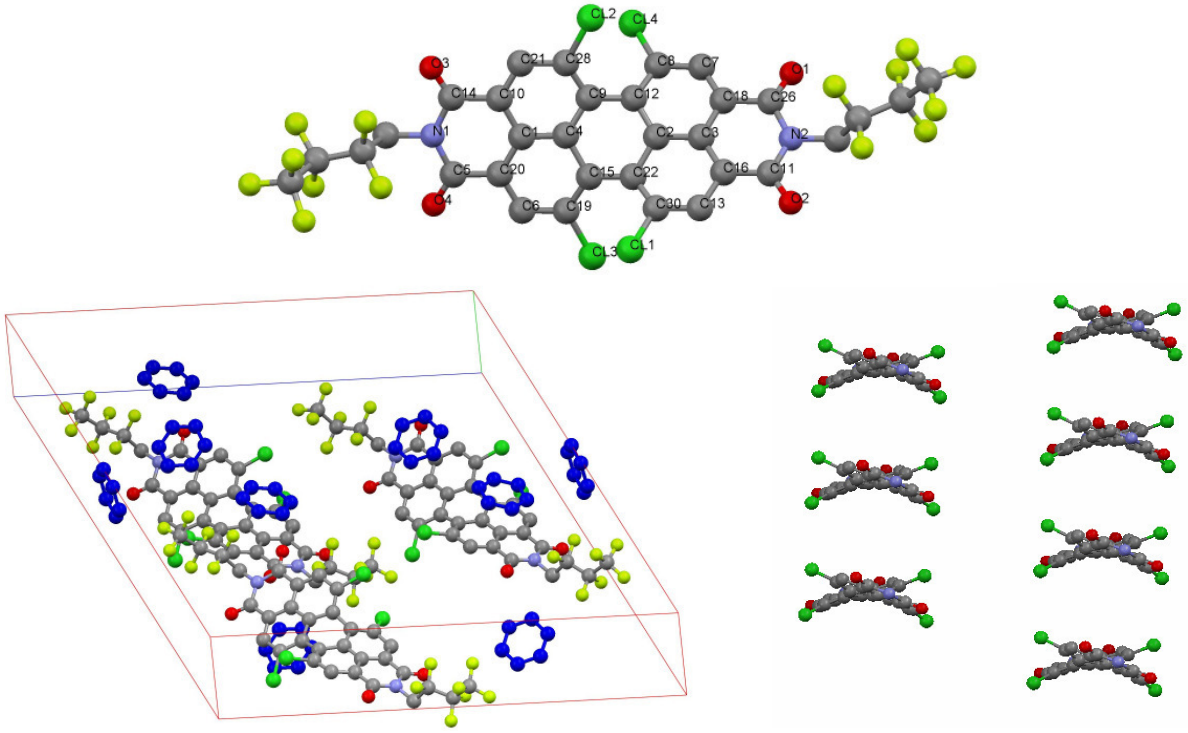

Figure 18. Single crystal structure with labels (top), packing with cell axis and disordered benzene (blue) (left) and side view on the stacks (right, for clarity solvent is omitted and only the perylene part is shown) of **1d**.

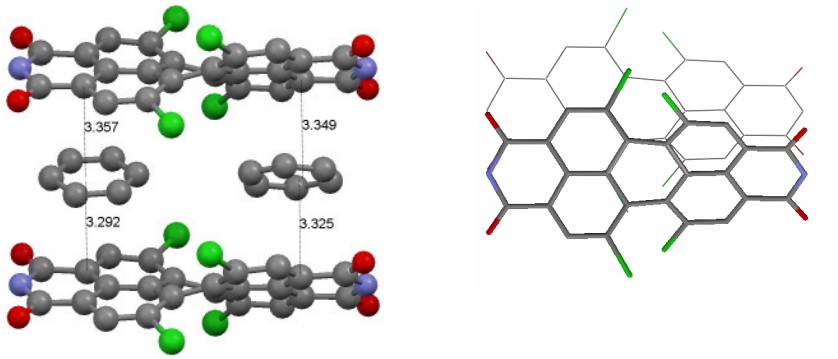

Figure 19. π–π distances between the molecules (left) and top view on the overlap of two neighboring molecules (right) of **1d**.

The crystal structure of **1e** is the first published one for a tetrabrominated perylene bisimide derivative and the dye crystallizes in the monoclinic space group C2, also with an inclusion of benzene between the perylene cores. In particular the torsion angle is very interesting. A "saturation" effect for the twisting of the perylene core was already suggested based on AM1 calculations.[19] Indeed the torsion angle (37.2°, C7-C8-C10-C11, Figure 20, top) increases only slightly compared to the tetrachlorinated compound **1d**. Having similar torsion angles and molecular dimensions as **1d**, the solid state of **1e** reveals quite identical packing attributes. The distances to the benzene molecules are ranging from 3.9 to 4.0 Å, and again only one isomer is found in the crystal (Figure 21). Though bearing the heaviest halogen (bromine) of the series, the inefficient inclusion of solvents and the highest torsion angles result in the lowest calculated density (1.838 g/cm^3) in series **1**.

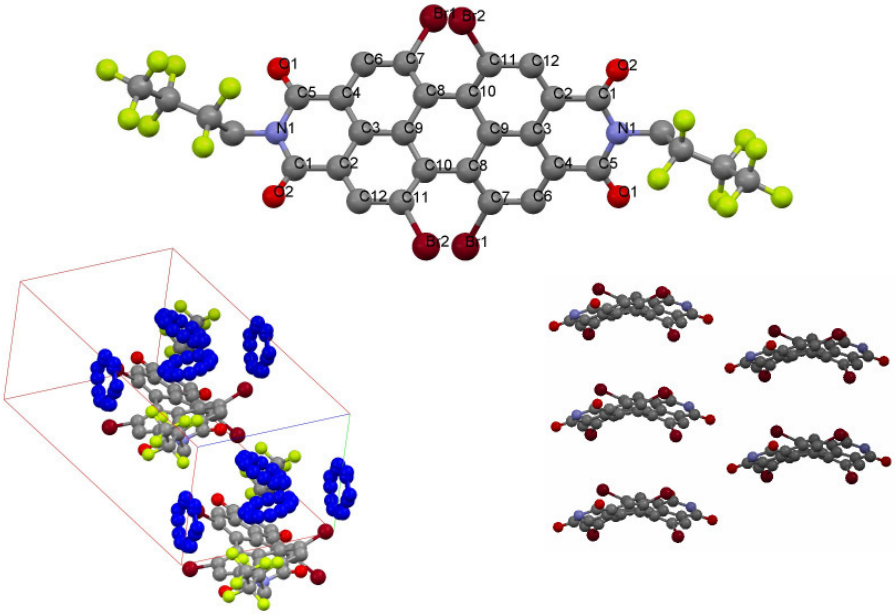

Figure 20. Single crystal structure with labels (top), packing with unit cell (left, with disordered benzene in blue) and side view on the stacks of **1e** (right, for clarity solvent is omitted and only the perylene part is shown).

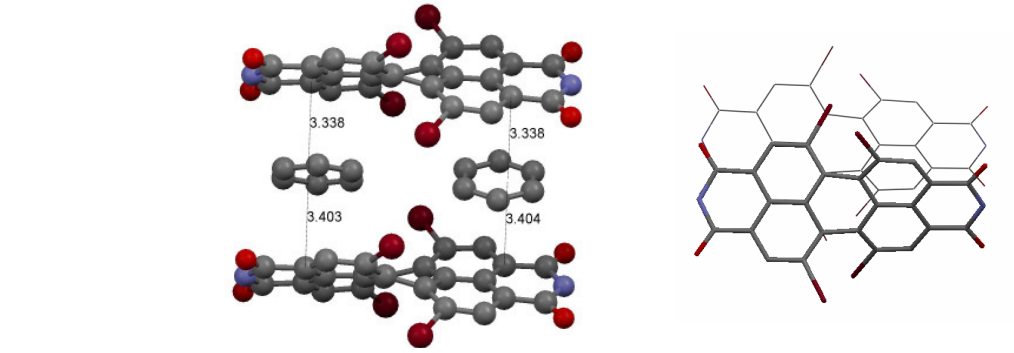

Figure 21. π–π distances between the molecules (left) and top view on the overlap of two neighboring molecules (right) of **1d**.

Notably, this is the first series of PBIs bearing identical imide substitutents but varying bay substituents that could be characterized by single crystal X-ray analysis. The experimentally obtained values for the torsion angle fit very well with the proposed non-linear increase of the torsion angles based on AM1 calculations (Figure 22).[19] Though the van der Waals radius of the bromine substituents is larger than the one of chlorine substituents, the accession of the torsion angle seems to have already reached the "level of saturation".

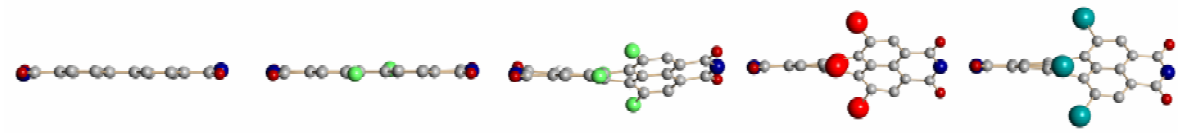

Figure 22. Side look onto the aromatic systems of **1a**, **1b**, **1c**, **1d** and **1e** showing a progressive twist of the perylene core.

This saturation behavior is nicely illustrated in a plot of experimental dihedral angles against the apparent overlap of the bay substituents (for calculation of the apparent overlap parameters, see ref 19 (Figure 23, Table 6).[a] From this plot several interesting conclusions arise:

Region A: For small apparent overlap, i.e. Σr^{*} < 2 Å a dense packing in stacks is maintained by increasing the distance between the two naphthalene subunits imide parts (1.466 (**1a**) to 1.472 Å (**1b**)) and increasing the angle (C-C-F) of the bay substituents from 120°(**1a**) to 122°(**1b**).

[a] For Figure 23 and Table 6 the empirically obtained data were used, as the distances and angles were taken directly from the single crystal X-ray analysis. Furthermore, the structures of five equally imide substituted dyes with different bay substituents could be obtained for the first time (especially the tetrabrominated derivative **1e**).

Region B: For 2 < Σr^* < 4 Å such planarization is obviously energetically not balanced any more by better packing leading now to increasing torsion (19.8 and 25.1°). Furthermore the distance between the naphthalene subunits and the angle (C-C-F) of the bay substituents (120.5°(**1c**)) are again slightly reduced.

Region C: When the overlap is again increased, i.e. Σr^* > 4 Å, the dihedral angle reaches its maximum value of about 37-38°. A further energetically less favored twisting in bay-position is apparently avoided by a distortion of other parts of the aromatic systems. The distance between the naphthalene subunit of the tetrabrominated dye **1e** is again enlarged to 1.474 Å (**1e**) and the angle (C-C-Br) of the bay substituents is now about 122°(**1e**).

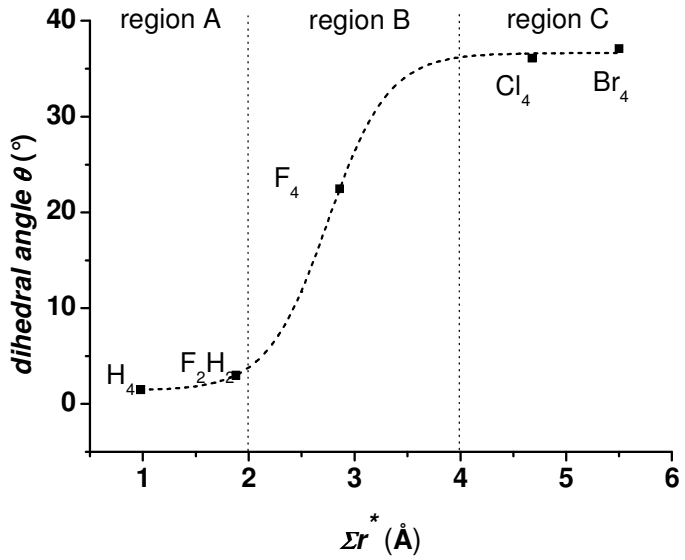

Figure 23. Dependence of the experimental dihedral angle and the apparent overlap for the discussed perylene bisimides calculated with values obtained by crystal structure of **1a**-**e**.

Table 6: Van der Waals radii, bond lengths, distance between substituents, overlap values and dihedral angles of **1a**, **1b**, **1c**, **1d** and **1e**.

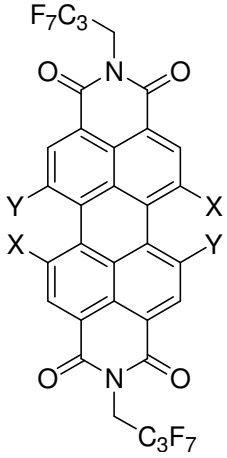

PBI	Subst.	r_{vdW}	a(C-Y)[a]	d(X,Y)[b]	$\sum r^*$(Å)	D. angle (θ)[a]
1a	X, Y=H	1.20	0.95	1.91	0.98	1.5
1b	X=H, Y=F	1.20/1.47	1.41	1.68	1.88	3.0
1c	X, Y=F	1.47	1.35	1.51	2.86	19.8/25.1
1d	X, Y=Cl	1.73	1.74	1.12	4.68	35.8/36.4
1e	X, Y=Br	1.86	1.89	0.97	5.50	37.2

[a] Distances and angles obtained from crystal structures; [b] theoretical distance between bay-substituents in a planar perylene.

The solid state packing of the derivatives **2b** and **2d** exhibit quite unusual crystal structures that are not related to previously found ones for perylene bisimides in the literature. Derivative **2b** crystallizes in the orthorhombic space group Pnna. The difluorinated perylene core is very similar to **1b** or even **1a** (Figure 24). Therefore the explanation of the unknown packing can only be given by consideration of the perfluorinated phenyl substituents at the imide nitrogens.

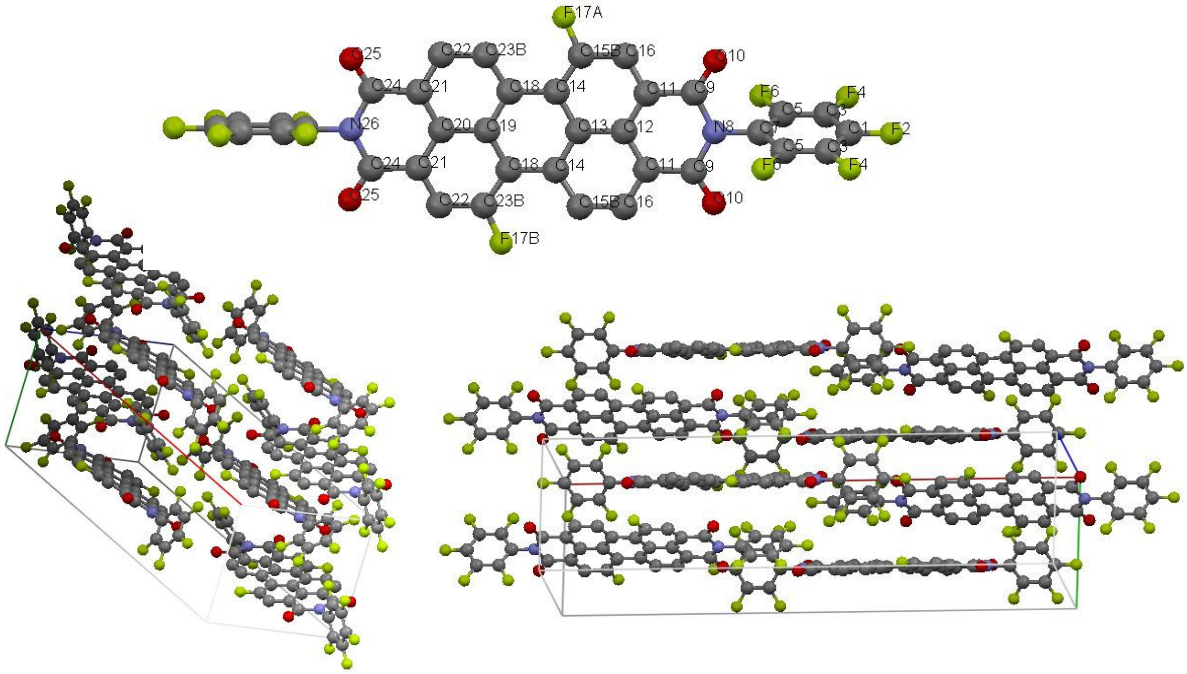

Figure 24. Single crystal structure with labels (top), packing with unit cell (left) and side view on the "brickstone" type stacks (right) of **2b**. The single crystals were obtained by slow crystallization of a chloroform/methanol mixture.

The bulky pentafluorophenyl groups have a large repulsion of their fluorine atoms with the oxygen atoms of the imide groups, leading to torsion angles of ~63° and ~88° of the N-C axis (e.g. C9-N8-C7-C5). The different values are probably caused by packing effects. Such pronounced twisting is also known for other phenyl substituents bearing e.g. methyl or diisopropyl in *ortho* position[22,18] that disfavor a more parallel orientation which would be required for a close parallel π–stacking of the dyes. Nevertheless, the molecules of **2b** are able to arrange in a side shifted brickstone like packing (Figure 24, right), which still enables close π–π contacts of less than 3.28 Å (Figure 25, left) due to an angulated arrangement of the perylene backbones. However, the π–π overlap of the vicinal PBIs is very small (Figure 25, right) and only the bisimide groups have a significant overlap with the neighbored π–surface. The angulated arrangement of the dye molecules leads to a less dense packing that is the

lowest among all dyes discussed so far (calculated density: 1.821 g/cm^3) It is noteworthy that a crystallization experiment in benzene afforded a parallel "herringbone" stacking with disordered toluene in the solid state (Figure 26). For this co-crystal, the distance between the perylene cores was larger than 6.8 Å, quite similar to **1d** and **1e**, while the torsion angles of the pentafluorophenyl substituents were less distinct (65° on both sides).

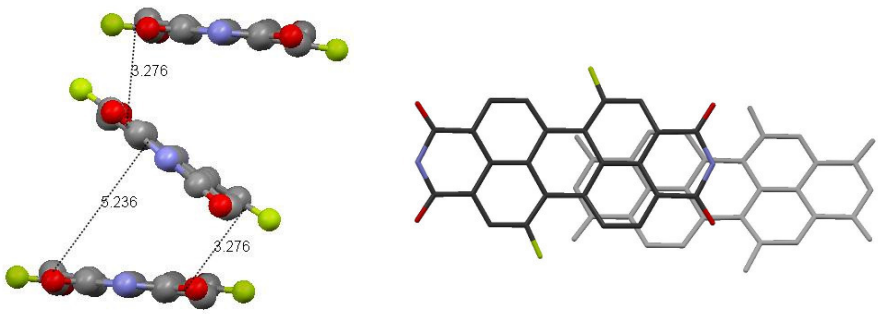

Figure 25. Minimal and maximal π–π-distances between the molecules (left) and view on the overlap of the closest two molecules (right) of **2b**.

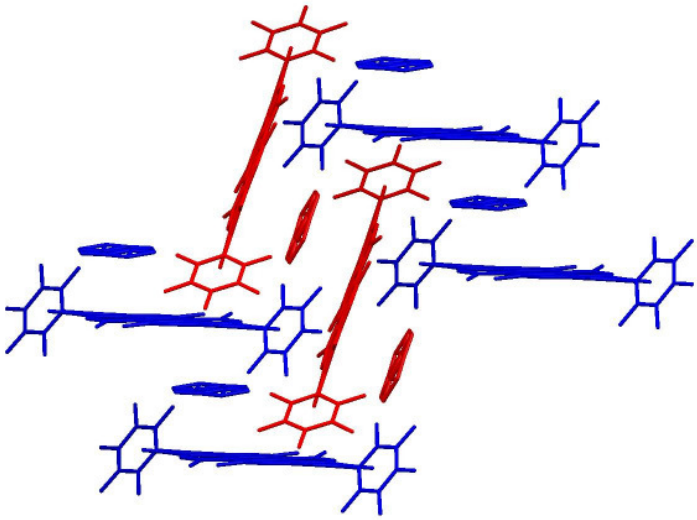

Figure 26. Crystal structure of **2b** with embedded disordered toluene molecules revealing a "herringbone" arrangement (blue and red = different stacks).

Tetrachlorinated perylene bisimide **2d** crystallizes in the triclinic space group P-1. For this derivative the perylene core is quite similar to **1d** with torsion angles in the bay position of 36.7° (C7-C8-C13-C14) and 35.8° (C11-C10-C19-C20, Figure 27, top). As already found in other solvent free crystal structures of tetrasubstituted PBIs, a 1:1 mixture of *M*- and *P*-enantiomers with two different distances (3.51 and 3.37 Å, Figure 28, left) –i.e. dimeric pairs–can be observed.

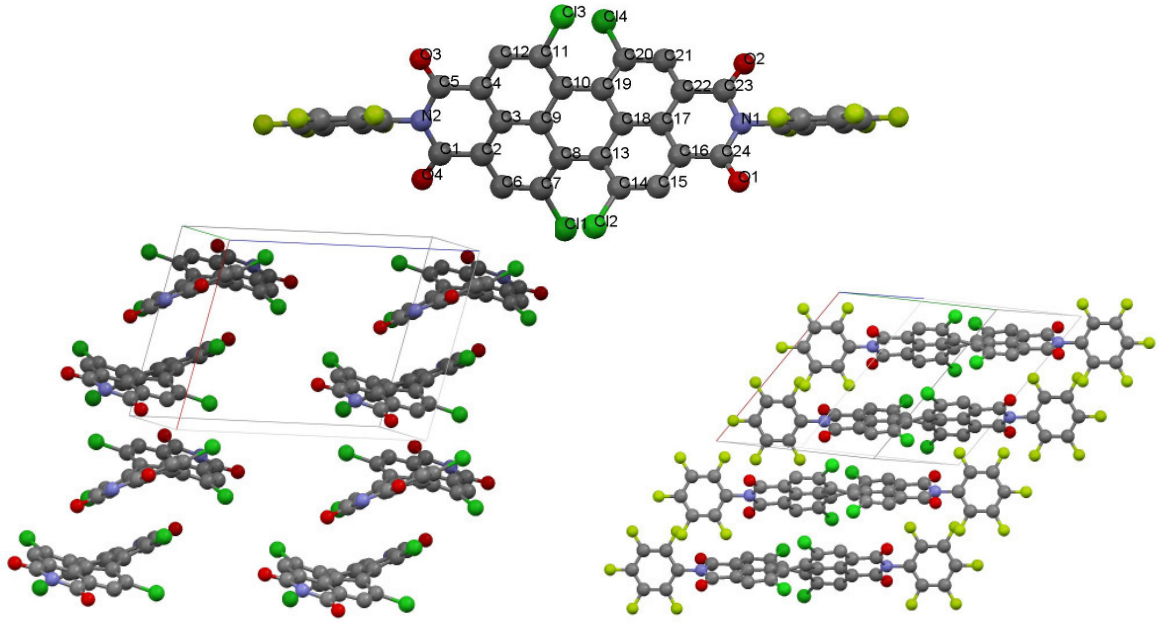

Figure 27. Single crystal structure with labels (top), packing with unit cell (left) and side view on the stacks (right) of **2d**.

The combination of the highly twisted aromatic core and the bulky imide substituents (torsion angles between 62° and 70°) makes pronounced π–π interactions even more difficult. Compared to **2b** the molecules of **2d** show a significant larger transverse shift in the crystal structure, resulting finally in a side shifted columnar arrangement (Figure 27, right). The closest enantiomers in one stack exhibit only a small π–π overlap of about 10%, the overlap with the second vicinal PBI is even smaller.

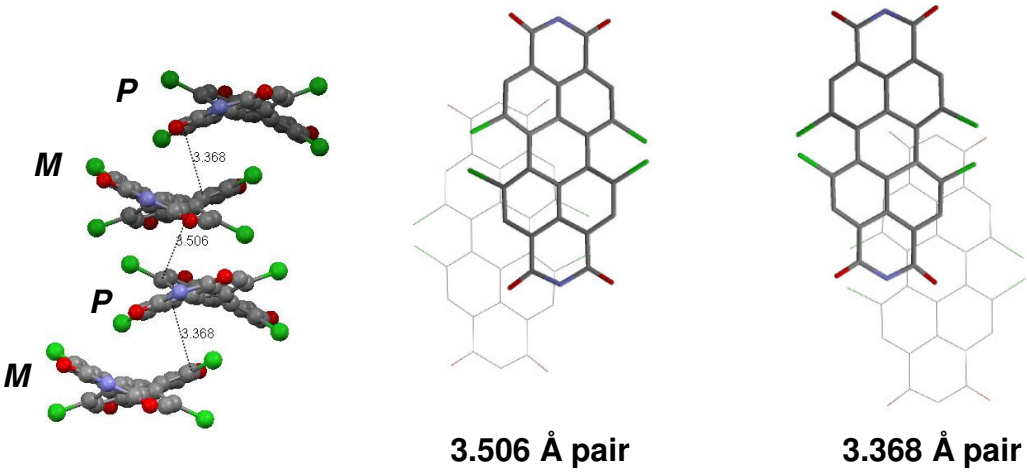

Figure 28. Minimal π–π-distances between the *M*- and *P*-enantiomers (left) and top view on the overlap of two neighboring molecules (middle, right) of **2d**.

As observed for **2b**, this very unusual packing could only be achieved by modified crystallization methods (slow diffusion of methanol into chloroform). The first crystal structure of **2d** showed also the typical inclusion of an aromatic solvent (toluene,

Figure 29) with distances of about 7.1 Å between the perylene cores. The solvent molecules were embedded in the perylene stacks with an average π–π distance of ~3.5 Å.

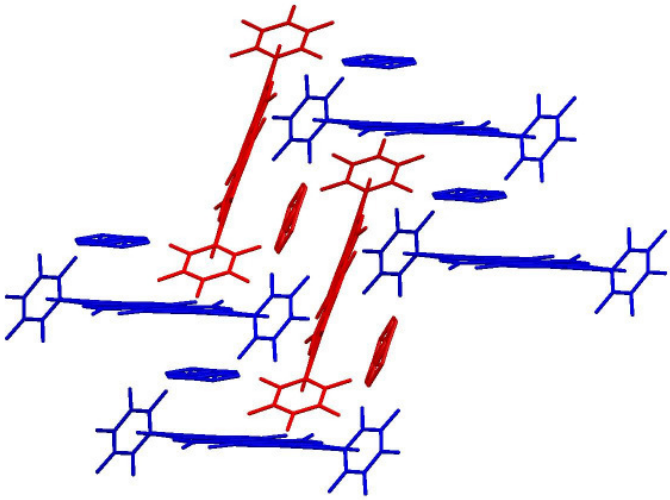

Figure 29. Co-crystal structure of **2d** revealing parallel stacking of the dyes with embedded disordered toluene molecules.

5.6 Performance in organic thin film transistors

To elucidate the potential of the synthesized perylene bisimide derivatives (series **1**-**4**) for electronic applications, OTFTs were built at Stanford University in the working group of Prof. Dr. Z. Bao (and coworkers Dr. J. H. Oh, Dr. M. M. Ling and S. Liu). The results of their investigations are summarized in the following part. For the top contact devices thin films were deposited by vacuum deposition techniques onto SiO_2 (300 nm)/n-doped silicon wafers which had been modified using a self-assembled monolayer of octadecyltriethoxysilane (OTS). Subsequently, gold electrodes were deposited through a shadow mask.

5.6.1 Series 1

The first devices of compounds of the series **1a**-**e** were prepared on surfaces with vacuum deposited OTS. The measured *I-V* characteristics of devices based on the five semiconductors are summarized in Table 7. The tetrabrominated PBI **1e** showed very low mobilities, which can be explained by the thermal instability of the dye leading partly to decomposition. Highly twisted tetrachlorinated dye **1d** did not decompose but showed very poor thin film quality, also resulting in low mobilities. Therefore the electronic attributes of TFTs of both dyes were not investigated in detail. Well-defined field effect characteristics were obtained for the perylene bisimides **1a**-**c** in the linear as well as the saturation regime (PBI **1a**, Figure 30).

Table 7: Summary of field-effect mobilities (μ), on/off rations (I_{on}/I_{off}), and threshold voltages (V_t) for TFTs with PBIs of series **1** prepared on OTS-treated substrates (vacuum deposition) at various temperatures (T_D). The highest mobilities are bold.

PBI	T_D [°C]	N_2 atmosphere			Air		
		μ [cm^2/Vs]	I_{on}/I_{off}	V_t[V]	μ [cm^2/Vs]	I_{on}/I_{off}	V_t[V]
1a	25	0.06	5.3×10^6	9-24	0.05	5.7×10^5	25-32
	90	0.45	5.8×10^5	12-28	0.34	5.2×10^5	27-46
	110	0.52	6.5×10^5	15-28	0.43	8.7×10^5	29-44
	125	**0.67**	$\mathbf{7.5\times10^5}$	**14-29**	**0.51**	$\mathbf{4.3\times10^6}$	**28-43**
	140	0.35	4.1×10^5	7-21	0.27	6.8×10^5	21-33
1b	25	0.06	2.3×10^6	32.2	0.06	6.0×10^5	35.6
	90	0.12	7.8×10^6	11.9	0.11	1.6×10^6	17.5
	125	**0.35**	$\mathbf{3.5\times10^7}$	**14.3**	**0.34**	$\mathbf{9.2\times10^6}$	**19.6**
1c	25	0.02	3.4×10^5	28.9	0.02	1.1×10^4	29.3
	90	0.03	2.2×10^5	5.56	0.02	1.4×10^5	24.8
	125	**0.03**	$\mathbf{8.1\times10^5}$	**1.53**	**0.03**	$\mathbf{2.7\times10^6}$	**34.3**
1d	125	5×10^{-4}	n.a.[a]	n.a.[a]		air-stable	
1e	125	3×10^{-5}	n.a.[a]	n.a.[a]		not tested	

[a] Due to low performance the properties of dyes **1d** and **1e** in OTFTs were not further investigated.

As generally observed for organic semiconductors, the charge carrier mobility of the three compounds rises with increasing substrate temperature during film deposition, due to increased crystallinity and larger grain sizes.[10,30] For all dyes the highest charge carrier mobilities were obtained at deposition substrate temperatures of 125 °C, leading to excellent mobilities of 0.67 cm^2/Vs for **1a** and 0.34 cm^2/Vs for **1b**, and moderate mobility of 0.03 cm^2/Vs for **1c**. At higher temperatures (150 °C) no suitable films of **1b** and **1c** could be deposited onto the substrate under the pressure conditions used in the experiments.

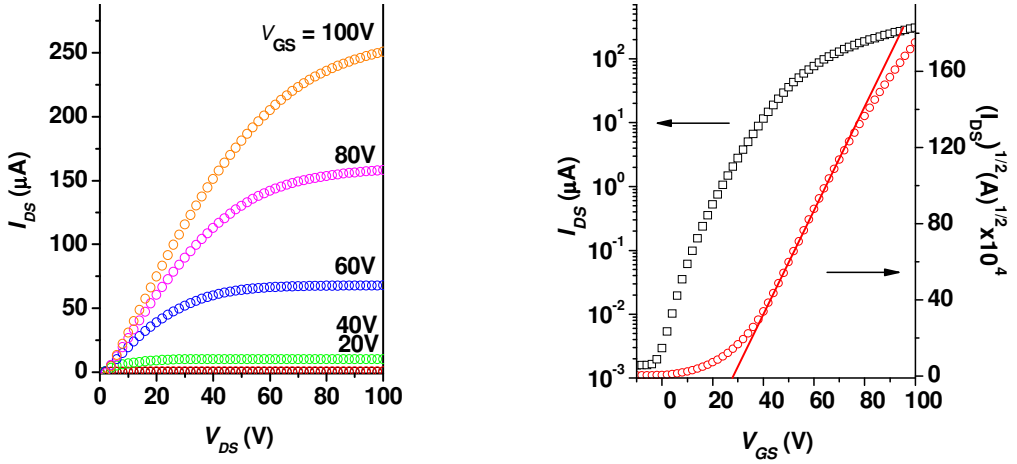

Figure 30. Current-voltage characteristics of a OTFT of PBI **1a** prepared at T_D = 125 °C: A plot of I_{DS} versus V_{DS} (left) and a plot of I_{DS} versus V_{GS} for V_{DS} = 100 V (right), the measurements were carried out under ambient environmental condition.

Also the AFM images (tapping mode) revealed that the grain size of the dyes, especially dye **1a** (Figure 31), became larger with increasing deposition temperature of the substrate. After deposition at 150 °C only some devices of **1a** showed transistor behavior. This is likely due to the significantly larger gaps between the grains and crack formation in the films.

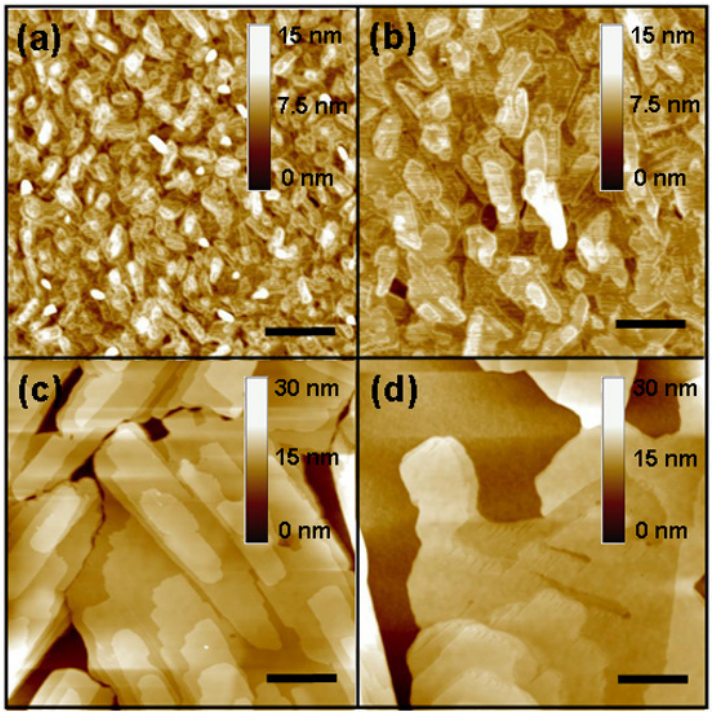

Figure 31. AFM topography images of **1a** thin films deposited onto OTS-treated SiO_2/Si substrates at various substrate temperatures: a) 25 °C, b) 90 °C, c) 125 °C, d) 150 °C, scale bar 400nm.

Considering the obtained solvent free single crystal structures for perylene derivatives **1a**-**c** the decreasing performance of the devices, going along with increasing torsion angles in bay position, is not astonishing. The two different distances between the *M*- and *P*-enantiomers of **1c** might provoke “dimer” traps in the thin film which are not suitable for maximization charge carrier transport. These disadvantageous packing attributes result also in a lower density (1.884 g/cm^3) of the crystal compared to **1a** and **b**, leading to reduced intermolecular interactions and presumably more pronounced vibrations of the molecules in the crystal. In addition **1c** did not precipitate easily in well ordered crystals during the crystallization experiments and on the substrate surface the vacuum deposited thin films were less regular and crystalline than the films of **1a** or **1b** (Figure 32).

The “herringbone” arrangement of PBI **1b** is more similar to well known solid state packing of established organic semiconductors like a-sexithiophene and pentacene.[31] Even though being per se not the perfect arrangement for ideal charge carrier transport,

some compounds (e.g. pentacene) show with this packing very high mobilities. The equidistant distances in the stacks of **1b** impede potential charge carrier traps, but the π–π overlap between the molecules is quite small. Interestingly, **1b** showed little differences in the transport properties, irrespective of using the pure 1,7 isomer or samples containing up to 15% contamination of the 1,6 isomer.

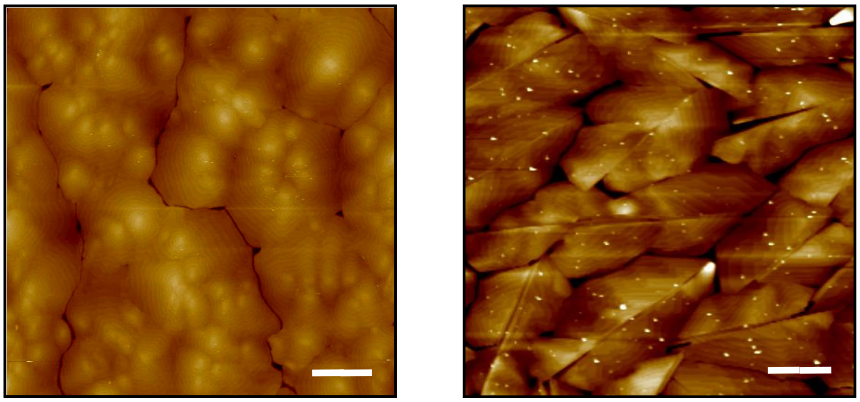

Figure 32. AFM topograpies for **1b** (left) and **1c** (right) thin films deposited at 125 °C onto OTS-treated SiO_2/Si substrates, scale bar 2 µm.

In contrast the packing of PBI **1a** (with the highest mobility) is very close to the ideal case. The molecules are arranged in slipped-stack parallel layers, and a two dimensional charge transport appears possible along the stacks and between the layers. The distance between the molecules within the stack is even smaller (3.31 Å) than that observed for the dicyano perylene bisimide derivative (3.40 Å)[13] which is known for its high charge carrier mobilities in air (Figure 1, R = perfluorobutyl, μ = 0.64 cm^2/Vs). Only in one dimension along the N-N axis the "isolating" perfluorinated alkyl chains reduce the potential of a pronounced three-dimensional charge carrier transport. As the maximum mobility is therefore strongly dependent on the orientation of the molecules between the electrodes, the vapor-deposited thin films of PBIs **1a**-**c** were analyzed by out of plane XRD measurements. While **1b** and **1c** showed non-uniform peaks, which displayed only a high crystallinity, the thin films of **1a** had a sharp primary peak at θ = 5.54°, which corresponds to a *d* spacing of 15.94 Å. Judging from a geometry-optimized length (21.78 Å) of the molecule, a tilt angle of 47° relative to the substrate normal is obtained, leading to a suggestion that the dye has favorable molecular orientations for charge transport between source and drain electrodes.

Next to the vacuum deposition of the OTS layer on the SiO_2 substrate another surface treatment was developed in Stanford. By deposition from solution a better

ordered coating was achieved. As the substrate treatment of the devices is one of the key parameters for high performance TFTs (e.g. thin films of PBI **1a** deposited on bare SiO_2 exhibited mobilities several orders of magnitude lower), this modification had again a substantial influence on the maximum mobilities. The most promising compounds of the first test series were examined again. Table 8 shows the increase of the mobility of **1a** to 1.44 cm^2/Vs and also the mobility of **1b** went up to 0.66 cm^2/Vs. Especially the value of **1a** is the highest reported mobility of an air-stable n-type semiconductor based on vacuum deposited TFTs.

Table 8: Increase of the maximum mobilities of differently treated substrate surfaces.

PBI	vacuum deposited OTS	solution deposited OTS
1a	0.72 cm^2/Vs	1.44 cm^2/Vs
1b	0.35 cm^2/Vs	0.66 cm^2/Vs

It is quite remarkable that TFTs of perylene bisimides **1a**-**d** exhibited mobilities in air close to those in nitrogen atmosphere. The performance of the TFTs of dye **1a**, without any electron-withdrawing groups at the perylene core, decreased only by 23%, while **1b** and **1c** with fluorine atoms in the bay position kept nearly entirely their mobility. Only the threshold voltages under ambient conditions were increased significantly showing that some more charges are trapped by oxygen or moisture.

The long time air stabilities of the two best derivatives **1a** and **1b** were investigated by testing their TFTs for more than 50 days under laboratory conditions. The mobility of **1a** (vacuum deposited OTS) decreased from 0.63 to 0.48 cm^2/Vs immediately after taking out the device from the glove box, but no further decrease was observed (Figure 33, left). The threshold voltage increased right after expose to air, but stayed in between 35 and 50 V (Figure 33, right). The on/off ratios improved compared to those in the nitrogen glove box, since the off current decreased by an order of magnitude. This might be due to the oxidation of unintentionally doped radical anions in air. The long time testing of TFTs of **1b** (vacuum deposited OTS) did not show any decrease at all and the performance stayed constantly at 0.34 cm^2/Vs. Its higher air-stability can be explained by the solid state packing. While for **1a** the intruding oxygen, after passing the perfluorinated alkyl chains, can diffuse easily between the perylene layers, the herringbone arrangements of **1b** might block the further entering of gas molecules. These observations are in clear contradiction to long time air-stability tests of the corresponding cyanated PBI derivative. A dramatic continuous decrease of the

performance by about 75% was observed during the first 50 days and the exponential decline continued for more than 400 days.[14] Furthermore, these effects were reported for several other core-cyanated perylene bisimide dyes with different perfluorinated imide substituents. Obviously only short term air-resistance of the electronic devices can be obtained by cyanation of the aromatic core, making this synthetic approach questionable for commercial applications.

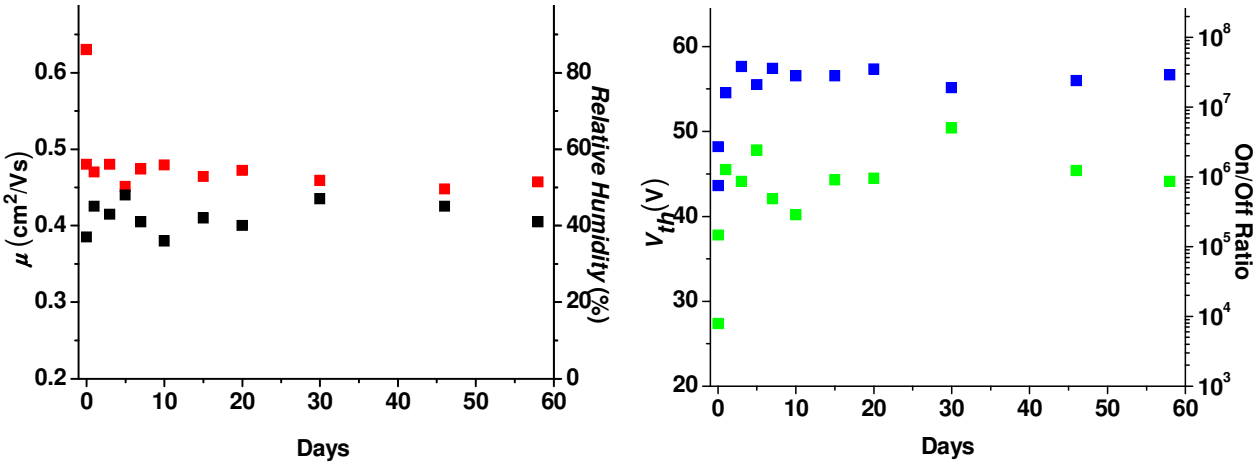

Figure 33. Air-stability measurements of a **1a** TFT (red) and relative humidity (black) (left), threshold voltage (green) and on/off ration (blue)(right).

To elucidate that the air stability of **1a** and **1b** can be attributed to an effect of the perfluorobutyl chains, a difluorinated perylene bisimide with halogen-free butyl chains (Chapter 4, PBI **4f**) was also tested in an OTFT. The mobilities in the glove box (N_2), especially on solution deposited OTS were even higher than thosefor **1b** (0.66 cm^2/Vs), showing values up to 0.89 cm^2/Vs and on/off ratios higher than 10^7. After exposure of the devices to laboratory conditions these outstanding attributes broke down very fast. The mobility decreased to 0.11 cm^2/Vs and the on/off ratio to 500. Similar observations were reported for naphthalene bisimides with perfluorinated alkyl substituents and their fluorine-free analogues.[32]

As already mentioned in the introduction, the reasons for the stability of n-type semiconductors towards air- and humidity might either be explained by adequate reduction potentials or by a dense crystalline packing, which hinders the intrusion of oxygen and moisture into the charge carrying thin layer at the gate dielectricum. The reduction potentials of the air stable PBIs **1a** and **1b** are higher (~0.12-0.15 V) than those of derivatives with simple alkyl groups at the imide position, but the reduction potential is by far not high enough to avoid reaction of radical anions with molecular

oxygen. An explanation for the long time stability must therefore be found in the special packing in the solid state. Unfortunately no single crystal of the PBI **4f (**Chapter 4) could be obtained, but the structures of the very similar dye **1a** and its corresponding fluorine free perylene were available. The space-filling illustration of their PBI stacks in solid state (Figure 34) shows the potential corroding surface for oxygen in the crystalline thin film. *Katz* et al proposed that the larger van der Waals radius of fluorine (compared to hydrogen) reduces the spacing between the imide alkyl substituents (Figure 34, left) from 4 Å to 2 Å and diminishes the possibility of O_2 intrusion.[11]

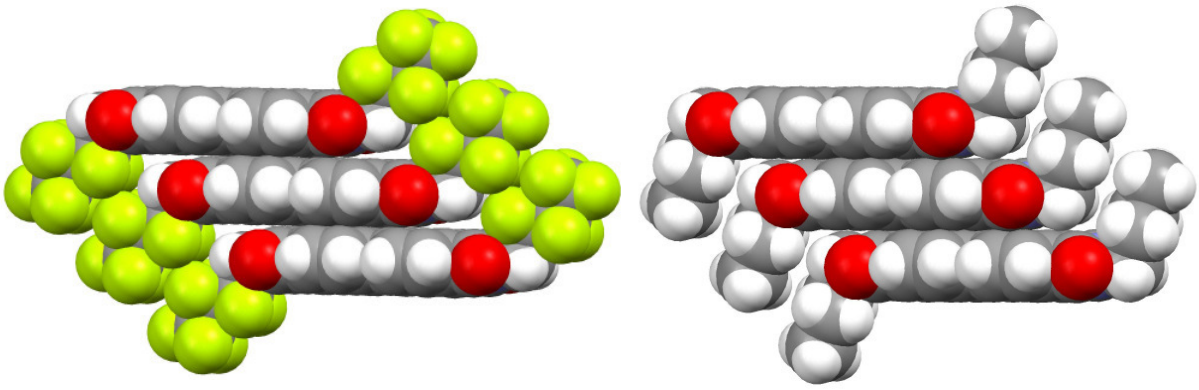

Figure 34. Space-filling depiction of single crystal structures of PBI **1a** (left) and its corresponding halogen-free dye (right), made of the corresponding cif file,[33] showing the potential "channel" for intrusion of oxygen between the fluorine-free butyl chains.

5.6.2 Series 2

The charge carrier mobilities of series **2** were also investigated with both kinds of surface treatments. As in series **1** the best mobilities could be obtained at deposition substrate temperatures of 125 °C. While the performance of the devices of series **1** increased only by factor 2 to 3 for the modified OTS treatment, PBIs **2b** and **2d** showed an accession by factor 10 and 24, respectively. The mobilities of **2b** changed from 0.04 cm^2/Vs to 0.99 cm^2/Vs (Table 9), while **2d** improved from 0.03 cm^2/Vs to 0.38 cm^2/Vs. As already mentioned perylene bisimide dye **2a** was synthesized by *Chen* et al[12] and tested in Stanford, too. Its mobilities on the former OTS treated substrate were the highest (0.07 cm^2/Vs) in the series, while no further results were published for the improved surface. As the brominated perylene bisimides are according to experience not stable during vacuum deposition, derivative **2e** was not tested.

Table 9: Summary of field-effect mobilities (μ), on/off rations (I_{on}/I_{off}), and threshold voltages (V_t) for TFTs with synthesized PBIs of compounds **2b** and **2d** prepared on OTS-treated substrates (solution deposited) at various temperatures (T_D). The highest mobilities are bold.

PBI	T_D [°C]	N_2 atmosphere			Air		
		μ [cm^2/Vs]	I_{on}/I_{off}	V_t[V]	μ [cm^2/Vs]	I_{on}/I_{off}	V_t[V]
2b	25	0.01	5.8×10^5	13.8	0.01	1.2×10^6	35.7
	90	0.77	5.9×10^6	9.68	0.40	3.3×10^6	41.8
	125	**0.99**	$\mathbf{1.2\times10^7}$	**8.59**	**0.54**	$\mathbf{1.2\times10^9}$	**38.7**
	150	0.14	2.1×10^4	28.3	0.01	3.5×10^2	40.2
2d	25	0.01	6.9×10^4	55.8	0.00	2.1×10^4	4.87
	90	0.25	8.7×10^6	28.2	0.25	9.1×10^6	31.2
	125	**0.38**	$\mathbf{3.7\times10^7}$	**19.9**	**0.27**	$\mathbf{4.7\times10^7}$	**29.8**
	140	0.20	4.6×10^6	21.1	0.18	5.1×10^7	34.5

To elucidate the very high accession of the mobilities with different surface treatments, the thin layers of **2b** and **2d** were investigated by AFM measurements. To clarify the growth mechanism, the first measurements were done on the sub-monolayer growth at a target thickness of only 3 nm. Figure 35 shows very clearly the deficient connected micro-crystallites of **2b** on the former OTS (middle) and also on bare SiO_2 (left), while the improved surface treatment (OTS deposition from solution) led to well accreted structures (left). This tendency goes on with increasing thickness of the layers. Figure 36 exhibits that for the best surface treatment (left) all crystallites are really well connected with each other, while for the former OTS surface (middle) the crystallites are larger, but have only little contact at the grain boundaries. The film on bare SiO_2 (right) shows only unfavorable attributes. The domains are very small and poorly connected with each other.

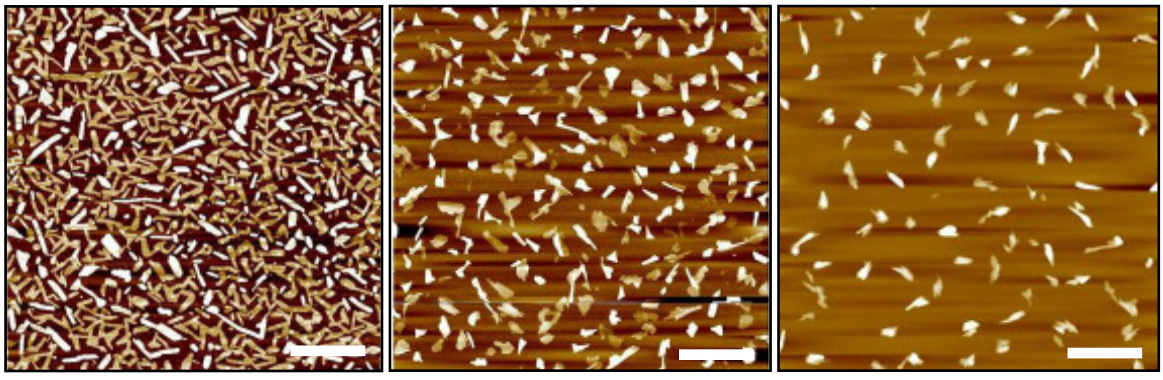

Figure 35. AFM topograpies for **2b** on solution deposited OTS (left), on vacuum deposited OTS (middle) and on bare SiO_2 (right), thickness 3 nm, scale bar 2 µm.

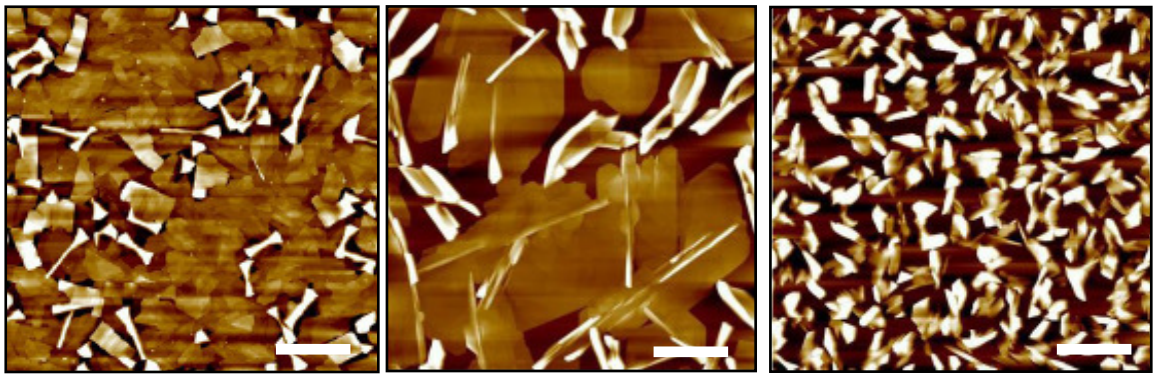

Figure 36. AFM topograpies for **2b** on solution deposited OTS (left), on vacuum deposited OTS (middle) and on bare SiO_2 (right), thickness 45 nm, scale bar 2 µm.

Next to the excellent mobility values, the on/off ratios of series **2** are also outstanding. While **1b** reached values over 10^7, derivative **2b** showed under exposure to air record values even over 10^9. The improvement is probably caused by the trapping of radical anions by oxygen in the off-state of the device. Furthermore, those extremely high numbers are up to now unreported for air-stable n-type organic semiconductors, whose ratios can normally be found between 10^4 and 10^5. These remarkable values extend the range of potential applications for this class of semiconductors significantly.

For perylene bisimides **2b** and **2d** a correlation between the single crystal structures and the high mobilities in OTFTs is more complicated than for series **1**, as uncommon packing motives were found. No parallel arrangements of the perylene cores are observable and also the π–π overlap between the chromophores is very small. As the thin films of all perylene bisimide derivatives show polycrystalline build-ups, it can be assumed that grain boundaries influence the charge carrier transport and that another limiting aspect for the mobility is presumably the smallest π–π distance between the perylene cores. Table 10 shows the highest mobilities and smallest distances of PBI derivatives (when a solvent free single crystal could be obtained).

Table 10: Summary of field-effect mobilities (μ) on solution deposited OTS, and smallest distances between the chromophores.

PBI.	highest mobility[a]	parallel stacking	smallest distance
1a	1.44 cm^2/Vs	yes	3.31 Å
1b	0.66 cm^2/Vs	yes	3.33 Å
1c	0.03 cm^2/Vs[b]	no	3.28/3.18 Å
2b	0.99 cm^2/Vs	no	3.28 Å
2d	0.38 cm^2/Vs	no	3.37/3.51 Å

[a] Obtained for solution processed OTS; [b] mobility available only for vacuum deposited OTS surface.

The best values were obtained for PBIs with small, uniform distances in the stack. The existence of *M*- and *P*- enantiomers (**1c** and **2d**) and changing distances seem to be more obstructive for a high performance TFT. These observations are not concordant with all charge carrier mobility measurements of twisted tetrasubstituted PBIs. PR-TRMC measurements revealed for a liquid crystalline tetrachlorinated PBI mobilities eight times higher than for its correspondent halogen-free PBI.[34] But in this case the better performance was explained by a higher order of the columnar stacks of the tetrachlorinated dye in the crystalline phase. This statement cannot count for series **1** and **2**, as all derivatives are highly crystalline and do not show phase transitions.

The devices of **2b** and **2d** were also tested under laboratory conditions (Table 9, right). The air stability was less pronounced than in series **1**, but still significantly larger than for fluorine-free PBI derivatives. The inferior performance compared to series **1** under the influence of oxygen and moisture can be related to the packing of the two derivatives. Due to the high torsion angle of the N-C axis of the perfluorinated imide substituents, a separation (as found for **1a** or **1b**) between aromatic core and imide substituents is no longer possible. This less dense packing of the pentafluorophenyl substituents makes the potential intrusion of oxygen into the thin layer easier. The slow propagation of oxygen continued apparently over the next days, shown by the highly varying mobility values of **2d** during long time measurements (Figure 37).

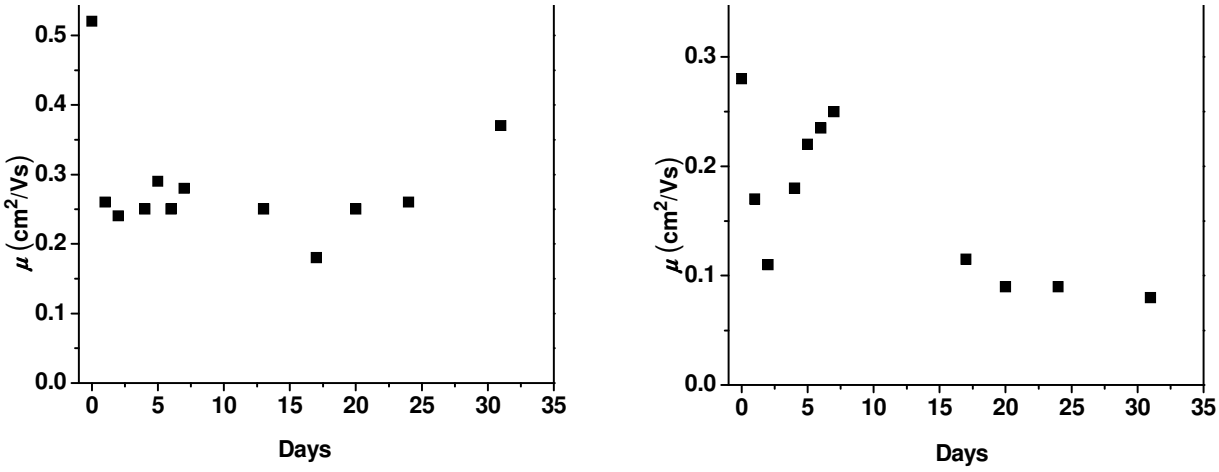

Figure 37. Air-stability measurements of a **2b** (left) and **2d** (right) over 30 days.

The devices of both derivatives did nevermore reach the performance of the first day during the tests in the following month and showed a further decrease of the measured mobilities for **2d**. This example shows very clearly that for the air-stability of the series **1**-**4** the position of the LUMOs is not deciding, as e.g. **2d** is easier to reduce than **1a**. In

fact, the separation of π–systems and perfluorinated alkyl or aryl substituents seems to be a main reason for longer resistance against moisture and air, since devices of **1a** and **1b**, which exhibited densely packed perfluorobutyl substituents, show excellent long time stability.

5.6.3 Series 3 and 4

The fluorine-free correspondent to dye **3a**, also known as a BASF "black pigment", is one of the few halogen free air stable n-type semiconductors with a reasonable charge carrier mobility of 0.11 cm^2/Vs according to measurements.[10] By fluorination of the phenyl part of the substituent the solid state packing was clearly changed as already revealed by the pigment color. Likewise the charge carrier mobility changed to give a much higher value of 0.62 cm^2/Vs (on solution deposited OTS). The air-stability of the device was also conserved and the mobility went down to 0.37 cm^2/Vs under exposition to oxygen.

The mobilities of **4a** and **4b** were tested only on the new OTS substrate. **4a** did obviously not pack in a favorable order and showed low mobilities of 0.05 cm^2/Vs. The first tests of **4b** exhibited mobilities of 0.11 cm^2/Vs, but annealing of the thin film for one hour at 150 °C improved the performance up to 0.61 cm^2/Vs. The lower charge carrier mobilities (compared to **1a**) were caused by deficient film quality, which could partly be overcome by annealing at a temperature of 150 °C. This process was not possible for dye **4a** with its very small trifluoroethyl substituents at the imide position. Furthermore **4a** and **4b** were not purified by column chromatography due to a low solubility, which might lead to higher remaining impurities in the thin layer despite forgoing purification by zone vacuum sublimation.

5.7 Conclusion

In summary, four series of perylene bisimide dyes bearing perfluorinated electron-withdrawing imide substituents were synthesized. The n-channel OFET characteristics for all compounds were tested at the University of Stanford and the solid state of the best derivatives was elucidated by single X-ray analysis and solid state UV/Vis spectroscopy. Furthermore, the correlation between torsion angle in bay position and charge carrier mobility was analyzed.

Highest n-channel charge carrier mobility could be mainly related to two different attributes. First of all a suitable substrate preparation is a key element for ideal ordered thin films, which are needed for unhindered transport in the active layer on top of the gate dielectricum. In addition, close π–π stacking interactions in the solid state are essential for efficient electron hopping, while parallel π–π stacking with high overlap between the chromophores seems to be less important.

As many of these n-type semiconductors showed impressive performance in air, the redox potentials of the dyes were also investigated. It was shown that air-stability relies less on low lying LUMOs compared to "normal" PBIs and more on the decreased possibility of intrusion of oxygen into the thin layer. In most instances perfluorinated imide substituents afforded electronic devices with long-lasting performance under ambient laboratory conditions.

Recapitulatory the best compounds exhibited a charge carrier mobility larger than 0.5 cm^2/Vs, which are one of the worldwide highest values for air-stable n-type semiconductors, and also exceptional high on/off ratios of more than 10^6.

5.8 Experimental Section

Material and methods. Di- and tetrabrominated perylene bisanhydrides **5c** and **5d** were synthesized according to literature.[35,36] For the synthesis of the dibromo perylene bisimide **1f** the isomeric mixture of the 1,7- and 1,6-isomers (in a ratio of about 9:1) and the pure 1,7-isomer were used.[36] The pure 1,7-dibrominated perylene bisanhydride was obtained according to literature. 2,2,2-Trifluoroethylamine, 2,2,3,3,4,4,4-heptafluorobutylamine, 2,2,3,3,4,4,5,5,5- nonafluoropentylamine, pentafluoroaniline, NMP, quinoline, zincacetate, acetic acid, potassium fluoride, 18-crown-6, sulfolane dichloromethane, chloroform, methanol, benzene, toluene and silica gel (Si 60; 40-63 μm) were purchased from commercial sources i.e. Merck, Fluka, Aldrich, or Fluka. Potassium fluoride was dried in vacuum (60 °C/10^{-3} mbar), sulfolane was fractionally destilled under vacuum prior to use. All other chemicals and solvents were used as received. 2-Pentafluorophenylethylamine[37] and the catalyst *N,N´*-dimethyl-imidazolidino-tetramethylguanidinium chloride (CNC^+)[18a] were synthesized according to literature procedure.

Thin layer chromatography. Thin layer chromatography was performed on

aluminium foils which were coated with silica gel 60 F_{254} and a concentration zone, purchased from Merck KGaA (Hohenbrunn, Germany).

Column chromatography. Flash and normal pressure column chromatography were done using silica gel Si60 (mesh size 0.032-0.063 mm) from Merck KGaA (Hohenbrunn, Germany) as stationary phase.

Melting points. Melting points were determined using a Olympus Bx41 polarization microscope (Olympus GmbH, Hamburg, Germany) equipped with a heating table (THMS 600, Linkam, Great Britain) and are uncorrected.

Mass Spectrometry (MS). MALDI-TOF mass spectrometry was performed on a Bruker Autoflex II spectrometer (Bruker Daltronics GmbH, Bremen, Germany). EI mass spectrometry was performed on a Finnigan MAT 90 spectrometer. High resolution mass spectra (HRMS) were recorded on an ESI MicroTOF Focus from Bruker Daltronics.

NMR spectroscopy. ^{1}H NMR spectra (400 MHz) were recorded on Bruker Advance 400 spectrometer; chemical shifts in $CDCl_3$ are given relative to $CHCl_3$ (δ = 7.26 ppm). ^{19}F NMR spectra (376.5 MHz) were recorded on Bruker Avance 400 spectrometer, chemical shifts in $CDCl_3$ are given relative to $CClF_3$ (δ = 0.00 ppm).

Absorption and fluorescence spectroscopy. For all measurements spectroscopic grade solvents (Uvasol®) from Merck were used. UV/Vis spectra were measured in quartz glass cuvettes under ambient conditions. The measurements were performed on a PE PE 950 spectrometer (Perkin Elmer GmbH, Rodgau, Germany). Fluorescence emission and excitation spectra were recorded on a PTI QM4-2003 fluorescence spectrometer and corrected against photomultiplier and lamp intensity. All fluorescence spectra are corrected. The fluorescence quantum yields were determined by optical dilute method[38] (A < 0.05) using *N,N´*-di(2,6-diisopropyl-phenyl)-perylene-3,4:9,10-tetracarboxylic acid bisimide (ϕ_{fl} = 1.00 in chloroform)[39] as reference. The solid state absorption spectra were also measured with a PE 950 spectrometer. The reflection was measured with a 10^{-4} M $BaSO_4$ trituration in an Ulbricht sphere.

Absolute fluorescence quantum yield determination in solid state. Absolute fluorescence quantum yields were determined on a Hamamatsu Absolute PL Quantum Yield Measurement System CC9920-02. The system is made up of an excitation source that uses a 150 W CW Xenon light source, a monochromator (250-700 nm, FWHM 10 nm), an integrating sphere, and a multi-channel spectrometer capable of simultaneously measuring multiple wavelengths between 300 and 950 nm and counting the number of absorbed and emitted photons. With this system the absolute fluorescence quantum yield of the pulverized dye was measured.

X-ray analysis. The X-ray diffraction data were collected on a Bruker X8 APEX diffractometer with a CCD area detector, using graphite-monochromated MoKα radiation. The structure was solved by using direct methods, refined, and expanded by using Fourier techniques with the SHELX software package (G. M. Sheldrick, SHELX-97, Universität Göttingen, 1997).[40] All non-hydrogen atoms were refined anisotropically. Hydrogen atoms were placed in idealized positions and included in structure factor calculations.

Electrochemical analysis. Cyclic voltammetry (CV) was performed with a BAS-Epsilon electrochemical analysor in a three electrode single-component cell under argon. Dichloromethane (HPLC grade) was used as solvent that was dried over calciumhydride and degassed prior to measurement. The supporting electrolyte tetrabutylammonium-hexafluorophosphate was recrystallized from ethanol/water and dried in high vacuum. The measurements were carried out at a concentration of 10^{-4} M with ferrocene as internal standard for the calibration of potential. Working electrode: Pt disc; reference electrode: Ag/AgCl; auxiliary electrode: Pt wire.

Device fabrication. Highly doped *n*-type (100) Silicon wafers (<0.004 Ω-cm) were used as substrates for the organic thin-film transistors (OTFTs). SiO_2 layers (300 nm) were thermally grown as gate dielectric onto Si substrates. Its unit area capacitance (C_i) was 10 nF/cm^2. The substrate surface was treated with *n*-octadecyl triethoxysilane [$C_{18}H_{37}Si(OC_2H_5)_3$, OTS]. A few drops of OTS (Aldrich Chemical Co.) were loaded on top of a preheated quartz block (~ 100 °C) inside a vacuum desiccator. The desiccator was immediately evacuated under vacuum (~ 25 mmHg) for 60 seconds. The SiO_2/Si substrate was treated for at least five hours to give a hydrophobic surface. The wafers

were subsequently baked at 110 °C for 15 min, and then rinsed with toluene, acetone, and isopropanol with drying under nitrogen after each step. Organic semiconductor thin films (40 nm) were vapor-deposited onto the Si/SiO_2 substrates held at well-defined temperatures between 25 and 150 °C with a deposition rate of 1.0 Å/s at 10^{-6} Torr, employing a vacuum deposition chamber (Angstrom Engineering, Inc., Canada).

Device characterization. Thin film transistors in top-contact configuration were used to measure the charge carrier mobility of the materials. Gold source and drain electrodes (typical channel lengths were 100 μm with width/length ratios of about 20) were vapor-deposited through a shadow mask. The current-voltage (*I-V*) characteristics of the devices were measured using a Keithley 4200-SCS semiconductor parameter analyzer. Key device parameters, such as charge carrier mobility (μ) and on-to-off current ratio (I_{on}/I_{off}), were extracted from the source-drain current (I_d) vs. gate voltage (V_g) characteristics employing standard procedures.

AFM. Measurements were performed by using a Multimode Nanoscope III (Digital Instruments/Veeco Metrology Group) AFM instrument in tapping mode.

Synthesis of series 1.

General imidization procedure A for perylene tetracarboxylic acid bisimides (1d-f).

The correspondent perylene-3,4:9,10-tetracarboxylic acid bisanhydride (**5b**-**d**) was dissolved in dry NMP under Argon. Then 2,2,3,3,4,4,4-heptafluorobutylamine and acetic acid were added. The mixture was stirred for 5 h at 90 °C and then poured into 2N HCl. The precipitate was filtered off and dried. The crude product was purified by column chromatography ($HCCl_3$) to give a red powder.

***N,N´*-Di(2,2,3,3,4,4,4-heptafluorobutyl)-1,6,7,12-tetrachloroperylene-3,4:9,10-tetracarboxylic acid bisimide (1d)**

According to general procedure **A**, 1.00 g (1.89 mmol) 1,6,7,12-tetrachloro-perylene-3,4:9,10-tetracarboxylic acid bisanhydride (**5b**), 1.06 g (5.35 mmol) hepta-fluorobutylamine and 680 mg acetic acid were dissolved in 20 ml dry NMP. The pure

product **1d** was isolated after column chromatography in a yield of 77% (1.30 g).
Mp: 401-410 °C; ^{1}H NMR ($CDCl_3$): δ 8.75 (s, 4H), 5.04 (t, 4H, ^{3}J(H,F) = 15.7 Hz); ^{19}F NMR (376.49 MHz, $CDCl_3$: δ -80.92 (t, 6F, ^{3}J(F,F) = 9.7 Hz), -116.41 (m, 4F), -128.15 (m, 4F); HR-MS (ESI (neg.-mode, chloroform, acetonitrile)): 924.8697 ($M+Cl^-$), calculated 924.8709 ($C_{32}H_8Cl_5F_{14}N_2O_4$); UV/Vis ($CH_2Cl_2$): λ_{max}/nm (ε_{max} /$M^{-1}cm^{-1}$) = 520 (38400), 486 (26700), 427 (12100); fluorescence (CH_2Cl_2): λ_{max} = 547 nm, fluorescence quantum yield ϕ_{fl} = 0.89; electrochemistry (CH_2Cl_2, 0.1M TBAHFP, vs. ferrocene): $E^{red}_{1/2}$ (PBI/PBI^-) = -0.74 V, $E^{red}_{1/2}$ (PBI^-/PBI^{2-}) = -0.95. V.
Single crystals of **1d** were obtained by recrystallization from benzene.
Crystal data of compound 1d. $C_{32}H_8Cl_4F_{14}N_2O_4$ + 2.5 (C_6H_6), orange bricks, monoclinic, space group C2, a = 27.0649(12), b = 7.0704(3), c = 26.3217(13) Å, α = 90°, β = 114.671(5)°, γ = 90°, V = 4577.1(4) Å^3, Z = 4, ρ_{calc} = 1.578 g/cm^3, μ = 0.363 mm^{-1}, F-(000) = 2180, T = 193(2) K, R_1 = 0.0917, wR_2 = 0.2550, 8962 independent reflections [$2\theta \leq 50.0°$] and 640 parameters.

***N,N´*-Di(2,2,3,3,4,4,4-heptafluorobutyl)-1,6,7,12-tetrabromoperylene-3,4:9,10-tetracarboxylic acid bisimide (1e).**

According to general procedure **A**, 500 mg (0.711 mmol) 1,6,7,12-tetra-bromoperylene-3,4:9,10-tetracarboxylic acid bisanhydride (**5c**), 500 g (2.60 mmol) heptafluorobutylamine and 340 mg acetic acid were dissolved in 10 ml dry NMP. Product **1e** was isolated after column chromatography in a yield of 66% (500 mg).
Mp: 440 °C (decomp.); ^{1}H NMR ($CDCl_3$): δ 8.89 (s, 4H), 5.03 (t, 4H, ^{3}J(H,F) = 15.7 Hz); ^{19}F NMR (376.49 MHz, $CDCl_3$): δ -80.95 (t, 6F, ^{3}J(F,F) = 9.8 Hz), -116.38 (m, 4F), -128.15 (m, 4F); HR-MS (apci (neg.-mode, chloroform)): 1065.6986 $(M)^-$, calculated 1065.6989 ($C_{32}H_8Br_4F_{14}N_2O_4$); UV/Vis ($CH_2Cl_2$): λ_{max}/nm (ε_{max} /$M^{-1}cm^{-1}$) = 529 (30500), 499 (21200), 442 (13700); fluorescence (CH_2Cl_2): λ_{max} = 568 nm, fluorescence quantum yield ϕ_{fl} = 0.54; electrochemistry (CH_2Cl_2, 0.1M TBAHFP, vs. ferrocene): $E^{red}_{1/2}$ (PBI/PBI^-) = -0.70 V, $E^{red}_{1/2}$ (PBI^-/PBI^{2-}) = -0.91 V.
Single crystals of **1e** were obtained by recrystallization from benzene.
Crystal data of compound 1e. $C_{32}H_8F_{14}Br_4N_2O_4$+ 3 ($C_6H_6$), orange needles, monoclinic, space group C2, a = 27.857(4), b = 7.1869(10), c = 13.0085(18) Å, α = 90°, β = 115.185(2)°, γ = 90°, V = 2356.8(6) Å^3, Z = 2, ρ_{calc} = 1.838 g/cm^3, μ = 3.52

mm^{-1}, *F*-(000) = 1276, *T* = 193(2) K, R_1 = 0.0273, wR_2 = 0.0666, 4631 independent reflections [$2\theta \leq 50.0°$] and 357 parameters.

***N,N´*-Di(2,2,3,3,4,4,4-heptafluorobutyl)-1,7-dibromoperylene-3,4:9,10-tetracarboxylic acid bisimide (1f).**

According to general procedure **A**, 469 mg (0.836 mmol) 1,7-dibromoperylene-3,4:9,10-tetracarboxylic acid bisanhydride (**5d**), 532 mg (2.67 mmol) heptafluorobutylamine and 342 mg acetic acid were dissolved in 17 ml dry NMP. Product **1f** was isolated after column chromatography in a yield of 94% (690 mg).

^{1}H NMR ($CDCl_3$): δ 9.54 (d, 2H, ^3J(H,H) = 8.2 Hz), 9.00 (s, 2H), 8.78 (d, 2H, ^3J(H,H) = 8.1 Hz), 5.04 (t, 4H, ^3J(H,F) = 15.3 Hz), literature known compound,[13b] improved yield.

***N,N´*-Di(2,2,3,3,4,4,4-heptafluorobutyl)-3,4:9,10-tetracarboxylic acid bisimide (1a).**

1.00 g (2.54 mmol) perylene-3,4:9,10-tetracarboxylic acid bisanhydride (**5a**), 1.43 g (7.19 mmol) heptafluorobutylamine and 920 mg acetic acid were dissolved in 15 ml dry NMP, stirred for 48 h at 200°C and then poured into 2N HCl. The crude product was filtered off and dried. Product **1a** was afforded after column chromatography in a yield of 25% (482 mg).

Mp: 421 °C (decomp.); ^{1}H NMR ($CDCl_3$): δ 8.78 (d, ^3J(H,H) = 8.0 Hz, 4H), 8.71 (d, ^3J(H,H) = 8.1 Hz, 4H), 5.04 (t, ^3J(H,F) = 15.5 Hz, 4H); ^{19}F NMR (376.49 MHz, $CDCl_3$): δ -80.97 (t, 6F, ^3J(F,F) = 9.8 Hz), -116.39 (m, 4F), -128.22 (m, 4F); HR-MS (apci (neg.-mode, chloroform)): 789.0264 ($M+Cl^-$), calculated 789.0268 ($C_{32}H_{12}F_{14}N_2O_4Cl$); UV/Vis ($CH_2Cl_2$): λ_{max}/nm (ε_{max} /$M^{-1}cm^{-1}$) = 524 (85200), 488 (50900), 457 (18500); fluorescence (CH_2Cl_2): λ_{max} = 531 nm, fluorescence quantum yield ϕ_{fl} = 1.00; electrochemistry (CH_2Cl_2, 0.1M TBAHFP, vs. ferrocene): $E^{red}_{1/2}$ (PBI/PBI^-) = -0.95 V, $E^{red}_{1/2}$ (PBI^-/PBI^{2-}) = -1.15 V; literature known compound,[41] improved synthesis and yield, fully characterized.

Single crystals of **1a** were obtained by recrystallization from toluene.

Crystal data of compound 1a. $C_{32}H_{12}F_{14}N_2O_4$, dark red needles, triclinic, space group P-1, a = 4.9104(4), b = 8.4835(7), c = 16.2891(13) Å, α = 97.489(4)°, β =

94.373(4)°, γ = 98.033(4)°, V = 663.08(9) Å^3, Z = 2, ρ_{calc} = 1.889 g/cm^3, μ = 0.191 mm^{-1}, F-(000) = 752, T = 193(2) K, R_1 = 0.0352, wR_2 = 0.0935, 2577 independent reflections [$2\theta \leq 50.0°$] and 235 parameters.

***N,N´*-Di(2,2,3,3,4,4,4-heptafluorobutyl)-1,7-difluoroperylene-3,4:9,10-tetracarboxylic acid bisimide (1b).**

40.0 mg (0.043 mmol) *N,N´*-Bis(2,2,3,3,4,4,4-heptafluorobutyl)-1,7-dibromo-perylene-3,4:9,10- tetracarboxylic acid bisimide (**1f**), 30 mg KF and 10 mg 18-crown-6 were heated to 160°C for 45 min in 1.5 ml sulfolane and then cooled down to room temperature. The reaction mixture was poured into water. After stirring for 1 h the precipitate was filtered and washed with water and dried under vacuum. The residue was purified by column chromatography ($HCCl_3$) to afford the product in a yield of 32% (11.0 mg).

Mp: 393-396 °C (decomp.); ^{1}H NMR ($CDCl_3$): δ9.23 (d, ^3J(H,H) = 5.3 Hz, 2H), 8.81 (d, ^3J(H,H) = 7.6 Hz, 2H), 8.62 (d, ^3J(H,F) = 13.5 Hz, 2H), 5.04 (t, ^3J(H,F) = 15.8 Hz, 4H); ^{19}F NMR (376.49 MHz, $CDCl_3$): δ -80.96 (t, 6H, ^3J(F,F) = 9.4 Hz), -102.23 (m, 2H), -116.38 (m, 4H), -128.18 (m, 4H); HR-MS (ESI (neg.-mode, chloroform, acetonitrile)): 790.0390 (M^-), calculated 790.0391 ($C_{32}H_{10}F_{16}N_2O_4$); UV/Vis (CH_2Cl_2): λ_{max}/nm (ε_{max} /M^{-1}cm^{-1}) = 509 (80100), 475 (46900), 445 (16500); fluorescence (CH_2Cl_2): λ_{max} = 516 nm, fluorescence quantum yield ϕ_{fl} = 1.00; electrochemistry (CH_2Cl_2, 0.1M TBAHFP, vs. ferrocene): $E^{red}_{1/2}$ (PBI/PBI$^-$) = -0.92 V, $E^{red}_{1/2}$ (PBI$^-$/PBI^{2-}) = -1.14 V.

Single crystals of **1b** were obtained by recrystallization from toluene.

Crystal data of compound 1b. $C_{32}H_{10}F_{16}N_2O_4$, orange needles, monoclinic, space group P2(1)/c, a = 17.4595(8), b = 5.2795(2), c = 15.2819(7) Å, α = 90.00°, β = 110.897(2)°, γ = 90.00°, V = 1315.99(10) Å^3, Z = 2, ρ_{calc} = 1.995 g/cm^3, μ = 0.208 mm^{-1}, F-(000) = 784, T = 193(2) K, R_1 = 0.0451, wR_2 = 0.1124, 2543 independent reflections [$2\theta \leq 50.0°$] and 244 parameters.

***N,N´*-Di(2,2,3,3,4,4,4-heptafluorobutyl)-1,6,7,12-tetrafluoroperylene-3,4:9,10-tetracarboxylic acid bisimide (1c).**

700 mg (0.956 mmol) *N,N´*-Bis(2,2,3,3,4,4,4-heptafluorobutyl)-1,6,7,12-tetrachloro-perylene-3,4:9,10-tetracarboxylic acid bisimide (**1d**), 1.09 g KF and 120 mg

(*N,N´*-dimethylimidazolidino)-tetramethylguanidinium chloride (CNC^+) (0.3 eq.) were stirred at 160 °C in 50 ml sulfolane for 2-3 h under argon. After cooling down to room temperature the reaction was quenched by addition of water and the precipitate separated by filtration, washed several times with water, and dissolved in CH_2Cl_2, dried over $MgSO_4$ and purified by silica gel column chromatography (pentane/DCM: 1/4). After removing the solvent under reduced pressure, the obtained solid material was redissolved in dichloromethane and precipitated by addition of methanol and dried in vacuum to give a red-orange powder in a yield of 8.6% (63.0 mg).

Mp: 322-328 °C; ^{1}H NMR ($CDCl_3$): δ 8.56 (t, ^3J(H,F) = 5.2 Hz, 4H), 5.04 (t, ^3J(H,F) = 15.3 Hz, 4H); ^{19}F NMR (376.49 MHz, $CDCl_3$): δ -80.95 (t, 6H, ^3J(F,F) = 8.8 Hz), -93.24 (t, 4H, ^3J(H,F) = 4.8 Hz,), -116.44 (m, 4H), -128.17 (m, 4H); HR-MS (ESI (neg.-mode, chloroform, acetonitrile)): 860.9886 ($M+Cl^-$), calculated 860.9891 ($C_{32}H_8F_{18}N_2O_4Cl$); UV/Vis (CH_2Cl_2): λ_{max}/nm (ε_{max} /$M^{-1}cm^{-1}$) = 502 (72400), 467 (44600), 438 (16200); fluorescence (CH_2Cl_2): λ_{max} = 512 nm, fluorescence quantum yield ϕ_{fl} = 0.90; electrochemistry (CH_2Cl_2, 0.1M TBAHFP, vs. ferrocene): $E^{red}_{1/2}$ (PBI/PBI^-) = -0.87 V, $E^{red}_{1/2}$ (PBI^-/PBI^{2-}) = -1.12 V.

Single crystals of **1c** were obtained by recrystallization from dichloromethane and methanol.

Crystal data of compound 1c. $C_{32}H_8F_{18}N_2O_4$, red needles, triclinic, space group P-1, a = 9.1985(5), b = 10.9675(6), c = 14.9248(7) Å, α = 87.475(2)°, β = 88.089(2)°, γ = 75.622(2)°, V = 1456.72(13) Å^3, Z = 2, ρ_{calc} = 1.884 g/cm^3, μ = 0.202 mm^{-1}, F-(000) = 816, T = 193(2) K, R_1 = 0.0414, wR_2 = 0.1014, 5656 independent reflections [$2\theta \leq 50.0°$] and 665 parameters.

Synthesis of series 2.

General imidization procedure B for perylene tetracarboxylic acid bisimides (2d-f).

To the correspondent perylene-3,4:9,10-tetracarboxylic acid bisanhydride (**5b**-**d**) dry NMP, 2,3,4,5,6-pentafluoroaniline, and acetic acid were added. The mixture was stirred for 28 h at 160 °C and then poured into 2N HCl. The precipitate was filtered off and dried. The crude product was purified by column chromatography to give a red powder.

***N,N´*-Di(pentafluorophenyl)-1,6,7,12-tetrachloroperylene-3,4:9,10-tetracarboxylic acid bisimide (2d).**

According to general procedure, 230 mg (0.434 mmol) 1,6,7,12-tetrachloroperylene-3,4:9,10-tetracarboxylic acid bisanhydride (**5b**), 550 mg (3.00 mmol) pentafluoroaniline and 170 mg acetic acid were dissolved in 8 ml dry NMP. Product **2d** was isolated after column chromatography (DCM) in a yield of 59% (220 mg).

Mp: 485 °C (subl.); ^{1}H NMR ($CDCl_3$): δ8.79 (s, 4H); ^{19}F NMR (376.498 MHz, $CDCl_3$): δ-143.70 (m, 4H), -151.43 (m, 2H), -161.48 (m, 4H); HR-MS (ESI (neg.-mode, chloroform, acetonitrile)): 892.8463 ($M+Cl^-$), calculated 892.8460 ($C_{36}H_4Cl_5F_{10}N_2O_4$); UV/Vis ($CH_2Cl_2$): λ_{max}/nm (ε_{max} /$M^{-1}cm^{-1}$) = 522 (43000), 488 (29400), 428 (12700); fluorescence (CH_2Cl_2): λ_{max} = 549 nm, fluorescence quantum yield ϕ_{fl} = 0.97; electrochemistry (CH_2Cl_2, 0.1M TBAHFP, vs. ferrocene): $E^{red}_{1/2}$ (PBI/PBI^-) = -0.69 V, $E^{red}_{1/2}$ (PBI^-/PBI^{2-}) = -0.89 V.

Single crystals of **2d** were obtained by recrystallization from dichloromethane and methanol.

Crystal data of compound 2d. $C_{36}H_4Cl_4F_{10}N_2O_4$, orange plates, triclinic, space group P-1,a = 11.7846(11), b = 12.0337(13), c = 13.2301(11) Å, α = 103.663(3)°, β = 100.758(3)°, γ = 117.633(3)°, V = 1516.5(3) $Å^3$, Z = 2, ρ_{calc} = 1.884 g/cm^3, μ = 0.503 mm^{-1}, F-(000) = 848, T = 193(2) K, R_1 = 0.0257, wR_2 = 0.0662, 5952 independent reflections [$2\theta \leq 50.0°$] and 505 parameters.

***N,N´*-Di(pentafluorophenyl)-1,6,7,12-tetrabromoperylene-3,4:9,10-tetracarboxylic acid bisimide (2e).**

According to general procedure, 350 mg (0.494 mmol) 1,6,7,12-tetrabromoperylene-3,4:9,10-tetracarboxylic acid bisanhydride (**5c**), 750 mg (4.10 mmol) pentafluoroaniline and 0.3 ml acetic acid were dissolved in 2 ml dry NMP. Product **2e** was afforded after column chromatography (DCM) in a yield of 41% (208 mg).

Mp: >500°C; ^{1}H NMR ($CDCl_3$): δ8.92 (s, 4H); ^{19}F NMR (376.498 MHz, $CDCl_3$): δ-143.62 (m, 4H), -151.38 (m, 2H), -161.41 (m, 4H); HR-MS (ESI (neg.-mode, chloroform, acetonitrile)): 1033.6739 (M^-), calculated 1033.6750 ($C_{36}H_4F_{10}Br_4N_2O_4$); UV/Vis ($CH_2Cl_2$): λ_{max}/nm (ε_{max} /$M^{-1}cm^{-1}$) = 533 (35100), 500 (24800), 443 (15500); fluorescence (CH_2Cl_2): λ_{max} = 569 nm, fluorescence quantum yield ϕ_{fl} = 0.64; electrochemistry (CH_2Cl_2, 0.1M TBAHFP, vs. ferrocene): $E^{red}_{1/2}$ (PBI/PBI^-) = -0.64 V,

$E^{red}_{1/2}$ (PBI^{-}/PBI^{2-}) = -0.84 V.

***N,N´*-Di(pentafluorophenyl)-1,7-dibromoperylene-3,4:9,10-tetracarboxylic acid bisimide (2f).**

According to general procedure **B**, 350 mg (0.636 mmol) 1,7-dibromoperylene-3,4:9,10-tetracarboxylic acid bisanhydride (**5d**), 750 mg (4.10 mmol) pentafluoroaniline and 0.3 ml acetic acid were dissolved in 2 ml dry NMP. Product **2f** was afforded after column chromatography (DCM) in a yield of 26% (210 mg).

^{1}H NMR ($CDCl_3$): δ8.12 (d, 2H, ^3J(H,H) = 8.1 Hz), 9.03 (s, 2H,), 9.58 (d, 2H, ^3J(H,H) = 8.1 Hz); HR-MS (ESI (neg.-mode, chloroform, acetonitrile)): 877.8542 (M^-), calculated 877.8540 ($C_{36}H_6Br_2F_{10}N_2O_4$).

***N,N´*-Di(pentafluorophenyl)-perylene-3,4:9,10-tetracarboxylic acid bisimide (2a).**

300 mg (756 µmol) perylene-3,4:9,10-tetracarboxylic acid bisanhydride (**5a**), 420 mg (2.29 mmol) pentafluoraniline and 98 mg zinc acetate were dissolved in 14 ml quinoline, stirred for 7 h at 200 °C and then poured into 2N HCl. The crude product was filtered off and dried. Product **1a** was afforded after column chromatography (DCM) in a yield of 19% (104 mg).

Mp: 338-342 °C (decomp.); ^{1}H NMR ($CDCl_3$): δ8.77 (d, 4H, ^3J(H,H) = 8.1 Hz), 8.82 (d, 4H, ^3J(H,H) = 8.0 Hz); MS (MALDI (neg.-mode, chloroform)): 722.023 (M^-), calculated 722.032 ($C_{36}H_8F_{10}N_2O_4$); UV/Vis (CH_2Cl_2): λ_{max}/nm (ε_{max} /$M^{-1}cm^{-1}$) = 527 (90200), 490 (54600), 459 (19800); fluorescence (CH_2Cl_2): λ_{max} = 534 nm, fluorescence quantum yield ϕ_{fl} = 1.00; electrochemistry (CH_2Cl_2, 0.1M TBAHFP, vs. ferrocene): $E^{red}_{1/2}$ (PBI/PBI^-) = -0.88 V, $E^{red}_{1/2}$ (PBI^-/PBI^{2-}) = -1.08 V; literature known compound,[42] fully characterized.

***N,N´*-Di(pentafluorophenyl)-1,7-difluoroperylene-3,4:9,10-tetracarboxylic acid bisimide (2b).**

128 mg (0.145 mmol) *N,N´*-Di(pentafluorophenyl)-1,7-dibromoperylene-3,4:9,10-tetracarboxylic acid bisimide (**2f**), 100 mg KF and 80 mg 18-crown-6 were heated to 160 °C for 45 min in 1.5 ml sulfolane and then cooled down to room temperature. The reaction mixture was poured into water. After stirring for 60 minutes the precipitate was filtered

and washed with water and dried under vacuum. The residue was purified by column chromatography (DCM) to afford the product in a yield of 45% (50 mg).

Mp: 465 °C (decomp.); ^{1}H NMR ($CDCl_3$): δ8.66 (d, 2H, ^3J(H,F) = 13.3 Hz), 8.85 (d, 2H, ^3J(H,H) = 7.5 Hz), 9.29 (m, 2H); ^{19}F NMR (376.498 MHz, $CDCl_3$): δ-101.88 (m, 2F), -143.66 (m, 4F), -151.71 (m, 2F), -161.67 (m, 4F); HR-MS (ESI (neg.-mode, chloroform, acetonitrile)): 792.98290 ($M+Cl^-$), calculated 792.98300 ($C_{36}H_6F_{12}N_2O_4Cl$); UV/Vis (CH_2Cl_2): λ_{max}/nm (ε_{max} /$M^{-1}cm^{-1}$) = 522 (92600), 476 (54800), 447 (19300); fluorescence (CH_2Cl_2): λ_{max} = 518 nm, fluorescence quantum yield ϕ_{fl} = 0.96; electrochemistry (CH_2Cl_2, 0.1M TBAHFP, vs. ferrocene): $E^{red}_{1/2}$ (PBI/PBI^-) = -0.86 V, $E^{red}_{1/2}$ (PBI^-/PBI^{2-}) = -1.08 V.

Single crystals of **2b** were obtained by recrystallization from dichloromethane and methanol.

Crystal data of compound 2b. $C_{36}H_6F_{12}N_2O_4$, red block, orthorhombic, space group Pnna, a = 31.880(2), b = 8.5607(6), c = 10.1357(7) Å, α = 90.00°, β = 90.00°, γ = 90.00°, V = 2766.2(3) Å^3, Z = 4, ρ_{calc} = 1.821 g/cm^3, μ = 0.174 mm^{-1}, F-(000) = 1504, T = 193(2) K, R_1 = 0.0406, wR_2 = 0.1072, 3272 independent reflections [$2\theta \leq$ 50.0°] and 260 parameters.

Synthesis of series 3.

***N,N´*-Di(2,3,4,5,6-pentafluorophenylethyl)-perylene-3,4:9,10-tetracarboxylic acid bisimide (3a).**

50 mg (0.711 mmol) perylene-3,4:9,10-tetracarboxylic acid bisanhydride (**5a**), 200 mg (0.974 mmol) pentafluorophenylethylamine and 5 mg zinc acetate were dissolved in 0.7 ml quinoline, stirred for 12 h at 180°C and then poured into 2N HCl. The crude product was filtered off and dried. Product **1a** was afforded after column chromatography ($HCCl_3$) in a yield of 15% (15 mg).

Mp: 408-413 °C; ^{1}H NMR ($CDCl_3$): δ8.67 (m, 8H), 4.53 (t, 4H, ^3J(H,H) = 6.6 Hz), 3.25 (t, 4H, ^3J(H,H) = 6.8 Hz);); ^{19}F NMR (376.498 MHz, $CDCl_3$): δ-143.72 (m, 2F), -152.21 (m, 1F), -161.99 (m, 2F); HR-MS (apci (pos.-mode, chloroform, acetonitrile)): 779.1025 $(M+H)^+$, calculated 779.1023 ($C_{40}H_{17}N_2O_4$), solubility not sufficient for UV/Vis spectroscopy; electrochemistry (CH_2Cl_2, 0.1M TBAHFP, vs. ferrocene): $E^{red}_{1/2}$ (PBI/PBI^-) = -1.01 V, $E^{red}_{1/2}$ (PBI^-/PBI^{2-}) = -1.21 V.

***N,N´*-Di(2,3,4,5,6-pentafluorophenylethyl)-1,6,7,12-tetrachloroperylene-3,4:9,10-tetracarboxylic acid bisimide (3b).**

1.00 g (1.89 mmol) 1,6,7,12-tetrachloroperylene-3,4:9,10-tetracarboxylic acid bisanhydride (**5b**), 1.59 g (7.54 mmol) pentafluorophenylethylamine and 0.7 ml acetic acid were dissolved in 35 ml dry NMP, stirred for 1h at 90°C and then poured into 2N HCl. The crude product was filtered off and dried. Product **1a** was afforded after column chromatography (DCM/*n*-hexane: 2/3) in a yield of 78% (1.35 g).

Mp: 421-425 °C; ^{1}H NMR ($CDCl_3$): δ8.65 (s, 4H), 4.51 (t, 4H, ^{3}J(H,H) = 6.7 Hz), 3.24 (t, 4H, ^{3}J(H,H) = 6.6 Hz); ^{19}F NMR (376.498 MHz, $CDCl_3$): δ-144.00 (m, 2F), -156.29 (m, 1F), -162.60 (m, 2F); HR-MS (esi (neg.-mode, chloroform, acetonitrile)): 913.9400 $(M)^-$, calculated 913.9397 ($C_{40}H_{12}Cl_4F_{10}N_2O_4$); UV/Vis ($CH_2Cl_2$): λ_{max}/nm (ε_{max} /$M^{-1}cm^{-1}$) = 520 (40900), 487 (28300), 427 (11200); fluorescence (CH_2Cl_2): λ_{max} = 546 nm, fluorescence quantum yield ϕ_{fl} = 0.93; electrochemistry (CH_2Cl_2, 0.1M TBAHFP, vs. ferrocene): $E^{red}_{1/2}$ (PBI/PBI^-) = -0.81 V, $E^{red}_{1/2}$ (PBI^-/PBI^{2-}) = -1.02 V.

Synthesis of series 4.

***N,N´*-Di(2,2,2-trifluoroethyl)-3,4:9,10-tetracarboxylic acid bisimide (4a).**

1.00 g (2.55 mmol) perylene-3,4:9,10-tetracarboxylic acid bisanhydride (**5a**), 1.5 ml (18.8 mmol) trifluoroethylamine and 1 ml acetic acid were dissolved in 10 ml dry NMP, stirred for 48 h at 200°C and then poured into 2N HCl. The crude product was filtered off. For removal of starting material the solid was refluxed in 2% $NaHCO_3$ solution, filtered off again and dried. 1.24 g (2.23 mmol) of product **4a** were obtained (yield 88%).

Mp: 475 °C (sublimation); HR-MS (EI): 554.0694 (M^+), calculated 554.0700 ($C_{28}H_{12}F_6N_2O_4$).

***N,N´*-Di(2,2,3,3,4,4,5,5,5-nonafluoropentyl)-3,4:9,10-tetracarboxylic acid bisimide (4b).**

2.23 g (5.69 mmol) perylene-3,4:9,10-tetracarboxylic acid bisanhydride (**5a**), 4.00 g (16.1 mmol) nonafluorobutylamine and 2.00 g acetic acid were dissolved in 34 ml dry NMP, stirred for 48 h at 200°C and then poured into 2N HCl. The crude product was filtered off. For removal of starting material the solid was refluxed in 2% $NaHCO_3$

solution, filtered off again and dried. The solid was recrystallized from toluene to give 655 mg (767 µmol, 13%) of product **4b**.

Mp: 358-363 °C; ^{1}H NMR ($CDCl_3$): δ 8.78 (d, 4H, ^{3}J(H,H) = 8.0 Hz), 8.72 (d, 4H, ^{3}J(H,H) = 8.1 Hz), 5.05 (t, 4H, ^{3}J(H,F) = 15.8 Hz); ^{19}F NMR (376.498 MHz, $CDCl_3$): δ -81.40 (m), -115.64 (m), -124.85 (m), -126.37 (m); HR-MS (esi (neg.-mode, chloroform, acetonitrile)): 854.0526 (M^-), calculated 854.0515 ($C_{34}H_{12}F_{18}N_2O_4$); UV/Vis (CH_2Cl_2): λ_{max}/nm (ε_{max} /$M^{-1}cm^{-1}$) = 524 (78600), 488 (47300), 457 (17600); fluorescence (CH_2Cl_2): λ_{max} = 530 nm, fluorescence quantum yield ϕ_{fl} = 1.00; electrochemistry (CH_2Cl_2, 0.1M TBAHFP, vs. ferrocene): $E^{red}_{1/2}$ (PBI/PBI^-) = -0.96 V, $E^{red}_{1/2}$ (PBI^-/PBI^{2-}) = -1.15 V.

5.9 References and Notes

[1] (a) C. W. Tang, *Appl. Phys. Lett.* **1986**, *48*, 183-185; (b) L. Schmidt-Mende, A. Fechtenkötter, K. Müllen, E. Moons, R. H. Friend, J. D. MacKenzie, *Science* **2001**, *293*, 1119-1122; (c) P. Peumans, S. Uchida, S. R. Forrest, *Nature* **2003**, *425*, 158-162; (d) S. E. Shaheen, C. J. Brabec, N. S. Sariciftci, F. Padinger, T. Fromherz, J. C. Hummelen, *Appl. Phys. Lett.* **2001**, *78*, 841-843.

[2] B. Geffroy, P. le Roy, C. Prat, *Polym. Int.* **2006**, *55*, 572-582.

[3] (a) Y. Noguchi, T. Sekitani, T. Someya, *Appl. Phys. Lett.* **2006**, *89*, 253507; (b) K. J. Lee, M. J. Motala, M. A. Meitl, W. R. Childs, E. Menard, A. K. Shim, J. A. Rogers, R. G. Nuzzo, *Adv. Mater.* **2005**, *17*, 2332-2336; (c) M. M. Ling, Z. Bao. *Chem. Mater.* **2004**, *16*, 4824-4840; (d) B. Yoo, T. O. Jung, D. Basu, A. Dodabalapur, B. A. Jones, A. Facchetti, M. R. Wasielewski, T. J. Marks, *Appl. Phys. Lett.* **2006**, *88*, 082104; (e) L. Zhou, A. Wanga, S.-C. Wu, J. Sun, S. Park, T. N. Jackson, *Appl. Phys. Lett.* **2006**, *88*, 083502; (f) R. C. G. Naber, B. de Boer, P. W. M. Blom, D. M. de Leeuw, *Appl. Phys. Lett.* **2005**, *87*, 203509; (g) C. D. Sheraw, L. Zhou, J. R. Huang, D. J. Gundlach, T. N. Jackson, M. G. Kane, I. G. Hill, M. S. Hammond, J. Campi, B. K. Greening, J. Francl, J. West, *Appl. Phys. Lett.* **2002**, *80*, 1088-1090; (h) D. Voss, *Nature*, **2000**, *407*, 442-444; (i) D. J. Gundlach, *Nat. Mater.* **2007**, *6*, 173-174; (j) H. Klauk, *Nat. Mater.* **2007**, *6*, 397-398; (k) A. Dodabalapur, *Mater. Today* **2006**, *9*, 24-39; (l) F. Würthner,

Angew. Chem. **2001**, *113*, 1069-1071; *Angew. Chem. Int. Ed.* **2001**, *40*, 1037-1039; (m) S. R. Forrest, *Nature* **2004**, *428*, 911-918.

[4] (a) S. Nadkarni, B. Yoo, D. Basu, A. Dodabalapur, *Appl. Phys. Lett.* **2006**, *89*, 184105; (b) S. De Vusser, S. Steudel, K. Myny, J. Genoe, P. Heremans, *Appl. Phys. Lett.* **2006**, *88*, 162116; (c) K. Hizu, T. Sekitani, T. Someya, J. Otsuki, *Appl. Phys. Lett.* **2007**, *90*, 093504; (d) H. Klauk, U. Zschieschang, J. Pflaum, M. Halik, *Nature* **2007**, *445*, 745-748.

[5] C. R. Newman, C. D. Frisbie, D. A. da Silva Filho, J.-L. Brédas, P. C. Ewbank, K. R. Mann, *Chem. Mater.* **2004**, *16*, 4436.

[6] (a) M. Yoon, S. A. DiBenedetto, A. Facchetti, T. J. Marks, *J. Am. Chem.* Soc. **2005**, *127*, 1348-1349; (b) M. Yoon, A. Facchetti, C. E. Stern, T. J. Marks, *J. Am. Chem. Soc.* **2006**, *128*, 5792-5801; (c) S. Ando, R. Muratami, J. Nishida, H. Tada, Y. Inoue, S. Tokito, Y. Yamashita, *J. Am. Chem. Soc.* **2005**, *127*, 14996-14997; (d) T. W. Lee, Y. Byun, B. W. Koo, I. N. Kang, Y. Y. Lyu, C. H. Lee, S. Y. Lee, *Adv. Mater.* **2005**, *17*, 2180-2184; (e) S. Kobayashi, T. Nishikawa, T. Takenobu, S. Mori, T. Shimoda, T. Mitani, H. Shimotani, N. Yoshimoto, S. Ogawa, Y. Iwasa, *Nat. Mater.* **2004**, *3*, 317-322; (f) E. J. Meijer, D. M. de Leeuw, S. Setayesh, E. Veenendaal, B. H. Huisman, P. W. M. Blom, J. C. Hummelen, U. Scherf, T. M. Klapwijk, *Nat. Mater.* **2003**, *2*, 678-682; (g) S. Kobayashi, T. Takenobu, S. Mori, A. Fujiwara, Y. Iwasa, *Appl. Phys. Lett.* **2003**, *82*, 4581-4583; (h) R. C. Haddon, A. S. Perel, R. C. Morris, T. T. M. Palstra, A. F. Hebard, R. M. Fleming, *Appl. Phys. Lett.* **1995**, *67*, 121-123; (i) S. Tatemichi, M. Ichikawa, T. Koyama, Y. Taniguchi, *Appl. Phys. Lett.* **2006**, *89*, 112108; (j) P. R. L. Malenfant, C. D. Dimitrakopoulos, J. D. Gelorme, L. L. Kosbar, T. O. Graham, A. Curioni, W. Andreoni, *Appl. Phys. Lett.* **2002**, *80*, 2517-2519.

[7] B.A. Jones, A. Facchetti, M. R Wasielewski, T. J. Marks, *J. Am. Chem.* Soc. **2007**, *129*, 15259-15278.

[8] D. M. deLeeuw, M. M. J. Simenon, A. R. Brown, R. E. F. Einerhand, *Synth. Met.* **1997**, *87*, 53-59.

[9] A. J. Jones, A. Facchetti, T. J. Marks, M. R. Wasielewski, *Chem. Mater.* **2007**, *19*, 2703-2705.

[10] M.-M. Ling, P. Erk, M. Gomez, M. Könemann, J. Locklin, Z. Bao, *Adv. Mater.* **2007**, *19*, 1123-1127.

[11] H. E. Katz, A. J. Lovinger, J. Johnson, C. Kloc, T. Slegrist, W. Li, Y.-Y. Lin, A. Dodabalapur, *Nature* **2000**, *404*, 478-481.

[12] H. Z. Chen, M. M. Ling, X. Mo, M. M. Shi, M. Wang, Z. Bao, *Chem. Mater.* **2007**, *19*, 816-824.

[13] (a) M. J. Ahrens, M. J. Fuller, M. R. Wasielewski, *Chem. Mater.* **2003**, *15*, 2684-2686; (b)A. J. Jones, M. J. Ahrens, M.-H. Yoon, A. Facchetti, T. J. Marks, M. R. Wasielewski, *Angew. Chem.* **2004**, *116*, 6523-6526; *Angew. Chem. Int. Ed.* **2004**, *43*, 6363-6366.

[14] R. T. Weitz, K. Amsharov, U. Zschieschang, E. B. Villas, D. K. Goswami, M. Burghard, H. Dosch, M. Jansen, K. Kern, H. Klauk, *J. Am. Chem. Soc.* **2008**, 10.1021/ja074675e.

[15] (a) J. Mizuguchi, *J. Appl. Phys.* **1998**, *84*, 4479-4486; (b) B. A. Gregg, *J. Phys. Chem.* **1996**, *100*, 852-859.

[16] W. Qiu, S. Chen, X. Sun, Y. Liu, D. Zhu, *Org. Lett.* **2006**, *8*, 867-870.

[17] F Würthner, V. Stepanenko, Z. Chen, C. Saha-Möller, N. Kocher, D. Stalke, *J. Org. Chem.* **2004**, *69*, 7933-7939.

[18] (a) A. Pleschke, A. Marhold, M. Schneider, A. Kolomeitsev, G.-V. Röschenthaler, *J. Fluorine Chem.* **2004**, *125*, 1031-1038; (b) F. Würthner, P. Osswald, R. Schmidt, T. E. Kaiser, H. Mansikkamäki, M. Könemann, *Org. Lett.* **2006**, *8*, 3765-3768.

[19] P. Osswald, F. Würthner, *J. Am. Chem. Soc.* **2007**, *129*, 14319–14326.

[20] F. Würthner, *Chem. Comm.* **2004**, 1564-1579.

[21] W. Qiu, S. Chen, X. Sun, Y. Liu, D. Zhu, *Org. Lett.* **2006**, *8*, 867-870.

[22] G. Klebe, F. Graser, E. Hädicke, J. Berndt, *Acta Crystallogr., Sect. B: Struct. Sci.* **1989**, *45*, 69-77.

[23] F. Graser, E. Hädicke, *Liebigs Ann. Chem.* **1984**, 483-494.

[24] I. Seguy, P. Jolinat, P. Destrule, R. Mamy, H. Allouchi, C. Couseille, M. Cotrait, H. Bock, *ChemPhysChem* **2001**, *2*, 448-452.

[25] I. Seguy, P. Jolinat, P. Destrule, R. Mamy, H. Allouchi, C. Couseille, M. Cotrait, H. Bock, *ChemPhysChem* **2001**, *2*, 448-452.

[26] J. Salbeck, H. Kunkely, H. Langhals, R. W. Saalfrank, J. Daub, *Chimia*, **1989**, *43*, 6-9.

[27] F. Graser, E. Hädicke, *Liebigs Ann. Chem.* **1980**, 1994-2011.

[28] S. R. Forrest, M. L. Kaplan, P. H. Schmidt, *J. Appl. Phys.* **1984**, *55*, 1492-1507.

[29] Z. Chen, M. G. Debije, T. Debaerdemaeker, P. Osswald, F. Würthner, *ChemPhysChem* **2004**, *5*, 137-140.

[30] *Organic Field-Effect Transistors* (Eds. Z. Bao and J. Locklin), Taylor and Francis, Boca Raton, **2007**.

[31] V. Coropceanu, J. Cornil, D. A. da Silva Filho, R. Silbey, J.-L. Brédas, *Chem. Rev.* **2007**, *107*, 926-952.

[32] (a) H. E. Katz, J. Johnson, A. J. Lovinger, L. Wenjie, *J. Am. Chem. Soc.* **2000**, *122*, 7787–7792; (b) H. E. Katz, J. Otsuki, K. Yamazaki, A. Suka, T. Takido, A. J. Lovinger, K. Raghavachari, *Chem. Lett.* **2003**, *32*, 508-509.

[33] F. Graser, E. Hädicke, *Liebigs Ann. Chem.* **1984**, 483-494.

[34] M. G. Debije, Z. Chen, J. Piris, R. B. Neder, M. M. Watson, K. Müllen, F. Würthner, *J. Mater. Chem.* **2005**, *15*, 1270-1276.

[35] W. Qiu, S. Chen, X. Sun, Y. Liu, D. Zhu, *Org. Lett.* **2006**, *8*, 867-870.

[36] F. Würthner, V. Stepanenko, Z. Chen, C. R. Saha-Möller, N. Kocher, D. Stalke, *J. Org. Chem.* **2004**, *69*, 7933-7939.

[37] R. Filler ,W. Chen, S. M. Woods, J*. Fluorine Chem.* **1995**, *73*, 95-100.

[38] *Principles of Fluorescence Spectroscopy* (Ed. J. R. Lakowicz), 2nd ed., Kluwer Academic/Plenum, New York, **1999**.

[39] G. Seybold, G. Wagenblast, *Dyes Pigm*. **1989**, *11*, 303-317.

[40] (a) G. M. Sheldrick, *SADABS 2.05: Program for Area Detector Absorption Correction*, University of Göttingen, **2002**; (b) G. M. Sheldrick, *SHELXL-97 – Program for Structure Refinement*, Universität Göttingen, **1997**.

[41] K. Deyama, H. Tomoda, H. Muramatsu, M. Matsui, *Dyes Pigm.* **1996**, *30*, 73-78.

[42] M.-M. Shi, H.-Z. Chen, J.-Z. Sun, J. Ye, M. Wang, *Chem. Comm.* **2003**, *14*, 1710-1711.

Chapter 6

Summary

This thesis deals with the synthesis of improved organic semiconductors, the detailed investigation of the molecular properties and the solid state arrangements revealed by single crystal X-ray diffraction and finally the development of structure-performance dependencies by measuring of the charge carrier mobilities of the derivatives in thin film transistors, which were built in the working groups of Prof. Dr. Frühauf (Stuttgart) and Prof. Dr. Bao (Stanford).

An overview of the history, functionality and principles of organic thin film transistors is given in Chapter 2. Also the performances of the most common organic semiconductors in (TFTs) are compared with each other. Furthermore, a structure-response relationship concerning the reduction potential and air-stability of literature known n-type compounds is debated.

In Chapter 3 four different acene derivatives with solubility providing substituents in mid position were synthesized (Figure 1). Two crystal structures of the highly soluble crystalline compounds were obtained revealing a parallel arrangement for the anthracene derivative and a “herringbone” order for the tetracene. The UV/Vis spectroscopy of the thin films showed the highest π–π interactions for the pentacene and anthradithiophene homologue due to the sufficient size of their aromatic systems. The better overlap between the molecules was also reflected in the significantly better charge carrier mobilities of the higher homologues in OTFTs prepared by spin-coating. Nevertheless, the mobilities stayed rather low due to insufficient crystallinity of the thin films and unoptimized preparation techniques for the transistors.

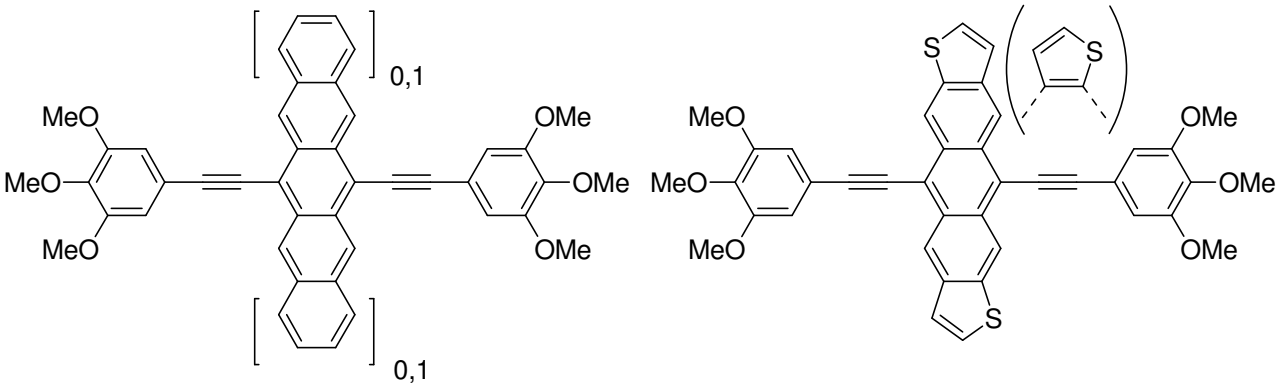

Figure 1. Synthesized acene derivatives of Chapter 3.

Chapter 4 explored the synthesis and properties of novel core di- and tetrafluorinated perylene bisimide dyes (Figure 2). Imidization of the difluorinated perylene bisanhydride led to lower yields than the Halex conversion of the dibrominated perylene bisimides. The fourfold exchange for the tetrafluorinated dyes was also less effective due to a higher sensibility of the obtained products. The physical attributes of the difluorinated derivatives were quite similar to unsubstituted PBIs as the π–system stayed planar, while the tetrafluorinated derivative showed a highly twisted perylene core similar to tetrachlorinated PBIs in the solid state packing.

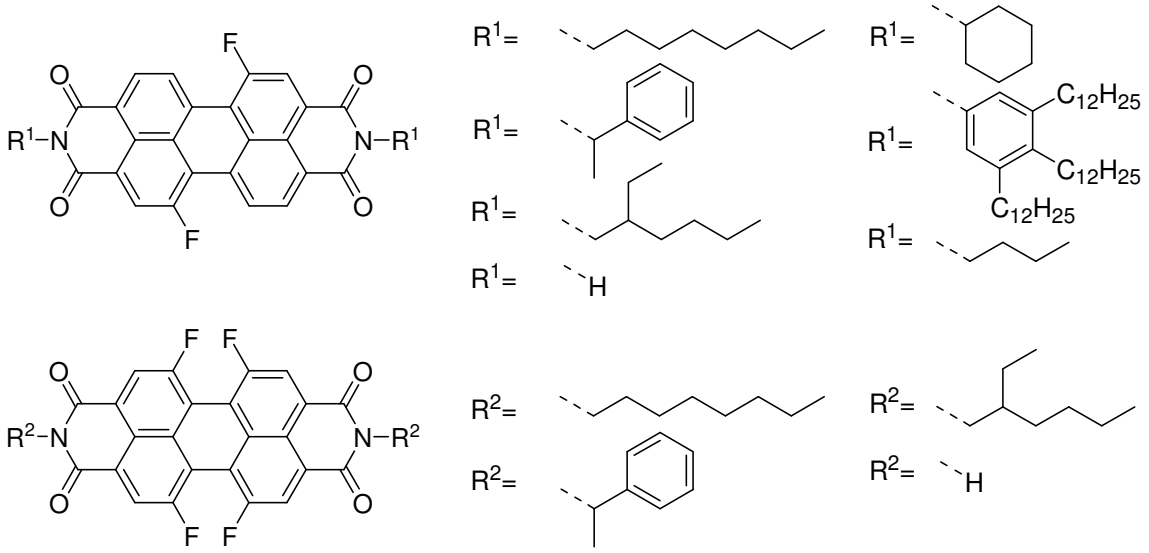

Figure 2. Synthesized core-fluorinated perylene bisimide dyes of Chapter 4.

Though fluorine has the highest electronegativity, cyclic voltammetry measurements revealed only slightly varied redox potentials of the dyes compared to their fluorine-free homologues. Furthermore, the imide substituents of the

difluorinated dyes were chosen to obtain insoluble pigments (R = hydrogen), highly crystalline compounds (R = butyl) and liquid crystalline derivatives (R = tridodecylphenyl). In literature several similar perylene bisimide dyes revealed outstanding mobilities in thin film transistors making these novel derivatives potential candidates for OTFTs prepared by vacuum deposition or spin-coating techniques. Exemplarily the difluorinated PBI with butyl substituents was tested as active layer in OTFTs and mobilities up to 0.89 cm^2/Vs were measured under nitrogen.

The use of electron deficient perylene bisimide dyes as potential air-stable organic n-type semiconductors in thin film transistors was investigated in Chapter 5. Four series of derivatives with varying bay and perfluorinated imide substituents were synthesized (Figure 3) and the solid state packing of the derivatives with the highest performance was analyzed by singe crystal X-ray diffraction.

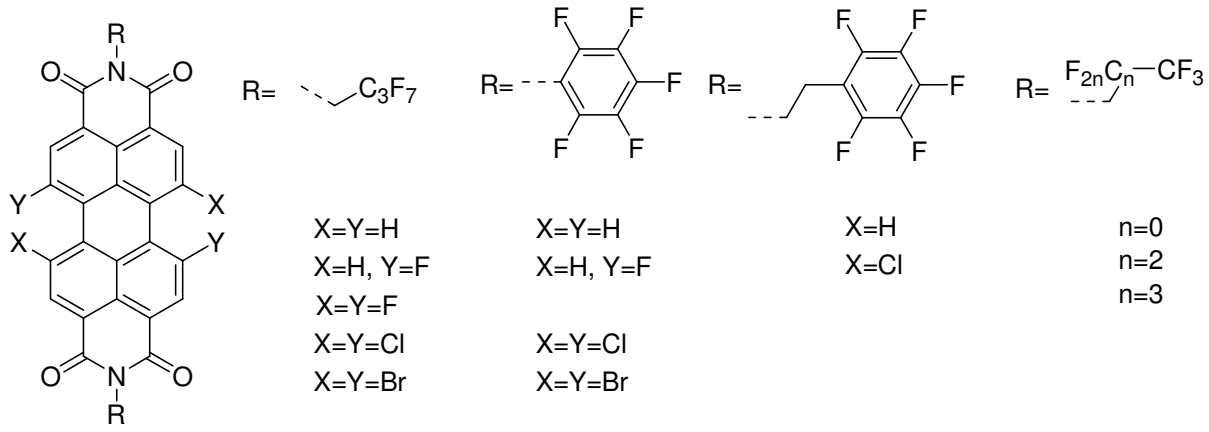

Figure 3. Synthesized perylene bisimide dyes for OTFTs of Chapter 5.

The best mobilities were obtained for PBIs with small and consistent π–π interactions, while dyes with highly twisted π–systems and *M*- and *P*-enantiomers in the crystal showed minor values. Next to the extremely high mobilities up to 1.44 cm^2/Vs and maximum on/off ratios of 10^9 all dyes showed adequate to excellent air stability in the electronic devices. The determination of the LUMOs of the dyes exhibited clearly that the stability of the OTFTs towards oxygen cannot be explained with the redox potentials. A special dense packing of the perfluorinated alkyl or phenyl substituents can obviously form a “barrier”, while normal hydrocarbons cannot hinder the intrusion of oxygen into the active thin layer. This can be seen exemplarily in the solid state of two perylene bisimide dyes (Figure 4)

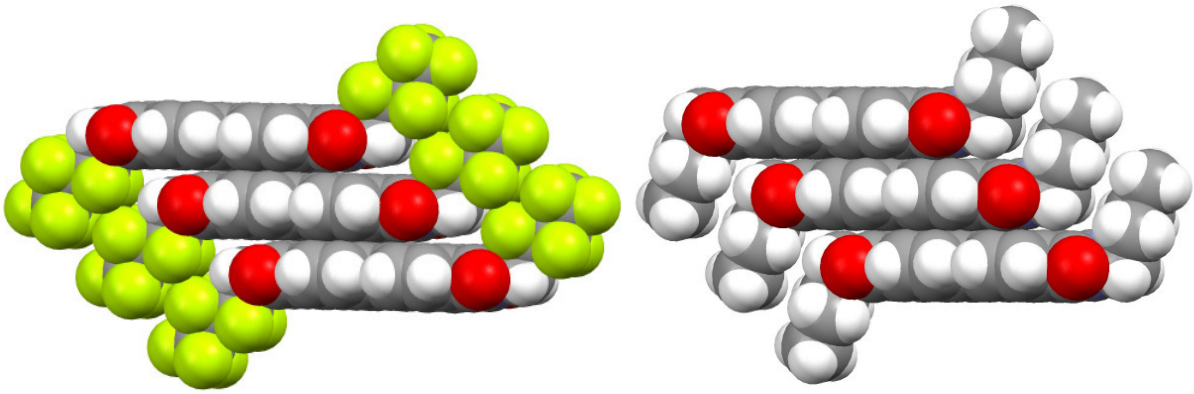

Figure 4. Space-filling depiction of single crystal structures of a PBI with perfluorinated alkyl chains, which was used as active layer of an air-stable OTFT (left) and its halogen-free corresponding dye (right) showing the potential “channel” for intrusion of oxygen between the butyl chains (right)

In conclusion the two main-goals of this thesis were achieved. Well soluble acene derivatives for spin-coated TFTs were obtained, showing charge carrier mobilities in the range of polymer p-type materials. Novel core-fluorinated perylene bisimide dyes were synthesized particularly and the use of electron deficient substituents lead to PBIs with outstanding air-stable mobilities in thin film transistors prepared by vacuum deposition techniques. The relationship between performance, air stability and solid state packing was elucidated in detail by single crystal X-ray diffraction analysis.

Chapter 7

Zusammenfassung

Das Ziel der vorliegenden Arbeit war die Synthese verbesserter organischer Halbleitermaterialien, detaillierte Untersuchungen ihrer Moleküleigenschaften sowie ihrer Packung mittels von Röntgenstrukturanalysen von Einkristallen sowie die Ableitung von Struktur-Eigenschaftsbeziehung mit Hilfe der Ladungsträgerbeweglichkeiten in Dünnschichttransistoren, welche in Kooperation mit der Arbeitsgruppe von Prof. Dr. Frühauf (Stuttgart) und Prof. Dr. Bao (Stanford) ermittelt wurden.

Ein Überblick über die Entwicklung und Funktionsweise von organischen Dünnschichttransistoren wird in Kapitel 2 gegeben. Auch die Leistungsfähigkeiten von Dünnschichttransistoren der bekanntesten organischen Halbleiter werden miteinander verglichen. Außerdem wird die Struktur-Eigenschaftsbeziehungen von luftstabilen n-Typ Derivaten bezüglich des Redoxpotentials diskutiert.

Kapitel 3 beschreibt die Synthese von vier verschiedenen Acenderivaten mit löslichkeitsvermittelnden Substituenten in der zentralen Position (Abbildung 1). Zwei Einkristallstrukturen der hochlöslichen kristallinen Verbindungen konnten erhalten werden, die eine parallele Anordnung der Anthracen- und eine „Fischgrätenstruktur“ der Tetracenmoleküle offenbarte. Die stärksten π–π Wechselwirkungen konnten durch Festkörper UV/Vis-Spektroskopie für die höheren Pentacen- und Anthradithiophen-Homologa nachgewiesen werden. Die signifikant

größere Überlappung ihrer aromatischen Systeme zeigte sich auch in den weitaus höheren Ladungsträgerbeweglichkeiten in organischen p-Kanal-TFTs, die durch Spin-Coating Verfahren hergestellt wurden. Allerdings waren die abgeschiedenen Dünnschichten amorph und die Transistorenherstellung nicht optimiert, was zu geringen Mobilitäten von 10^{-5} cm^2/Vs für den Lochtransport führte.

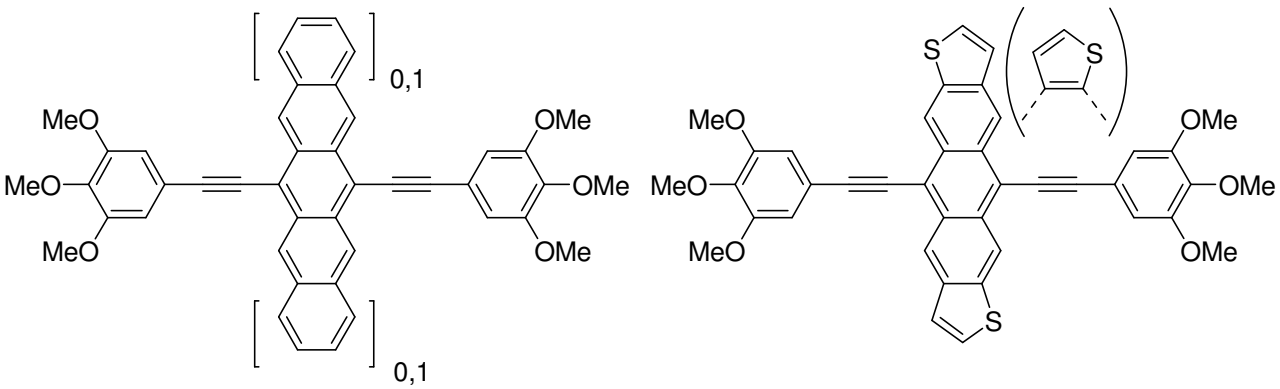

Abbildung 1. Hergestellte Acenderivate in Kapitel 3.

Kapitel 4 beschäftigt sich mit der Synthese und den Eigenschaften neuer di- und tetrafluorierter Perylenbisimidfarbstoffe (Abbildung 2). Imidisierung von difluorierten Perylenbisanhydrid führte zu geringeren Ausbeuten als die Halogen-Austauschreaktion aus den entsprechenden dibromierten PBIs. Wegen einer höheren Empfindlichkeit des entstehenden Produktes war auch der vierfache Austausch bei tetrachloriertem Farbstoffen weniger effizient. Die physikalischen Eigenschaften der difluorierten Derivate waren denen der halogenfreien PBIs sehr ähnlich, da sie ebenfalls ein planares π–System besitzen. Für ein tetrafluoriertes Derivat wurde jedoch ein stark verdrilltes aromatisches System und eine ähnliche Packung im Festkörper gefunden wie sie für vierfach chlorsubstituierte Perylenbisimide bekannt ist. Des Weiteren zeigten Cyclovoltammetriemessungen, dass eine Kernfluorierung nur einen sehr kleinen Einfluss auf die Redoxpotentiale hat, obwohl Fluor die höchste Elektronegativität besitzt. Insgesamt wurde bei der Auswahl der Imidreste darauf geachtet, neben unlöslichen Pigmentfarbstoffen (z.B. R = H) auch hochkristalline Verbindungen (z.B. R = butyl) und gutlösliche, flüssigkristalline Derivate (R = tridodecylphenyl) zu erhalten. Da viele veröffentlichte PBIs mit ähnlicher Grundstruktur ausgezeichnete Feldeffektmobilitäten zeigten, sind diese kernfluorierten Derivate ebenfalls sehr aussichtsreichen Kandidaten für organische Dünnschichttransistoren, die entweder durch Abscheidung aus Lösung

oder durch Vakuumauftragung hergestellt werden können. Exemplarisch wurde das difluorierte PBI mit Butylresten in der Imidposition auf Feldeffektmobilitäten in TFTs untersucht und Werte bis zu 0.89 cm^2/Vs gemessen (unter N_2-Atmosphäre).

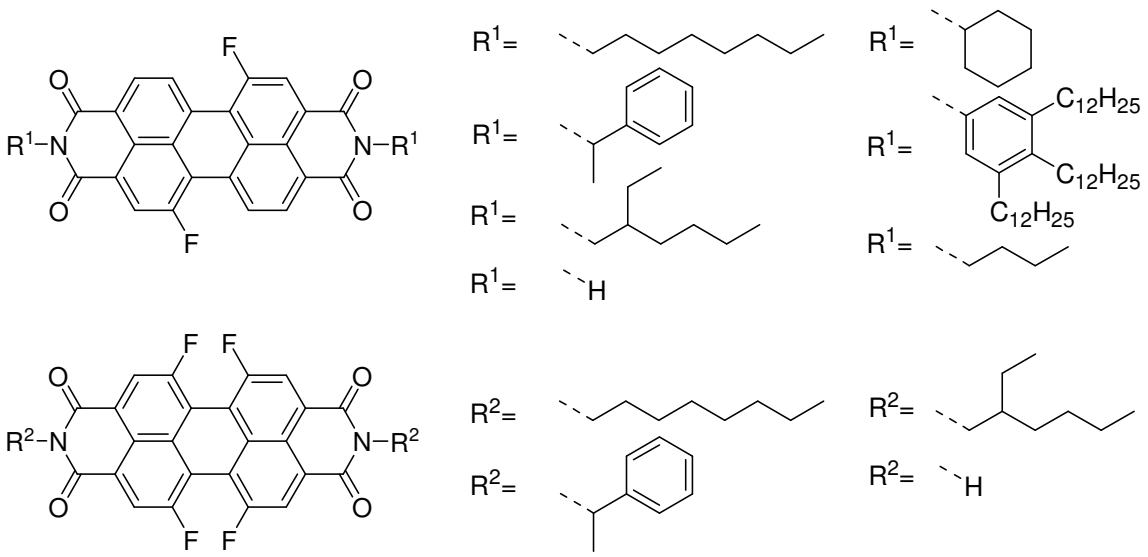

Abbildung 2. Synthetisierte kernfluorierte PBIs in Kapitel 4.

Die Synthese von sehr elektronenarmer Perylenbisimiden als potentielle luftstabile, organische n-Halbleiter in Dünnschichttransistoren war der Schwerpunkt in Kapitel 5. Vier verschiedene Serien mit variierenden Bucht- und perfluorierten Imidsubstituenten wurden synthetisiert und die Festkörperpackungen der besten Derivate durch Einkristallröntgenstrukturanalyse bestimmt (Abbildung 3).

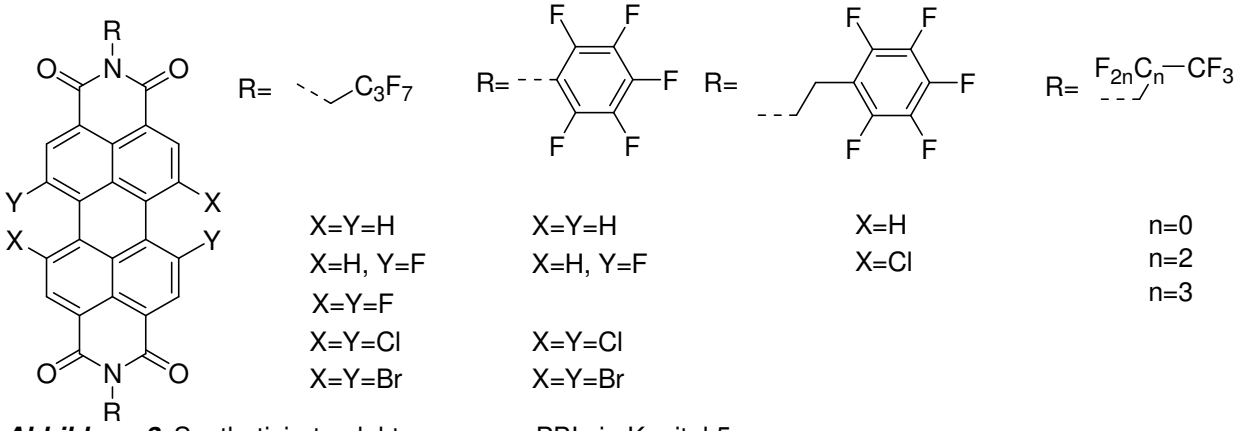

Abbildung 3. Synthetisierte elektronenarme PBIs in Kapitel 5.

Die besten Ladungsträgermobilitäten wurden für Farbstoffe mit kleinen und gleichmäßigen π–π Abständen erhalten, während stark verdrillte Systeme mit *M*- and *P*-Enantiomeren im Festkörper geringere Mobilitäten zeigten. Neben extrem hohen Beweglichkeiten bis zu 1.44 cm^2/Vs (PBI **1a**) und maximalen ein/aus Verhältnissen

von 10^9 (PBI **2b**) zeigten alle Farbstoffe gute bis exzellente Luftstabilität in Feldeffekttransistoren. Die genaue elektrochemische Bestimmung der LUMOs zeigte eindeutig, dass die Stabilität gegenüber Sauerstoff nicht durch die Redoxpotentiale erklärt werden kann. Offensichtlich wird durch eine dichtere Packung der perfluorierten Alkyl- oder Phenylsubstituenten das Eindringen von Sauerstoff in die aktive Schicht verhindert. Bei einer Separierung der π–Systeme und perfluorierten Imidreste (Abbildung 4, links) und dem Vorliegen dicht gepackter PBI-Stapel wurden die besten Werte an Luft erzeilt.

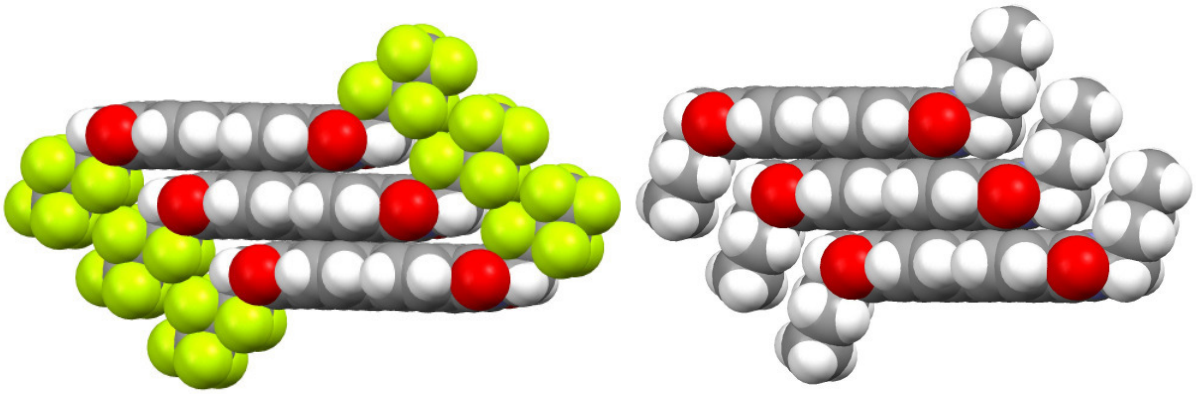

Abbildung 4. Kalotten Modell der Packung im Einkristall für das an Luft in OFETs verwendbare PBI **1a** mit perfluorierten Butylketten (links) und das entsprechende halogenfreie Analogon (rechts) mit einem größeren Abstand zwischen den Substituenten.

Zusammenfassend konnten die beiden Hauptziele der Arbeit erreicht werden. Gutlösliche Acenderivate für Spin-Coating Verfahren konnten hergestellt werden deren TFTs Ladungsträgerbeweglichkeiten im Bereich polymerer p-Halbleitermaterialien liegen. Vor allem wurden jedoch neuartige Perylenbisimidfarbstoffe synthetisiert, die durch Einführung elektronenziehender Halogenreste herausragende Elektronenbeweglichkeiten in Dünnschichttransitoren an Luft aufwiesen (durch Vakuumsublimation hergestellt). Der Zusammenhang zwischen Ladungsträgermobilität, Luftstabilität und Festkörperpackung wurde detailliert durch Einkristallstrukturanalysen aufgeklärt.

List of Publications and Patents

Publications

“Air-stable n-channel organic thin-film transistors with high field-effect mobility based on *N,N’*-bis(heptafluorobutyl)-3,4:9,10-perylene diimide.”
J. H. Oh, S. Liu, Z. Bao, R. Schmidt, F. Würthner *Appl. Phys. Lett.* **2007**, *91*, 212107.

“Core-fluorinated perylene bisimide dyes: air stable n-channel organic semiconductors for thin film transistors with exceptionally high on-to-off current ratios.”
R. Schmidt, M. M. Ling, J. H. Oh, M. Winkler, M. Könemann, Z. Bao, F. Würthner *Adv. Mat.* **2007**, *19*, 3692-3695.

“Highly soluble acenes as semiconductors for thin film transistors.“
R. Schmidt, S. Göttling, D. Leusser, D. Stalke, A.-M. Krause, F. Würthner *J. Mater. Chem.* **2006**, *16*, 3708–3714.

“Synthesis and optical and electrochemical properties of core-fluorinated perylene bisimides.”
F. Würthner, P. Osswald, R. Schmidt, T. E. Kaiser, H. Mansikkamäki, M. Könemann *Org. Lett.* **2006**, *8*, 3765–3768.

“Electronic and crystal engineering of acenes for solution-processible self-assembling organic semiconductors.“
F. Würthner, R. Schmidt *ChemPhysChem* **2006**, *7*, 793–797.

Patents

“Fluorinated rylenetetracarboxylic acid derivatives and use thereof.”
M. Koenemann, P. Osswald, R. Schmidt, F. Wuerthner, WO2007093643.

“Verwendung von *N,N'*-Bis(1,1-dihydroperfluor-C3-C5-alkyl)-perylen-3,4:9,10-tetracarbonsäurebisanhydriden“
M. Koenemann, R. Schmidt, F. Wuerthner, not yet laid open.

“Fluorinated naphthalene diimide dyes with perfluorinated imide substituents in OTFTs”
M. Koenemann, C. Roeger, R. Schmidt, F. Wuerthner, not yet laid open.